REACTIONS OF COPPER COMPLEXES WITH DIOXYGEN AND OXO TRANSFER REAGENTS: TOWARD ELUSIVE COPPER-OXYL SPECIES

A DISSERTATION
SUBMITTED TO THE FACULTY OF THE GRADUATE SCHOOL
OF THE UNIVERSITY OF MINNESOTA
BY

Sungjun Hong

IN PARTIAL FULFILLMENT OF THE REQUIREMENTS
FOR THE DEGREE OF
DOCTOR OF PHILOSOPHY

William B. Tolman, Advisor

July 2010

Acknowledgements

I would like to thank several people for helping me reach this accomplishment. First, I thank my advisor, Professor William B. Tolman, for his encouragement over the years and allowing me the opportunity to work on interesting and challenging projects and to develop as an independent scientist. I also thank Professor Lawrence Que, Jr., and John Lipscomb for allowing me access to their facilities. I'd like to thank Dr. Victor Young, Jr. for all of his help with X-ray Crystallography. Thanks also to my master degree research advisor, Professor Ho-Gyeom Jang, for his guidance and advice to pursue this career.

I would like to thank all past and present Tolman group members for helpful discussions. In particular, thanks to Aalo Gupta for his endeavor to work on Resonance Raman experiments as well as to make our lab a fun place to work. Also, thanks to Drs. Lyndal Hill and Itsik Bar-Nahum for their advice and guidance.

I would like to especially thank my wife, Moonyeon Youn, for her constant love, respect and encouragement. I would not be here where I am today without her, who has always helped me to achieve my goals. I also would like to show my deep love to my lovely daughter Hannah and son Ian. They always made me laugh and gave me the inspiration to follow my own path.

Abstract

The binding and activation of dioxygen by Cu ions is central to the function of numerous biological systems. Among the enzymes activate dioxygen for the functionalization of organic substrates, those catalyzed by the mononuclear copper enzymes dopamine β-monooxygenase (DβM) and peptidylglycine α-hydroxylating monooxygenase (PHM) are less understood. Despite extensive research on these enzymes, the exact nature of the active species responsible for substrate functionalization is not resolved, with two provocative proposals involving either a Cu^{II}-superoxo or a mononuclear Cu^{II}-oxyl species having been put forth. The goal of this research is to understand the reaction catalyzed by the PHM and DβM enzymes on a fundamental chemical level via a small molecule synthetic model approach, with particular emphasis on generating and/or characterizing a Cu-oxygen species that is capable of performing similar reactions to those seen in the DβM and PHM enzymes.

Chapter 1 contains a general overview of dioxygen activation in biological systems and gives a review of the structure and proposed catalytic mechanisms of DβM and PHM, followed by a summary of recent synthetic efforts toward mononuclear Cu/O_2 adducts and Cu-oxyl species. Chapter 2 describes the synthesis and characterization of the copper(I) complexes of the electron-deficient β-diketiminate and analogous 4-nitroformazan supporting ligands, and their O_2-reactivity studies, portions of which have

been previously reported.[1] Chapter 3 describes a bio-inspired synthetic route toward a mononuclear Cu-oxyl species that involves decarboxylation of copper(I)-α-ketocarboxylate complexes by dioxygen; portions of the work have been communicated previously.[2] Chapter 4 then describes results obtained from reactions of copper(I) complexes of bidentate N-donor ligands with pyridine- and trimethylamine N-oxides or PhIO. Portions of this work were previously reported.[3]

[1] Hong, S.; Hill, L. M. R.; Gupta, A. K.; Naab, B. D.; Gilroy, J. B.; Hicks, R. G.; Cramer, C. J.; Tolman, W. B. "Effects of Electron-Deficient β-Diketiminate and Formazan Supporting Ligands on Copper(I)-Mediated Dioxygen Activation." *Inorg. Chem*. **2009**, *48*, 4514-4523.

[2] Hong, S.; Huber, S. M.; Gagliardi, L.; Cramer, C. C.; Tolman, W. B. "Copper(I)-α-Ketocarboxylate Complexes: Characterization and O_2 Reactions That Yield Copper-Oxygen Intermediates Capable of Hydroxylating Arenes." *J. Am. Chem. Soc*. **2007**, *129*, 14190-14192.

[3] Hong, S.; Gupta, A. K.; Tolman, W. B. "Intermediates in Reactions of Copper(I) Complexes with N-Oxides: From the Formation of Stable Adducts to Oxo Transfer." *Inorg. Chem*. **2009**, *48*, 6323-6325.

TABLE OF CONTENTS

LIST OF TABLES

Page

LIST OF SCHEMES

Pages

LIST OF FIGURES

Pages

ABBREVIATIONS

ATP	Adenosine triphosphate
BF	Benzoylformate
DβM	Dopamine β-monooxygenase
DFT	Density functional theory
DMF	Dimethylformamide
EPR	Electron paramagnetic resonance
ESI-MS	Electrospray ionization mass spectrometry
ET	Electron transfer
EXAFS	Extended X-ray absorption fine structure
FTIR	Fourier transform infrared spectroscopy
LMCT	Ligand-to-metal charge transfer
LUMO	Lowest unoccupied molecular orbital
MF	Mesitoylformate
MLCT	Metal-to-ligand charge transfer
NMR	Nuclear magnetic resonance
PHM	Peptidylglycine α-hydroxylating monooxygenase
TEMPO	2,2,6,6-Tetramethyl-1-piperidinyloxy radical
THF	Tetrahydrofuran
XAS	X-ray absorption spectroscopy

CHAPTER 1. BINDING AND ACTIVATION OF DIOXYGEN BY COPPER SYSTEMS

1.1. Dioxygen Activation

By definition, aerobic life requires use of dioxygen (O_2) in key metabolic processes. For instance, dioxygen functions as a terminal electron acceptor in cellular respiration. The reduction of O_2 to water then generates electron and proton gradients that are subsequently used to synthesize ATP (adenosine triphosphate) to store energy. Dioxygen is also an important reactant in transformations of organic molecules in biological processes (cf. Scheme 1-1).

$$C_6H_{12}O_6\ (aq) + 6\ O_2\ (g) \longrightarrow 6\ CO_2\ (g) + 6\ H_2O\ (l)$$

$$\Delta G = -2880\ kJ\ per\ mole\ of\ C_6H_{12}O_6$$

Scheme 1-1. Simplified reaction of glucose with O_2.

In general, such reactions involve the cleavage of the oxygen-oxygen bond and formation of C-O and O-H bonds. Despite the strong thermodynamic driving force (here, $\Delta G = -2880$ kJ), the rates of reaction of dioxygen with organic molecules under ambient conditions are low due to (a) the unfavorable one-electron reduction potential of O_2

(ranging from ~ –0.2 to –0.5 V vs NHE depending on the medium)[4] and (b) spin restrictions. Dioxygen has two unpaired electrons residing in two degenerate antibonding molecular orbitals (π_{2px}^* and π_{2py}^*; Scheme 1-2). Thus, the electronic ground state of O_2 is a triplet ($^3\Sigma_g^-$), while most organic compounds are ground state singlets. Direct reaction of triplet O_2 with singlet organic compounds is a spin-forbidden process and thus has a large kinetic barrier.

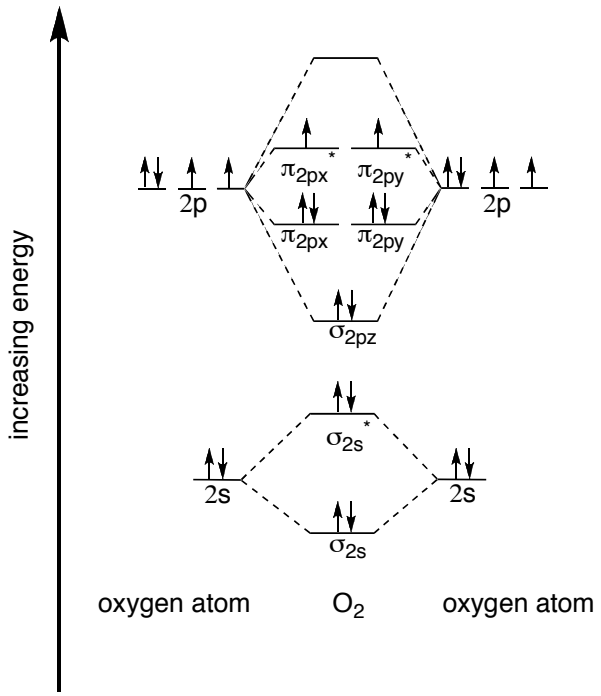

Scheme 1-2. Molecular orbitals energy diagram for O_2.

An obvious question that arises from these observations is: how do organisms employ O_2 to maintain their life under ambient conditions? In general, the metabolic

[4] Bielski, Benon H. J.; Cabelli, Diane E.; Arudi, Ravindra L.; Ross, Alberta B. "Reactivity of perhydroxyl/superoxide radicals in aqueous solution." *J. Phys. Chem. Ref. Data*. **1985**, *14*, 1041-1100.

processes described above are catalyzed by a sequence of enzymes. With respect to O_2-involving reactions in organisms, the enzymes often contain transition metal ions (called metalloenzymes). Among the various transition metal ions found in biology, Fe and Cu are the most commonly observed in metalloenzymes. One of the key roles played by transition metal ions in metalloenzymes is to facilitate the binding and activation of dioxygen via formation of metal-oxygen intermediates that then can rapidly react with organic substrates. Understanding the wide-range of interesting O_2-dependent metabolic processes performed by metalloenzymes is of fundamental importance. In addition, appreciation of these processes has direct practical applications. For example, understanding how metalloenzymes that catalyze selective oxidation reactions of organic substrates with dioxygen could inform the design of new environmentally benign catalysts useful for converting abundant feed-stocks (e.g. aliphatic alkanes) to value-added synthons (e.g. alkenes, alcohols, aldehydes, ketones, etc.).

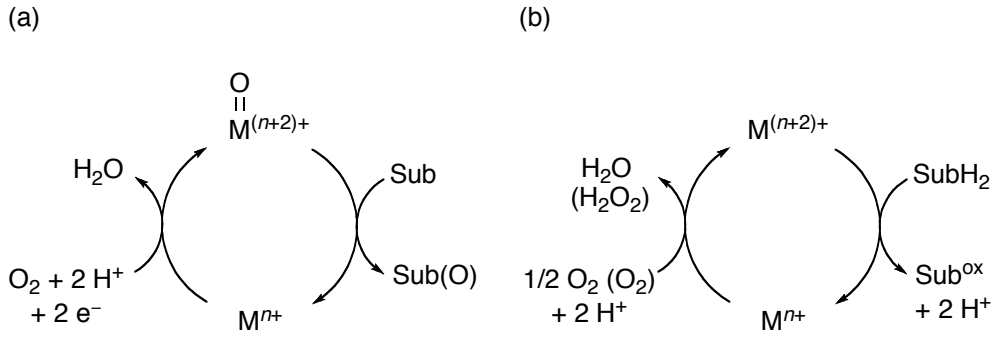

Scheme 1-3. Simplified catalytic cycles of some metalloenzyme-catalyzed reactions. (a) Oxygenase pathway, which involves the substrate oxidation through oxygen-atom transfer from O_2, often via a high-valent metal-oxygen intermediate. (b) Oxidase pathway, which simply utilizes O_2 as a two-electron/two-proton acceptor in the oxidation of the substrate.

Metalloenzymes that activate dioxygen are generally divided into two categories, oxygenases and oxidases, depending on the fate of the oxygen atoms from O_2. Oxygenases effect oxygen-atom transfer from dioxygen to the substrate, whereas oxidases simply use dioxygen as an electron/proton acceptor in substrate oxidation to yield water or hydrogen peroxide (H_2O_2). In general, the mechanisms of both types of enzymes involve reaction of the reduced metal center (M^{n+}) with dioxygen. Through sequential electron and/or proton transfer processes, the dioxygen can be reduced into superoxo ($O_2^{-\bullet}$), peroxo (O_2^{2-}) or even oxo (O^{2-}) species. All of these species can then participate in reaction pathways leading either to the incorporation of the oxygen atoms into the organic substrates (oxygenases) or to the reduction of O_2 to water or H_2O_2 (oxidases).

Understanding what factors govern the course of formation of metal-oxygen intermediates and their properties is of great importance in both biological and catalytic systems. Significant insights into dioxygen activation by these metalloenzymes have been obtained through a combination of chemical, structural, spectroscopic, and computational approaches applied both to enzymes and to synthetic model systems.[5] The goal of studies of synthetic models systems is to elucidate the underlying principles of metalloenzyme structure and function, including structure, spectroscopy, magnetic and electronic structure, reactivity, and chemical mechanism, through studies of synthetic complexes

[5] a) Holm, R. H.; Kennepohl,P.; Solomon. E. I. "Structural and Functional Aspects of Metal Sites in Biology" *Chem. Rev.* **1996**, *96*, 2239-2314. b) Costas, M.; Mehn. M. P.; Jensen. M. P.; Que Jr., L. "Dioxygen Activation at Mononuclear Nonheme Iron Active Sites: Enzymes, Models, and Intermediates" *Chem. Rev.* **2004**, *104*, 939-986. c) Siegbahn, P. E. M.; Borowski, T. "Modeling Enzymatic Reactions Involving Transition Metals" *Acc. Chem. Res.* **2006**, *39*, 729-738. d) Nam, W. "Dioxygen Activation by Metalloenzymes and Models" *Acc. Chem. Res.* **2007**, *40*, 465. e) Mirica, L. M.; Ottenwaelder, X.; Stack, T. D. P. "Structure and Spectroscopy of Copper−Dioxygen Complexes" *Chem. Rev.* **2004**, *104*, 1013-1045.

designed to replicate the active site. Because synthetic analogs can be used to investigate the effects of systematic variations in coordination geometry, ligation, local environment, and other factors, synthetic models studies may often provide insights that cannot be easily achieved from studies of the enzymes themselves.

As an example of the utility of the synthetic modeling approach that is particularly relevant to the thesis research describe here, consider how reversible binding of O_2 to the oxygen carrier hemocyanin (Hc) was discovered. This protein found in the blood of mollusks and anthropods reversibly binds O_2 by using two copper ions closely located to one another. Initial studies showed that the binding of O_2 to reduced form of Hc (two Cu^I ions) resulted in the oxidized O_2-bound form (called oxyHc). This form was found to display unique spectral features (UV-vis: 345 nm, ε =21,000 M^{-1} cm^{-1} and 550 nm, ε =800 M^{-1} cm^{-1},[6] resonance Raman (rR): 741 cm^{-1}, $\Delta^{18}O_2$ = 44 cm^{-1}).[7] The rR data fall in the range expected for the O-O stretching vibration of the peroxide ion (O_2^{2-}), suggesting the presence of such an entity in oxyHc. However, the binding mode of the peroxide moiety to the copper ions and the electronic origins of the characteristic UV-vis transitions remained unclear until a key discovery was made in efforts to prepare synthetic models of the oxyHc active site. Structural characterization of a Cu/O_2 species formed by reaction of a synthetic Cu^I model complex with O_2 showed two copper(II) ions

[6] a) Heirwegh, K.; Borginon, H.; Lontie, R. "Separation and absorption spectra of α- and β-hemocyanin of Helix pomatia." *Biochim. Biophys. Acta*. **1961**, *48*, 517-526. b) Van Holde, K. E. "Physical studies of hemocyanins. III. Circular dichroism and absorption spectra." *Biochemistry*. **1967**, *6*, 93-99.

[7] a) Freedman, T. B.; Loehr, J. S.; Loehr, T. M. "A resonance Raman study of the copper protein, hemocyanin. New evidence for the structure of the oxygen-binding site." *J. Am. Chem. Soc*. **1976**, *98*, 2809-2815. a) Ling, J-S; Nestor, L. P.; Czernuszewicz, R. S.; Spiro, T. G.; Fraczkiewicz, R.; Sharma, K. D.; Loehr, T. M.; Sanders-Loehr, J. "Common Oxygen Binding Site in Hemocyanins from Arthropods and Mollusks. Evidence from Raman Spectroscopy and Normal Coordinate Analysis." *J. Am. Chem. Soc*. **1994**, 116, 7682-7691.

linked by a side-on bound η^2:η^2-peroxide moiety.[8] Importantly, this species exhibited remarkably similar UV-vis and rR spectroscopic features to those of oxyHc, implicating that O_2 binding in oxyHc also occurs in the same fashion. The subsequent structural characterization of oxyHc from horseshoe crab[9] and octopus[10] eventually confirmed the side-on binding mode of O_2 that was first suggested by the pioneering synthetic modeling work.

My research builds upon this work and has a related goal: to evaluate the mechanisms of O_2 activation by copper-containing metalloenzymes through the synthetic modeling approach. The enzymes that motivate this research are described below.

1.2. O_2 Activation by Copper Enzymes

Copper-containing enzymes perform a variety of biologically important functions including electron transfer, O_2-transport, oxygenation, oxidation, and iron homeostasis.[11]

---

[8] a) Kitajima, N. Fujisawa, K.; Morooka, Y.; Toriumi, K. "μ-η^2:η^2-Peroxo binuclear copper complex, [Cu(HB(3,5-($Me_2CH)_2$pz)$_3$)]$_2$(O_2)." *J. Am. Chem. Soc*. **1989**. *111*, 8975-8976. b) Kitajima, N.; Koda, T.; Hashimoto, S.; Kitagawa, T.; Morooka, Y. "An accurate synthetic model of oxyhemocyanin." *J. Chem. Soc. Chem. Commun*. **1988**, *2*, 151-152. c) Kitajima, N.; Koda, T.; Hashimoto, S.; Kitagawa, T.; Morooka, Y. "Synthesis and characterization of the dinuclear copper(II) complexes [Cu(HB(3,5-Me_2pz)$_3$)]$_2$X (X = O^{2-}, $(OH)_2^{2-}$, CO_3^{2-}, O_2^{2-})." *J. Am. Chem. Soc*. **1991**, *113*, 5664-5671. d) Kitajima, N.; Fujisawa, K.; Fujimoto, C.; Morooka, Y.; Hashimoto, S.; Kitagawa, T.; Toriumi, K.; Tatsumi, K.; Nakamura, A. "A new model for dioxygen binding in hemocyanin. Synthesis, characterization, and molecular structure of the μ-η^2:η^2 peroxo dinuclear copper(II) complexes, [Cu(HB(3,5-R_2pz)$_3$)]$_2$(O_2) (R = isopropyl and Ph)." *J. Am. Chem. Soc*. **1992**, *114*, 1277-1291.

[9] Magnus, K. A.; Ton-That, H.; Carpenter, J. E. "Recent Structural Work on the Oxygen Transport Protein Hemocyanin." *Chem. Rev*. **1994**, *94*, 727-735.

[10] Cuff, M. E.; Miller, K.I.; Van Holde, K. E.; Hendrickson, W. A. "Crystal structure of a functional unit from Octopus hemocyanin." *J. Mol. Biol*. **1998**, *278*, 855-870.

[11] a) Lippard, S. J.; Berg, J. M. "*Principles of Bioinorganic Chemistry"* b) Blackman, A. G.; Tolman, W. B. "Copper-Dioxygen and Copper-Oxo Species Relevant to Copper Oxygenases and Oxidases" Structure & Bonding, Vol. 97; Springer-Verlag: Berlin, 2000; Vol. 97, pp 179-211. c) Solomon, E. I.; Chen, P.; Metz, M.; Lee, S. K.; Palmer, A. E. "Oxygen Binding, Activation, and Reduction to Water by Copper Proteins."

The active sites of these enzymes are similarly variable, with structures that include 1-3 copper ions, or a combination of other transition metal ions like Fe or Zn. A subset of copper-containing proteins that bind and/or activate dioxygen are listed in Table 1-1, arranged according to the number of copper ions that are postulated to be involved in the dioxygen activation process.[5a]

Table 1-1. Copper-containing Proteins that Bind and/or Activate Dioxygen.

No. Cu ions involved in O_2 activation	Protein (abbreviation)	Reaction performed
1	amine oxidase (AO)	Oxidases $XH_2 + O_2 \rightarrow X + H_2O_2$
	galactose oxidase (GAO)	
	glyoxal oxidase (GLO)	
	quercetin 2,3-dioxygenase (QDO)	Dioxygenases $X + O_2 \rightarrow XO_2$
2 (uncoupled)[a]	dopamine β-monooxygenase (DβM)	Monooxygenases $X + O_2 + 2e^- + 2H^+ \rightarrow XO + H_2O$
	peptidylglycine α-amidating monooxygenase (PHM)	
2	Tyrosinase (Tyr)	
	hemocyanin (Hc)	Dioxygen transport $2Cu^{1+} + O_2 \leftrightarrow Cu^{2+}{}_2(O_2{}^{2-})$
	catechol oxidase	Oxidases $O_2 + 4e^- + 4H^+ \rightarrow 2H_2O$
3	multicopper oxidases	
	laccase (Lc)	
	ascorbase oxidase (AO)	
	ceruloplasmin (Cp)	
	Fet3	
1 (+ other metal)	cytochrome *c* oxidase (with Fe)	

[a] These proteins contain two copper ions separated by ~ 11Å, but it is unclear if one or both activate dioxygen. X stands for substrate.

Angew. Chem. Int. Ed. **2001**, *40*, 4570-4590. d) Lewis, E. A.; Tolman, W. B. "Reactivity of Dioxygen-Copper Systems" *Chem. Rev.* **2004**, *104*, 1047-1076.

It is worth noting that similar active site structures can be associated with different functions. For example, both Hc and Tyr contain two copper centers in their active sites with each copper ion coordinated by three histidine imidazole residues. Moreover, the catalytic core polypeptide domains in the two proteins are superimposible. As described above, in Hc reversible binding of O_2 occurs to form a peroxide level intermediate, which is ligated in a μ–η^2:η^2 configuration (Scheme 1-4, top).[9,12] Yet, while an identical (μ–η^2:η^2–peroxo)dicopper(II) unit has also been identified in Tyr, this unit promotes hydroxylation of the aromatic ring of the phenol substrate according to the proposed mechanism shown in Scheme 1-4.

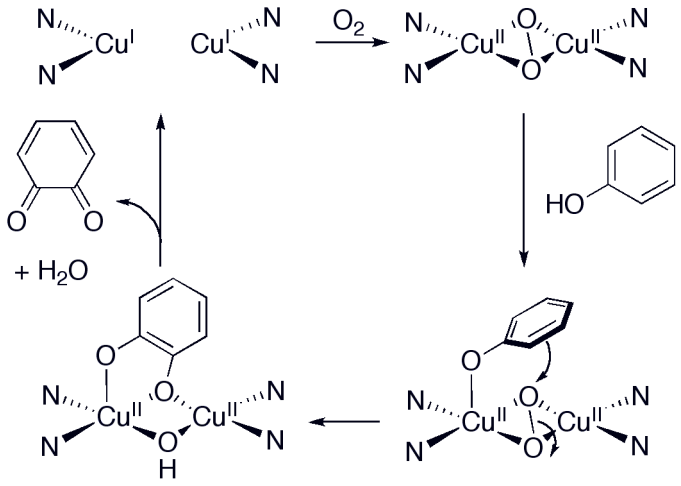

Scheme 1-4. Proposed catalytic cycle for Tyr. The symbol "N" refers to a histidine imidazole group. Axial ligands are omitted for clarity.

These differences in reactivity have been ascribed to differences in the accessibility of substrates to the oxygenated active site (inaccessible in Hc, enabled in Tyr). This point

[12] Solomon, E. I.; Sundaram, U. M.; Machonkin, T. E. "Multicopper Oxidases and Oxygenases." *Chem. Rev*. **1996**, *96*, 2563-2605.

highlights the importance of the ternary structure and 'second-sphere' environment of metalloenzymes that are major contributors to modulation of active site properties such as electronic structure, redox potential, reaction stereochemistry, and reaction mechanism. In this sense, metalloenzymes can be considered as elaborately designed inorganic metal complexes.[12]

It is also worth noting mechanistic similarities among the copper proteins listed in Table 1-1, notwithstanding their diverse active site structures. For example, in all cases it appears that the reaction with O_2 proceeds with the reduced Cu^I form to yield an adduct. This adduct or an intermediate derived therefrom then either functionalizes substrates or undergoes reduction to water (or H_2O_2). Nonetheless, many mechanistic questions have yet to be resolved, such as how and what type of an adduct or intermediate species are formed, what electronic and geometric properties are associated with them, and what species is(are) responsible for functionalizing substrate.

A key goal of my thesis work has been to address these and related questions, with a specific focus on dioxygen activation at single copper sites exemplified by those thought to be involved in O_2 biniding in dopamine β-monooxygenase (DβM) and peptidylglycine α-hydroxylating monooxygenase (PHM).[13] Both enzymes are found exclusively in higher eukaryotes and are responsible for the biosynthesis of neurotransmitters and hormones. While DβM catalyzes the benzylic hydroxylation of dopamine to norepinephrine

[13] a) Stewart, L.C.; Klinman, J.P. "Dopamine Beta-Hydroxylase of Adrenal Chromaffin Granules: Structure and Function" *Ann. Rev. Biochem*. **1998**, *57*, 551-590. b) Eipper, B. A.; Stoffers, P. A.; Mains, R. E. "The Biosynthesis of Neuropeptides: Peptide alpha-Amidation" *Annu. Rev. Neurosci.* **1992**, *15*, 57–85. c) Klinman, J.P. "The copper-enzyme family of dopamine β-monooxygenase and peptidylglycine α-hydroxylating monooxygenase: resolving the chemical pathway for substrate hydroxylation. *J. Biol. Chem*. **2006**, 281, 3013-3016.

(DβM),[13a] the transformation of C-terminal glycine-extended peptides to their α-hydroxylated products is catalyzed by PHM (Scheme 1-5).[13b] Despite their different functions, DβM and PHM exhibit key similarities. Each enzyme catalyzes the stereospecific insertion of an O-atom from dioxygen into a C-H bond. Moreover, both enzymes exhibit high sequence homologies and remarkable structural analogies at their catalytic active sites that suggest mechanistic similarities as well.[14] In view of the significance of these issues to my research and in order to provide the foundation for the experimental approach I have taken, a detailed discussion of the structural and mechanistic aspects of these enzymes is warranted.

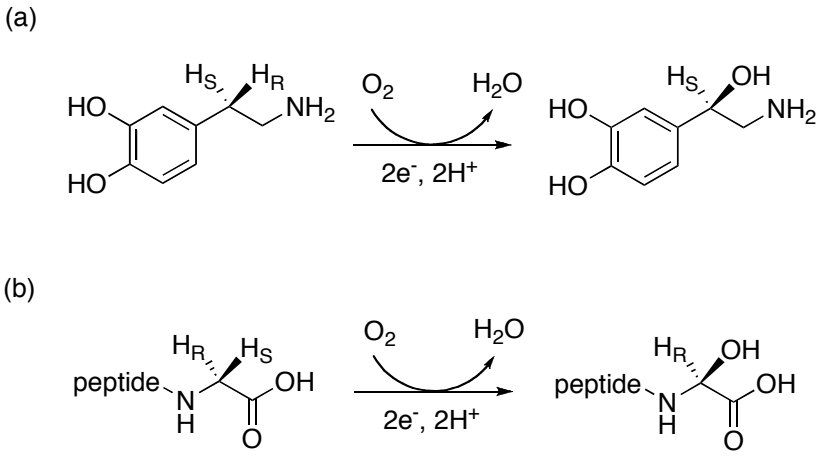

Scheme 1-5. Reactions catalyzed by (a) dopamine β-monooxygenase (DβM) and (b) peptidylglycine α-hydroxylating monooxygenase (PHM).

[14] a) Lamoroux, A.; Vigny, A.; Faucon Biguet, V.; Darmon, M. C.; Frank, R.; Henry, J. P.; Mallet, J. "The primary structure of human dopamine-β-hydroxylase: insights into the relationship between the soluble and the membrane-bound forms of the enzyme" *EMBO J.* **1987**, *6*, 3931–3937. b) Southan, C.; Kruse, L. I. "Sequence similarity between dopamine β-hydroxylase and peptide α-amidating enzyme: Evidence for a conserved catalytic domain" *FEBS Lett.* **1989**, *255*, 116-120. c) Eipper, B. A.; Quon, A. S. W.; Mains, R. E.; Boswell, J. S.; Blackburn, N. J. "The Catalytic Core of Peptidylglycine α-Hydroxylating Monooxygenase: Investigation by Site-Directed Mutagenesis, Cu X-ray Absorption Spectroscopy, and Electron Paramagnetic Resonance" *Biochemistry.* **1995**, *34*, 2857–2865.

1.3. Structure and Mechanistic Insights for Dopamine β-Monooxygenase and Peptidylglycine α-Hydroxylating Monooxygenase.

1.3.1. Structure of Active Sites in DβM and PHM

Both DβM and PHM are copper-containing monoxygenases, with one oxygen from dioxygen incorporated into the hydroxylated product and the other liberated in the form of water. Thus, the reduction of O_2 to water is a four-electron/two-proton process, with two electrons originating from substrate and two electrons from an exogenous electron donor such as ascorbic acid (naturally occurring biological reducing reagent). This seemingly simple reaction, however, consists of a series of complicated chemical steps; the reduction of O_2 to water requires an O-O bond breaking through sequential proton/electron transfer before or after insertion of an O-atom into a C–H bond. The first event of this reaction is a binding of O_2 to one or two of the copper centers. Subsequent electron transfer to the bound O_2 generates a Cu/O_2 intermediate(s) that participates in the substrate modification. These reactions are strongly influenced by the coordination environment of the copper centers, such as types and spatial arrangement of their ligands.

Initial information pertaining to the copper coordination environment in these enzymes was obtained through extensive biochemical, kinetic and spectroscopic studies, most notably Extended X-ray Absorption Fine Structure (EXAFS) work.[15,16] Both

[15] a) Klinman, J. P.; Krueger, M.; Brenner, M.; Edmondson, D. E. "Evidence for two copper atoms/subunit in dopamine β-monooxygenase catalysis." *J. Biol. Chem*. **1984**, *259*, 3399-3402. b) Blackburn, N. J.; Concannon, M.; Shahiyan, S. K.; Mabbs, F. E.; Collison, D. "Active Site of Dopamine β-Hydroxylase.

enzymes contain two distinct copper sites that play different roles.[15a,b] In the oxidized form of the enzymes (Cu^{II}/Cu^{II}), EXAFS experiments showed that the metal ions are coordinated by 2–3 histidine ligands and 1–2 O/N ligands, which are likely water-derived oxygen ligands. Reduction to the Cu^{I}/Cu^{1} oxidation state is accompanied by loss of a solvent ligand and the gain of a sulfur donor from a methionine. This results in significant structural changes in coordination numbers and geometry for both copper centers. One site (called Cu_A for DβM and Cu_H for PHM, respectively) changes from a 4- or 5-tetragonal geometry to a 2- or 3-coordinate configuration, with one of three copper-imidazolyl bonds being elongated. The second site (called Cu_B for DβM and Cu_M for PHM) changes from a 4- or 5-coordinate tetragonal geometry to a trigonal or tetrahedral coordination with a short Cu-S bond at 2.27 Å for PHM[16a] and 2.25 Å for DβM.[15e] Hence, it was suggested that the Cu_A (or Cu_H) site consists of three histidine N-donors and the other Cu_B (or Cu_M) site has two histidine N-donors and one methionine S-donor, with additional water-derived O-donors present in the oxidized enzymes. The results from CO-binding studies[15c] showed that CO (a competitive inhibitor for O_2)

Comparison of Enzyme Derivatives Containing Four and Eight Copper Atoms per Tetramer Using Potentiometry and EPR Spectroscopy" *Biochemistry*. **1988**, *27*, 6001-6008. c) Blackburn, N. J.; Pettingill, T. M.; Seagraves, K. S.; Shigeta, R. T. "Characterization of a carbon monoxide complex of reduced dopamine beta-hydroxylase. Evidence for inequivalence of the Cu(I) centers" *J. Biol. Chem*. **1990**, *265*, 15383-15386. d) Stewart, L. C.; Klinman, J. P. "Characterization of Alternate Reductant Binding and Electron Transfer in the Dopamine β-Monooxygenase Reaction" *Biochemistry*. **1987**, *26*, 5302-5309. e) Reedy, B. J.; Blackburn, N. J. "Preparation and Characterization of Half-Apo Dopamine β–hydroxylase by Selective Removal of Cu_A. Identification of a Sulfur Ligand at the Dioxygen Binding Site by EXAFS and FTIR Spectroscop" *J.Am.Chem.Soc*. **1994**, *116*, 1924-1931.

[16] a) Eipper, B. A.; Quon, A. S. W.; Mains, R. E.; Boswell, J. S.; Blackburn, N. J. "The Catalytic Core of Peptidylglycine α-Hydroxylating Monooxygenase: Investigation by Site-Directed Mutagenesis, Cu X-ray Absorption Spectroscopy, and Electron Paramagnetic Resonance." *Biochemistry*. **1995**, *34*, 2857-65. b) Boswell, J. S.; Reedy, B. J.; Kulathila, R.; Merkler, D.; Blackburn, N. J. "Structural investigations on the coordination environment of the active-site copper centers of recombinant bifunctional peptidylglycine α-amidating enzyme." *Biochemistry*. **1996**, *35*, 12241-50. c) Blackburn, N. J.; Rhames, F. C.; Ralle, M.; Jaron, S. "Major changes in copper coordination accompany reduction of peptidylglycine monooxygenase: implications for electron transfer and the catalytic mechanism." *J. Biol. Inorg. Chem*. **2000**, *5*, 341-353.

preferentially binds to Cu_B (or Cu_M), leading to speculation that this site is the likely one at which O_2 binding and substrate hydroxylation occur. In separate studies, it was concluded that ascorbic acid binding occur near the Cu_A (or Cu_H) site, and that it functions as an electron transfer conduit for funneling electrons to Cu_B (or Cu_M).[15d]

While there is no crystallographic data available to date for DβM, a series of X-ray structures of different forms of PHM have been reported.[17] The first such structure was obtained for the oxidized form of rat PHM (ox-PHM_{CC}).

Figure 1-1. Crystal structure of PHM_{CC} that shows the inderdomains containing the two active site copper centers.[17a] (pdb 1PHM)

[17] a) Prigge, S. T.; Kolhekar, A. S.; Eipper, B. A.; Mains, R. E.; Amzel, L. M. "Amidation of bioactive peptides: the structure of peptidylglycine alpha- hydroxylating monooxygenase." *Science*. **1997**, *278*, 1300-1305. b) Prigge, S.T.; Kolhekar, A.S.; Eipper, B.A.; Mains, R.E.; Amzel, L.M. "Substrate-mediated electron transfer in peptidylglycine α-hydroxylating monooxygenase." *Nat Struct Biol*. **1999**, *6*, 976-983. c) Prigge, Sean. T.; Eipper, Betty. A.; Mains, Richard. E.; Amzel, L. Mario. "Dioxygen binds end-on to mononuclear copper in a precatalytic enzyme complex." *Science*. **2004**, *304*, 864-867.

As illustrated in Figures 1-1 and 1-2, the structure revealed the relative disposition of the two copper centers per subunit and their respective ligands, which are in good agreement with those proposed by spectroscopic studies. The two copper centers are located at the interdomain space, where the domain 1 binds one copper (Cu_H) and the domain 2 binds the other copper (Cu_M). The two coppers are separated by ~ 11 Å over either side of a solvent-filled interdomain cleft.

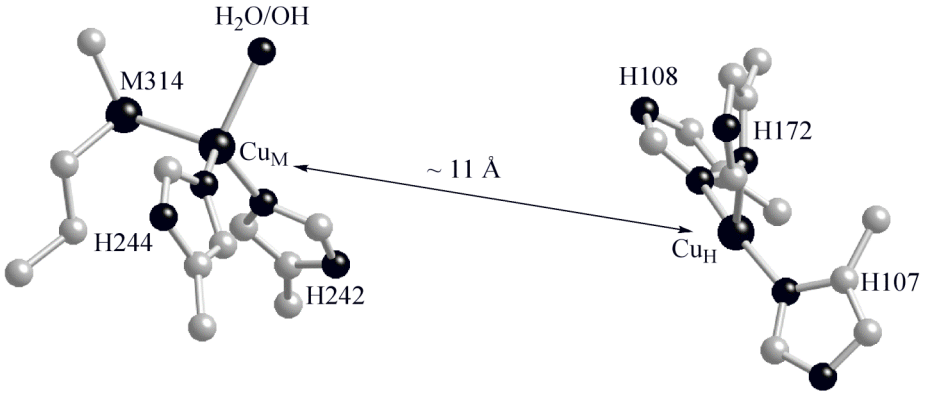

Figure 1-2. Coordination geometries at the two copper centers in PHM_{CC}.[17a]

The coordination geometry of the Cu_H site can be regarded as square pyramidal with three histidine ligands (T-shape) and two vacant coordination positions (presumably filled by water molecules that were not located). The Cu_M site has two histidine ligands, one methionine sulfur and one solvent-derived molecule (putative binding site for O_2) in an approximately tetrahedral geometry.

Subsequently, the structures of the reduced- (red-PHM_{CC}) and peptide substrate N-α-acetyl-3,5-diiodotyrosylglycine (Ac-Dil-YG) bound forms (ox-PHM_{CC}-sub) of PHM_{CC} were solved.[17b] Comparisons of these structures with that of ox-PHM_{CC} are

revealing. First, the overall features for all three structures are very similar, including the very small root mean square deviation (α-carbons) and similar Cu-Cu distances. These observations suggest that the significant interdomain motion does not take place upon reduction and substrate binding. Moreover, the coordination geometries of both copper sites in red-PHM_{CC} are very similar to those seen in ox-PHM_{CC}; the Cu_H site remains planar T-shaped and the Cu_M site remains tetrahedral. These findings are in sharp contrast with the previously reported EXAFS data for PHM[16c] that indicated significant structural changes upon reduction. The basis for these differences between the spectroscopic and crystallographic results has yet to be resolved.

In ox-PHM_{CC}-sub, the substrate is bound in the cleft between the two domains through multiple bonding interactions with several conserved active site residues (Asn 316, Tyr 318 and Arg 240) as shown in Figure 1-3. For example, the carboxylate of the substrate is anchored by a bidentate salt bridge to the guanidinium of Arg 240 and a hydrogen bond to Tyr 318. In addition, the backbond amide is hydrogen bonded to Asn 316. The diiodotyrosine side chain is positioned at the loose hydrophobic pocket that is spacious enough to accommodate virtually any amino acid side chain. These structural features led the authors to suggest a possible electron-transfer pathway from Cu_H to Cu_M. In ox-PHM_{CC}-sub, a water molecule occupies a position between the side chain of Gln 170 and the carboxylate oxygen of the bound substrate (~ 3 Å from Gln 170 and 3 Å from the substrate carboxylate). These interactions are absent in red-PHM_{CC} and ox-PHM_{CC}. Instead, the direct hydrogen bond between Gln 170 and His 108 is present in red-PHM_{CC}, whereas a water molecule bridges Gln 170 and His 108 in ox-PHM_{CC}. The

authors surmised that in the substrate-bound reduced state both the hydrogen bonding between Gln 170 and His 108 and the water-mediated hydrogen bonding between Gln 170 and substrate carboxylate are present. This atomic positioning could provide the shortest connection between the two coppers ions in an electron transfer pathway, but only when the substrate binds at the reduced enzyme, thus "gating" electron transfer.

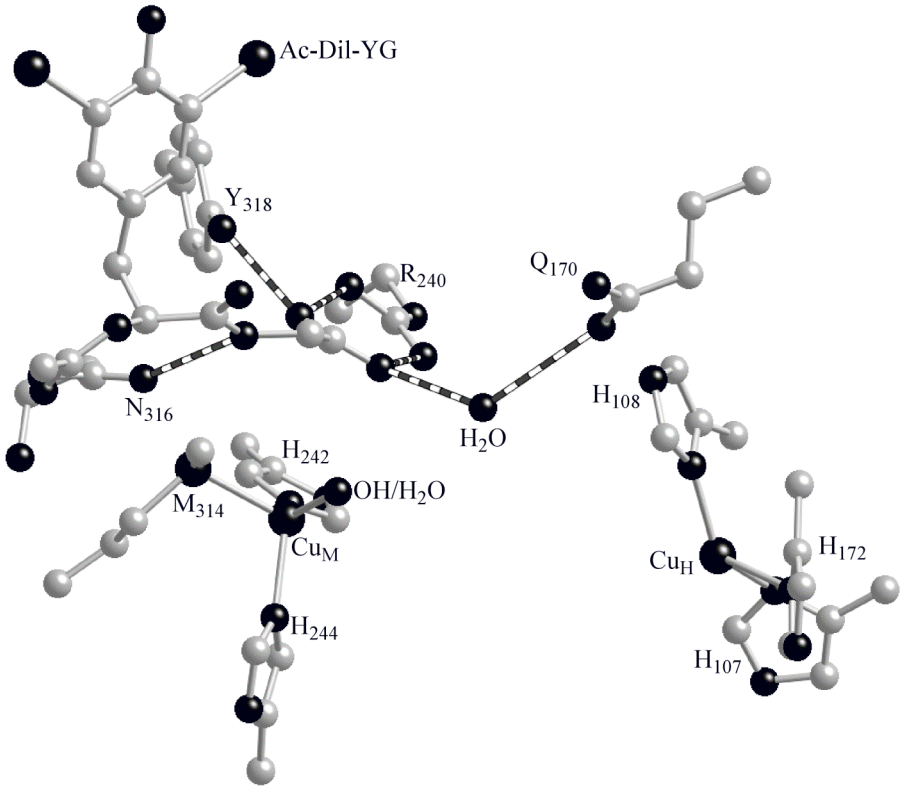

Figure 1-3. Representation of the active sites in ox-PHM$_{CC}$-sub. Bonding interactions between peptide substrate (Ac-Dil-YG), side chains from protein and water are indicated by multi-band cylinder bonds.[17b] (pdb 1OPM)

Additional insights were provided by the structure of the precatalytic enzyme complex containing dioxygen and the substrate analog N-acetyl-diiodotyrosyl-D-threonine (ITY),[17c] as depicted in Figure 1-4.

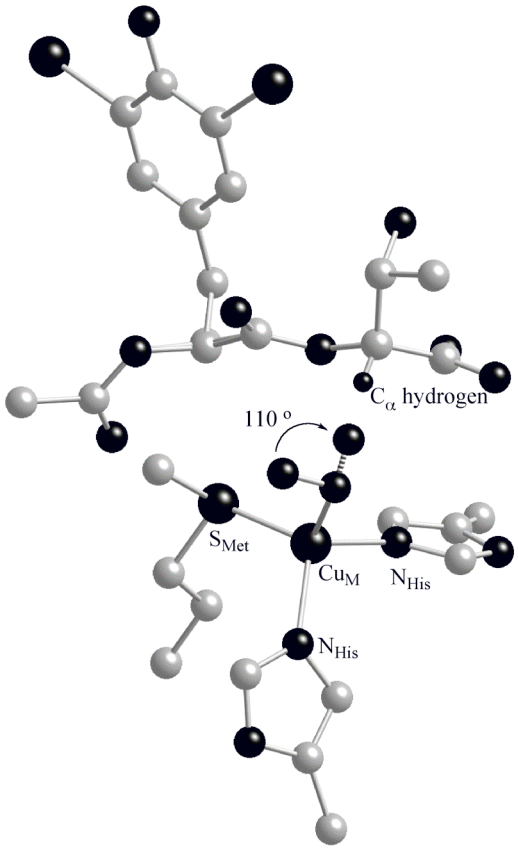

Figure 1-4. Representation of the Cu_M site in pre-catalytic complex of PHM with bound substrate and dioxygen. The arrow shows the rotation of the distal oxygen atom through Cu-O bond that would bring the distal oxygen within ~ 2.2 Å of the pro-*S* hydrogen. Both rotated oxygen and C_α hydrogen are made for an illustrative purpose. (pdb 1SDW)

The overall coordination geometries of the copper ions are similar to those shown in the other crystal structures. However, the fourth coordination position at the Cu_M site, which is occupied by a water in ox-PHM_{CC}-sub, is ligated by a diatomic species

identified as two O atoms bound in an end-on fashion, with Cu-O distances of 2.11 Å to the proximal oxygen and 2.78 Å to the distal oxygen. The O-O distance of 1.23 Å is similar to that of free dioxygen (1.22 Å).[18] The distal oxygen is 3.16 Å from the estimated position of the *pro-S* hydrogen of the substrate analog. Simple rotation of the distal oxygen by ~ 110° through the Cu-O bond, however, brings this oxygen ~ 2.2 Å from the hydrogen atom, an ideal position for attack during catalytic turnover. In addition, the previously proposed electron transfer pathway through hydrogen bonds including the bound substrate, His 108, Gln 170 and a water is also observed in this structure with a subtle movement of the water toward a position between His 108 and the carboxylate of the bound substrate. Thus, the authors suggest that rotational motion of the copper-bound oxygen could provide a gating effect on facilitating the electron transfer and the C-H bond functionalization steps.

The results from the PHM and DβM structural studies have shed light on some aspects of the mechanism of action in these enzymes, but many unanswered questions remain pertaining to the electron transfer pathway between the two copper centers, the unsual nature of the Cu_H site relative to usual copper sites that perform this function in biology,[5a,12] how O_2 is reduced, and how substrate is hydroxylated. Additional experiments, analyses, and derived hypotheses focused on these issues are described in the following section.

[18] Gubelmann, M. H.; Williams, A. F. "The structures and reactivity of dioxygen complexes of the transition metals." *Struct. Bonding (Berlin)*. **1983**, *55*, 1-65.

1.3.2. Mechanism of Substrate Oxidation by DβM and PHM

As described in the previous section, DβM and PHM contain two copper ions that are separated over ~ 11Å by a solvent-filled cleft between two protein domains. In view of this relatively long distance, it is unlikely that both copper ions act together to bind and activate O_2. Instead, it is widely believed that each of copper centers performs a separate function; Cu_A (or Cu_H) participates in electron transfer from ascorbate to Cu_B (or Cu_M), where binding and activation of O_2 and substrate take place. Both copper centers undergo oxidation from the +1 to +2 oxidation level to provide two electrons to O_2 in the oxidative half-reaction (top cycle in Scheme 1-6). The remaining two electrons required for O_2-reduction to water are provided by the substrate, which undergoes the hydroxylation. The subsequent reduction of two Cu^{II} ions to Cu^{I} by ascorbate and release of the product (or vice versa) completes the catalytic cycle (bottom cycle in Scheme 1-6).

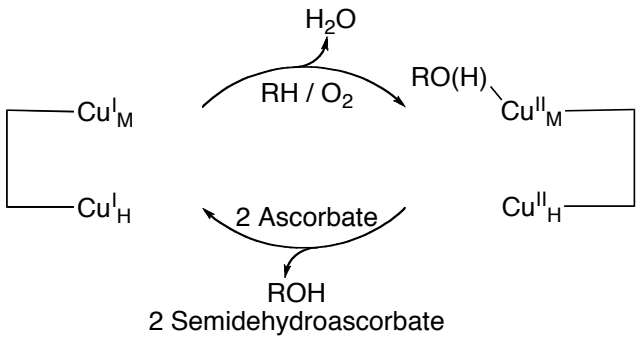

Scheme 1-6. Simplified reaction scheme catalyzed by PHM.

According to this model of the overall reaction cycle, long-range (> 11Å) electron transfer (ET) step between the two copper sites during catalysis is required. A number of mechanisms have been proposed for this ET step. For instance, one intriguing mechanism was proposed on the basis of CO-binding studies on PHM either in the absence or presence of various peptide substrates as a probe of the interaction of the Cu(I) sites with O_2.[19] According to this mechanism, free superoxide generated at Cu_H was postulated to cross the solvent channel to Cu_M, essentially delivering an electron in the process. A conserved residue, Tyr 79, situated at 4 Å from Cu_H, was postulated to assist in the channeling of the superoxide between the two copper centers. However, this mechanism cannot fully explain the possible leakage of the superoxide that would be expected to occur to some degree. This would result in uncoupling between O_2 consumption and substrate hydroxylation, yet this is not observed for either enzyme (see below).

Another mechanism involves a substrate-mediated electron-transfer pathway in which Gln 170 plays a critical role, as described in the previous section.[17] Arguing against this mechanism, recent site-specific mutagenesis studies on PHM_{CC} showed that mutation of this key residue (Gln170) to an Ala results in little change in enzyme reactivity.[20] Similarly, a recent kinetic study on PHM with substrates that are significantly different with regard to their structural features such as steric bulk, hydrophobicity and length, indicated close similarities between the primary kinetic

---

[19] Jaron, S.; Blackburn, N. J. "Does superoxide channel between the copper centers in peptidylglycine monooxygenase? A new mechanism based on carbon monoxide reactivity." *Biochemistry*. **1999**, *38*, 15086-15096.

[20] Bell, J.; El Meskini, R.; D'Amato, D.; Mains, R. E.; Eipper, B. A. "Mechanistic Investigation of Peptidylglycine α-Hydroxylating Monooxygenase via Intrinsic Tryptophan Fluorescence and Mutagenesis." *Biochemistry*. **2003**, *42*, 7133-7142.

parameters and their isotope effects.[21] These results effectively rule out a mechanism in which the extended backbone of the peptide substrate provides a pathway for the ET step. Thus, the mechanism of the long-range electron transfer still remains an open question.

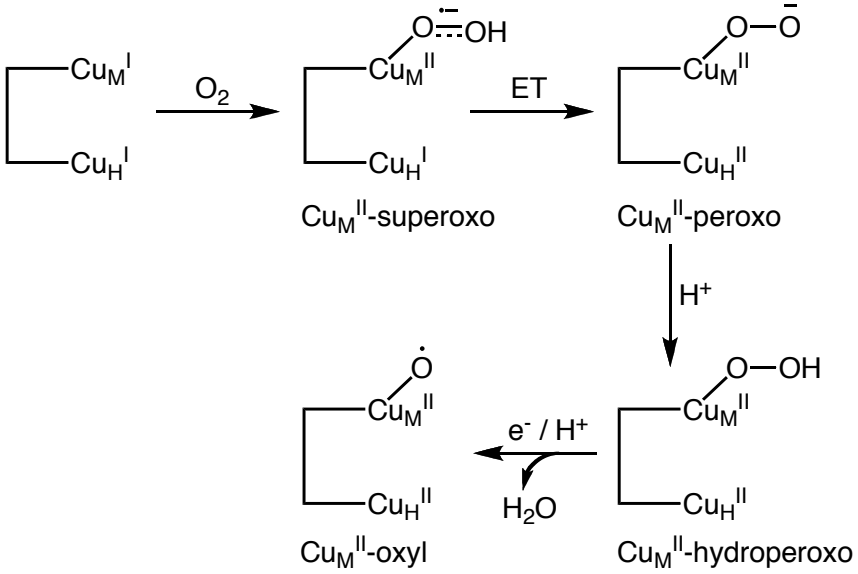

Scheme 1-7. Various active Cu/O_2 species possibly formed during catalysis in DβM and PHM.

Another critical issue concerns whether the ET step occurs before or after the key C-H bond cleavage step. This issue is unavoidably related to that concerning the nature of the active species responsible for the substrate hydroxylation. That is, depending on the timing of the ET step, many possible active species may be envisioned, including one-electron reduced Cu^{II}-superoxo, two-electron reduced Cu^{II}-peroxo or -hydroperoxo, and Cu^{II}-oxyl radical species, as depicted in Scheme 1-7. Identification of such species is one

[21] Francisco, W. A.; Wille, G.; Smith, A. J.; Merkler, D. J.; Klinman, J. P. "Investigation of the Pathway for Inter-Copper Electron Transfer in Peptidylglycine α-Amidating Monooxygenase." *J. Am. Chem. Soc.* **2004**, *126*, 13168-13169.

of the greatest challenges for understanding these enzymes. If the ET step occurs before the substrate activation, one of the latter three species is the candidate. If the ET occurs later, the only reasonable species capable of hydroxylating the substrate is the Cu^{II}-superoxo unit. These remain open questions because none of these various species have been observed by spectroscopic means so far, the only intermediate having been identified being the precatalytic O_2 complex with unknown oxidation level or kinetic viability.

Our current understanding of the enzymes has been informed by extensive kinetic studies that have been used to evaluate selected mechanistic proposals. Common among many of these proposals is the notion that the substrate hydroxylation involves hydrogen atom abstraction by a Cu/O_2 species to yield a free radical intermediate.[22] A Cu_M^{II}-superoxo intermediate is one possible species that could initiate the C-H bond cleavage prior to the ET step from the other Cu site (Cu_H). Working with this idea in mind, two closely related mechanisms have been put forth (Scheme 1-8).

For both, in the presence of substrate, the reduced enzyme reversibly interacts with O_2 in an energetically uphill process to yield a very low equilibrium concentration of a Cu_M^{II}-superoxo species in which the bound O_2 fragment exists in either an end-on or a side-on binding mode. This initially formed Cu_M^{II}-superoxo species is expected to be

[22] a) Fitzpatrick, Paul F.; Flory, Donald R., Jr.; Villafranca, Joseph J. "3-Phenylpropenes as mechanism-based inhibitors of dopamine β-hydroxylase: evidence for a radical mechanism." *Biochemistry*. **1985**, *24*, 2108-2114. b) Fitzpatrick, Paul F.; Villafranca, Joseph J. "Mechanism-based inhibitors of dopamine β-hydroxylase containing acetylenic or cyclopropyl groups." *J. Am. Chem. Soc*. **1985**, *107*, 5022-5023. c) Fitzpatrick, P. F.; Villafranca, J. J. "Mechanism-based inhibitors of dopamine β-hydroxylase. *Arch. Biochem. Biophys*. **1987**, *257*, 231-250. d) Zabriskie, T. M.; Cheng, H.; Vederas, J. C. "Mechanism-based inactivation of peptidylglycine α-hydroxylating monooxygenase (PHM) by a substrate analog, D-phenylalanyl-L-phenylalanyl-D-vinylglycine: inhibition of formation of peptide C-terminal amides." *J. Am. Chem. Soc*. **1992**, *114*, 2270-2272. e) Kulathila, R.; Merkler, K. A.; Merkler, D, J.; Kulathila, R. "Enzymic formation of C-terminal amides." *Nat. Pro. Rep*. **1999**, *16*, 145-154.

diamagnetic due to antiferromagnetic coupling between the two radical centers, which is in line with the failure to observe any Cu^{II} EPR signal during a single turnover experiment.[22] It is then proposed that the Cu_M^{II}-superoxo abstracts an H-atom from the substrate to generate a substrate radical and a Cu_M^{II}-OOH species.

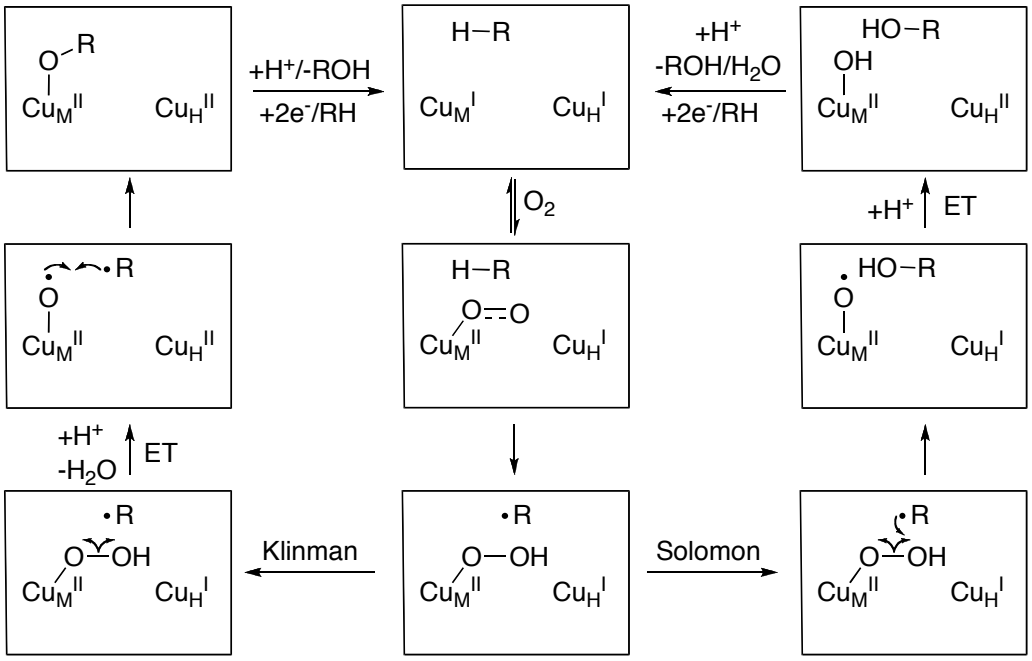

Scheme 1-8. Proposed mechanisms for PHM and DβM. The left cycle by Klinman et al.[23] and the right cycle by Solomon et al[24]. ET stands for the electron transfer.

At this point, the two mechanisms differ with respect to the subsequent product formation and electron transfer steps. In the mechanism proposed by Klinman (the left

[23] Evans, John. P.; Ahn, Kyunghye.; Klinman, Judith. P. "Evidence that dioxygen and substrate activation are tightly coupled in dopamine β-monooxygenase. Implications for the reactive oxygen species." *J. Biol. Chem*. **2003**, *278*, 49691-49698.

[24] Chen. P.; Solomon. E. I. "Oxygen activation by the noncoupled binuclear copper site in peptidylglycine α-hydroxylating monooxygenase. Reaction mechanism and role of the noncoupled nature of the active site." *J. Am. Chem. Soc*. **2004**, *126*, 4991-5000.

cycle in Scheme 1-8), electron transfer from the Cu_H site to the Cu_M-OOH species occurs to produce a water and a novel Cu_M^{II}-oxyl species. The resultant highly reactive Cu_M^{II}-oxyl species then rapidly combines with the substrate radical to form an alkoxide complex. Release of the product through protonation and reduction of Cu^{II} to Cu^{I} completes the catalytic cycle. On the other hand, Solomon et al. proposed that the substrate hydroxylation involves a "water-assisted" direct OH transfer from the Cu_M^{II}-OOH species to the substrate radical to yield an outer-sphere alcohol product and a Cu^{II}-oxyl species. The high energy of the latter species would provide the driving force for subsequent electron transfer. Although these mechanisms differ with respect to the order of the ET step and the alcohol product formation steps, they have in common the initiation of the H-atom abstraction by the Cu_M^{II}-superoxo species.

Several pieces of evidence support these mechanistic hypotheses. For example, sizable O-18 isotope effects on *V/K* that are increased by substrate deuteration were observed (see Table 1-2).[25,26] Experimentally, these values were obtained in the limit of low O_2 and saturating substrate. Thus, O-18 isotope effects on *V/K* reflect all steps from the binding of O_2 through the first irreversible step. Under this specific condition, the C-H bond cleavage is irreversible and rate-determining. As a result, the sensitivity of the oxygen isotope effect to the substrate deuteration means that any activation of O_2 proceeding to the C-H bond cleavage must be fully reversible.

---

[25] Tian, G.; Berry, J. A.; Klinman, J. P. "Oxygen-18 kinetic isotope effects in the dopamine β-monooxygenase reaction: Evidence for a new chemical mechanism in non-heme, metallomonooxygenase." *Biochemistry*. **1994**. *33*. 226-234.

[26] Francisco, W. A.; Blackburn, N. J.; Klinman, J. P. "Oxygen and Hydrogen Isotope Effects in an Active Site Tyrosine to Phenylalanine Mutant of Peptidylglycine α-Hydroxylating Monooxygenase: Mechanistic Implications." *Biochemistry*. **2003**, *42*, 1813-1819.

Table 1-2. O-18 Isotope Effects on *V/K* for PHM and DβM with Dopamine and Hippuric Acid as Substrates.

Substrate	DβM[a]	PHM[b]
protiated	1.0197 ± 0.0003	1.0173 ± 0.0009
deuterated	1.0256 ± 0.0003	1.0212 ± 0.0018

[a] Taken from ref 25. [b] Taken from ref 26.

Another critical experimental result concerns the intrinsic isotope values, along with the individual rate constants for each isolated chemical step. By using substrate or substrate analogs with similar reactivities, the results of the measured deuterium and tritium isotope effect values for DβM and PHM enabled determination of the intrinsic primary and secondary isotope effects for the isolated C-H bond cleavage (see Table 1-3).[27,28,29] The remarkable similarities between the intrinsic isotope effects for both enzymes imply identical transition-state structures for the C-H activation processes. The intrinsic primary isotope effect of ~ 12 in both enzymes exceeds the semiclassical maximum value of 7. This finding is indicative of quantum-mechanical tunneling in the

[27] Miller, S. M.; Klinman, J. P. "Magnitude of intrinsic isotope effects in the dopamine β-monooxygenase reaction." *Biochemistry*. **1983**, *22*, 3091-3096.
[28] Miller, S. M.; Klinman, J. P. "Secondary isotope effects and structure-reactivity correlations in the dopamine β-monooxygenase reaction: evidence for a chemical mechanism." *Biochemistry*. **1985**, *24*, 2114-2127.
[29] Francisco, W. A.; Merkler, D. J.; Blackburn, N. J.; Klinman, J. P. "Kinetic Mechanism and Intrinsic Isotope Effects for the Peptidylglycine α-Amidating Enzyme Reaction." *Biochemistry*. **1998**, *37*, 8244-8252.

C-H bond activation reaction. This hypothesis is further supported by the temperature independence of the intrinsic isotope effect in wild-type PHM.[30]

Table 1-3. Comparison of Intrinsic Parameters for DβM and PHM with Dopamine and Hippuric Acid as Substrates.

parameter	DβM	PHM[d]
1° k_H/k_D	10.9 ± 1.9[a]	1.0173 ± 0.0009
2° k_H/k_D	1.19 ± 0.06[b]	1.0212 ± 0.0018
$k_{C\text{-}H}$ (s^{-1})	1200 ± 540[c]	810 ± 120

[a] Taken from ref 27. [b] Taken from ref 28. [c] Taken from ref 30. [d] Taken from ref 29. For dopamine, bond dissociation energy = 85 kcal/mol.[31] For hippuric acid, bond dissociation energy = 87 kcal/mol.[32]

When the magnitude of the intrinsic isotope effect is known, kinetic isotope effect measurements can provide individual microscopic rate constants.[33] Accordingly, rate constants of 810 ± 120 s^{-1} and 1200 ± 540 s^{-1} have been calculated for the C–H bond cleavage step in PHM and DβM, respectively. If the ET step comes into play before the C-H activation, it should occur at a rate faster than ~ 10^3 s^{-1} for the C-H cleavage because this step is rate-determining. Given that the two copper sites in these enzymes are

[30] Francisco, W. A.; Knapp, M. J.; Blackburn, N. J.; Klinman, J. P. "Hydrogen Tunneling in Peptidylglycine α-Hydroxylating Monooxygenase." *J. Am. Chem. Soc*. **2002**, *124*, 8194-8195.

[31] Weast, R. C., Ed. (1971) *CRC Handbook of Chemistry and Physics*, 51st ed., The Chemical Rubber Co., Cleveland, OH.

[32] Armstrong, D. A.; Yu, D.; Rauk, A. "Oxidative damage to the glycyl α-carbon site in proteins: an ab initio study of the C-H bond dissociation energy and the reduction potential of the C-centered radical." *Can. J. Chem*. **1996**, *74*, 1192-1199.

[33] Ahn, N.; Klinman, J. P. "Mechanism of modulation of dopamine β-monooxygenase by pH and fumarate as deduced from initial rate and primary deuterium isotope effect studies." *Biochemistry*. **1983**, *22*, 3096-3106.

separated by over ~ 11 Å via a fully solvent exposed cleft and there is no evidence for a through-substrate electron pathway (see above), this scenario appears to be very unlikely. On the other hand, under the condition in which both substrate and O_2 are saturated, the product dissociation from the enzyme active sites has been shown to be a rate-limiting step.[28] This rate constant (k_d) was calculated to be ~ 40 s^{-1} for hippuric acid with PHM.[29] If the ET step follows the C-H cleavage, it has to occur faster than the rate for k_d (~ 40 s^{-1}). This far less stringent limit for the ET step seems to be more reasonable if we assume that it would occur via a direct electron tunneling through bulk water between two copper centers.[34] Although this electron tunneling through water in these enzymes would not be expected to occur as fast as the predicted rate (10^9 s^{-1}) considering the significant structural change upon the oxidation (see the structural description), it should remain faster than the rate for k_d to accommodate catalysis and there would be no need to invoke substrate or free superoxide as an electron conduit.

This assumption was further reinforced by a recent elaborate study of the relationship between O_2 consumption and substrate hydroxylation in DβM.[22] There are two major findings in this study. First, a significant change in substrate reactivity does not perturb the stoichiometry of O_2 uptake relative to substrate hydroxylation. Thus, even with 4-(trifluoromethyl)phenethylamine as a substrate with an apparent reaction rate that is much lower (ca. 3 orders of magnitude) compared to those of similar substrates studied, the ratio of O_2 consumption to product formation remains at unity. Moreover, a

[34] Ponce, A.; Gray, H. B.; Winkler, J. R. "Electron Tunneling through Water: Oxidative Quenching of Electronically Excited $Ru(tpy)_2^{2+}$ (tpy = 2,2':6,2"-terpyridine) by Ferric Ions in Aqueous Glasses at 77 K. *J. Am. Chem. Soc*. **2000**, *122*, 8187-8191.

kinetic isotope effect of ~ 18 using a β,β-dideuterated analog as the substrate[22c] indicates that the C-H cleavage is fully rate-determining with this substrate. If either one or both copper ions undergo(es) oxidation(s) before substrate activation, it should result in a steady state accumulation of an enzyme complex that contains the activated oxygen intermediate. Thus, it is expected that the lifetime of the activated oxygen intermediate would increase as the reactivity of the substrate decreases, and ultimately reach at the highest level with the inert substrate. Given that the active sites in PHM are fully exposed to solvent, some degree of the leakage of this activated oxygen species (either superoxide or peroxide) should occur, resulting in the deviation from unity for the ratio between the product formation and O_2 consumption. However, this is not observed in these enzymes in which O_2 consumption and substrate hydroxylation are completely coupled.

In a second key finding, the authors failed to observe reoxidation of the reduced enzyme by O_2 in the presence of an inert substrate analog (β,β-difluorophenethylamine, DFPA), which is not able to undergo the C-H activation. This result suggests that copper reoxidation is tightly coupled to C-H activation. In other words, there is no electron transfer from the copper sites to incoming O_2 prior to C-H activation. Even if it did occur, it takes place at an undetectable level in a fully reversible process, which is in line with the observation from the sensitivity of the oxygen isotope effect to substrate deuteration.[25,26]

Taking all of the aforementioned experimental results into account, any mechanism that involves highly reduced oxygen species such as Cu^{II}-OO^{-}, Cu^{II}-OOH, or Cu^{II}-$O^{\bullet}$ seems very unlikely. For instance, the Cu^{II}-OOH species has been proposed as a

reactive oxygen species on the basis of early pH-dependent isotope effects for DβM.[33] The formation of this species from O_2 requires two consecutive long-range proton-coupled electron transfer processes. Thus, it seems very unlikely that this species would be formed at an undetectable level in a fully reversible manner. Furthermore, the involvement of this species is also incompatible with the results from an early study of the relationship between the magnitude of the O-18 kinetic isotope effect and substrate reactivity.[25] If the Cu^{II}-OOH species indeed initiates H-atom abstraction from the substrate, a normal O-18 isotope effect would be expected; that is, greater O-O bond breaking in the peroxo moiety occurs as the reaction becomes less favorable (more product-like transition state), resulting in larger O-18 kinetic isotope effect with decreasing substrate reactivity. However, the experimental results showed an inverse O-18 isotope effect. To explain this, an alternative mechanism has been suggested. In this mechanism, the Cu^{II}-OOH species first undergoes reductive cleavage of the O-O bond by abstracting the H-atom from a conserved tyrosine residue (PHM: Y318; DbM: Y484) near the Cu_M site to produce a Cu^{II}-O$^{\bullet}$ species, water and a tyrosyl radical. The resulting Cu^{II}-O$^{\bullet}$ species then initiates the substrate hydroxylation. However, recent site-specific mutagenesis studies with PHM[26] indicated that the Y318F mutant had no impact on V_{max}, identical O-18 isotope effect to that of the wild-type enzyme, and exhibited only a 3-4 fold reduction in the rate constant for C-H bond cleavage. These findings were argued to remove the Cu^{II}-O$^{\bullet}$ species from consideration.

There is some experimental evidence suggesting that both PHM and DβM enzymes use a Cu^{II}-superoxo intermediate to initiate their catalysis by C-H bond

cleavage. Nonetheless, there is no consensus on the identity of the active species of these enzymes. Except for the one example,[35] none of the synthetic Cu^{II}-superoxo species that have been characterized spectroscopically or isolated as discrete crystalline compounds show the aliphatic C-H bond activation chemistry akin to those catalyzed by these enzymes (see the section 1-4). Moreover, a series of recent DFT studies on these enzymes showed conflicting results with regard to the energetics of the C-H bond cleavage by various Cu/O_2 intermediates, leaning more toward the mechanism involving a Cu-oxyl species.[36]

As an example, Kamachi et al. investigated dopamine hydroxylation by three possible oxidants, Cu^{II}-superoxo, -hydroperoxo and -oxyl species, in DβM with DFT/QM-MM calculations.[36a,b] They calculated the activation energy for the H-atom abstraction by these species and found that the corresponding H-atom abstraction barriers were 3.8, 17 and 40 kcal/mol for the Cu-oxo, -superoxo, and -hydroperoxo, respectively. On the basis of these results, they speculated that the dopamine hydroxylation can be initiated by the Cu^{II}-superoxo species, but the Cu^{II}-oxyl species has stronger oxidation power that is enough to promote the H-atom abstraction with a low activation barrier if this species could be effectively formed at the active site of DβM.

---

[35] Kunishita, A.; Kubo, M.; Sugimoto, H.; Ogura, T.; Sato, K.; Takui, T.; Itoh, S. "Mononuclear Copper(II)- Superoxo Complexes that Mimic the Structure and Reactivity of the Active Centers of PHM and DβM." *J. Am. Chem. Soc*. **2009**, *131*, 2788-2789.

[36] a) Kamachi, T.; Kihara, N.; Shiota, Y.; Yoshizawa, K. "Computational Exploration of the Catalytic Mechanism of Dopamine β-Monooxygenase: Modeling of Its Mononuclear Copper Active Sites." *Inorg. Chem*. **2005**, *44*, 4226-4236. b) Yoshizawa, K.; Kihara, N.; Kamachi, T.; Shiota, Y. "Catalytic Mechanism of Dopamine β-Monooxygenase Mediated by Cu(III)-Oxo." *Inorg. Chem*. **2006**, *45*, 3034-3041. c) Crespo, A.; Marti, M. A.; Roitberg, A. E.; Amzel, L. M.; Estrin, D. A. "The catalytic mechanism of peptidylglycine α-hydroxylating monooxygenase investigated by computer simulation." *J. Am. Chem. Soc*. **2006**, *128*, 12817-12828.

Crespo et al. also investigated the molecular basis of the H-abstraction mechanism in PHM using QM-MM calculations.[36c] Their computed potential energy profiles for the H-abstraction reaction by Cu^{I}-$O_2^{\bullet-}$, Cu^{II}-$O_2^{\bullet-}$, and Cu^{II}-OOH species indicate that none of these species can promote H-atom abstraction. Instead, they found that the Cu^{I}-$O_2^{\bullet-}$ species, which is a resonance form of a Cu^{II}-OO^{-}, spontaneously undergoes two consecutive protonation steps from the surrounding solvent to form a water molecule and a $[L_3^{\bullet+}Cu^{III}O]^{2+} \leftrightarrow [L_3^{\bullet+}Cu^{II}O^{\bullet-}]^{2+}$ ($L_3^{\bullet+}$ having significant positive charge and unpaired electron density localized over the three ligands coordinated to Cu_M). Then, the produced $[CuO]^{2+}$ species abstracts the substrate H-atom in concerted fashion with almost zero activation energy (less than 2 kcal/mol). On the basis of these findings, the authors concluded that the probable active species in PHM is $[L_3^{\bullet+}Cu^{III}O]^{2+}$ that closely resembles its iron analogue active species in cytochrome P450 enzymes (Compound I, $[Por^{\bullet+}Fe^{IV}O]$, Por = porphyrin).[37]

In an effort to solve the mechanistic puzzles for the PHM and DβM enzymes, many research groups have synthesized model complexes and investigated their oxygenation chemistry.[38] These studies have deepened our understanding of fundamental aspects including the binding and activation of O_2 at copper centers, electronic and

---

[37] Sono, M.; Roach, M. P.; Coulter, E. D.; Dawson, J. H. "Heme-Containing Oxygenases." *Chem. Rev.* **1996**, *96*, 2841-2887.

[38] a) Hatcher, L. Q.; Karlin, K. D. "Oxidant types in copper-dioxygen chemistry: the ligand coordination defines the Cu_n-O_2 structure and subsequent reactivity." *J. Biol. Inorg. Chem*. **2004**, *9*, 669-683. b) Itoh, S. "Mononuclear copper active-oxygen complexes." *Curr. Opin. Chem. Biol*. **2006**, *10*, 115-122. c) Cramer, C. J.; Tolman, W. B. "Mononuclear Cu-O_2 Complexes: Geometries, Spectroscopic Properties, Electronic Structures, and Reactivity." *Acc. Chem. Res*. **2007**, *40*, 601-608. d) Suzuki, M. "Ligand Effects on Dioxygen Activation by Copper and Nickel Complexes: Reactivity and Intermediates." *Acc. Chem. Res*. **2007**, *40*, 609-617. e) Itoh, S.; Fukuzumi, S. "Dioxygen activation by copper complexes. Mechanistic insights into copper monooxygenases and copper oxidases." *Bull. Chem. Soc. Jpn*. **2002**, *75*, 2081–2095. f) Schindler, S. "Reactivity of Copper(I) Complexes Towards Dioxygen." *Eur. J. Inorg. Chem.* **2000**, 2311–2326.

geometric properties of the resulting Cu/O_2 species, and their reactivity patterns toward substrates. However, understanding of the mononuclear Cu/O_2 intermediates that are most relevant to the postulated active species in catalysis by these enzymes is in its infancy. Perhaps least understood is the mononuclear Cu^{II}-oxyl species that have been characterized only in the gas phase.[39] The following section will focus on the most recent synthetic model studies on PHM and DβM.

1.4. Synthetic Model Studies Relevant to DβM and PHM

1.4.1. 1:1 Cu/O_2 Adducts

Despite the extensive studies on DβM and PHM using biochemical, kinetic, spectroscopic, X-ray crystallographic, and theoretical methods, there is still debate about the identity of the active species responsible for H-atom abstraction. To resolve this issue, much effort has been focused on synthesizing copper(I) model complexes, evaluating their reactivity toward O_2, and identifying/characterizing the resulting Cu/O_2 species.[38] Among the many such species that have been studied, dinuclear species ($[Cu_2/O_2]$) are arguably the best understood. In contrast, only a handful of mononuclear Cu/O_2 species of most relevance to postulated intermediates in catalysis by DβM and PHM have been characterized spectroscopically[35,40] or crystallographically[41,42,43,44] so far. The scarcity of

---

[39] Schroeder, D.; Holthausen, M. C.; Schwarz, H. "Radical-Like Activation of Alkanes by the Ligated Copper Oxide Cation (Phenanthroline)CuO^+." *J. Phys. Chem. B* **2004**, *108*, 14407-14416.

[40] a) Weitzer, M.; Schindler, S.; Brehm, G.; Schneider, S.; Hoermann, E.; Jung, B.; Kaderli, S.; Zuberbuehler, A. D. "Reversible Binding of Dioxygen by the Copper(I) Complex with Tris(2-

these species is in a large part due to their tendency to further react with Cu^{I} precursors to form thermodynamically stable dinuclear and/or multinuclear complexes. Thus, stabilization of the 1:1 Cu/O_2 intermediates and evaluation of their geometric, spectroscopic, electronic, and reactivity properties represent significant research goals. The recent successes in this area are summarized below in order to place my research in perspective.

Several crystal structures of such 1:1 Cu/O_2 species and their in-depth characterization via experiment and theory have been reported.[41-44] In 1994, Kitajima et al.[41] oxygenated a copper(I) precursor with a sterically demanding tris(pyrazolyl)hydroborate ligand ($HB(3\text{-}tBu\text{-}5\text{-}iPrpz)_3$ = hydrotris(3-*tert*-butyl-5-*iso*-propyl-1-pyrazolyl)borate). UV-vis spectroscopy, manometry measurements ($Cu:O_2$ = 0.9), FT-IR spectroscopy ($\nu_{O\text{-}O}$ = 1116 cm^{-1} for $^{16}O_2$ and 1060 cm^{-1} for $^{18}O_2$), ^{1}H NMR spectroscopy (diamagnetic), and Cu K-edge X-ray absorption spectroscopy data (Cu^{II}

---

dimethylaminoethyl)amine (Me6tren) Ligand." *Inorg. Chem*. **2003**, *42*, 1800-1806. b) Zhang, C. X.; Kaderli, S.; Costas, M.; Kim, E.; Neuhold, Y.; Karlin, K. D.; Zuberbuehler, A. D. "Copper(I)-Dioxygen Reactivity of [(L)CuI]+ (L = Tris(2-pyridylmethyl)amine): Kinetic/Thermodynamic and Spectroscopic Studies Concerning the Formation of Cu-O2 and Cu2-O2 Adducts as a Function of Solvent Medium and 4-Pyridyl Ligand Substituent Variations." *Inorg. Chem*. **2003**, *42*, 1807-1824. c) Börzel, H.; Comba, P.; Hagen, K. S.; Kerscher, M.; Pritzkow, H.; Schatz, M.; Schindler, S.; Walter, O. "Copper-Bispidine Coordination Chemistry: Syntheses, Structures, Solution Properties, and Oxygenation Reactivity." *Inorg. Chem*. **2002**, *41*, 5440-5452. d) Karlin, K. D.; Kaderli, S.; Zueberbuehler, A. D. "Kinetics and Thermodynamics of Copper(I)/Dioxygen Interaction." *Acc. Chem. Res*. **1997**, *30*, 139-147. e) Karlin, K. D.; Tolman, W. B.; Kaderli, S.; Zuberbuehler, A. D. "Kinetic and thermodynamic parameters of copper-dioxygen interaction with different oxygen binding modes." *J. Mol. Catal. A: Chem*. **1997**, *117*, 215-222.

[41] Fujisawa, K.; Tanaka, M.; Moro-oka, Y.; Kitajima, N. "A Monomeric Side-On Superoxocopper(II) Complex: Cu(O2)(HB(3-tBu-5-iPrpz)3)." *J. Am. Chem. Soc.* **1994**, *116*, 12079–12080.

[42] Aboelella, N. W.; Lewis, E. A.; Reynolds, A. M.; Brennessel, W. W.; Cramer, C. J.; Tolman, W. B. "Snapshots of Dioxygen Activation by Copper: The Structure of a 1:1 Cu/O2 Adduct and Its Use in Syntheses of Asymmetric Bis(μ-oxo) Complexes." *J. Am. Chem. Soc.* **2002**, *124*, 10660–10661.

[43] Reynolds, A. M.; Gherman, B. F.; Cramer, C. J.; Tolman, W. B. "Characterization of a 1:1 Cu/O2 Adduct Supported by an Anilido-Imine Ligand." *Inorg. Chem.* **2005**, *44*, 6989–6997.

[44] Würtele, C.; Gaoutchenova, E.; Harms, K.; Holthausen, M. C.; Sundermeyer, J.; Schindler, S. "Crystallographic Characterization of a Synthetic 1:1 End-On Copper Dioxygen Adduct Complex." *Angew. Chem., Int. Ed.* **2006**, *45*, 3867–3869.

oxidation state) support a formulation of the oxygenated product as a Cu^{II}-superoxo species.

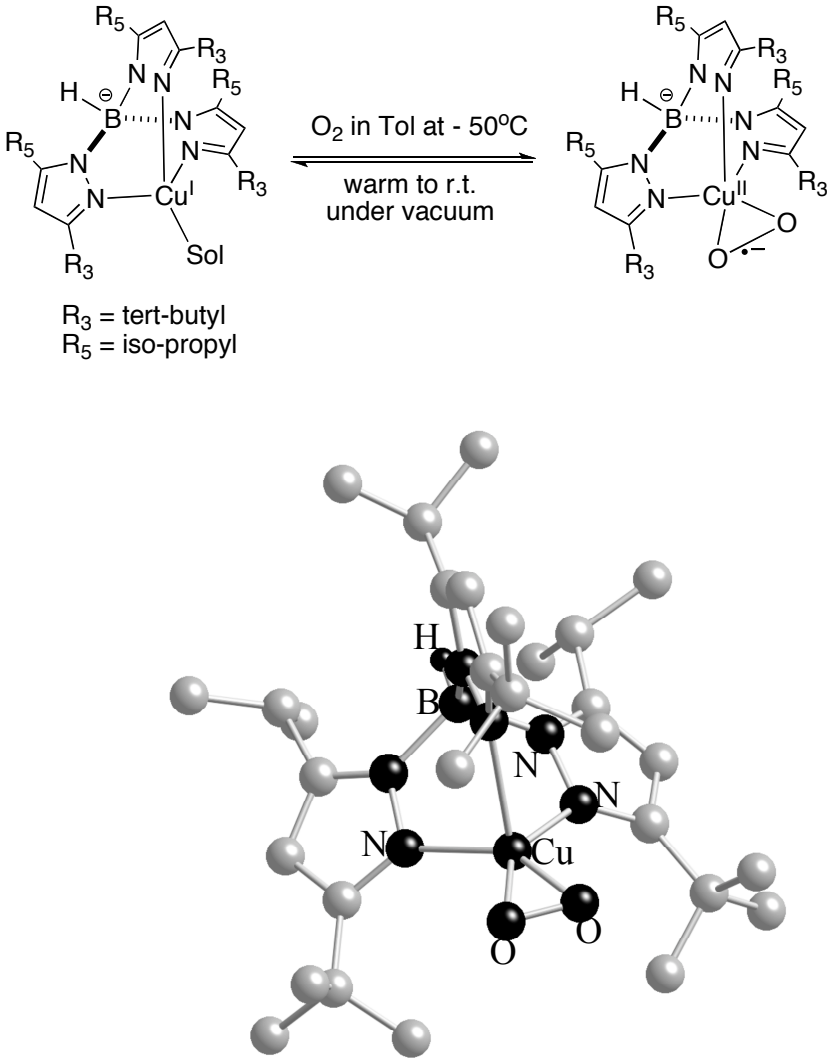

Figure 1-5. Reversible formation of the side-on bound Cu^{II}-superoxo species from the reaction between Cu(DMF)[HB(3-*t*Bu-5-*i*Prpz)$_3$] and O_2, and crystal structure of Cu(O_2)[HB(3-*t*Bu-5-*i*Prpz)$_3$].[41]

In later work,[45] investigation into the electronic structure of this and related Cu^{II}-superoxo species showed them to have a diamagnetic, singlet ground state with a low-lying triplet state at ~ 1500 cm^{-1} higher in energy, with the singlet ground state involving a strong covalent interaction between a Cu^{II} *xy* and in-plain π^* orbital of the superoxide. In the crystal structure of $Cu(O_2)$[HB(3-*t*Bu-5-*i*Prpz)$_3$] (Figure 1-5), the coordination geometry at the copper center can be regarded as a square pyramidal with two nitrogens and two oxygens in an equatorial position and with the third nitrogen in an apical position. This complex features side-on (η^2) coordination of the O_2 fragment, and the Cu–N and –O distances are typical for Cu^{II} compounds. Yet, the O-O distance of 1.22(3) Å is so short that is close to that of free O_2 (1.208 Å).[18] This is perhaps attributed to the low quality of the single crystals (R = 11.6 % and R_W = 8.46 %) and the fact that the data collection was carried out at room temperature (in of itself unusual, considering the thermal instability typically associated with such species), which would result in underestimation of the O-O distance due to librational disorder of the O_2 moiety. This hypothesis is further supported by the results from DFT calculations on a series of reported side-on 1:1 metal/O_2 complexes.[46] This study analyzed O-O and M-O bonding in these series. It was noted that the O-O distance of 1.262(8) Å in the analogous $Co(O_2)$[HB(3-*t*Bu-5-*i*Prpz)$_3$] complex[47] measured at room temperature is similar to that

---

[45] Chen, P.; Root, D. E; Campochiaro, C.; Fujisawa, K.; Solomon, E. I. "Spectroscopic and electronic structure studies of the diamagnetic side-on Cu^{II}-superoxo complex Cu(O2)[HB(3-R-5-^{i}Prpz)3]: Antiferromagnetic coupling versus Covalent delocalization." *J. Am. Chem. Soc*. **2003**, *125*, 466-474.

[46] Cramer, C. J.; Tolman, W. B.; Theopold, K. H.; Rheingold, A. L. "Variable Character of O-O and M-O Bonding in Side-on (η2) 1:1 Metal Complexes of O_2." *Proc. Natl. Acad. Sci. U.S.A.* **2003**, *100*, 3635–3640.

[47] Egan, J. W., Jr.; Haggerty, B. S.; Rheingold, A. L.; Sendlinger, S. C.; Theopold, K. H. "Crystal structure of a side-on superoxo complex of cobalt and hydrogen abstraction by a reactive terminal oxo ligand." *J. Am. Chem. Soc*. **1990**. *112*. 2445-2446.

of the Cu analog, but the measured ν_{O-O} (961 cm^{-1}) for the former is 151 cm^{-1} lower than that of the latter (1112 cm^{-1}). The O-O distance and ν_{O-O} value are closely related to each other with respect to the degree of charge transfer from the metal to O_2 fragment. This apparent discrepancy between two closely related side-on bound metal-superoxo species led to the reevaluation of the crystal structure of the cobalt analog at low temperature (150 K). In this low temperature structure, the O-O bond distance was found to be 1.355(3) Å, consistent with that predicted by DFT theory (1.380 Å). This result clearly illustrates how the librational mode of the bound O_2 fragment would result in significant underestimation of the O-O distance at high temperature.

Notwithstanding problems associated with its X-ray structure and solution properties, the $Cu(O_2)[HB(3\text{-}t\text{Bu-}5\text{-}i\text{Prpz})_3]$ is notable as the first crystallographically characterized side-on bound 1:1 Cu^{II}-superoxo species. It is worth noting that the key factors that led to the stabilization and isolation of the 1:1 Cu/O_2 adduct were the use of low temperatures and sterically hindered supporting ligands to prevent decomposition processes and dimerization. Unfortunately, studies of the reactivity of this species have yet to be reported.

Recently, Schindler and coworkers successfully generated a 1:1 Cu/O_2 adduct by using a sterically conjested and superbasic tren derivative (TMG_3tren = 1,1,1-tris{2-[N^2-1,1,3,3-tetramethylguanidino)]ethyl}-amine).[44] The copper(I) precursor readily reacts with O_2 at low temperature in acetone or propionitrile to form a dark-green 1:1 Cu/O_2 species, whose formation is completely reversible (see Figure 1-6).

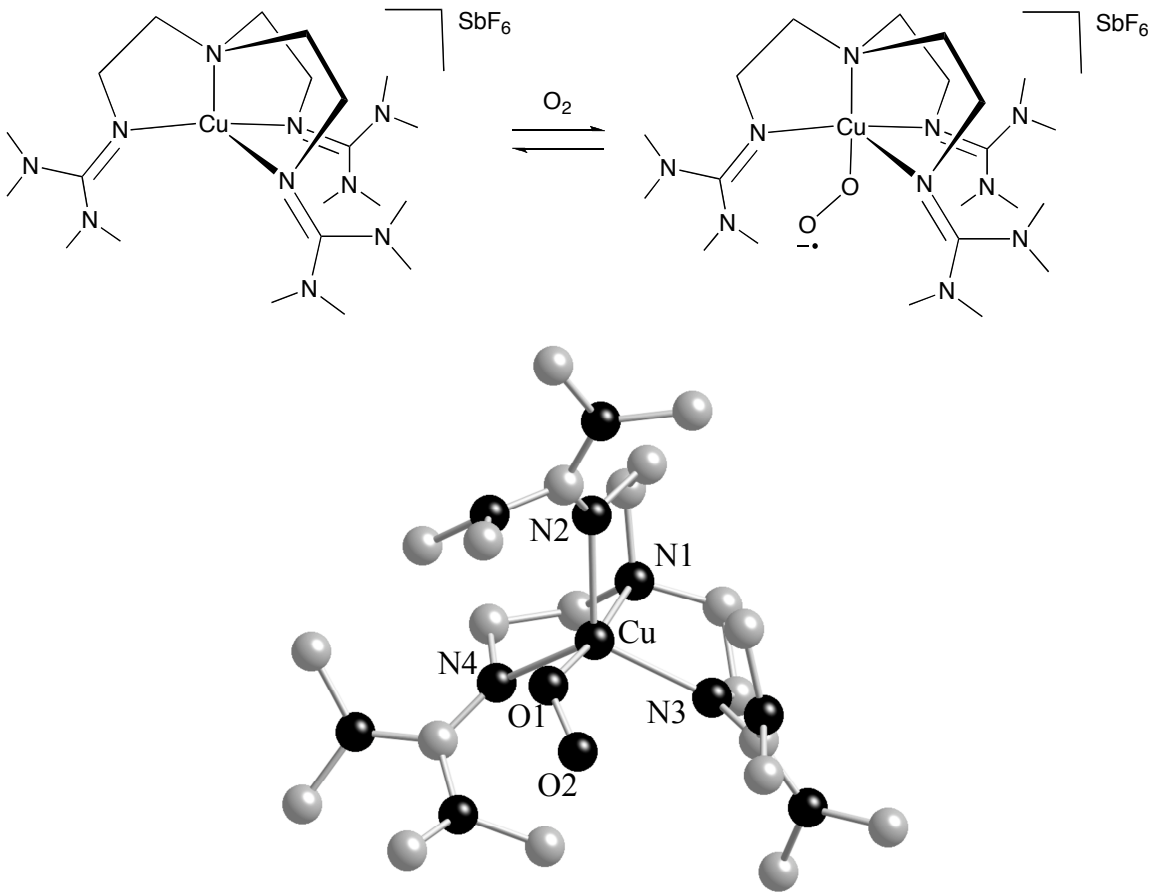

Figure 1-6. Reversible formation of the end-on bound Cu^{II}-superoxo species from the reaction between $[Cu(TMG_3tren)]^+$ and O_2, and the crystal structure of $[Cu(O_2)(TMG_3tren)]^+$ (the counteranion, co-crystallized acetones, hydrogen atoms and the 6% disorder position of O_2 are not shown for clarity).

The $\nu_{O\text{-}O}$ value (1117 cm^{-1} for $^{16}O_2$ and 1059 cm^{-1} for $^{18}O_2$)[48] for this species is typical for metal-superoxide complexes (~1075-1296 cm^{-1}).[49] The results from resonance Raman experiments did not allow the binding mode of O_2 moiety (side-on vs end-on) to

[48] Schatz, M.; Raab, V.; Foxon, S. P.; Brehm, G.; Schneider, S.; Reiher, M.; Holthausen, M. C.; Sundermeyer, J.; Schindler, S. "Dioxygen complexes: Combined spectroscopic and theoretical evidence for a persistent end-on copper superoxo complex." *Angew. Chem. Int. Ed*. **2004**. *43*. 4360-4363.

[49] a) Hill, H. A. O.; Tew, D. G. "Dioxygen, Superoxide and Peroxide. In *Comprehensive Coordination Chemistry*; Wilkinson, G., Gillard, R. D., McCleverty, J. A., Eds.; Pergamon: Oxford, 1987; Vol. 2, pp 315–333. b) Nakamoto, K. *Infrared and Raman Spectra of Inorganic and Coordination Compounds, Part B*, 5th ed.;Wiley-Interscience: New York, 1997; pp 154–168.

be determined, so the authors performed DFT calculations, showing that two isomers are energy minima. One isomer (**1**) features a tetradentate N-coordination and an end-on O_2 ligand, and a second isomer (**2**) features a tridentate N-coordination with an one dissociated ligand arm from the copper center and a side-on O_2 ligand; **1** was found to be 29.4 kcal/mol more stable than **2**. Moreover, the computed $\nu_{O\text{-}O}$ value for **1** is almost identical with the experimental value. Thus, the authors postulated that the dark-green oxygenated intermediate is more likely an end-on bound Cu^{II}-superoxo species.

This postulate was unambiguously confirmed by a single crystal X-ray structure determination.[44] As shown in Figure 1-6, the O_2 fragment binds to Cu in an end-on (η^1) fashion as an axial ligand in a trigonal-bipyramidal geometry. The Cu-N and -O distances are typical for Cu^{II} complexes. Importantly, the O-O distance of 1.280(3) Å falls in the range characteristic of metal-superoxide complexes (~1.2-1.3 Å). This complex represents the first example of the end-on 1:1 Cu^{II}-superoxo species that is thoroughly characterized by UV-visible and resonance Raman spectroscopies, DFT calculations, and single crystal X-ray crystallography. Recent reactivity studies of this species toward external substrates show interesting results, implying the involvement of the putative $[CuO]^+$ intermediate during the course of the intra-ligand hydroxylation processes (*vide infra*).

An entirely different 1:1 Cu/O_2 adduct was isolated by Tolman and coworkers and characterized through a combination of spectroscopic methods, extensive kinetic studies,

X-ray crystallography, and theory. [42-43,50-51]

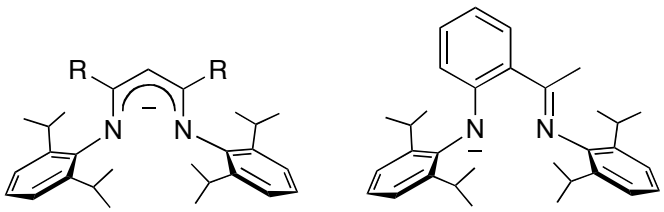

1, R = Me
2, R = tBu

3

Scheme 1-9. β-diketiminate and anilido-imine ligands.

By using the strongly electron-donating, mono-anionic β-diketiminate or anilido-imine ligands with bulky aromatic ring substituents (Scheme 1-9), the formation of dicopper species could be completely blocked upon low-temperature oxygenation of the corresponding Cu^{I} precursors. In contrast to the previous described Cu^{II}-superoxo species, the oxygenation to yield [$LCu(O_2)$] intermediates was irreversible. Because all [$LCu(O_2)$] intermediates (L = **1** through **3**) showed very similar spectroscopic features, attention is placed on the complex [(**1**)$Cu(O_2)$]. This complex exhibits absorption features at 385 nm ($\varepsilon \approx 2400\ M^{-1}\ cm^{-1}$) and 600 nm (broad, $\varepsilon \approx 200\ M^{-1}\ cm^{-1}$), is EPR silent, and has a $Cu:O_2$ uptake ratio of 1.0(2):1. A $\nu_{O\text{-}O}$ value of 968 cm^{-1} that shifted by 51 cm^{-1} with $^{18}O_2$ was observed. This value is significantly lower than typical for metal-superoxide complexes, but is higher than the region typical for metal-peroxides (~750-

[50] Spencer, D. J. E.; Aboelella, N. W.; Reynolds, A. M.; Holland, P. L.; Tolman, W. B. β-Diketiminate Ligand Backbone Structural Effects on $Cu(I)/O_2$ Reactivity: Unique Copper-Superoxo and Bis(μ-oxo) Complexes. *J. Am. Chem. Soc.* **2002**, *124*, 2108–2809.

[51] Aboelella, N. W.; Kryatov, S. V.; Gherman, B. F.; Brennessel, W. W.; Young, V. G., Jr.; Sarangi, R.; Rybak-Akimova, E. V.; Hodgson, K. O.; Hedman, B.; Solomon, E. I.; Cramer, C. J.; Tolman, W. B. "Dioxygen Activation at a Single Copper Site: Structure, Bonding, and Mechanism of Formation of 1:1 Cu/O_2 Adducts." *J. Am. Chem. Soc.* **2004**, *126*, 16896–16911.

930 cm^{-1}). Upon use of a statistical mixture of O_2 isotopomers ($^{18}O_2$, $^{18}O^{16}O$, and $^{16}O_2$), the resonance Raman spectrum showed three peaks, the middle one being at 943 cm^{-1} with an identical line width to those of the peaks from $^{18}O_2$ and $^{16}O_2$. These results are consistent with, but do not prove a symmetrical binding of O_2 to copper.[41] Thus, the complex [(**1**)Cu(O_2)] was initially formulated as a side-on bound (η^2) Cu^{II}-superoxo species.[47] However, the X-ray crystallographic,[42,43] DFT,[51] and X-ray absorption results[50,51] suggest that a completely different formalism for the bonding is appropriate that is more akin to a side-on bound Cu^{III}-peroxo.

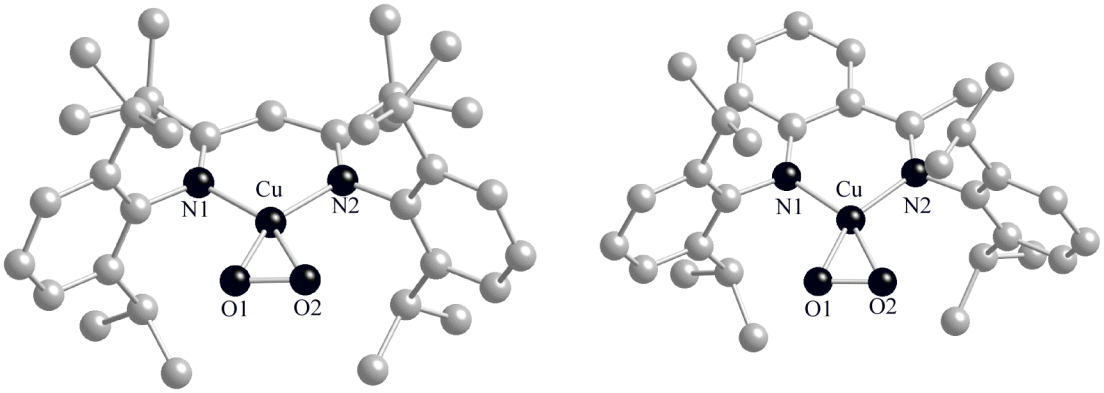

Figure 1-7. Representation of the crystal structures of [(**2**)Cu(O_2)] (left) and [(**3**)Cu(O_2)] (right).

The crystallographically determined O-O distances of 1.44(2) Å[42] and 1.392(2) Å[43] for [LCu(O_2)] (L = **2** or **3**, respectively) are more close to the values characteristic for metal-peroxo complexes (~1.4-1.5 Å) although the value for L = **2** is not particularly reliable due to severe disorder problems associated with the structure. Further insights were provided by a DFT study on [(**2**)Cu(O_2)], from which it was concluded that the copper center is in a Cu^{III} oxidation state. Theoretical calculations also predicted that the

side-on singlet state of all of the [LCu(O_2)] intermediates is a minimum energy structure with O-O distances in a range of 1.358 – 1.378 Å, in reasonable agreement with the experimental values. More definitive evidence for the copper oxidation state in [LCu(O_2)] intermediates was provided by X-ray absorption spectroscopic data (XAS).[50,51] The spectra of Cu K-edge XAS for [(**1**)Cu(O_2)] exhibited a pre-edge feature at ~ 8980.7 eV, which is ~ 2 eV higher in energy than those typical for Cu^{II} complexes (8978.8 ± 0.4 eV). This result clearly demonstrated that the copper ion of [(**1**)Cu(O_2)] complex is in +3 oxidation state. Similarly, Cu L-edge XAS data also supported the Cu^{III} oxidation state of [(**1**)Cu(O_2)], as evidenced by ~ 2 eV shifts of key peaks to higher energy than those typical for Cu^{II} complexes (~ 930 eV). Two main contributors to this ~ 2 eV higher energy shift for both pre-edge energies are the effective nuclear charge (Z_{eff}) of the absorbing atom (in this case, Cu ion) and ligand field strength (LF). To evaluate the relative contributions of these two terms to pre-edge transition energies, time-depedant (TF) DFT calculations were performed. The results indicated that while the Z_{eff} term leads to similar energy shifts in the Cu 1s, 2p, and 3d orbitals, the LF term predominantly affects the energy of the lowest unoccupied Cu 3d orbital (LUMO). That is, the stronger the ligand donors, the more destabilization of the Cu 3d orbital. For [(**1**)Cu(O_2)], the strongly electron donating β-diketiminate ligand makes the Z_{eff} for the Cu^{III} ion essentially the same as other Cu^{II} complexes, but with greater destabilization of the LUMO, as supported by the shorter Cu-N distances (avg. d_{Cu-N} = ~ 1.86 Å) and larger N character (~ 18%) in the LUMO for [(**1**)Cu(O_2)] compared with ~ 2.25 Å and ~ 12% for the side-one bound Cu^{II}-superoxo analog, Cu(O_2)[HB(3-*t*Bu-5-*i*Prpz)$_3$], respectively.

Taken together, all copper(I) complexes of either β-diketiminates or the anilido-imine ligand give rise to the side-on 1:1 Cu/O_2 intermediate upon oxygenation, which lies closer to the Cu^{III}-peroxo formalism within the continuum of the Cu^{II}-superoxo and the Cu^{III}-peroxo extremes. This can be attributed to the strongly electron donating character of the β-diketiminates and anilido-imine ligands, rendering the electron flow from the copper center to O_2 fragment more favorable toward Cu^{III} and peroxide levels.

This electronic structure is thought to be related to a general lack of reactivity of the $[LCu(O_2)]$ species (L = **1** through **3**) with various substrates including phenols, phenolates, thioanisole, ferrocene or acids such as HBF_4.[52] The results from the reaction between $[(\mathbf{1})Cu(O_2)]$ and various phosphines are notable. Instead of oxidizing the phospines to the corresponding phospine oxides, the phosphines simply replace the bound O_2 from $[(\mathbf{1})Cu(O_2)]$ species to yield Cu^{I}-phosphine adducts. Detailed kinetic analyses of these reactions revealed an associative mechanism. These results indicate that the steric bulk of the supporting ligands does not prevent other substrates from approaching the Cu/O_2 core. Thus, the poor oxidizing power of these species likely has an electronic origin. This hypothesis was further examined by theoretical calculations.[53] This study predicted that these species would be difficult to reduce and protonate due to their reduced radical character (Cu^{II}-superoxo vs Cu^{III}-peroxo). Thus, the H-atom abstraction from the hydrocarbon substrate by these species is thermodynamically unfavorable. However, theory predicts that use of the less electron donating ligands could generate a

[52] Reynolds, A. M.; Lewis, E. L.; Aboelella, N. W.; Tolman, W. B. "Reactivity of a 1:1 copper–oxygen complex: Isolation of a Cu(II)-*o*-iminosemiquinonato species." *Chem. Commun.* **2005**, 2014–2016.

[53] Gherman, B. F.; Tolman, W. B.; Cramer, C. J. "Characterization of the structure and reactivity of monocopper-oxygen complexes supported by β-diketiminate and anilido-imine ligands." *J. Comput. Chem.* **2006**, *27*, 1950-1961.

side-on bound analog having more Cu^{II}-superoxo character and this analog would have more favorable reduction potential and basicity.

1.4.2. Mononuclear Cu-Oxyl Species.

Mononuclear copper-oxyl species ($[Cu^{II}\text{-}O^{-\bullet} \leftrightarrow Cu^{III}=O^{2-}]^{+}$) have been implicated as a possible reactive intermediate in catalysis by PHM and DβM,[36] but are less well understood. Such species have been characterized by theory[36,53,54] and only observed in the gas phase.[39] Theory predicts that they can be best described as a Cu^{II}-oxyl radical species rather than a Cu^{III}-oxo complex analogous to Fe^{IV}=O cores.[54b] One unpaired electron resides in one of the oxygen p-orbitals, thus resulting in a $O(p)^5$ configuration, an oxyl radical. The other unpaired electron is located in one of the Cu atom d-orbitals. These two unpaired electrons are ferromagnetically coupled to give rise to a triplet electronic ground state (S = 1). The only net bonding interaction between the copper(II) ion and the oxyl moiety is a half σ-bond, thus indicatting weak Cu-O bonding. These electronic structures and metal-oxygen bonding pictures for the Cu^{II}-oxyl species markedly contrast with those of the Fe^{IV}=O analogs. The latter features one strong σ- and two half π-bonds, leading to a net double bond interaction between the iron(IV) ion and the oxo group. The Fe^{IV}=O species have significant spin density on the oxygen atoms resulting from the strong covalency of the Fe-O π-bonding. However, the Cu^{II}-oxyl

[54] a) Nakao, Y.; Hirao, K.; Taketsugu, T. "Theoretical study of first-row transition metal oxide cations." *J. Chem. Phys.* **2001**, *114*, 7935-7940. b) Decker, A.; Solomon, E. I. "Dioxygen activation by copper, heme and non-heme iron enzymes: comparison of electronic structures and reactivities." *Curr. Opin. Chem. Biol.* **2005**, *9*, 152-163.

species have true radical character with unpaired electron density on the oxygen atom. Due to the weak Cu-O bond and the significant radical character of the oxygen atom, the mononuclear Cu^{II}-oxyl species are predicted to be powerful oxidants and to be difficult to observe. Nonetheless, recent experimental results implicate that such species may be involved as a transient intermediate during the course of either ligand modification processes or exogenous substrate activations.[55,56,57,58]

Ito and coworkers[55] synthesized a mononuclear Cu^{II}-cumylperoxo species by reacting the copper(II) complex of a tridentate ligand with cumene hydroperoxide in the presence of base in acetonitrile at –40 °C. The Cu^{II}-cumylperoxo species was characterized by UV-visible spectroscopy (λ_{max} = 465 nm, ε =1100 M^{-1} cm^{-1}), resonance Raman experiments, and an EPR experiment (99% spin remained). Interestingly, this transient Cu^{II}-alkylperoxo complex gradually decomposed via a first-order kinetics even at –40 °C to give a bis(μ-hydroxo)dicopper(II) complex (64% isolated yield without any ligand modification) and acetophenone in 92 % yield. To explain these observations, they speculated that the Cu^{II}-cumylperoxide first underwent a homolytic cleavage of the O-O bond to yield LCu^{II}-$O^{\bullet}$ and a cumyloxyl radical. The Cu^{II}-$O^{\bullet}$ species would abstract a H-

---

[55] a) Kunishita, A.; Teraoka, J.; Scanlon, J. D.; Matsumoto, T.; Suzuki, M.; Cramer, C. J.; Itoh, S. "Aromatic Hydroxylation Reactivity of a Mononuclear Cu(II)-Alkylperoxo Complex." *J. Am. Chem. Soc.* **2007**, *129*, 7248-7249. b) Kunishita, A.; Ishimaru, H.; Nakashima, S.; Ogura, T.; Itoh, S. "Reactivity of Mononuclear Alkylperoxo Copper(II) Complex. O-O Bond Cleavage and C-H Bond Activation." *J. Am. Chem. Soc.* **2008**, *130*, 4244-4245.

[56] Comba, P.; Knoppe, S.; Martin, B.; Rajaraman, G.; Rolli, C.; Shapiro, B.; Stork, T. "Copper(II)-mediated aromatic ortho-hydroxylation: a hybrid DFT and ab initio exploration." *Chem. Eur. J.* **2008**, *14*, 344-357.

[57] Maiti, D.; Lee, D-H.; Gaoutchenova, K.; Wuertele, C.; Holthausen, M. C.; Narducci, S., Amy, A.; Sundermeyer, J.; Schindler, S.; Karlin, K. D. "Reactions of a copper(II) superoxo complex lead to C-H and O-H substrate oxygenation: modeling copper-monooxygenase C-H hydroxylation." *Angew. Chem. Int. Ed.* **2008**, *47*, 82-85.

[58] Maiti, D.; Narducci. S. Amy, A.; Karlin, K. D. "Copper-Hydroperoxo-Mediated N-Debenzylation Chemistry Mimicking Aspects of Copper Monooxygenases." *Inorg. Chem.* **2008**, *47*, 8736-8747.

atom from the surrounding medium to yield a Cu^{II}-OH complex, which subsequently dimerized to form the final dicopper(II) product. The cumyloxyl radical species would be expected to undergo the well-known β-scission to yield the acetophenone product.

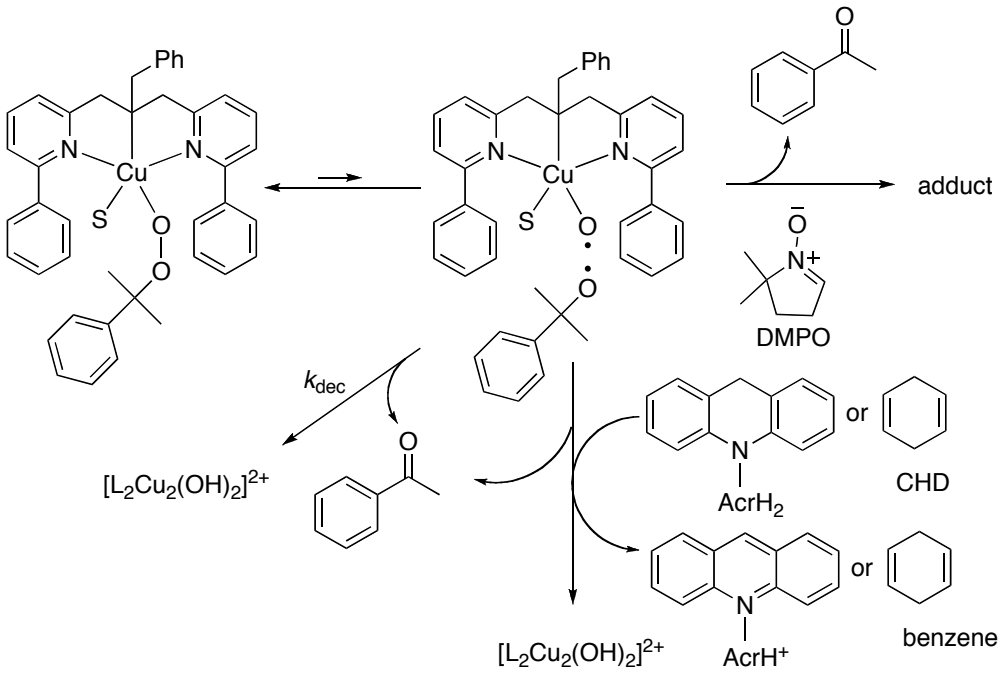

Scheme 1-10. Proposed reaction pathway to formation of an active Cu^{II}-oxyl species via a homolytic O-O bond cleavage of the Cu^{II}-cumylperoxo.[55]

To test this idea, the authors added excess 5,5-dimethyl-1-pyrroline-*N*-oxide (DMPO) to the Cu^{II}-cumylperoxo solution in order to intercept the putative Cu^{II}-$O^{\bullet}$ species. Indeed, they observed formation of the expected 1:1 adduct between the Cu^{II}-$O^{\bullet}$ and DMPO, as evidenced by ESI-MS and EPR measurements. More significantly, this Cu^{II}-cumylperoxo species showed one-electron oxidation chemistry with the exogenous substrates having relatively weak C-H bonds. For example, addition of 10-methyl-9,10-dihydroacridine to the acetonitrile solution of the Cu^{II}-alkylperoxo at –40 °C resulted in

formation of *N*-methylacridinium ion as a sole oxidation product (49% yield based on the Cu^{II}-cumylperoxo species), without perturbing the yield of the acetophenone. A detailed kinetic investigation showed a large kinetic isotope effect of $k^H/k^D = 19.2$, indicating that H-atom abstraction is rate-determining. Although these observations provide some evidence for the suggested homolytic cleavage pathway, the underlying mechanism (stepwise O-O bond scission and C-H bond activation of substrate *vs* its concerted variant) could not be dissected, in paticular without accounting for the methyl radical that must form after the cumyloxyl radical decomposition.

As described above, the $[Cu(TMG_3tren)]^+$ complex reversibly yields the mononuclear end-on bound Cu^{II}-superoxide intermediate upon oxygenation below −78 °C. With respect to its reactivity, the Cu^{II}-superoxide intermediate shows some interesting implications.[57] Addition of various substituted phenol substrates to the Cu^{II}-superoxide intermediate at −80 °C after removal of excess O_2 results in oxidation, oxygenation, or hydroperoxidation similar to those seen in other related system.[59] More importantly, the major copper-containing product after completion of the reaction was found to be a Cu^{II}-alkoxide species (~65% or more) derived from an intramolecular hydroxylation of the ligand methyl (α to nitrogen) C-H bond. When using $^{18}O_2$ to produce the starting Cu^{II}-superoxo species, one ^{18}O-atom was found to be incorporated into the final Cu^{II}-alkoxide product, as evidenced by ESI-MS data. Interestingly, this reaction was not observed in the absence of phenol substrate, nor by just warming the

[59] Maiti, D.; Fry, H. C.; Woertink, J. S.; Vance, M. A.; Solomon, E. I.; Karlin, K. D. "A 1:1 Copper-Dioxygen Adduct is an End-on Bound Superoxo Copper(II) Complex which Undergoes Oxygenation Reactions with Phenols." *J. Am. Chem. Soc*. **2007**. *129*. 264-265.

Cu^{II}-superoxo solution to room temperature, which resulted in O_2 release and reformation of the starting Cu^{I} complex. Thus, these results rule out the role of the Cu^{II}-superoxo itself in effecting the intramolecular ligand hydroxylation.

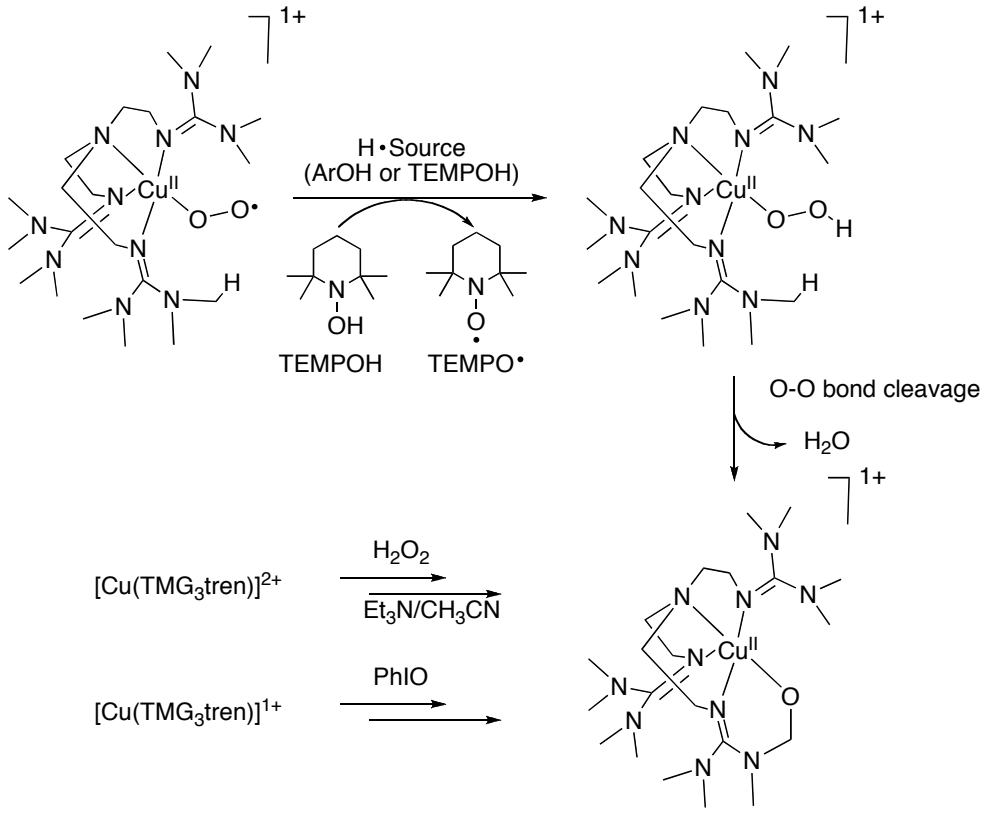

Scheme 1-11. Various routes to form hydroxylated product.[57]

A similar result was obtained by using TEMPOH as a H-atom donor that does not suffer from any substrate oxidation reactions like those observed in the cases of phenol substrates. Time-dependant EPR spectra in conjunction with UV-visible spectroscopy clearly indicated that the intensity of the EPR signal arising from the TEMPO radical increases as the reaction progresses. This result implies that the Cu^{II}-superoxo

intermediate abstracts an H-atom from TEMPOH to produce a Cu^{II}-hydroperoxo species and a TEMPO radical. The authors suggested that this Cu^{II}-hydroperoxo species leads to the ligand alkyl hydroxylation. To test this hypothesis, they investigated the reaction of a copper(II) analogue with a slight excess of H_2O_2/Et_3N, and they found the formation of the identical Cu^{II}-alkoxide product. Moreover, the same Cu^{II}-alkoxide product also formed in almost quantitative yields by reacting the copper(I) precursor with iodosylbenzene (PhIO), a well known oxo-transfer reagent. This result may be attributed to a $[CuO]^+$ or perhaps a Cu(OIPh) species. Overall, this system provides important precedent for aliphatic C-H bond hydroxylation by a structurally defined end-on Cu^{II}-superoxo species. But, this reaction occurs only upon addition of H-atom donors (phenols or TEMPOH) to the Cu^{II}-superoxo species. Thus, the nature of the active oxidant (Cu-OOH or its variants) responsible for this unusual ligand transformation remains unclear.

Karlin and coworkers performed a series of reactivity studies of discrete Cu^{II}-OOH complexes of TMPA deriviatives (TMPA = tris(2-pyridylmethyl)amine). In these studies, they attached various alkylamine substituents to one of the pyridyl side arms to investigate intramolecular oxidation chemistry.[58,60] Warming of the solution containing mononuclear Cu^{II}-OOH complexes, which were produced by adding excess of H_2O_2/Et_3N to Cu^{II} precursors, effected well-known oxidative *N*-dealkylation reactions. With *N,N*-dibenzylamine as the internal substrate,[58] one of the main organic products after removing the copper ions from the crude reaction mixtures was found to be a singly *N*-

[60] Maiti, D; Narducci Sarjeant, A. A.; Karlin, K. D. "Copper(II)-Hydroperoxo Complex Induced Oxidative N-Dealkylation Chemistry." *J. Am. Chem. Soc*. **2007**, *129*, 6720-6721.

dealkylated one (~48%) along with a corresponding benzaldehyde (~43%), as shown in Scheme 1-12.

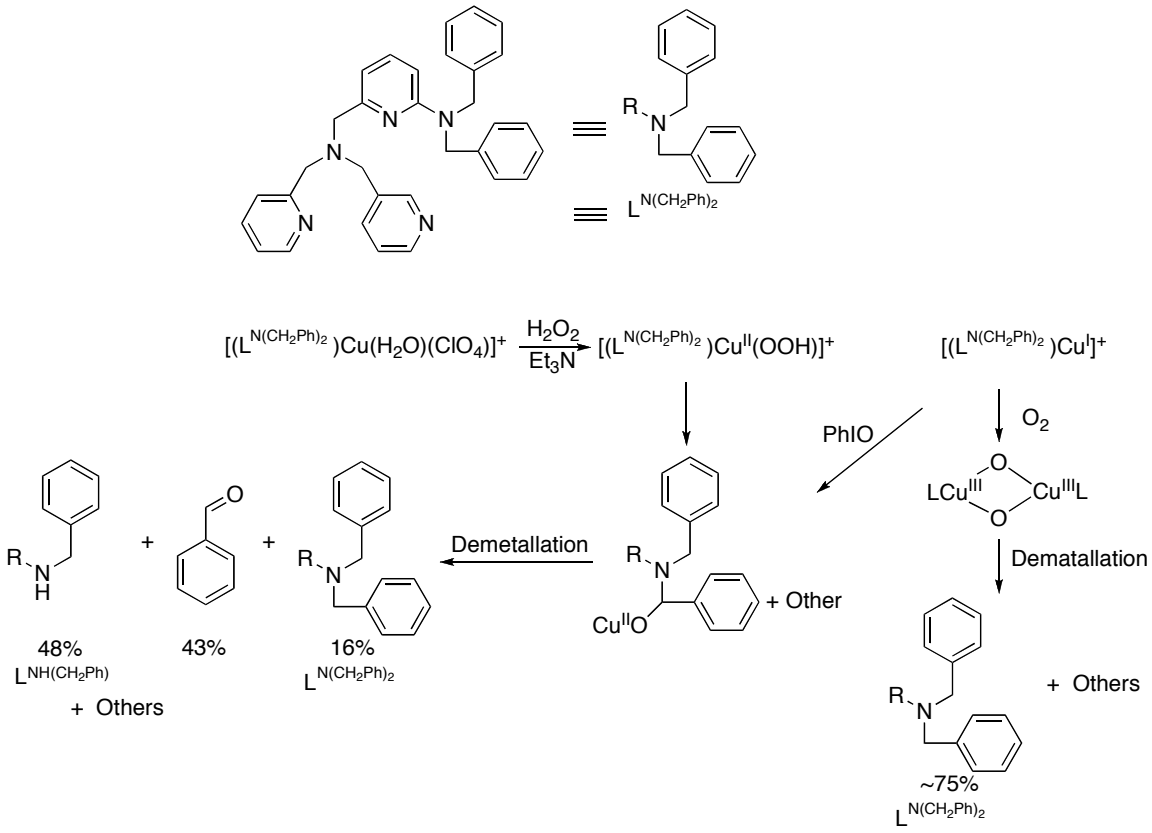

Scheme 1-12. Scheme for reactions of Cu^{I} and Cu^{II} with O_2 and H_2O_2 or PhIO, respectively.

This copper oxidative *N*-dealkylation reaction has been proposed to proceed via a N–Cα H-atom abstraction to produce an alkoxyamine intermediate.[11d,61] ESI-MS measurements on the crude reaction mixtures before removal of the Cu^{II} ions revealed the

[61] a) Shearer, J.; Zhang, C. X.; Zakharov, L. N.; Rheingold, A. L.; Karlin, K. D. "Substrate oxidation by copper-dioxygen adducts: mechanistic considerations." *J. Am. Chem. Soc*. **2005**, *127*, 5469-5483. b) Itoh, K.; Hayashi, H.; Furutachi, H.; Matsumoto, T.; Nagatomo, S.; Tosha, T.; Terada, S.; Fujinami, S.; Suzuki, M.; Kitagawa, T. "Synthesis and Reactivity of a (μ-1,1-Hydroperoxo)(μ-hydroxo)dicopper(II) Complex: Ligand Hydroxylation by a Bridging Hydroperoxo Ligand." *J. Am. Chem. Soc*. **2005**, *127*, 5212-5223.

presence of the corresponding Cu^{II}-alkoxide species, where the incorporated oxygen atom was found to come from the bound hydroperoxide. In a supplementary experiment, the authors analyzed the decayed products of the oxygenated species derived from the O_2 reaction with the Cu^{I} analogue to test whether or not the Cu^{I}/O_2 chemistry could also effect similar results. The copper(I) precursor resulted in the bis(μ-oxo)dicopper(III) species upon oxygenation, which spontaneously decayed as the temperature increased. After removing the copper ions from the decayed reaction mixtures, the organic products were analyzed. In contrast to results seen in Cu^{II}/H_2O_2 chemistry previously,[58] one of the main recovered organic products was an intact ligand along with a very small amount of oxidative *N*-dealkylated ones. Thus, this result eliminates the involvement of the $Cu^{III}_2(\mu\text{-}O)_2$ core in the observed *N*-dealkylation chemistry with the Cu^{II}-OOH systems. More interestingly, the same Cu^{II}-alkoxide species was detected by reacting Cu^{I} precursor with PhIO. Although the authors could not determine yields of the organic products from this reaction due to the experimental difficulties, they succeeded in monitoring the reaction progress using ESI-MS measurements as a function of time. At an early stage, the peak at *m/z* = 564, corresponding to a putative cupryl species, $[(L^{N(CH2Ph)2})Cu^{III}{=}O]^{+}$, was observed along with a minor Cu^{II}-alkoxide product. Theoretical fitting on these peaks predicted a ratio of cupryl to alkoxide product of 7:3. The cupryl peak completely disappeared after ~5 to 6 min, and only the alkoxide peak remained. The authors were also able to determine a kinetic isotope value (k_H/k_D) of ~1.9 based on product distributions from the reaction of the partially deuterated analogous ligand complex $[(L^{N(CH3CD3)})Cu^{I}]^{+}$ with PhIO. This value is in good agreement with the previously

determined $k_H/k_D \approx 1.9$ for the $[(L^{N(CH3CD3)})Cu^{II}(OOH)]^+$ reaction,[60] implying that both $[(L)Cu^{II}(OOH)]^+$ and $[(L)Cu^{I}]^+$/PhIO reactions proceed through a common intermediate. Taken together, all data presented above suggest that a putative Cu^{II}-oxyl reactive intermediate forms during the course of the oxidative *N*-dealkylation processes by the Cu^{II}-OOH species, but decisive direct evidence for such species remains elusive.

As described in this section, there are some precedents implicating that a mononuclear Cu^{II}-oxyl species could be involved in some oxidation reactions toward either internal or external substrates. It is interesting to note, however, that all examples shown above begin with either Cu^{II}-alkylperoxo or -hydroperoxo, that is, the Cu^{II} precursors containing the significantly preactivated O_2 moieties, which then participate in the oxidation reactions either in a concerted manner or in a stepwise fashion, with O-O bond cleavage happening prior to substrate oxidation. In the latter case, this may lead to the formation of a highly reactive Cu^{II}-oxyl species, but the existence of such species has yet to be confirmed. Thus, further studies need to be carried out to prove firmly the existence of a Cu^{II}-oxyl species.

1.5. Perspectives and Research Plans

Metalloenzymes use transition metal cofactors to effect a reductive activation of molecular oxygen for the generation of active-oxygen species.[5,11-12] In this context, PHM and DβM belong to a unique class of such enzymes, where they employ two copper ions, but O_2 activation to cleave C-H bond occurs solely at one copper site. The extensive body

of work on PHM and DβM has led to proposals that a Cu^{II}-superoxo intermediate initiates such C-H bond cleavage.[24-27] Even if this is the case, the exact nature of the C-H bond cleavage step, and the timing and mechanism of the subsequent electron transfer between two copper centers has yet to be resolved. Moreover, the recent theoretical studies[33] on these enzymes imply an alternative manifold for this process including a mononuclear $[CuO]^{1+ \text{ or } 2+}$, which is closely related with a well-studied cytochrome P450 iron-oxo oxidant.[37]

Aside from the biological studies, synthetic bioinorganic Cu/O_2 chemistry over last two decades has played a significant role in understanding fundamental coordination chemistry issues. As a result of these studies, a diverse array of copper-oxygen intermediated has been identified, with a specific emphasis on the dicopper-dioxygen complexes. In contrast, little is known about the mononuclear copper-oxygen analogues in a large part due to their intrinsic instability toward a rapid trapping reaction by a second equivalent of the Cu^{I} reagent. Nonetheless, recent advances in the ligand design has led to isolation and characterization of several such 1:1 Cu/O_2 species structurally[41-44] and/or spectroscopically.[35,40] With these results, we have began to understand their geometric, spectroscopic, and electronic properties. Yet, there are many things to be learned, in particular with respect to the structure/reactivity relationship. Although there is some indirect evidence to implicate the existence of a mononuclear Cu^{II}-oxyl species,[52-55] direct observation of such a highly reactive species has proven to be far more challenging.

Thus, the goals of my thesis research are as follows. First, I aimed to evaluate the O_2 chemistry of Cu^I complexes by using a range of supporting ligands with varing steric and electronic profiles. More specifically, within the framework of β-diketiminate ligands, I examined how changing of the electron donating character affects the overall oxygenation chemistry and the chemical and physical properties of subsequent Cu/O_2 intermediates. The results of these studies will be described in Chapter 2. The second goal was to develop new synthetic approaches toward an elusive $[CuO]^+$ species. We proposed two such routes; One is inspired by α-ketoglutarate-dependent non-heme iron enzymes, in which analogous $[Fe^{IV}=O]^{2+}$ moiety is generated by O_2-induced decarboxylation of an α-ketocarboxylate bound to Fe^{II} center in a bidentate fashion, and is generally thought to be an active species for C-H bond activation.[5b,62] If we could extend this chemistry to Cu(I) congener, we speculated that a $[CuO]^+$ or related species could be generated via a similar reaction pathway. The experimental observations and theoretical predictions resulting from this work are described in Chapter 3.

Another possible route to $[CuO]^+$ species is to treat various Cu(I) complexes with oxo-transfer reagents such as PhIO or derivatives as well as aliphatic and/or aromatic N-oxides. This route might provide a $[CuO]^+$ or related species via a heterolytic X-O bond cleavage (i.e., $XO + M^{n+} \rightarrow X + M^{n+2}=O^{2-} + X$; (M = transition metals and X = PhI or

[62] a) Abu-Omar, M. M.; Loaiza, A.; Hontzeas, N. "Reaction mechanisms of mononuclear non-heme iron oxygenases." *Chem. Rev.* **2005**. *105*. 2227-2252. b) Hausinger, R. P. "Fe(II)/α-ketoglutarate-dependent hydroxylases and related enzymes." *Crit. Rev. Biochem. Mol. Biol.* **2004**. *39*. 21–68. c) Krebs, C.; Fujimori, D. G.; Walsh, C. T.; Bollinger, J. M., Jr. "Non-Heme Fe(IV)-Oxo Intermediates." *Acc. Chem. Res.* **2007**. *40*. 484-492.

amines), as seen in a number of such reactions with copper[58,60,63] or other transition metal centers.[64] The results of these studies are discussed in Chapter 4.

[63] Reglier, M.; Amadei, E.; Tadayoni, R.; Waegell, B. "Pyridine nucleus hydroxylation with copper oxygenase models." *J. Chem. Soc., Chem. Commun*. **1989**. *8*. 447-450.

[64] Selected examples: a) Que, L., Jr. "The road to non-heme oxoferryls and beyond." *Acc. Chem. Res*. **2007**. *40*. 493-500. b) Rohde, J.-U.; In, J.-H.; Lim, M. H.; Brennessel, W. W.; Bukowski, M. R.; Stubna, A.; Münck, E.; Nam, W.; Que, L., Jr. "Crystallographic and Spectroscopic Evidence for a Nonheme Fe^{IV}=O Complex." *Science* **2003**. *299*. 1037–1039. c) Song, W.; Seo, M. S.; DeBeer George, S.; Ohta, T.; Song, R.; Kang, M.; Tosha, T.; Kitagawa, T.; Solomon, E. I.; Nam, W. "Synthesis, Characterization, and Reactivities of Manganese(V)-Oxo Porphyrin Complexes." *J. Am. Chem. Soc.* **2007**. *129*. 1268-1277. d) Rowe, G. T.; Rybak-Akimova, E, V.; Caradonna, J. P. "Unraveling the Reactive Species of a Functional Non-Heme Iron Monooxygenase Model Using Stopped-Flow UV-Vis Spectroscopy." *Inorg. Chem*. **2007**. *46*. 10594-10606. e) Qin, K.; Incarvito, C. D.; Rheingold, A. L.; Theopold, K. H. "Hydrogen Atom Abstraction by a Chromium(IV) Oxo Complex Derived from O_2." *J. Am. Chem. Soc.* **2002**. *124*. 14008-14009. f) Gross, Z.; Ini, S. "Dual Role of Pyridine N-Oxides in Ruthenium Porphyrin-Catalyzed Asymmetric Epoxidation of Olefins." *Inorg. Chem*. **1999**. *38*. 1446-1449.

CHAPTER 2. SYNTHESIS, CHARACTERIZATION, AND DIOXYGEN REACTIVITY OF ELECTRON-DEFICIENT COPPER(I) COMPLEXES

2.1. Introduction

The work described in this chapter is " reproduced with permission from Hong, S.; Hill, L. M. R.; Gupta, A. K.; Naab, B. D.; Gilroy, J. B.; Hicks, R. G.; Cramer, C. J.; Tolman, W. B. "Effects of Electron-Deficient β-Diketiminate and Formazan Supporting Ligands on Copper(I)-Mediated Dioxygen Activation." *Inorg. Chem*. **2009**, *48*, 4514-4523. Copyright [2009] American Chemical Society." As discussed in Chapter 1, both PHM and DβM enzymes utilize copper ions and O_2 to catalyze stereospecific hydroxylation of their respective substrates via an H-atom abstraction mechanism.[22-24,26,28,30,65] The exact nature of the active species responsible for such H-atom abstraction is still being debated, with one theory being that the reaction is performed by a 1:1 Cu^{II}-superoxo entity.[5] Thus, much effort in synthetic bioinorganic chemistry has focused on isolation and characterization of such species.[66] However, trapping such species so that they may be characterized by conventional spectroscopic tools or X-ray crystallography has been difficult. The basis of their scarcity is mainly due to their propensity to further react with another molecule of the Cu^{I} complex present in the solution to yield peroxo- or bis(μ-oxo)dicopper species. In some cases, 1:1 Cu/O_2 complexes have been identified as

[65] Bollinger, J. M., Jr.; Krebs, C. "Enzymatic C-H activation by metal-superoxo intermediates." *Curr. Opin. Chem. Biol.* **2007**, *11*, 151-158.
[66] Selected recent reviews: see references 5e,11d,38a,38b.

transient intermediates in low-temperature stop-flow kinetic studies of oxygenation of Cu^I complexes.[40b,e] X-ray structures of 1:1 Cu/O_2 species have been reported recently.[41-44] To sufficiently attenuate the reaction of the initially formed 1:1 Cu/O_2 species with Cu^I starting materials, sterically bulky supporting ligands have been used. For example, β-diketiminate (and anilidoimine)[44] ligands (Scheme 2-1), which are strongly electron-donating, monoanionic, and bidentate donors, have found to be useful for studying the O_2 reactivity of their Cu^I complexes. By virtue of their tunable steric and electronic profiles through variation of substituents on their carbon frameworks (R and R') and/or aromatic rings (R''), it is possible to systematically investigate how supporting ligand electronic and structural features influence the O_2 reactivity of their Cu^I complexes and the stability of the resulting Cu/O_2 species. [50,67]

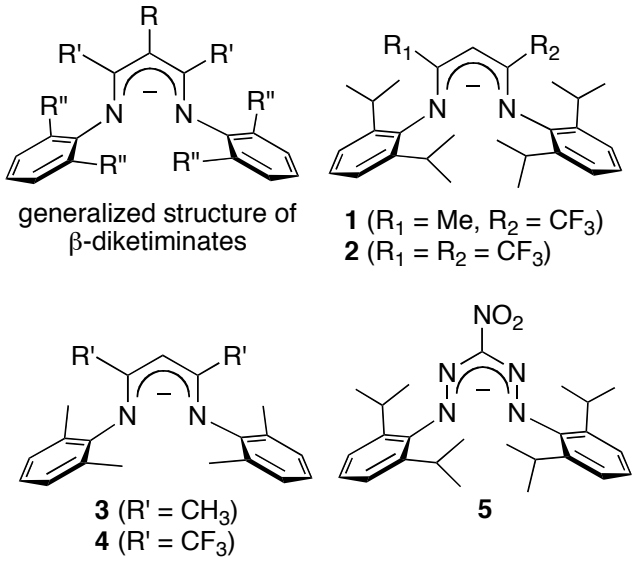

Scheme 2-1. Diketiminate and formazan ligands.

[67] Spencer, D. J. E.; Reynolds, A. M.; Holland, P. L.; Jazdzewski, B. A.; Duboc-Toia, C.; Le Pape, L.; Yokota, S.; Tachi, Y.; Itoh, S.; Tolman, W. B. "Copper Chemistry of β-Diketiminate Ligands: Monomer/Dimer Equilibria and a New Class of Bis(μ-oxo)dicopper Compounds." *Inorg. Chem*. **2002**, *41*, 6307-6321.

While Cu^{I} complexes of these ligands typically yield bis(μ-oxo)dicopper(III) species during low-temperature oxygenation,[50,67] some Cu^{I} complexes of more sterically hindered variants (R = H, R' = Me or tBu, and R'' = iPr) react with O_2 to produce side-on bound monocopper-dioxygen adducts (Scheme 2-2).[50,51]

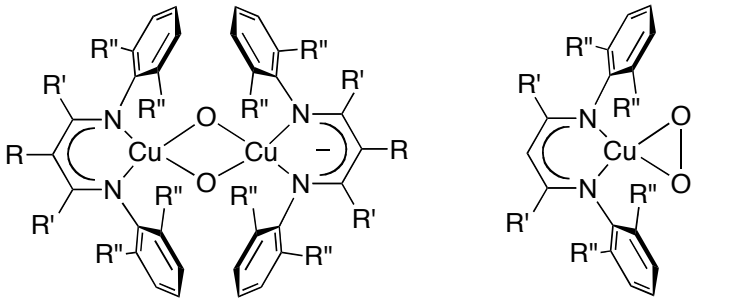

Scheme 2-2. Intermediates derived from oxygenation of copper(I) complexes of various β-diketiminate ligands.

Detailed spectroscopic and theoretical studies showed that these adducts are best described as Cu^{III}-peroxo species with unusually strong Cu-O bonds and a weakened O-O bond as a result of the powerful electron donation of the diketiminate ligands.[51,68] For instance, the Cu^{I} complex of the ligand featuring R = H, R' = Me, and R'' = iPr irreversibly reacted with O_2 at −80 °C in THF to yield a green-colored species (λ_{max} = 385 nm, ε = 2400 M^{-1} cm^{-1} and 600 nm, ε = 200 M^{-1} cm^{-1}).[50] This green species is EPR silent and has a $Cu:O_2$ uptake ratio of 1.0(2):1, as evidenced by spectrophotometric

[68] Sarangi, R.; Aboelella, N.; Fujisawa, K.; Tolman, W. B.; Hedman, B.; Hodgson, K. O.; Solomon, E. I. "X-ray Absorption Edge Spectroscopy and Computational Studies on $LCuO_2$ Species: Superoxide-Cu^{II} versus Peroxide-Cu^{III} Bonding." *J. Am. Chem. Soc.* **2006**, *128*, 8286-8296.

titration data. The resonance Raman spectrum of this species has an O-isotope sensitive band at 968 cm^{-1} that shifted by 51 cm^{-1} when $^{18}O_2$ was used. The resonance Raman data obtained by using a statistical mixture of $^{18}O_2$, $^{18}O^{16}O$, and $^{16}O_2$ show an additional single peak at 943 cm^{-1} with a line width identical to those of peaks derived from $^{16}O_2$ and $^{18}O_2$. Despite being not conclusive, in particular without information for the Cu-O stretching region, this result is indicative of a symmetric side-on (η^2) ligation of the O_2 fragment to the copper center. In later work, the side-on ligation was unambiguously confirmed by an X-ray crystal structure determination of this green species, although its structure suffered from a whole molecule disorder problem.[42]

The position of the O-isotope sensitive resonance Raman band of this green species is especially notable. The $\nu_{O\text{-}O}$ value (968 cm^{-1}) of the green species is significantly lower than those typical for metal-superoxide complexes (~1075-1295 cm^{-1}), but more similar to those seen in metal-peroxide complexes (~750-930 cm^{-1}).[69] This indicates that the bound O_2 fragment is more peroxo-like in character. This interpretation was further corroborated by X-ray absorption spectroscopy (XAS).[51,68] Cu K-edge XAS has been used as a diagnostic tool for distinguishing Cu^{II} and Cu^{III} oxidation states.[70] Cu K-edge spectra contain many complicated features that are strongly influenced by ligand environment, coordination geometry, and metal's oxidation state. Yet, a pre-edge feature, a weak, electric dipole forbidden but quadrupole-allowed 1s → 3d transition, is found to

---

[69] a) Vaska, L. "Dioxygen-Metal Complexes: Toward a Unified View." *Acc. Chem. Res.* **1976**, *9*, 175–183. b) Valentine, J. S. "The dioxygen ligand in mononuclear group VIII transition metal complexes." *Chem. Rev.* **1973**, *73*, 235–245. c) Gubelmann, M. H.; Williams, A. F. "The structure and reactivity of dioxygen complexes of the transition metals." *Struct. Bonding (Berlin, Ger.)* **1983**, *55*, 1–65.

[70] DuBois, J. L.; Mukherjee, P.; Stack, T. D. P.; Hedman, B.; Solomon, E. I.; Hodgson, K. O. "A Systematic K-edge x-ray Absorption Spectroscopic Study of Cu(III) Sites." *J. Am. Chem. Soc.* **2000**, *122*, 5775-5787.

be mainly affected by the metal's oxidation state with a minor contribution from ligand fields (LF). Consistent with expectation that increased effective nuclear charge (Z_{eff}) of a Cu^{III} ion relative to a Cu^{II} analog gives rive to higher binding energies for 1s core electrons, pre-edges for Cu^{III} complexes appear at 8981 ± 0.5 eV, which are ~ 2 eV higher in energy for Cu^{II} counterparts (8978.8 ± 0.4 eV). The pre-edge value of ~ 8980.7 eV for the green species falls into the range of Cu^{III} complexes, clearly demonstrating that the copper ion is in the +3 oxidation state. More detailed XAS studies on the green species in conjunction with DFT calculations[68] provided further insights. The Cu L-edge spectrum, in particular a strong, electric-dipole allowed 2p → 3d transition, also supported the Cu^{III} oxidation state of the green species, as evidenced by ~ 2 eV shifts of key peaks to higher energy than those typical for Cu^{II} complexes (~ 930 eV). As described above, two main contributors to this~ 2 eV higher energy shift for both pre-edge energies are the Z_{eff} of the absorbing atom (in this case, Cu ion) and the LF. To evaluate the relative contributions of these two terms to pre-edge transition energies, time-dependant (TF) DFT calculations were performed. The results indicated that while the Z_{eff} term leads to similar energy shifts in the Cu 1s, 2p, and 3d orbitals, the LF term predominantly affects the energy of the lowest unoccupied Cu 3d orbital (LUMO). That is, the stronger the ligand donors, the more the destabilization of the Cu 3d orbital. For the green species, the strongly electron donating β-diketiminate ligand makes the Z_{eff} for the Cu^{III} ion essentially the same as other Cu^{II} complexes, but results in greater destabilization of the LUMO, as supported by the shorter Cu-N distances (avg. d_{Cu-N} = ~ 1.86 Å) and larger N character (~ 18%) in the LUMO for the green species compared

with ~ 2.25 Å and ~ 12% for the side-on bound Cu(II)-superoxo analog, respectively.[41] As a result, the 1:1 Cu/O_2 adducts derived from the β-diketiminates and anilido-aniline ligands were found to be poor oxidants, as revealed by a lack of the reactivity with various potential H-atom donors including phenols.[52]

Given that the structure of the O_2-bound pre-catalytic form of the PHM contains an end-on Cu^{II}-superoxo moiety[17c] rather a side-on Cu^{III}-peroxo and the former species is thought to be responsible for the H-atom abstraction from substrate,[3e,24] we performed theoretical calculations in order to understand how changing in the electron donating power of the β-diketiminate ligands affects the reactivity of the oxygenated species.[53] The calculations predicted that the green species is very difficult both to reduce and to protonate. Accordingly, this species is not suitable for abstracting H-atoms from the substrate. Instead, the calculations indicated that use of a less electron-donating β-diketiminate ligand would increase Cu^{II}-superoxo character, leading to enhanced C-H bond activation reactivity. Moreover, an end-on Cu^{II}-superoxo isomer is predicted to be more oxidizing than the side-on analog. Finally, the calculations also predicted that the end-on Cu^{II}-superoxo isomer is only ~ 5 kcal mol^{-1} higher in energy than the side-on product, and that decreasing the electron-donating power of the diketiminate could decrease this energy gap and potentially enable isolation of the end-on Cu^{II}-superoxide form.[51,53,68]

In order to test this hypothesis experimentally, copper(I) complexes of **1** and **2** featuring CF_3 replacements for the backbone methyl groups were synthesized and

characterized.[71] These modifications were aimed to influence only the electron donating capabilities of the ligands while maintaining the steric profiles at the Cu^{I} centers. Comparisons of the structural features of $LCu(NCCH_3)$ (L = **1** and **2**) with those of the parent Cu^{I} complex support this underlying notion. All three Cu^{I} complexes show very similar structure parameters to one another. One thing to note is that the C(backbone)-N-C(aryl) angles increase by ~ 2 º on average as each backbone methyl group is replaced by a CF_3. This indicates that slightly larger steric profiles for the CF_3 substituents push the aryl ring toward the Cu center. However, the main effect of the CF_3 substituents is observed in the electronic properties of the Cu^{I} complexes. As expected, replacement of the backbone methyl group in **1** by a CF_3 group to yield **2** indeed results in a 14 cm^{-1} increase in the ν(CO) value for LCuCO and a ~300 mV increase in the $E_{1/2}$ value for $LCu(NCCH_3)$. Collectively, these findings are in line with **2** being a poorer electron donor that yields a more Lewis acidic and less readily oxidized copper(I) center.

Due to this difference in ligand electron-donating power, the dioxygen reactivity of (**1**) and (**2**)$Cu(NCCH_3)$ was found to be markedly changed. Whereas (**1**)$Cu(NCCH_3)$ yielded a side-on Cu^{III}-peroxide, no intermediate was observed for (**2**)$Cu(NCCH_3)$. For example, oxygenation of (**1**)$Cu(NCCH_3)$ in THF at −80 °C resulted in development of new features at 415 nm (sh, ε = 1700 M^{-1} cm^{-1}) and 540 nm (ε = 125 M^{-1} cm^{-1}), which bleached upon warming. The resonance Raman spectra for the oxygenated intermediate exhibited an O-isotope sensitive band at 977 cm^{-1} that shifted to 928 cm^{-1} when $^{18}O_2$ was used. The $\nu_{O\text{-}O}$ value of 977 cm^{-1} for this intermediate is higher than 968 cm^{-1} for the

[71] Hill, L. M. R.; Gherman, B. F.; Aboelella, N. W.; Cramer, C. J.; Tolman, W. B. "Electronic tuning of β-diketiminate ligands with fluorinated substituents: effects on the O2-reactivity of mononuclear Cu(I) complexes." *Dalton Trans*. **2006**, *41*, 4944-4953.

green species. This is in a good agreement with the weaker electron-donating nature of **1** relative to the parent β-diketiminate ligand, leading to decreased reduction of the O_2 ligand. However, the difference exerted by one CF_3 replacement is not big enough to significantly affect the bonding in the CuO_2 unit.

To gain further information about how additional CF_3 replacement influences the oxygenation of the copper(I) precursor and the bonding and/or geometry in the resulting CuO_2 moiety, DFT calculations were performed on these systems. For each ligand, theory predicted that the singlet state is more stable than the corresponding triplet state by 2-10 kcal/mol in both side-on (η^2) and end-on (η^1) O_2 coordination. Also, the free energy of oxygenation was predicted to increase by ~ 5 kcal/mol for each CF_3 addition to the ligand backbone. As a result, while the oxygenation for the parent ligand (–50 °C, in THF) is calculated to be exergonic by 9.9 kcal/mol, for **1** and **2** (–80 °C, in THF) the corresponding values are –5.1 and +0.4 kcal/mol, respectively. This is consistent with the failure to observe oxygenation of (**2**)Cu($NCCH_3$) experimentally. With respect to the relative energy of η^2 versus η^1 O_2 binding to the copper ion, $\Delta E(\eta^2-\eta^1)$, each CF_3 group reduces this energy gap by ~ 2 kcal/mol, with the value of –4.7 kcal/mol for the parent ligand.[51] For **2**, the end-on O_2 coordination to the copper is predicted to be almost isoenergetic with the side-on isomer ($\Delta E(\eta^2-\eta^1)$ = –0.4 kcal/mol). This is in fairly good agreement with the previous theoretical prediction (see above). In this context, a synthetic challenge is obvious. Although use of less electron-donating bidendate N-donor ligands favors the end-on O_2 ligation to the copper center over the side-on congener, it renders the overall oxygenation of the corresponding copper(I) precursor thermodynamically

unfavorable. Therefore, a balance must be achieved such that the ligand electronics result in the end-on Cu^{II}-superoxo at the expense of the side-on Cu^{III}-peroxide variant while maintaining favorable thermodynamics for O_2 binding.

We assumed that while not observed, a 1:1 Cu/O_2 adduct from oxygenation of (**2**)Cu($NCCH_3$) might be present at a low equilibrium concentration with the predicted free energy of oxygenation being only +0.4 kcal/mol. To prove this idea, we sought to trap a similar 1:1 adduct supported by **4**. We envisioned that this ligand framework would have similar electronic/redox properties to those of **2**, but by virtue of its reduced steric bulk could enable the irreversible formation of a bis(μ-oxo)dicopper(III) complex like that known for **3**.[10a] Likewise, we turned our attention to nitroformazan **5** as a potential supporting ligand analogous to the diketiminates.[72,73] Although some transition metal complexes of **5** or related ligands have been reported,[73,74] Cu^{I} variants and their oxygenation chemistry have never been explored. In addition, because of its unique properties including lower electron-donating capability and non-innocent properties,[75,76] (**5**)Cu($NCCH_3$) might result in interesting O_2 chemistry.

This Chapter describes the synthesis and characterization of copper(I) complexes of electron-deficient ligands **4** and **5**, along with the results of their low-temperature

---

[72] Gilroy, J. B.; Otieno, P. O.; Ferguson, M. J.; McDonald, R.; Hicks, R. G. "Synthesis and Characterization of 3-Cyano- and 3-Nitroformazans, Nitrogen-Rich Analogues of β-Diketimine Ligands." *Inorg. Chem*. **2008**, *47*, 1279-1286.

[73] Gilroy, J. B.; Patrick, B. O.; McDonald, R.; Hicks, R. G. "Transition Metal Complexes of 3-Cyano- and 3-Nitroformazans." *Inorg. Chem*. **2008**, *47*, 1287-1294.

[74] Gilroy, J. B.; Ferguson, M. J.; McDonald, R.; Hicks, R. G. "Synthesis and characterization of palladium complexes of 3-nitroformazans." *Inorg. Chim. Acta*. **2008**, *361*, 3388-3393.

[75] Koivisto, B. D.; Hicks, R. G. "The magnetochemistry of verdazyl radical-based materials." *Coord. Chem. Rev*. **2005**, *249*, 2612-2630.

[76] Gilroy, J. B.; Ferguson, M. J.; McDonald, R.; Patrick, B. O.; Hicks, R. G. "Formazans as β-diketiminate analogues. Structural characterization of boratatetrazines and their reduction to borataverdazyl radical anions." *Chem. Commun*. **2007**, *2*, 126-128.

oxygenation reactions and, detailed spectroscopic[77] and theoretical studies[78] on oxygenated species.

2.2. Synthesis and Characterization of Copper(I) Complexes

2.2.1. Synthesis of Copper(I) Complexes

The protonated forms of **4**[79] and **5**[72] were synthesized according to published procedures. The complexes $LCu(NCCH_3)$ (L = **4** and **5**) were prepared by reacting $[Cu_4Mes_4]$ (Mes = mesityl)[80] with the protonated ligands in CH_3CN under an inert atmosphere in good yields (75–80%) (Scheme 2-3). Analytically pure crystalline products suitable for X-ray crystallography were obtained through recrytallization either in CH_3CN (for L = **4**) or from slow diffusion of pentane into a concentrated THF solution (for L = **5**) at –20 °C. All copper(I) complexes were fully characterized by ^1H and $^{13}C\{^1H\}$ NMR spectroscopy, elemental analysis, cyclic voltammetry, UV-visible spectroscopy and single crystal X-ray crystallography, the details of which are described in the following sections.

---

[77] Resonance raman experiments were preformed by Aalo K. Gupta, and preliminary EPR data and analysis were performed by our collaborator at the Medical College of Wisconsin, Prof. William Antholine.

[78] Theoretical calculations were performed by our collaborator at the University of Minnesota, Prof. Christopher Cramer.

[79] Carey, D. T.; Cope-Eatough, E. K.; Vilaplana-Mafe, E.; Mair, F. S.; Pritchard, R. G.; Warren, J. E.; Woods, R. J. "Structures and reactions of monomeric and dimeric lithium diazapentadienyl complexes with electrophiles: synthesis of α-C,C'-dialkyl-β-diimines, and dissolution-reversible synthesis of an α-alkoxylithium-b-diimine." *Dalton Trans*. **2003**, *6*, 1083-1093.

[80] Tsuda, T.; Yazawa, T.; Watanabe, K.; Fujii, T.; Saegusa, T. "Preparation of thermally stable and soluble mesitylcopper(I) and its application in organic synthesis." *J. Org. Chem*. **1981**, *46*, 192-194.

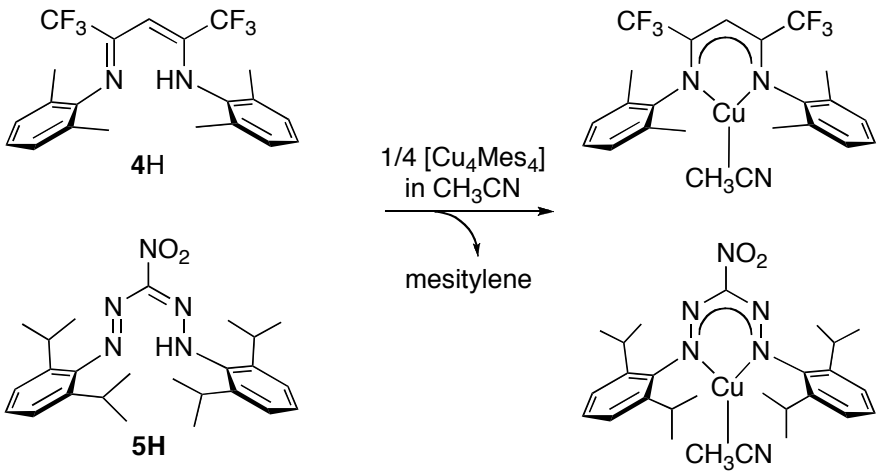

Scheme 2-3. Synthesis of $LCu(NCCH_3)$ (L = **4** and **5**).

2.2.2. Spectroscopic Characterizations

The ^1H NMR spectra of the complexes $LCu(NCCH_3)$ (L = **4** and **5**) display sharp signals that are shifted downfield relative to the protonated ligands, indicating incorporation of the copper ion into the ligands. Notably, the signals from the N-H protons of the protonated ligands shown at 12-14 ppm disappear upon complexation, and the signals from the liberated mesitylene appear in the expected regions in the crude reaction mixtures. In addition, the coordination of an acetonitrile to the copper center is evident from a singlet at 0.20 ppm for the methyl hydrogens.

As depicted in Figure 2-1, the visible region of the electronic absorption spectrum for (**4**)$Cu(NCCH_3)$ in THF at ambient temperature displays a weak band around 500 nm (ε = 460 M^{-1} cm^{-1}) and strong bands at 280 nm (ε = 18900 M^{-1} cm^{-1}) and 381 nm (ε = 16600 M^{-1} cm^{-1}). Although the origin of the former band is not clear at this point, it appears to be related to the unique eletronic/structural properties of **4**, because this band

is absent in other copper(I) complexes of β-diketiminate ligands (R = H, R' = CH_3 or tBu) (see Scheme 2-1 for ligand structure).[50-51,67] However, the latter bands are commonly seen in Cu^I complexes of β-diketiminates. [50-51,67] These features have been assigned as ligand-based π–π^* transitions on the basis of their energy, intensity, and sensitivity to the electronic properties of a central methine β-diketiminate backbone substituent (R). For example, the bands appearing in the range of 340 – 381 nm with intensity over 19000 M^{-1} cm^{-1} were found to be blue-shifted as R became more electron-withdrawing. Thus, for (**4**)Cu($NCCH_3$) the bands below 400 nm appear to have the same origin.

Formazans are intensely colored owing to strong charge-transfer transitions in the visible region involving the formazan backbone and the N-aryl substituents.[72,73] Upon complexation with transition metal ions, these low energy bands tend to be red-shifted relative to the corresponding protonated ligands, due to increased delocalization within the formazan backbone associated with fixed conformation of the formazanato anion. This is also the case for (**5**)Cu($NCCH_3$), which exhibits three major absorption features at 352, 410 and 650 nm. These bands are significantly red-shifted compared to those (334, 398 and 532 nm) of the protonated 3-nitroformazan ligand. This observation is also indicative of incorporation of the copper ion into the ligand framework.

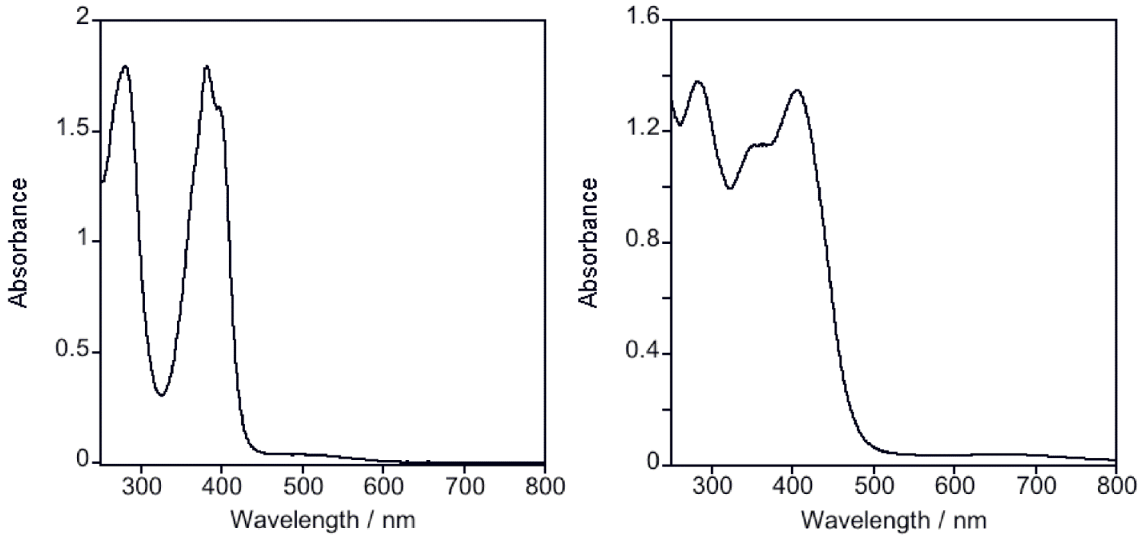

Figure 2-1. UV-vis spectra of (left) (**4**)Cu($NCCH_3$) and (right) (**5**)Cu($NCCH_3$) in THF at ambient temperature, using concentration of 0.1 mM.

2.2.3. X-ray Crystallography

The X-ray crystal structures of LCu($NCCH_3$) (L = **4** or **5**) are shown in Figure 2-2. For (**5**)Cu($NCCH_3$), its low-quality crystal led to a weak diffraction data set. Moreover, the diffraction patterns indicated that the crystal either contains multiple fragments or might be twinned. However, we could not find any appropriate twin law to model the structure. Instead, the best solution for this compound was obtained by using only the most intense diffraction data. Consequently, the final structure contains many disorder problems that we could not refine. Nonetheless, its structure unambiguously shows the atomic connectivities within this molecule, but analysis of interatomic distances and angles for (**5**)Cu($NCCH_3$) can only be deemed approximate.

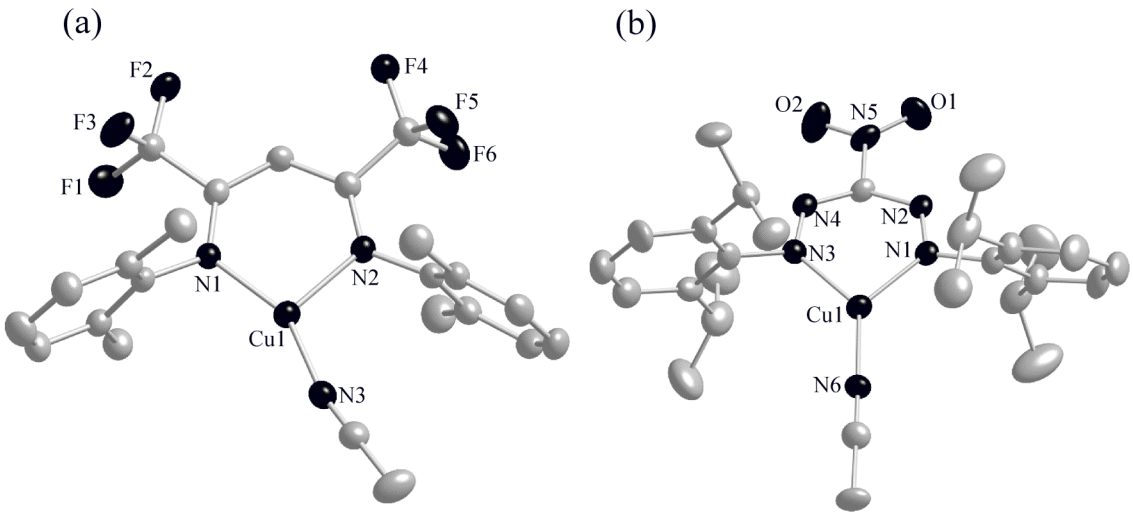

Figure 2-2. Representation of the X-ray crystal structures of (a) (**4**)Cu($NCCH_3$) and (b) (**5**)Cu($NCCH_3$). For **5**, only one of two molecules in an asymmetric unit is given. All non-hydrogen atoms are shown as 50 % thermal ellipsoids. Hydrogen atoms are omitted for clarity.

Table 2-1. Selected bond lengths (Å) and angles (deg)[a] for LCu($NCCH_3$) (L = **4** or **5**).

(**4**)Cu(CH_3CN)		(**5**)Cu(CH_3CN)[b]	
Cu1-N1	1.902(2)	Cu1-N1	1.943(5)
Cu1-N2	1.998(2)	Cu1-N3	1.953(6)
Cu1-N3	1.871(2)	Cu1-N6	1.877(8)
N1-Cu1-N2	99.01(9)	N1-Cu1-N3	93.0(2)
N1-Cu1-N3	148.46(9)	N1-Cu1-N6	132.7(3)
N2-Cu1-N3	111.57(9)	N3-Cu1-N6	134.0(3)

[a]Estimated standard deviations are given in parentheses. [b]Data for only one of two molecules in an asymmetric unit is given.

Both compounds exhibit three coordinate Cu^I ions and gross structural features

similar to other known Cu^{I} complexes with β-diketiminate ligands.[50-51,67] In (**4**)Cu($NCCH_3$), the Cu^{I} ion adopts a geometry close to T-shaped, with divergent Cu-N (diketiminate) distances of 1.902(2) and 1.998(2) Å. This asymmetry in Cu-N bonds seems to be largely due to a crystal packing effect, because the analogous copper(I) complex of **2** has symmetric Cu-N distances of ~ 1.94 Å.[71] Even with **1**, the asymmetry of the ligand backbone does not translate into significant asymmetric coordination of the diketiminate nitrogen donors to the copper center (1.9431 vs 1.9307 Å). The C(backbone)-N-C(aryl) angles in (**4**)Cu($NCCH_3$) (122-125°) are wider than those in the copper complex of the analogue **3** (116-120°).[67] This trend is also seen in the copper(I) complexes of **1** and **2**, as described above. We hypothesize that this angle widening is due to steric pressure from the CF_3 groups that place the aryl substituents closer to the bound metal ion. The effect has important implications in reactivity studies (see below).

Although analysis of bond distances and angles for (**5**)Cu($NCCH_3$) should be done with caution due to the reasons discussed above, we can say that the values lie in the range of other Cu^{I} complexes with β-diketiminate ligands.[50-51,67] In contrast to (**4**)Cu($NCCH_3$), the complex with **5** shows more symmetrical binding of the formazanato nitrogens to the copper center, leading to a coordination geometry close to Y-shaped. Because the formazanato ligand does not have substituents on the N2 and N4 atoms, the copper complex has smaller angles of N2-N1-C_{aryl} and N4-N3-C_{aryl} of 109 and 110°, notwithstanding the fact that this ligand contains the more bulky 2,6-diisopropyl substituted phenyl rings.

2.2.4. CO Binding and Electrochemistry

In order to obtain information concerning the relative degree of electron donating ability to the copper(I) ion as a function of ligand set, we synthesized Cu^{I}-CO adducts by bubbling CO gas into solutions of the copper(I) complexes either in C_6D_6 or in THF. Although we could not observe the peak corresponding to the CO in $^{13}C\{^{1}H\}$ spectra for both CO adducts in C_6D_6, the ^{1}H NMR spectra clearly show complete loss of the signals from the coordinated acetonitrile, indicating the replacement of the solvent molecule with CO. The coordination of CO to the copper center was further corroborated by FT-IR spectra of the CO adducts prepared *in-situ* in THF (Figure 2-3).

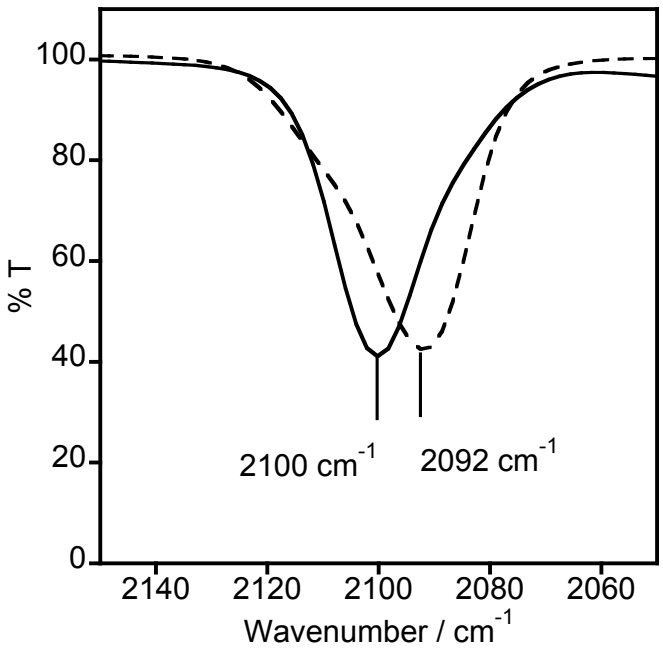

Figure 2-3. FT-IR spectra of LCu(CO) adducts (L = **4** or **5**) in THF at ambient temperature. Solid line for (**4**)Cu(CO) and dashed line for (**5**)Cu(CO).

Both CO adducts display strong peaks around 2100 cm^{-1} corresponding to the CO stretching vibrations. In general, the CO stretching frequency of metal carbonyl adducts serves as a good measure of relative electron density at a metal site. It also provides information of the donor properties of the supporting ligand coordinated to a metal ion. Thus, the ν(CO) value decreases as the electron density at the metal center increases as a result of the presence of a greater electron donating ligand, in turn due to the stronger π-back-bonding interaction effected through the metal center that weakens the CO bond. It was demonstrated[18] that displacement of a backbone methyl group in **1** by a CF_3 group to yield **2** increases the CO stretching frequency by ~ 13 cm^{-1} for LCu(CO). A similar effect is evident from the ν(CO) values for the complexes of **4** and **5** (see Table 2-2). For **2** and **4**, both ligands have two backbone CF_3 groups, and they exhibit almost identical ν(CO) values of 2097 cm^{-1} and 2100 cm^{-1} for their copper(I) carbonyl complexes, respectively, despite their aryl substituents being different (iPr vs Me). This implies analogous electron-donating properties for these two ligands. Similarly, the electron donating ability of **5** appears to be in the range of **2** and **4**.

To further support this result, gas-phase theoretical values of the CO stretching frequencies for all Cu^{I}-CO adducts were calculated at the *m*PW level after correction by 19 cm^{-1}, which is the difference between *m*PW and experiment for CO gas. The calculated values show a similar trend (8 cm^{-1} increment per CF_3 group) going from **1** to **2**. The analogous trend can also be applied to the complexes of **3** and **4** if we assume that each CF_3 replacement has an equal contribution to the shift of the ν(CO) value (9 cm^{-1}

increment per CF_3 group). Thus, these results reflect the degree to which the ligand influences the molecular electronic structure.

Table 2-2. Properties of Copper(I) complexes of Diketiminate and Formazan Ligands.

ligand	ν (CO)		$E_{1/2}$ (mV)
	exptl (cm^{-1})	calcd (cm^{-1})[a]	
1	2083	2074	110
2	2097	2082	411
3	2071	2070	b
4	2100	2088	134
5	2092	2084	103

[a] Computed values for copper(I) carbonyl complexes at the *m*PW level after correction by 19 cm^{-1}, which is the difference between *m*PW and experiment for CO gas. [b] Value reported previously but under different conditions than those used in this work (CH_3CN solvent), and this fact along with previously noted complications with reproducibility for this complex makes comparison of the ν(CO) values more useful for drawing comparisons among the complexes listed.[67]

To further probe the effects of **4** and **5** on the redox properties of their copper(I) complexes, we performed electrochemistry experiments. Cyclic voltammograms (see Figure 2-4) of THF solutions of $LCu(NCCH_3)$ (L = **4** or **5**) with $TBAPF_6$ (0.3 M, TBA = tetrabutylammonium) at ambient condition exhibited pseudoreversible waves with $E_{1/2}$ values of + 134 mV (**4**) and + 103 mV (**5**) versus Fc/Fc^+ ($\Delta E_{p,c}$ = 118 and 112 mV, respectively, at a scan rate of 20 mV s^{-1}). These values are compared to data for related compounds obtained under similar conditions in Table 2-2. As noted previously, the CF_3 group increases the $E_{1/2}$ value for $LCu(NCCH_3)$ (L = **1** or **2**) by ~ 300 mV. However, the

$E_{1/2}$ value of (**4**)Cu(NCCH$_3$) is 277 mV lower than that for (**2**)Cu(NCCH$_3$). This result contradicts the conclusions based on the ν(CO) values.

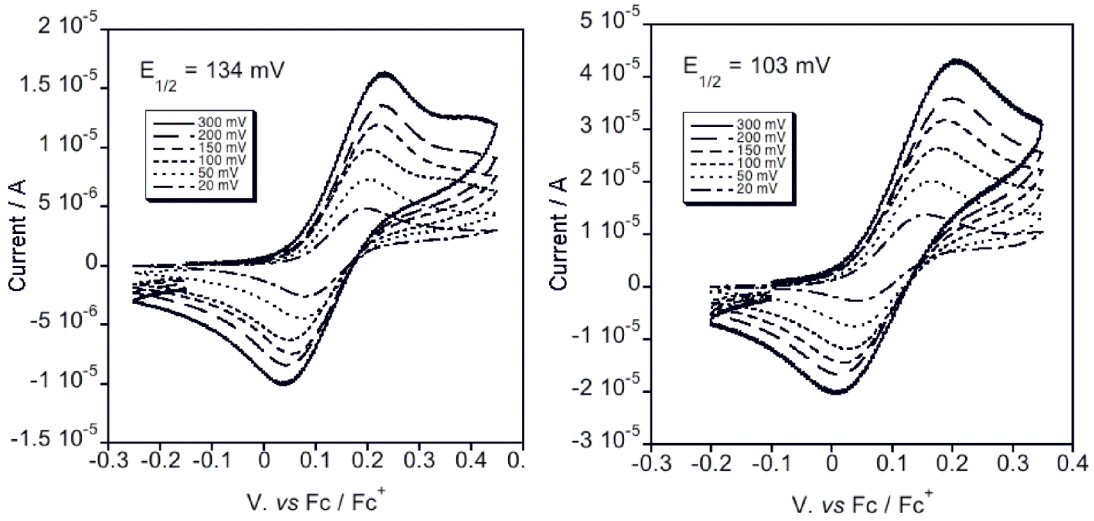

Figure 2-4. Cyclic voltammograms recorded for (left) (**4**)Cu(NCCH$_3$) and (right) (**5**)Cu(NCCH$_3$) using Pt working and auxiliary electrodes, a Ag wire/AgNO$_3$ (10 mM in CH$_3$CN) reference electrode, and a BAS Epsilon potentiostat connected to a 22 mL cell in an inert-atmosphere glovebox. Experiments were performed using analyte concentrations of 1 mM in THF with 0.3 M Bu$_4$NPF$_6$ (sample volumes of ~5 mL) at room temperature. The ferrocene/ferrocenium couple was recorded for reference. The scan rates were varied from 20-300 mV s^{-1} (see insets).

This apparent discrepancy between ν(CO) and $E_{1/2}$ values for the complexes of **2** and **4** can be explained by two possible effects of differing aryl substituents. One is the greater hydrophobicity of the diisopropylphenyl group in **2** compared to the dimethylphenyl group in **4**. For **2**, this effect would result in the relative destabilization of the more highly charged Cu^{II} species, which in turn would increase the $E_{1/2}$ value. Another effect is mainly steric; while the copper(I) complex of the more sterically hindered **2** likely remains three coordinate upon oxidation, the smaller steric profile for **4** could enable binding of two (or more) solvent molecules upon oxidation of its copper(I) complex, resulting in enhanced

stability for the copper(II) state and a smaller $E_{1/2}$ value. Thus, these hydrophobic and steric influences often make use of the $E_{1/2}$ values as markers for the relative electron density at the metal center problematic. On the contrary, these effects do not perturb the ν(CO) values significantly, as evidenced by the similar ν(CO) values for **2** and **4**. In this regard, we view the ν(CO) values as more reliable indicators for the purpose of comparisons of the relative Lewis acidity at the metal center. Thus, on the basis of the ν(CO) data, the nitroformazan **5**, and diketiminates **2** and **4** have similar electron-donating characteristics.

2.3. Dioxygen Reactivity of Copper(I) Complexes

2.3.1 Oxygenation of Copper(I) Complexes at Room Temperature

One of the main goal of my work is to address how the steric profile of the ligands (**4** and **5**) having similar electronic characteristics with **2** could affect the overall oxygenation processes of their copper(I) complexes. As mentioned previously, the copper(I) complex of **2** was found to be inert toward dioxygen over a wide temperature range (from –80 to 25 °C) (*vide supra*). Thus, in order to test effects of the steric profiles of **4** and **5** on the O_2 chemistry of their copper(I) compounds, we first performed the oxygenations for $LCu(NCCH_3)$ (L = **4** and **5**) at ambient temperature. Both copper(I) complexes in THF readily reacted with O_2 at room temperature to yield red-brown solutions, from which $L_2Cu_2(OH)_2$ could be isolated as crystalline solids in modest yield (40-44%). These compounds were characterized by elemental analysis and X-ray crystallography.

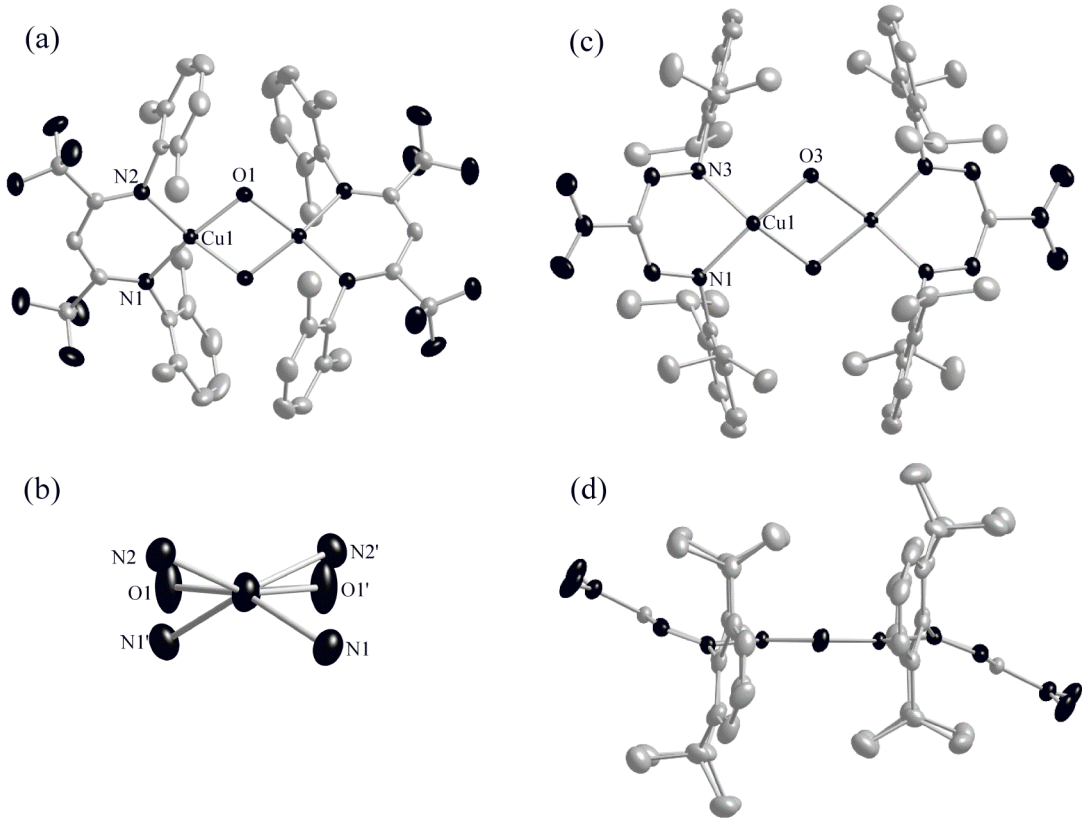

Figure 2-5. Representation of the X-ray structures with all non-hydrogen atoms shown as 50% thermal ellipsoids. (a) For (**4**)$_2$Cu$_2$(OH)$_2$. (b) View along Cu-Cu vector; C and F atoms are omitted for clarity. (c) For (**5**)$_2$Cu$_2$(OH)$_2$; three THF molecules are omitted for clarity. (d) Alternative view by rotating (c) by 90°.

Table 2-3. Selected bond lengths (Å) and angles (deg).

(**4**)$_2$Cu$_2$(OH)$_2$		(**5**)$_2$Cu$_2$(OH)$_2$	
Cu1-O1	1.9121(18)	Cu1-O3	1.9179(13)
Cu1-O1’	1.9105(18)	Cu1-O3’	1.9294(13)
Cu1-N1	1.943(2)	Cu1-N1	1.9519(15)
Cu1-N2	1.940(2)	Cu1-N3	1.9646(15)
Cu1-Cu1’	3.0195(6)	Cu1-Cu1’	3.0278(5)
O1-Cu1-O1’	75.44(9)	O3-Cu1-O3’	76.19(6)
O1-Cu1-N1	157.40(9)	O3-Cu1-N1	172.51(6)
O1-Cu1-N2	97.82(8)	O3-Cu1-N3	98.50(6)
O1’-Cu-N1	97.93(8)	O3’-Cu-N1	96.95(6)
O1’-Cu1-N2	159.07(9)	O3’-Cu1-N3	173.05(6)
N1-Cu1-N2	95.28(8)	N1-Cu1-N3	88.09(6)
		Cu1-O3-Cu1’	103.81(6)

The crystal structures of $L_2Cu_2(OH)_2$ (L = **4** and **5**) are depited in Figure 2-5. In (**4**)$_2$Cu$_2$(OH)$_2$, two copper ions with a Cu-Cu distance of 3.0915(6) Å adopt distorted square planar geometries with N_2O_2 donor atoms characterized by a τ_4 value of 0.31, where $\tau_4 = 0$ is for the perfect square planar and $\tau_4 = 1.00$ for the prefect tetrahedral

geometries.[81] Like (**4**)Cu($NCCH_3$), canting of the aryl rings toward the coordinated Cu ion by the CF_3 groups is also evident by C(backbone)-N-C(aryl) angles of almost 123°. This effect causes a large structural distortion of the metal ions in $(\mathbf{4})_2Cu_2(OH)_2$ toward the tetragonal geometries. For comparison, the analog derived from **3**, featuring two backbone methyl groups,[82] displays an almost perfect square planar geometry within the $N_4O_4Cu_2$ core. That is, twisting of the ligand planes with respect to each other seemingly helps to minimize unfavorable steric repulsions between the two aryl groups. This is evident from a relative large dihedral angle between the N atoms (N1-Cu1-N2/N1'-Cu1'-N2') of 56.31°.

In contrast, the structure of $(\mathbf{5})_2Cu_2(OH)_2$ shows a planar $N_4O_4Cu_2$ core, with a Cu-Cu distance of 3.0278(5) Å. Each copper ion adapts a square pyramidal geometry with an additional oxygen atom from the coordinated THF solvent located at an axial position. In this case, interligand interactions are minimized by two factors; the first is through a canting of the ligand backbones away from the plane of the core by ~27° (Figure 2-4(d)). The second factor is the lack of substituents on the N atoms adjacent to the ligated N atoms that results in small N-N-C(aryl) angles of ~112° and a decreased steric profile for the formazan, notwithstanding the presence of the isopropyl substituents on the aryl rings. The formazancopper metallocycle appears as a boatlike conformation because of displacement of the central C atom and the Cu atom away from the plane defined by the formazan N atoms. Similar conformational properties have been seen for

---

[81] Yang, L.; Powell, D. R.; Houser, R. P. "Structural variation in copper(I) complexes with pyridylmethylamide ligands: structural analysis with a new four-coordinate geometry index, τ_4." *Dalton Trans*. **2007**, *9*, 955-964.

[82] Dai, X.; Warren, T. H. "Dioxygen activation by a neutral β-diketiminato copper(I) ethylene complex." *Chem. Commun*. **2001**, *19*, 1998-1999.

related formazan complexes.[72-73,75]

The formation of bis(μ-hydroxo)dicopper(II) compounds upon oxygenation of $LCu(NCCH_3)$ (L = **4** and **5**) at room temperature is remarkable, given the lack of the O_2 reactivity of the copper(I) complex of **2** that features similar electronic properties to those of **4** and **5**. As noted previously, theory predicts that the oxygenation of (**2**)$Cu(NCCH_3)$ at –80 °C is slightly endergonic by 0.4 kcal/mol. The fact that this compound does not react with O_2 even at room temperature is puzzling. We initially speculated that the oxygenation of (**2**)$Cu(CH_3CN)$ yields a very small amount of a 1:1 Cu/O_2 adduct. However, **4** and **5** enable a similar 1:1 Cu/O_2 to further react with another molecule of the copper(I) precursor to generate dicopper-dioxygen species by virtue of their reduced steric profiles. This second reaction might drive the overall reaction downhill, even though the formation of a 1:1 Cu/O_2 adduct is endorgonic.

2.3.2 Oxygenation of Copper(I) Complexes at Low Temperature

To prove the hypothesis described above and to identify the dicopper-dioxygen species that is presumably an intermediacy on the path to the bis(hydroxo)dicopper(II) final product, we performed the oxygenation of $LCu(NCCH_3)$ (L = **4** and **5**) in THF at – 80 °C. Upon oxygenation, new strong absorption features in the UV-vis spectra were observed (Figure 2-6). These features remained unchanged upon removal of excess O_2 by purging with Ar, but completely disappeared upon warming. These results indicated the irreversible oxygenation of $LCu(NCCH_3)$ to form thermally sensitive intermediates. Importantly, the UV-vis spectra of the final decayed products are almost identical with those obtained by the room-temperature oxygenation (data not shown), suggesting that the low-temperature

oxygenated intermediates decay via as-yet defined pathways to form the same bis(μ-hydroxo)dicopper(II) compounds. The most prominent peaks of the oxygenated species appear at 470 nm (ε ~ 15 000 M^{-1} cm^{-1}, **4**) and 525 nm (ε ~ 23 000 M^{-1} cm^{-1}, **5**). The high intensity of these two bands is indicative of charge-transfer (CT) transitions associated with Cu/O_2 intermediates.[5e,11d,38a-b] For example, bis(μ-oxo)dicopper(III) species typically have two strong absorption bands at 300 – 330 nm (ε ~ 10 000 to 20 000 M^{-1} cm^{-1}) and 400 – 450 nm (ε ~ 10 000 to 30 000 M^{-1} cm^{-1}), while μ-η^2:η^2-peroxodicopper(II) species exhibit a high-energy CT band at ~ 340 – 380 nm (ε ~ 18 000 to 20 000 M^{-1} cm^{-1}) and a lower energy band at ~ 510 – 550 nm (ε ~ 1000 M^{-1} cm^{-1}).[83] The spectroscopic features of the intermediates formed resemble those of the bis(μ-oxo)dicopper(III) species, althought the band position for the complex derived from **5** is significantly red-shifted relative to that typically observed. Spectrophotometric titrations results also confirmed the requisite 2:1 Cu/O_2 stoichiometry (insets to plots in Figure 2-6).

[83] Henson, M. J.; Mukherjee, P.; Root, D. E.; Stack, T. D. P.; Solomon, E. I. "Spectroscopic and Electronic Structural Studies of the $Cu(III)_2$ Bis-μ-oxo Core and Its Relation to the Side-On Peroxo-Bridged Dimer." *J. Am. Chem. Soc*. **1999**. *121*. 10332-10345.

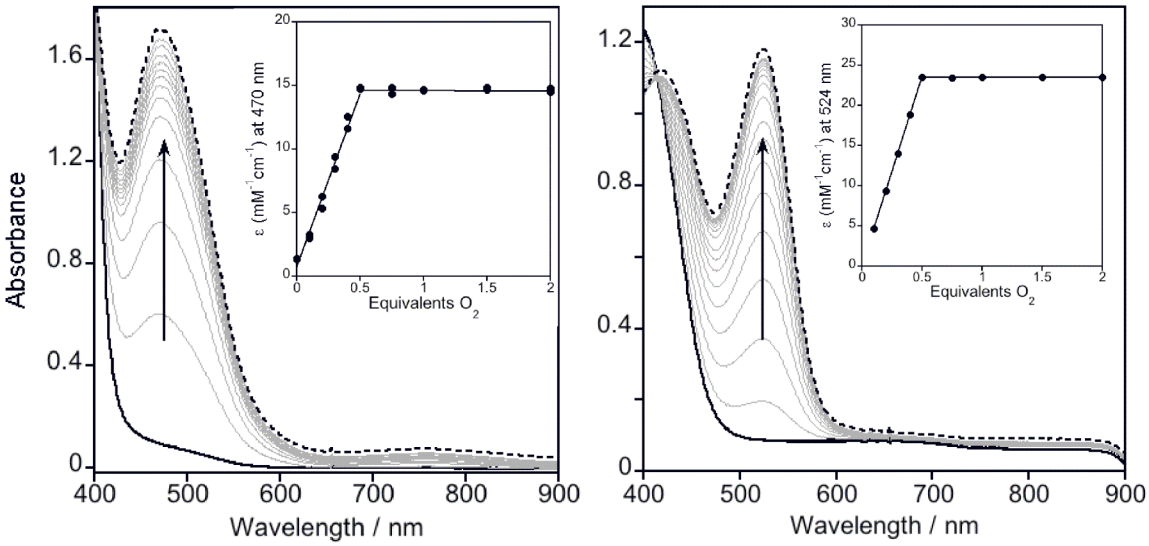

Figure 2-6. UV-vis changes accompanying oxygenation of (left) (**4**)Cu(NCCH$_3$) and (right) (**5**)Cu(NCCH$_3$) at -80 °C in THF, using starting concentrations of 0.2 mM and 0.1 mM, respectively. The initial and final spectra are in solid and dotted line, respectively. The insets show the results of spectrophotometric titrations of the complexes with O_2 as linear fits to (left) data for two replicate runs or (right) average data from three replicate runs.

In order to provide further insight into the nature of the intermediates formed, we performed resonance Raman (rR) spectroscopy experiments on samples prepared using $^{16}O_2$ and $^{18}O_2$ with excitation wavelengths of 457.9 nm (**4**) or 514.5 nm (**5**). For (**4**)Cu(NCCH$_3$), the rR data show two peaks at 598 and 610 cm^{-1} that are replaced by a single peak at 566 cm^{-1} when $^{18}O_2$ is used. The two peaks shown with $^{16}O_2$ are likely ascribed to a Fermi doublet associated with a symmetric vibration of a Cu_2O_2 core that converts into a single peak with $^{18}O_2$. This pattern has been seen previously for other known bis(μ-oxo)dicopper species.[83,84] Although detailed analysis of rR data for

[84] Holland, P. L.; Cramer, C. J.; Wilkinson, E. C.; Mahapatra, S.; Rodgers, K. R.; Itoh, S.; Taki, M.; Fukuzumi, S.; Que, L., Jr.; Tolman, W. B. "Resonance Raman spectroscopy as a probe of the bis(μ-oxo)dicopper core." *J. Am. Chem. Soc.* **2000**. *122*. 792-802.

(**5**)Cu($NCCH_3$) is complicated due to an additional overlapping peak at 581 nm, the oxygenated product exhibits a peak at 581 nm that is shifted to 558 nm with $^{18}O_2$. In addition, the frequency-doubled overtone bands associated with these primary peaks are observed as shown in the inset to Figure 2-7(b). These resonance Raman spectra for both oxygenated species fall in the range of those typical of bis(μ-oxo)dicopper species ($\nu_{(O-O)}$ ~ 600 cm^{-1} and $\Delta\ ^{18}O_2$ ~ 28 cm^{-1}). Furthermore, both oxygenated species are EPR silent. The combined data for both cases **4** and **5** are consistent with the assignment of the 470 and 525nm transitions, respectively, as CT transitions involving bis(μ-oxo)dicopper cores.

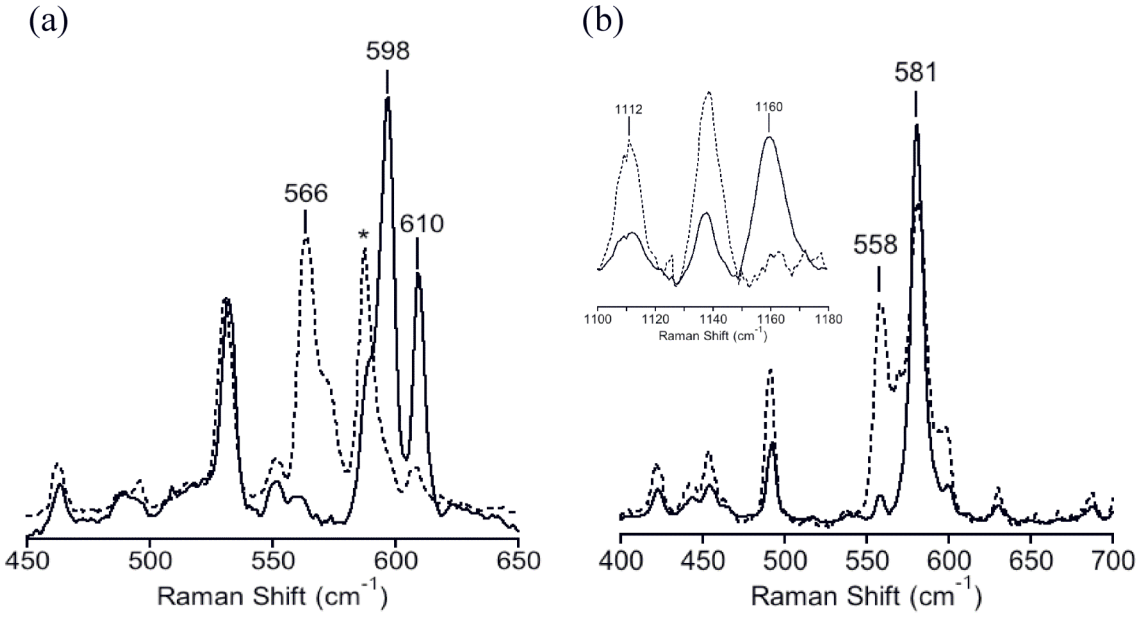

Figure 2-7. rR spectra of the frozen solutions resulting from oxygenations of (a) (**4**)Cu($NCCH_3$) (40 mM) (λ_{ex} = 457.9 nm, 77 K) and (b) (**5**)Cu($NCCH_3$) (10 mM) (λ_{ex} = 514.5 nm, 77 K) in THF at – 80 °C, using $^{16}O_2$ (solid line) or $^{18}O_2$ (dashed line). The inset to plot (b) shows overtone bands.

2.4. Computational Evaluation of Oxygenation Reactions

As noted in the structural descriptions of copper(I) complexes of **4** or **5** and their room temperature oxygenated bis(μ-hydroxo)dicopper(II) species, DFT calculations at the *m*PW level of theory were performed by Prof. Christopher Cramer in order to address how subtle changes of the steric profiles for the supporting ligands (**3** *vs* **4** or **5**) can influence the oxygenation reaction and to gain additional insight into the structural and spectroscopic characteristics of the bis(μ-oxo)dicopper(III) species ligated by **4** and **5**. One of he key findings was that the computed energy-minimized geometries of the bis(μ-oxo)dicopper(III) species of **4** and **5** share the overall structural characteristics shown in the crystal structures of bis(μ-hydroxo)dicopper(II) species, except for shorter Cu-Cu (2.860 Å for **4** and 2.783 Å for **5**) and Cu-O distances (1.832 Å for **4**, and 1.829 and 1.833 Å for **5**). As seen in the crystal structures in Figure 2-2 and 2-5, the lack of substituents at the N_2 and N_4 atoms of formazan underly the shorter Cu-Cu distance in the complex of **5** compared to that of **4**. This effect becomes clear when the $CuNC_{ipso}$ angles for the computed [LCu(CO)] species are compared to each other; in **4** this angle is predicted to be 115.5°, but the corresponding angle in **5** is predicted to increase to 120.6°.

Another key finding is that the effect of the electron donating or withdrawing groups in the ligands on the geometrical parameters of the Cu_2O_2 rhomb structures is negligible. That is, the Cu-Cu (2.836 Å) and Cu-O (1.831 Å) distances of the bis(μ−oxo)dicopper(III) complex of **3**, which contains two backbone CH_3 groups instead of CF_3 ones, are predicted at the *m*PW1 level to be quite similar to those for the bis(μ−oxo)dicopper(III) of **4**. This observation is further supported by the experimental

and computed resonance Raman data (Table 2-4). The experimentally observed breathing frequencies of the bis(μ-oxo)dicopper(III) complex of **3** and **4** differ by only 4 cm^{-1} (608 cm^{-1} and $\Delta^{18}O_2$ = 27 cm^{-1} for the complex of **3** and 604 cm^{-1} in that of **4** given that the pair of peaks at 598 and 610 cm^{-1} result from a Fermi resonance). This experimental observation also agrees with theory in that the fundamental core frequency for the bis(μ-oxo)dicopper(III) complex of **4** is only 5 cm^{-1} smaller than that of **3** with an almost identical isotope shift. For the complex of **5**, the corresponding frequency is predicted to strongly couple with aryl bending and formazan modes, which make its assignment more difficult. However, one such frequency is predicted to occur at 608 cm^{-1} ($\Delta^{18}O_2$ = 20 cm^{-1}), keeping in mind that the analysis in this case is more tentative.

Table 2-4. Experimental and computed[a] rR data.

$[L_2Cu_2(O)_2]$	Experimental value		Computed value	
	$^{16}O_2$ (cm^{-1})	$\Delta[^{18}O_2]$ (cm^{-1})	$^{16}O_2$ (cm^{-1})	$\Delta[^{18}O_2]$ (cm^{-1})
3[b]	608	27	582	24
4	598 and 610		577	25
5	581	23	565	20

[a] at the *m*PW level of theory. [b] see ref 67.

We also calculate energetics for the following reaction, which may provide information about the differential stability of the bis(μ-oxo)dicopper(III) complexes derived from **2, 4** and **5**.

$$2[LCu(CO)] + O_2 \rightarrow [L_2Cu_2(O)_2] + 2CO$$

The computed 298K free energies of this reaction at the *m*PW level are predicted to be 25.4 and 9.9 kcal mol^{-1} for L = **4** and **5**, respectively. This result clearly indicates that the bis(μ-oxo)dicopper(III) complex of **5** is much stable than that of **4**, which may result from the reduced steric clash between aryl rings in the former, as noted above. The corresponding value with **2** is predicted to be even larger (45.6 kcal mol^{-1}), as expected from the much more unfavorable steric interactions from the isopropyl substituted phenyl rings. This result also supports the failure to experimentally observe the formation of the bis(μ-oxo)dicopper(III) complex with **2**.[71]

The bis(μ-oxo)dicopper(III) complex of **4** and **5** displayed an unusually red-shifted CT absorption. Thus, we performed time-dependant DFT (TD-DFT) calculations using B3LYP to understand the nature of the longest wavelength absorptions in these species. In the case of the complex with **4**, TD B3LYP predicts there to be only a single excitation having significant oscillator strength at low energy, and the wavelength of the transition is predicted to be 540 nm. This prediction is well to the red of the experimentally observed value, which is typical of charge-transfer excitations with TD

B3LYP.[85] The transition itself is computed to be an excitation out of the antibonding π* orbital formed from the out-of-plane O $2p_z$ orbitals (sometimes called the π_v* orbital) into an antibonding combination of Cu d_{xy} orbitals and the σ_u* orbital formed by the antibonding combination of the O $2p_y$ orbitals along the O–O axis (Figure 2-8a). This excitation is exactly the same as that predicted by Estiú and Zerner, at the INDO/S level, to occur at lowest energy for a bis(μ-oxo)dicopper core supported by three imidazole ligands per copper atom.[86] In the case of the complex with **4**, the donor orbital is predicted also to be substantially delocalized onto the diketiminate aryl rings, but the core contribution is dominated by the O–O π_v*.

The most intense low-energy absorption for the bis(μ-oxo)dicopper complex with **5**, on the other hand, is predicted to occur at 548 nm at the TD B3LYP level, and involves excitation from an occupied orbital comprised of the O $2p_y$ σ_u* orbital and formazan in-plane ligand orbitals into the π_σ* orbital that is formed as an antibonding combination of the Cu d_{xy} orbitals and the O $2p_x$ π* orbital (Figure 2-8b). This acceptor orbital also has a significant formazan π* component. The excitation is very similar to that proposed by Henson et al. based on SCF-Xa-SW calculations for the lowest-energy excitation in a bis(μ-oxo)dicopper core supported by two ammonia ligands per copper.[25] In the case considered by Henson et al., however, there was substantial contribution to the occupied orbital by the Cu d_{xy} orbitals, while in this case they are predicted to make negligible contribution to the occupied orbital. There is thus a more substantial overall charge-

[85] Cramer, C. J. "*Essentials of Computational Chemistry: Theories and Models*, 2nd ed.; John Wiley & Sons: Chichester, U.K., 2004; pp 501-504.
[86] Estiú, G. L.; Zerner, M. C. "Calculations on the Electronic Structure and UV-Visible Spectrum of Oxyhemocyanin." *J. Am. Chem. Soc*. **1999**. *121*. 1893-1901.

transfer character to this excitation which likely contributes to its intensity. The unique characteristics of the formazan ligand, with its framework orbitals lying at high energy in the occupied orbital manifold, is responsible for this interesting variation.

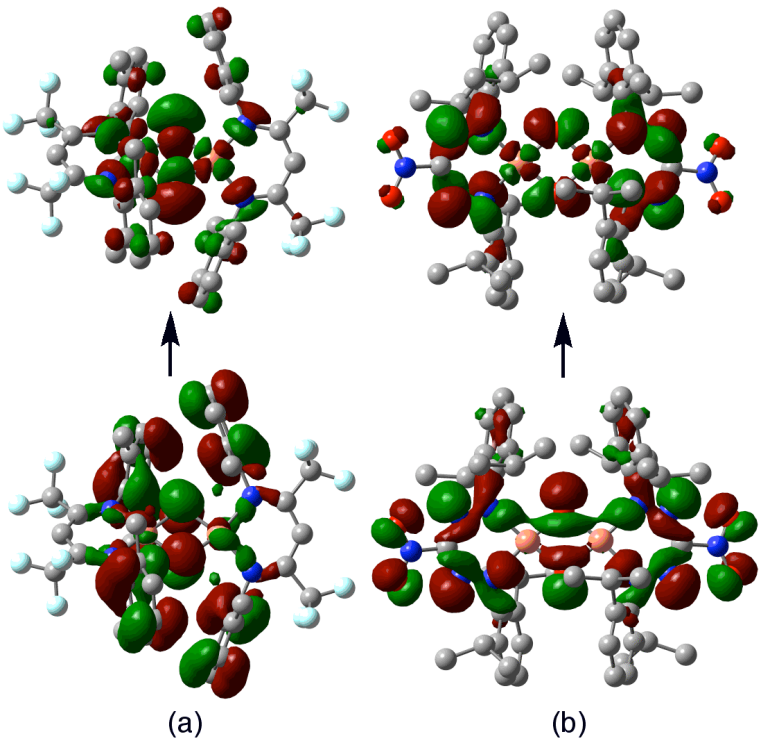

Figure 2-8. Predicted donor (below) and acceptor (above) Kohn-Sham molecular orbitals for the longest wavelength transitions observed for **4** (a) and **5** (b). The 0.02 a.u. isodensity surfaces are visualized and hydrogen atoms are removed for clarity. Cu atoms are peach, F atoms are aqua, O atoms are red, N atoms are blue, and C atoms are grey; the molecules are oriented with the Cu–Cu axis horizontal.

2.5. Decay of Bis(μ-oxo)dicopper Complexes

The bis(μ-oxo)dicopper(III) complexes have been implicated in a vast array of reactivity, including oxidative *N*-dealkylation, aliphatic or aryl ring hydroxylation, alcohol oxidation, phenol coupling and oxygenation of phosphines and sulfides.[7] Although we did not investigate the reactivity of the bis(μ-oxo)dicopper(III) complexes of **4** and **5**, the characteristic CT bands associated with these species bleached upon warming to above – 50 °C, where the main decayed products were identified as bis(μ-hydroxo)dicopper(II) species together with many other side products that were not characterized. The same species were produced more cleanly by oxygenating the corresponding copper(I) compounds at ambient temperature. Interestingly, we noticed formation of an additional intermediate species during the decay process for the bis(μ-oxo)dicopper(III) complexes of **5** (Figure 2-9). Its formation and decay was more conveniently monitored by oxygenating (**5**)Cu($NCCH_3$) at temperature above –50 °C. This new intermediate features a narrow low energy band at 742 nm with ε ~ 1100 M^{-1} cm^{-1} per copper. While d-d transitions of copper(II) complexes often appear in this region of the UV-vis spectrum, such an assignment seems unlikely in view of the band shape and intensity observed here. As seen in Figure 2-9, both formation (k = 0.037 s^{-1}) and decay (k = 0.0024 s^{-1}) of the 742 nm feature obeys a first-order rate law. The data shown in Figure 2-10 revealed that the formation rates of the intermediate in THF or d_8-THF at –30 °C have a modest kinetic isotope effect (k_H/k_D = 1.6), suggesting an attack on the solvent C-H(D) bond during the transformation of the bis(μ-oxo)dicopper to the

intermediate.[87]

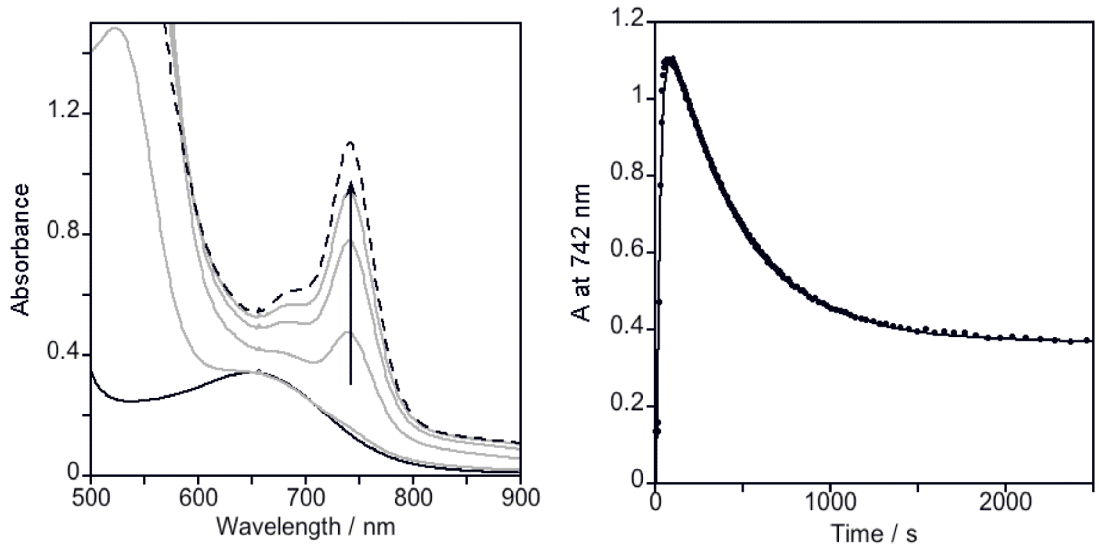

Figure 2-9. (left) UV-vis spectral change upon oxygenation of (**5**)Cu($NCCH_3$) (1.0 mM) in THF at – 10 °C. Solid line for starting material and dotted line for intermediate (right) Time trace for formation and decay of intermediate monitored at 742 nm (black dot) and fit to bi-exponential equation ($A_t = A_1 – A_2*\exp(-k_1*t) + A_3*\exp(-k_2*t)$, $k_1 = 0.037$ and $k_2 = 0.0024$).

[87] Attempts to identify product of oxidation of the solvent via gas chromatography/mass spectrometry analysis after allowing the intermediate to decompose were unsuccessful, however.

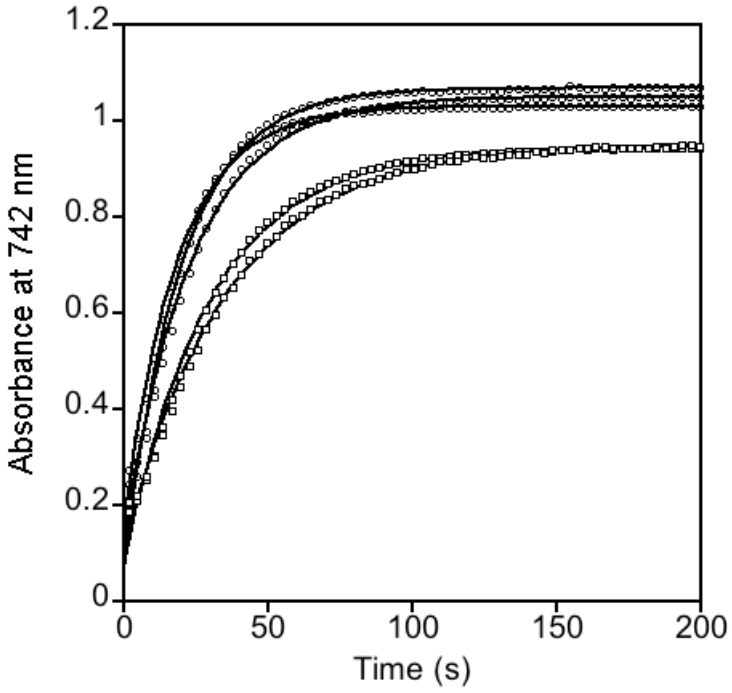

Figure 2-10. Time traces for formation of the intermediate generated upon oxygenation of (**5**)Cu($NCCH_3$) at –30 °C, with data monitored at 742 nm and fit to exponential equations. Circles are for runs in THF and squares are for runs in THF-d_8. Average values of rate constants are k(THF) = 0.048 s^{-1} and k (THF-d_8) = 0.030 s^{-1}, giving k_H/k_D = 1.6.

Moreover, the 4 K X-band EPR spectrum of the intermediate features an isotropic signal at g ~ 2.0 and its double integration indicates a total spin quantity of ~ 77% relative to the bis(μ-oxo)dicopper(III) precursor. These spectroscopic features are reminiscent of a related boron-formazan species.[75] Its chemically one electron reduced form is a borataverdazyl radical anion that exhibits similar spectroscopic features (a band at 738 nm in the solid-state electronic spectrum and an isotropic EPR signal at g ~ 2.0 in the solid state). In addition, the acceptor orbital of $(\mathbf{5})_2Cu_2(O)_2$ has significant contributions from formazan π^* orbitals (Figure 2-8b) that are analogous to the singly occupied molecular orbital of verdazyls, a well-established family of stable organic

radials.[88] On the basis of these observations, we speculate that the 742 nm absorption feature and the signal in the EPR spectrum arises from a species comprising the ligand-centered radical.

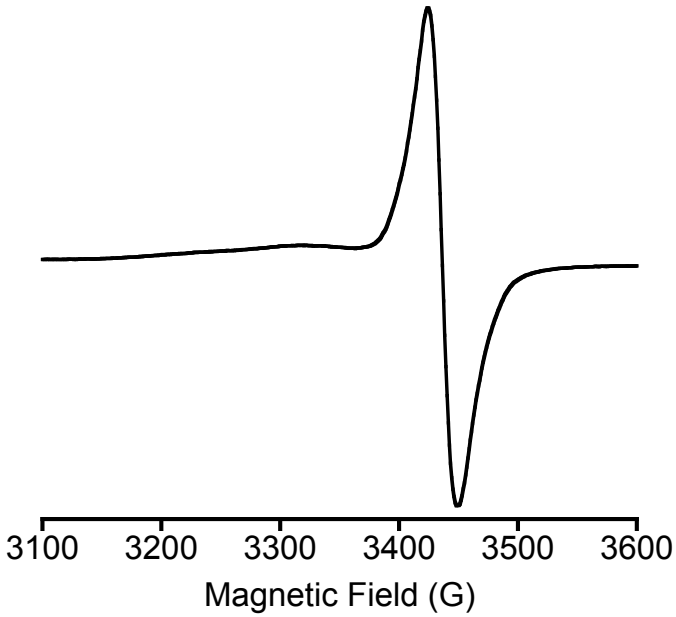

Figure 2-11. X-band EPR spectrum of the intermediate (4 K).

Scheme 2-4 depicts possible decomposition pathways to $(\mathbf{5})_2Cu_2(OH)_2$ via a proposed formazl radical ligand intermediate (**A** or **B**).[76] As indicated by the kinetic isotope effect, the initial mixed-valent (μ-hydroxo)(μ-oxo)Cu(II)Cu(III) species generated upon hydrogen atom abstraction from the bis(μ-oxo)dicopper species would be expected to undergo rapid internal electron transfer processes involving either transfer from a Cu^{II} ion to the formazan ligand (**A**) or from the formazan to a Cu^{III} ion (**B**). Given

[88] Gilroy, J. B.; McKinnon, S. D. J.; Kennepohl, P.; Zsombor, M. S.; Ferguson, M. J.; Thompson, L. K.; Hicks, R. G. "Probing Electronic Communication in Stable Benzene-Bridged Verdazyl Diradicals." *J. Org. Chem*. **2007**. *72*. 8062-8069.

that the borataverdazyl radical anion was formed by reduction rather than oxidation,[76] any Cu-based hyperfine splitting in the EPR spectrum is absent and the formazan is more likely to accommodate an additional electron in its π^* orbitals by theory, the former process to result in species **A** would appear more likely. However, we cannot rule out the second process to yield **B** if strong antiferromanetic coupling between two copper(II) centers and little coupling between these centers and a formazan radical are assumed.

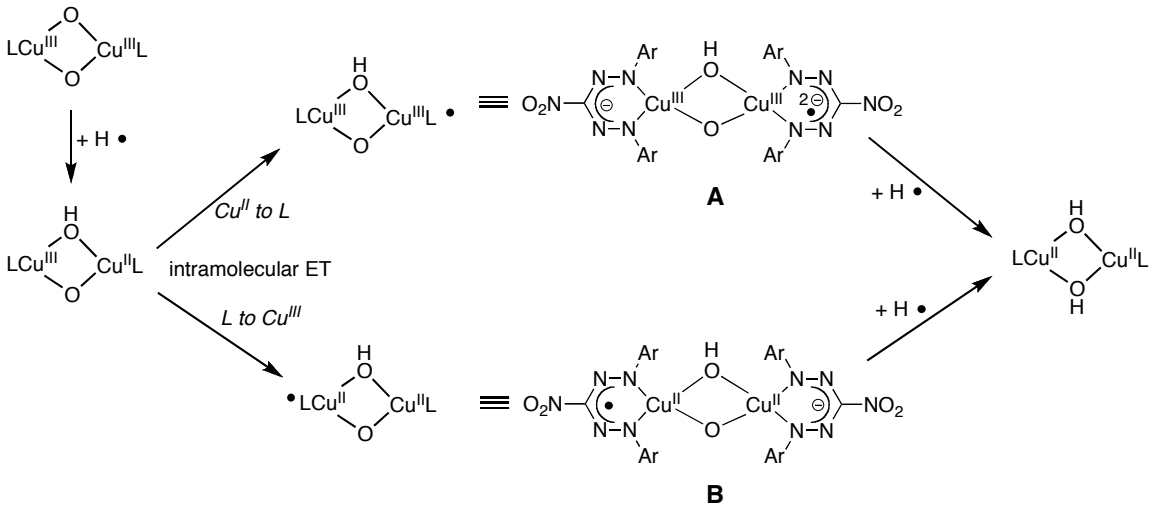

Scheme 2-4. Proposed decay pathways of $(\mathbf{5})_2Cu_2(O)_2$ to form the bis(hydroxo)dicopper(II) complex.

2.6. Conclusions and Perspectives

In this chapter we described the synthesis and characterization of copper(I) complexes of a sterically less hindered β-diketiminate ligand featuring two CF_3 backbone substituents and a nitro-formazan analogue, and studied their dioxygen reactivity. The main goal of this research was to evaluate how subtle change of steric profiles of the

ligands can influence the oxygenation chemistry of the copper(I) complexes.

We have shown that the copper(I) complexes of **4** and **5** feature electron-deficient metal centers similar with those of other β-diketiminate ligands (**3**), as evidenced by the high ν(CO) frequencies for the species [LCu(CO)]. In contrast to the lack of O_2 reactivity previously reported for [(**2**)Cu(CH_3CN)], which is similarly electron-poor but more sterically congested by the diisopropylphenyl versus dimethylphenyl group, both [LCu(CH_3CN)] (L = **4** and **5**) readily reacted with O_2 at room temperature to yield bis(μ-hydroxo)dicopper species, which were structurally characterized by X-ray crystallography. Moreover, oxygenation of these compounds at – 80 °C resulted in the formation of bis(μ-oxo)dicopper species, whose identities were confirmed on the basis of UV-vis and resonance Raman spectroscopy, spectrophotometric titration data, EPR silence, and theory. We assumed that although O_2 binding to copper centers in all cases are thermodynamically unfavorable due to the poor electron-donating nature of the ligands, in the cases of **4** and **5** the facile dimerization of the 1:1 Cu/O_2 transient intermediate by virtue of their reduced steric profiles drives the reactions forward.

The nitroformazan exhibits unusual electronic, steric and coordination properties. To the best of my knowledge, the synthesis of the copper(I) complex with this ligand and its oxygenation chemistry has not been explored prior to this research. The bis(μ-oxo)dicopper species derived from this ligand features a unique low energy CT band at 524 nm, which is notably far in the red compared to those seen previously. We attributed this unusual behavior to the substantial ligand orbital contributions to the $[Cu_2O_2]^{2+}$ core transition on the basis of theory. Interestingly, we observed the novel intermediate

featuring the relatively sharp absorption band at the lower energy region and the isotropic EPR signal at g ~ 2.0 during the decay process of the bis(μ-oxo)dicopper species. These spectroscopic and/or physiological data led us to formulate the intermediate as a metalloverdazyl radical. We speculate that this radical species is formed via a mechanism involving H-atom abstraction from the solvent by the bis(μ-oxo)dicopper species followed by a rapid internal redox isomerization.

2.7. Experimental Section

General Considerations. All solvents and reagents were obtained from commercial sources and used as received unless otherwise noted. The solvents tetrahydrofuran (THF), pentane, and Et_2O were dried over Na/benzophenone and distilled under Ar or passed through solvent purification columns (Glass Contour, Laguna, CA). Acetonitrile (CH_3CN) was dried over CaH_2 and distilled under Ar prior to use. [Cu_4Mes_4] (Mes = mesityl),[75] and the protonated forms of **4**[74] and **5**[70] were prepared according to published procedures. All metal complexes were prepared and stored in a Vacuum Atmospheres inert atmosphere glovebox under a dry nitrogen atmosphere or were manipulated using standard inert atmosphere vacuum and Schlenk techniques.

Physical Methods. NMR spectra were recorded on either Varian VI-300 or VI-500 spectrometers at room temperature. Chemical shifts (δ) for ^1H (300 MHz) and ^{13}C (75 MHz) NMR spectra were referenced to residual protium in the deuterated solvent. UV-vis spectra were recorded on an HP8453 (190-1100 nm) diode array spectrophotometer. Low temperature spectra were acquired through the use of a Unisoku low temperature UV-Vis cell holder. When necessary, UV-Vis spectra were corrected for

drifting baselines due to minimal frosting of the UV cells caused by the low-temperature device. This was achieved by subtracting the average of a region with no absorbance (i.e., baseline, typically 950-1000 nm) from the entire spectrum. X-band EPR spectra were recorded on a Bruker E-500 spectrometer with an Oxford Instruments EPR-10 liquid helium cryostat (4-20K, 9.61 GHz). Resonance Raman spectra were recorded on an Acton 506 spectrometer using a Princeton Instruments LN/CCD-11100-PB/UVAR detector and ST-1385 controller interfaced with Winspec software. The spectra were obtained at –196 °C using a backscattering geometry. Excitation at 457.9 and 514.5 nm was provided by a Spectra Physics BeamLok 2065-7S Ar Laser. Raman shifts were externally referenced to liquid indene. Elemental analyses were performed by Robertson Microlit Lab. ESI-MS (electrospray ionization mass spectra) were recorded on a Bruker BioTOF II instrument. IR spectra were obtained using a ThermoNicolet Avatar 370 FT-IR equipped with an ATR attachment, using a CaF_2 solution cell (Intermatioinal Crystal Labs). Cyclic voltammograms were recorded using Pt working and auxiliary electrodes, a Ag wire/$AgNO_3$ (10 mM in CH_3CN) reference electrode, and a BAS Epsilon potentiostat connected to a 22 mL cell in an inert-atmosphere glovebox. Experiments were performed using analyte concentrations of 1 mM in THF with 0.3 M tetrabutylammonium hexafluorophosphate, $TBAPF_6$, (sample volumes of ~5 mL) at room temperature. The ferrocene/ferrocenium couple was recorded for reference.

[(4)Cu(CH_3CN)]. In an inert atmosphere, to a solution of the ligand precursor H(**4**) (100 mg, 0.24 mmol) in CH_3CN (5 mL) was added [Cu_4Mes_4] (44 mg, 0.06 mmol). After the reaction mixture was vigorously stirred overnight, it was filtered through a plug of Celite to remove any insoluble residue. The solvent was removed from the filtrate in vacuo to give a brown residue. The product was isolated in analytically pure form by allowing a concentrated solution of the residue in CH_3CN to stand for 3 d at –20 °C. The

resulting orange crystals were separated from the mother liquor, washed with cold pentane (~ 5 mL) and dried in vacuo (93 mg, 75 %). ^{1}H NMR (300 MHz, benzene-d_6): δ 6.99 (d, J = 7.5 Hz, 4H), 6.91 (t, J = 7.5 Hz, 2H), 6.11 (s, 1H), 2.11 (s, 12H), 0.28 (s, 3H) ppm. ^{13}C{^{1}H} NMR (75.0 MHz, benzene-d_6): δ 152.40, 148.56, 143.57, 130.33, 124.39, 123.23, 119.43, 83.77, 19.19, 0.27. UV-vis [λ_{max}, nm (ε, $M^{-1}cm^{-1}$) in THF]: 280 (18,900), 381 nm (16,600), 500 nm (460). Anal. Calc. for $C_{23}H_{22}CuN_3F_6$: C, 53.33; H, 4.28; N, 8.11. Found: C, 53.56; H, 4.08; N, 8.08.

[(5)Cu(CH$_3$CN)]. This compound was synthesized following the same procedure as described above, except using H(**5**) as the starting material and crystallizing the product by slow diffusion of pentane into a concentrated THF solution at –20 °C (99 mg, 80 %). ^{1}H NMR (300 MHz, benzene-d_6): δ 7.15 (m, 6H), 3.40 (septet, J = 6.9 Hz, 4H), 1.24 (d, J = 6.9 Hz, 24H), 0.17 (s, 3H) ppm. ^{13}C{^{1}H} NMR (75.0 MHz, benzene-d_6): δ 151.46, 141.24, 127.85, 124.29, 29.06, 25.02, 23.71, 0.27 ppm. UV-vis [λ_{max}, nm (ε, $M^{-1}cm^{-1}$) in THF]: 287 (11,700), 352 (9,480), 410 (10,500), 650 (380). Anal. Calc. for $C_{27}H_{37}CuN_6O_2$: C, 59.92; H, 6.89; N, 15.53. Found: C, 59.75; H, 6.91; N, 15.74.

LCu(CO) (L = 4 or 5). General procedure. The complex LCu(CH$_3$CN) (L = **4** or **5**) (37 μmol) was dissolved in benzene-d_6 (0.8 mL) in a screw-capped NMR tube. Carbon monoxide was gently bubbled through the solution for 20 min at ambient temperature, during which time the color changed to gold for L = **4** and dark-red for L = **5**. Both CO adducts were immediately characterized by ^{1}H and ^{13}C NMR spectroscopy. For IR characterization, the complex LCu(CH$_3$CN) (37 μmol) was dissolved in THF (2 mL) in a 10 mL Schlenk tube and stirred with CO bubbling at ambient pressure for 2 h, during which time the solvents evaporated. Approximately half of the dried solid (golden to dark red) was dissolved in THF (0.4 mL) and the IR spectrum recorded immediately. (**4**)Cu(CO): ^{1}H NMR (300 MHz, benzene-d_6): δ 6.96 – 6.86 (m, 6H), 6.16 (s, 1H), 2.13

(s, 12H). $^{13}C\{^{1}H\}$ NMR (75.0 MHz, benzene-d_6): δ 153.65, 149.30, 129.92, 125.48, 122.89, 119.09, 85.67, 19.12. FT-IR (THF): 2100 cm^{-1} (ν_{CO}). (**5**)Cu(CO): ^{1}H NMR (300 MHz, benzene-d_6): δ 7.24 – 7.08 (m, 6H), 3.24 (sept, , J = 6.9 Hz, 4H), 1.20 (s, 24H). $^{13}C[1H]$ NMR (75.0 MHz, benzene-d_6): δ 151.62, 151.34, 141.30, 129.92, 124.52, 29.09, 25.40, 23.43. FT-IR (THF): 2092 cm^{-1} (ν_{CO}).

$L_2Cu_2(OH)_2$ (L = 4 or 5). Solutions of $LCu(CH_3CN)$ (L = **4** or **5**) in THF (~50 mg in 10 mL) were oxygenated by bubbling of O_2 at ambient temperature for ~1 min. For L = **4**, the resulting red-brown solution was layered with ~ 10 ml pentane and allowed to stand at –20 °C. Red single crystals formed after several days, and were either mounted for analysis by X-ray crystallography or collected by decanting the mother liquor, washing with cold pentane, and drying in vacuo (19 mg, 40%). Anal. Calc. for $C_{42}H_{40}Cu_2F_{12}N_4O_2$: C, 51.06; H, 4.08; N, 5.67. Found: C, 51.76; H, 4.30; N, 5.27. Red single crystals of the product of the reaction of (**5**)$Cu(CH_3CN)$ were obtained by slow evaporation of the red-brown reaction solution, and were isolated similarly (21 mg, 44%). Anal. Calc. for $C_{50}H_{70}Cu_2N_{10}O_6$: C, 58.06; H, 6.82; N, 13.54. Found: C, 57.67; H, 6.91; N, 13.28.

Low Temperature Oxygenations of $LCu(CH_3CN)$ (L = 4 or 5). (a) UV-vis Spectroscopy. An anaerobically prepared THF solution of (**4**)$Cu(CH_3CN)$ (0.2 mM) or (**5**)$Cu(CH_3CN)$ (0.1 mM) in a septum-sealed quartz cuvette was cooled to –80 °C, and a dry stream of O_2 was bubbled through the solution for ~ 20 min or ~ 100 s, respectively. The spectroscopic changes are shown in Figure 5. The final spectrum was not perturbed by removal of excess O_2 from the solution by an Ar purge. For L = **5**, after bubbling Ar for 30 min through the solution to remove remaining unreacted O_2, the solution was warmed above –50 °C resulting in the disappearance of the band at 525 nm and growth of a new sharp feature at 742 nm, which subsequently decayed (Figure 8). The same

intermediate spectrum was also generated by directly oxygenating (**5**)Cu(CH_3CN) above –50 °C.

(b) Resonance Raman Spectroscopy. An Ar-filled Schlenk flask or NMR tube was charged with 1 mL of a THF solution of LCu(CH_3CN) (L = **4** or **5**; 40 mM for L = **4** and 10 mM for L = **5**) by syringe and cooled to –80 °C by submersion in an acetone/dry ice bath while maintaining an argon purge. Dry O_2 was bubbled through the solution (30 min for L = **4** and 10 min for L = **5**). Samples were frozen either in a copper cup attached to a liquid N_2 cooled coldfinger (L = **4**) or by immersing the NMR tube in liquid N_2 (L = **5**). For reactions with $^{18}O_2$, a 10 mL Schlenk tube charged with 1 mL of a THF solution of LCu(CH_3CN) (L = **4** or **5**) was frozen in liquid N_2 and ~ 10 mL $^{18}O_2$ was vacuum-transferred to the flask. The resulting mixture was warmed to –80 °C by submersion in an acetone/dry ice bath and stirred for 3 h to ensure complete reaction. Samples for analysis by resonance Raman spectroscopy were prepared either by transferring a sample of the reaction mixture to a copper cup or to a precooled NMR tube (–80 °C) followed by immersion in liquid N_2.

(c) EPR Spectroscopy. A 10 mL Schlenk flask was charged with a THF solution of LCu(CH_3CN) (L = **4** or **5**) (2 mM) and was cooled to –80 °C in an acetone/dry ice bath. Dry O_2 was bubbled through the solution (30 min for L = **4** and 10 min for L = **5**), and the resulting solution transferred *via* a pre-cooled syringe to a pre-cooled (–80 °C) EPR tube, which was immersed in liquid N_2 for subsequent analysis by EPR spectroscopy. Also, a quartz cuvette was charged with a THF solution of (**5**)Cu(CH_3CN) (2 mM), cooled to –30 °C, and oxygenated by bubbling dry O_2 with monitoring of the feature at 742 nm by UV-vis spectroscopy. Aliquots of the solution were rapidly transferred at various time points *via* a syringe to a pre-cooled (–80 °C) EPR tube, which was immersed in liquid N_2 for subsequent analysis by EPR spectroscopy.

(d) Spectrophotometric O_2 Titrations. A 1 mL sample of a stock solution of $LCu(CH_3CN)$ (L = **4** or **5**) in THF (1.0 mM for **4**, 0.5 mM for **5**) was placed in a 0.2 cm path-length UV-vis cuvette, cooled to –80 °C and the headspace evacuated. Spectra were taken before and after cooling to ensure that no sample degradation had occurred. An O_2 saturated THF solution (10 mM) was prepared by bubbling dry O_2 gas through argon-saturated THF in a 10 mL Schlenk tube at 25 °C for 15 min.[i] Using a graduated gastight syringe, portions of the 10 mM O_2 saturated THF solution (10, 20, 30, 40, 50, 75, 100, 150, and 200 μL), were injected into the cuvette where it was left to equilibrate with stirring. The progress of oxygenation was followed by monitoring the absorption band at 470 nm (**4**) or 524 nm (**5**) in the UV-vis spectrum until no further increase in absorbance was observed. The Cu:O_2 stoichiometry reported in the text was calculated from two (L = **4**) or three (L = **5**) replicate runs.

Table 2-5. Summary of X-ray Crystallographic Data.

	[(**4**)Cu(CH_3CN)]
empirical formula	C23 H22 Cu F6 N3
formula weight (g/mol)	517.98
temperature (K)	173(2)
crystal system	Monoclinic
space group	P2(1)/n
a (Å)	8.0421(12)
b (Å)	23.357(4)
c (Å)	12.1307(19)
α (deg)	90
β (deg)	90.679(2)
γ (deg)	90
V ($Å^3$)	4212.7(8)
Z	4
crystal size (mm^3)	0.3 × 0.3 × 0.2
θ range (deg)	1.74 to 25.05
abs coeff. (mm^{-1})	1.023
reflns collected	21659
unique reflns	4047
parameters	302
R1, *w*R2 (for I > 2σ(I))	0.0373, 0.0912
goodness-of-fit	1.033
largest peak, hole ($e/Å^{-3}$)	0.329, -0.531

$R1 = \Sigma||F_0|-|F_c||/\Sigma|F_0||$. $wR_2 = [\Sigma[w(F_0^2-F_c^2)^2]/\Sigma w(F_0^2)^2]]^{1/2}$
where $w = q / [\sigma^2 (F_0^2) + (aP)^2 + bP + d + e \times sin(\theta)$.
$GooF = S = [\Sigma[w(F_0^2-F_c^2)^2] / (n-p)]^{1/2}$

Table 2-6. Summary of X-ray Crystallographic Data.

	$[(\mathbf{4})_2Cu_2(OH)_2]$	$[(\mathbf{5})_2Cu_2(OH)_2]$
empirical formula	C42 H40 Cu2 F12 N4 O2	C62 H94 Cu2 N10 O9
formula weight (g/mol)	987.86	1250.55
temperature (K)	173(2)	173(2)
crystal system	Monoclinic	Monoclinic
space group	C2/c	P2(1)/n
a (Å)	12.5411(14)	12.7689(16)
b (Å)	17.913(2)	14.1614(18)
c (Å)	19.003(2)	17.642(2)
α (deg)	90	90
β (deg)	99.300(2)	90.187(2)
γ (deg)	90	90
V ($Å^3$)	4212.7(8)	3190.1(7)
Z	4	2
crystal size (mm^3)	0.5 × 0.2 × 0.1	0.4 x 0.3 x 0.3
θ range (deg)	2.00 to 25.05	1.84 to 25.09
abs coeff. (mm^{-1})	1.104	0.729
reflns collected	18939	30970
unique reflns	3723	5634
parameters	288	400
R1, *w*R2 (for I > 2σ(I))	0.0299, 0.0654	0.0287, 0.0709
goodness-of-fit	1.047	1.073
largest peak, hole ($e/Å^{-3}$)	0.279, -0.281	0.488, -0.292

$R1 = \Sigma||F_0|-|F_c||/\Sigma|F_0||$. $wR_2 = [\Sigma[w(F_0^2-F_c^2)^2]/\Sigma w(F_0^2)^2]]^{1/2}$ where $w = q / [\sigma^2 (F_0^2) + (aP)^2 + bP + d + e \times sin(\theta)$. GooF = $S = [\Sigma[w(F_0^2-F_c^2)^2] / (n-p)]^{1/2}$

CHAPTER 3. SYNTHESIS, CHARACTERIZATION, AND DIOXYGEN REACTIVITY OF COPPER(I)-α−KETOCARBOXYLATE COMPLEXES

3.1. Introduction

As described in Chapter 1, a mononuclear copper-oxyl [$Cu^{III}=O^{2-} \leftrightarrow Cu^{II}-O^{-\bullet}$] species has been invoked as a possible active intermediate in catalysis by copper-containing enzymes such as dopamine β-monooxygenase and peptidylglycine α-hydroxylating monooxygenase.[25] Recent theoretical studies on these enzymes also suggest that the copper-oxyl species initiates H-atom abstraction from substrates.[36] Experimental evidence to support this notion has begun to emerge in the literature.[55b,57-58] For example, model complexes containing Cu^{II}-OOR (R = H or alkyl) units with various N-donor supporting ligands were postulated to undergo homolytic O-O bond scission to yield putative copper-oxyl species that induce either intramolecular ligand hydroxylation[55b,57]or oxidative N-dealkylation[58] processes. However, the exact nature of the active species in these model complexes remains elusive. There is an obvious prerequisite for generating $[CuO]^+$ species from the reaction of copper(I) complexes with O_2; four electrons are required to fully cleave the O-O double bond. While most copper(I) complexes react with O_2 to form a variety of Cu_2/O_2 species with varing degrees of O_2 reduction and multiple copper oxidation levels, formation of a 1:1 Cu/O_2 species is relatively rare.[5e,11d,38a-b] Even for the latter species, the O_2 fragment is at most either at the superoxide or peroxide level depending on the amount of the charge transfer from the copper center to O_2. Consequently, one must provide extra-electrons to the bound O_2

moiety of the 1:1 Cu/O_2 species in order to completely break the O-O bond.

In this context, it is useful to consider how related high-valent $[Fe^{IV}=O]^{2+}$ species have been successfully isolated or characterized in model studies and enzymes.[62c,64a,89] Among various routes by which $[Fe^{IV}=O]^{2+}$ moieties may be accessed is that used by α-ketoacid-dependent non-heme iron enzymes.[5b,62a-b] These enzymes constitute one of the largest family of non-heme iron enzymes and catalyze many biologically important transformations including substrate hydroxylations, desaturations and ring-expansions. Aside from the α-ketoacid, these enzymes require dioxygen and iron(II) for their catalytic functions. The iron(II) is bound to two histidine imidazolyls and a carboxylate from a Glu residue, the so-called 2-His-1-carboxylate facial triad.[90] The remaining coordination sites are occupied by water molecules that can be the binding sites for the α-ketoacid and O_2 (or NO, an O_2 surrogate) (Figure 3-1).

---

[89] For examples, see: a) Nam, W. "High-Valent Iron(IV)-Oxo Complexes of Heme and Non-Heme Ligands in Oxygenation Reactions." *Acc. Chem. Res*. **2007**, *40*, 522-531. b) Shaik, S.; Hirao, H.; Kumar, D. "Reactivity of High-Valent Iron-Oxo Species in Enzymes and Synthetic Reagents: A Tale of Many States." *Acc. Chem. Res*. **2007**, *40*, 532-542. c) Shaik, S.; Kumar, D.; de Visser, S. P.; Altun, A.; Thiel, W. "Theoretical perspective on the structure and mechanism of cytochrome P 450 enzymes." *Chem. Rev*. **2005**, *105*, 2279-2328. d) Harvey, J. N.; Poli, R.; Smith, K. M. "Understanding the reactivity of transition metal complexes involving multiple spin states." *Coord. Chem. Rev*. **2003**, *238-239*, 347-361. e) Bautz, J.; Comba, P.; Lopez de Laorden, C.; Menzel, M.; Rajaraman, G. "Biomimetic high-valent non-heme iron oxidants for the cis-dihydroxylation and epoxidation of olefins." *Angew. Chem. Int. Ed*. **2007**, *46*, 8067-8070. f) Kryatov, S. V.; Rybak-Akimova, E. V.; Schindler, S. "Kinetics and Mechanisms of Formation and Reactivity of Non-heme Iron Oxygen Intermediates." *Chem. Rev*. **2005**, *105*, 2175-2226.

[90] Hegg, E. L.; Que, L, Jr. "The 2-His-1-carboxylate facial triad. An emerging structural motif in mononuclear non-heme iron(II) enzymes." *Eur. J. Biochem*. **1997**, *250*, 625-629.

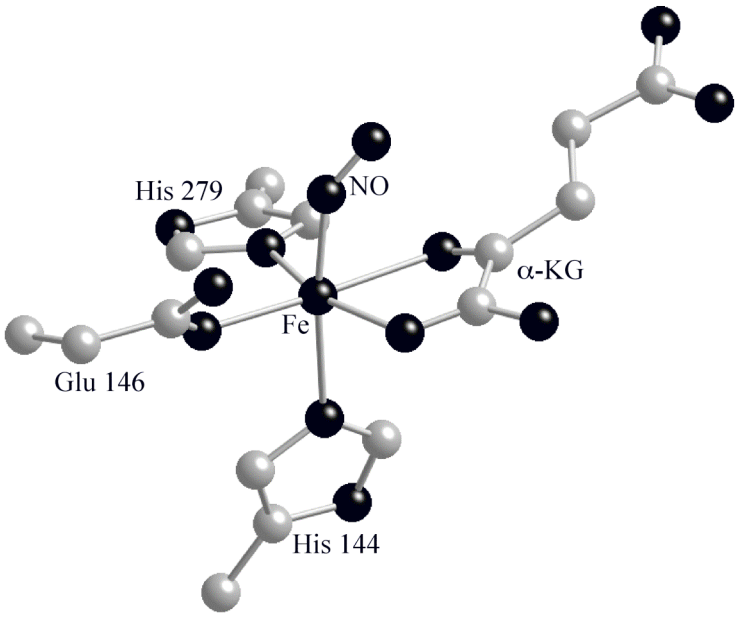

Figure 3-1. Crystal structure of NO adduct in Clavaminate Synthase. (pdb 1GVG)[91]

A general mechanism for these enzymes has been proposed (Scheme 3-1). In the first step, the α-ketoacid binds the iron center in a bidentate fashion leading to displacement of two water molecules from the coordination sphere. Substrate binding in the vicinity of the iron active site then results in the loss of the remaining water molecule, generating a coordinatively unsaturated metal center ready to bind and activate O_2 to yield a transient Fe^{III}-superoxo species. Subsequent steps involve the oxidative decarboxylation (loss of CO_2) of the bidentate α-ketoacid complex of Fe^{II} via attack at the ketocarbon by the transient Fe^{III}-superoxo species to yield a formally Fe^{II}-peracid, which then undergoes a heterolytic O-O bond scission to generate a $[Fe^{IV}=O]^{2+}$ intermediate that is ultimately responsible for oxidizing the external substrate. The Fe^{II}

[91] Zhang, Z.; Ren, J. S.; Harlos, K.; McKinnon, C. H.; Clifton, I. J.; Schofield, C. J. "Crystal structure of a clavaminate synthase-Fe(II)-2-oxoglutarate-substrate-NO complex: evidence for metal centered rearrangements." *FEBS. Lett.* **2002**, *517*, 7-12.

ion and the α-ketoacid cofactor each provide two electrons to ensure complete O-O bond breaking, with two oxidizing equivalents stored at the metal center in the $[Fe^{IV}=O]^{2+}$ intermediate. Typically, one O-atom from O_2 is incorporated in the carboxylic acid derived from the α–ketoacid and the other is transferred to substrate.

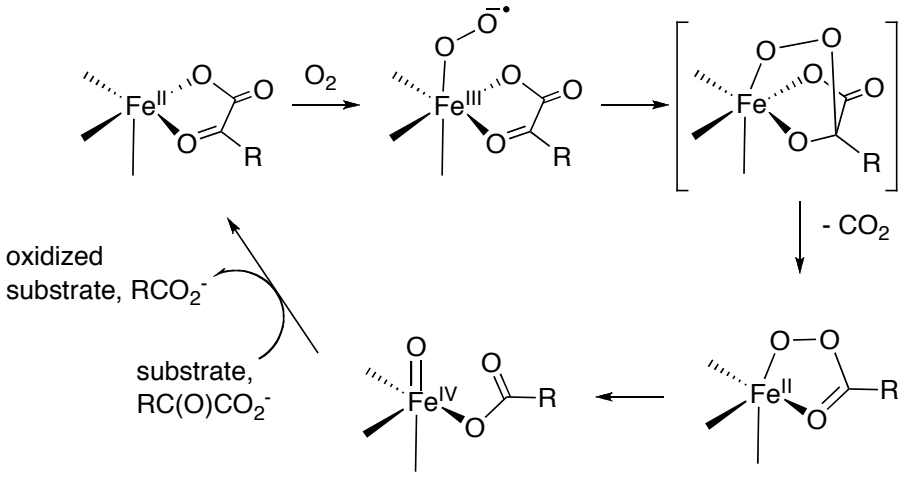

Scheme 3-1. General O_2-activation mechanism for α–ketoacid dependent non-heme iron enzymes.

Several $[Fe^{II}(L)(\alpha\text{-ketoacid})]$ (L = tridentate or tetradentate N-donor ligands) complexes have been reported as structural and/or functional models of the α-ketoacid dependent non-heme iron enzymes.[92,93,94] These complexes display bidentate

[92] a) Chiou, Y.-M.; Que, L., Jr. "Models for α-Keto Acid-Dependent Non-heme Iron Enzymes: Structures and Reactivity of $[Fe^{II}(L)(O_2CCOPh)](ClO_4)$ Complexes." *J. Am. Chem. Soc.* **1995**, *117*, 3999-4013. b) Chiou, Y.-M.; Que, L., Jr. "Model Studies of α-Keto Acid-Dependent Nonheme Iron Enzymes: Nitric Oxide Adducts of $[Fe^{II}(L)(O_2CCOPh)](ClO_4)$ Complexes." *Inorg. Chem.* **1995**, *34*, 3270-3278. c) Hegg, E. L.; Ho, R. Y. N.; Que, L., Jr. "Oxygen Activation and Arene Hydroxylation by Functional Mimics of α-Keto Acid-Dependent Iron(II) Dioxygenases." *J. Am. Chem. Soc.* **1999**, *121*, 1972-1973. d) Mehn, M. P.; Fujisawa, K.; Hegg, E. L.; Que, L., Jr. "Oxygen activation by nonheme iron(II) complexes: α-Keto carboxylate versus carboxylate." *J. Am. Chem. Soc.* **2003**, *125*, 7828-7842. f) Mukherjee, A.; Martinho, M.; Bominaar, E. L.; Muenck, E.; Que, L., Jr. "Shape-selective interception by hydrocarbons of the O2-derived oxidant of a biomimetic nonheme iron complex." *Angew. Chem., Int. Ed.* **2009**, *48*, 1780-1783.

[93] Ha, E. H.; Ho, R. Y. N.; Kisiel, J. F.; Valentine, J. S. "Modeling the Reactivity of α-Ketoglutarate-Dependent Non-Heme Iron(II)-Containing Enzymes." *Inorg. Chem.* **1995**, *34*. 2265-2266.

coordination of the α-ketoacid and exhibit unique visible chromophores arising from metal-to-α-ketoacid charge transfer transitions (MLCT).[95] The binding mode of the α-ketoacid to the iron(II) center in these model complexes is flexible in solution(monodentate vs bidentate), but only bidentate α-ketoacid complexes give rise to the diagonistic visible absorption features. Interestingly, six-coordinate iron complexes with neutral tetradentate N4 ligands take days to undergo oxidative decarboxylation,[92a] whereas the iron complexes of monoanionic tridentate Tp^{R2} ligands (Tp = hydrotrispyrazole borate, R = Me or Ph) react with O_2 within hours.[92c,93,94] This significant difference in reaction rates emphasizes the importance of a vacant site for O_2 binding in promoting the oxidative decarboxylation of the bound α-ketoacid.

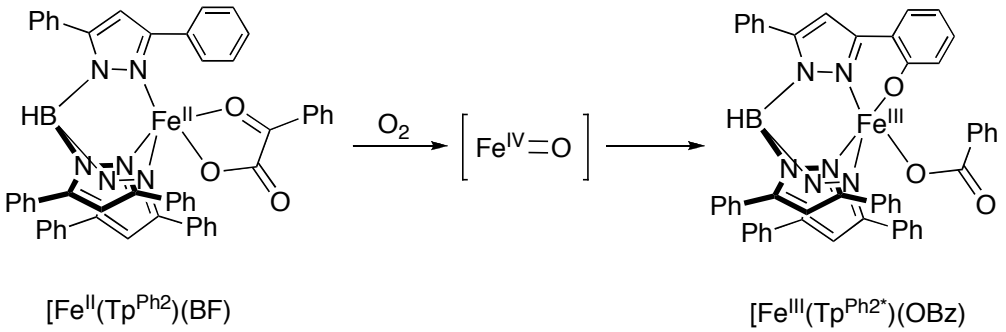

$[Fe^{II}(Tp^{Ph2})(BF)]$ $[Fe^{III}(Tp^{Ph2*})(OBz)]$

Scheme 3-2. Reaction of $[Fe^{II}(Tp^{Ph2})(BF)]$ with O_2 in benzene at 25 °C.

---

[94] Hikichi, S.; Ogihara, T.; Fujisawa, K.; Kitajima, N.; Akita, M.; Moro-oka, Y. "Synthesis and Characterization of the Benzoylformato Ferrous Complexes with Hindered Tris(pyrazolyl)borate Ligand as a Structural Model for Mononuclear Non-Heme Iron Enzymes." *Inorg. Chem*. **1997**, *36*, 4539-4547.

[95] a) Pavel, E. G.; Zhou, J.; Busby, R. W.; Gunsior, M.; Townsend, C. A.; Solomon, E. I. "Circular Dichroism and Magnetic Circular Dichroism Spectroscopic Studies of the Non-Heme Ferrous Active Site in Clavaminate Synthase and Its Interaction with α-Ketoglutarate Cosubstrate." *J. Am. Chem. Soc*. **1998**, *120*, 743-753. b) Ryle, M. J.; Padmakumar, R.; Hausinger, R. P. "Stopped-Flow Kinetic Analysis of Escherichia coli Taurine/α-Ketoglutarate Dioxygenase: Interactions with α-Ketoglutarate, Taurine, and Oxygen." *Biochemistry*. **1999**, *38*, 15278-15286.

One of these model complexes, $[Fe^{II}(Tp^{Ph2})(BF)]$ (BF = benzoylformate),[92c,f] mimics the enzymatic reaction (Scheme 3-2). Oxygenation of this complex leads to intramolecular arene hydroxylation of the ligand in 70% yield within hours at room temperature, along with the benzoic acid derived from BF. The analogous Fe^{II} complex containing the benzoate instead of the benzoylformate also reacts to give the ligand hydroxylation, but at much slower rate (a few days) and in lower yield (~50%), demonstrating the key role the α-ketoacid plays in O_2 activation.[92d] In a series of studies with para-substituted BF derivatives, the rates of the oxidative decarboxylation were shown to increase as the substituent becomes more electron-withdrawing. This result suggests that the oxidative decarboxylation involves nucleophilic attack at the ketocarbon of the BF, presumably by the Fe^{III}-superoxide as in the proposed mechanism depicted in Scheme 3-1. More interestingly, it was demonstrated that while not observed or detected, the oxidant, presumably $[Fe^{IV}=O]^{2+}$, could be trapped with exogenous hydrocarbon substrates. The trapping efficiency was found to be modulated not only by the strength of the target C-H bond but also by the shape of the substrates.[92f] For example, the oxygenation of $[Fe^{II}(Tp^{Ph2})(BF)]$ in the presence of excess cyclohexene reduced the yield of the ligand hydroxylation by a factor of four and resulted in the formation of cyclohexadiene as the sole organic product. In contrast, other organic substrates such as toluene, ethylbenzene and diphenylmethane having comparable C-H bond strengths to that of cyclohexene did not influence the yield of the ligand hydroxylation. Similarly, cyclohexane, which has a similar steric profile but a stronger C-H bond relative to cyclohexene, also did not intercept the oxidant. This shape selectivity in the biomimetic model complexes is especially notable. To explain this, the authors speculated that the

cavity around the iron center formed by the phenyl substituents of the Tp ligand discriminates among various hydrocarbons according to their shape.

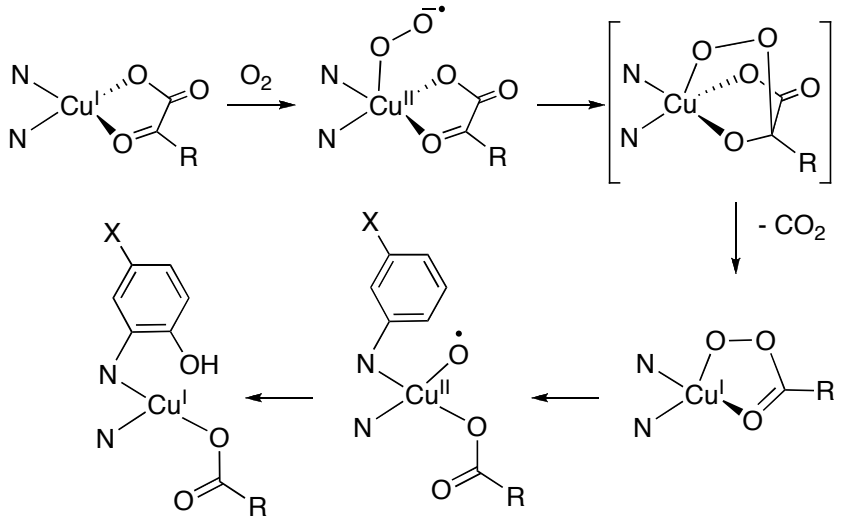

Scheme 3-3. Proposed reaction mechanism of Cu^{I}-α-ketocarboxylate complexes with O_2.

Inspired by the results from the previous Fe^{II} model studies, we hypothesized that Cu^{I} analogues of α-ketoacids might react similarly with O_2 to generate novel Cu^{I}-peracid and/or derived Cu-oxyl [$Cu^{III}=O^{2-} \leftrightarrow Cu^{II}\text{-}O^{-\bullet}$] species, which could subsequently be trapped in intra- or intermolecular fashion. Specifically, we envisioned a copper-based mechanism akin to that shown for iron (Scheme 3-3). To test this idea, we targeted several Cu^{I}-α-ketoacid complexes for synthesis and characterization, together with a simple Cu^{I}-OTf variant (OTf = trifluoromethanesulfonate). Comparative O_2 reactivity studies were then performed. The chapter will discuss the results from these experiments

along with computational evaluations of the observed O_2 activation process.[96] Portions of the work presented in this chapter have been previously published elsewhere.[2]

3.2. Ligand Design and Synthesis

Recent theoretical calculations indicated that a mononuclear Cu-oxyl species should be a powerful oxidant,[36,39,53] perhaps even more reactive than the related $[Fe^{IV}=O]^{2+}$ moiety. Thus, it was expected that direct observation of such a species would be challenging. In this context, we initially sought to intercept a mononuclear copper-oxyl by using a supporting ligand with an arene substituent appropriately positioned to be susceptible to intramolecular attack via a reaction similar to those seen in the Fe^{II} model complexes.[92] In addition, the ligands have to provide enough steric bulk to prevent any unwanted side reactions such as a dimerization to yield Cu_2/O_2 complexes. Moreover, given that the open coordination site for O_2 binding has been shown to be critical for initiating the oxidative decarboxylation of the bound α-ketoacid as discussed above, the ligand framework should lead to low-coordinate copper complexes to allow for the binding of α–ketoacids and O_2. Finally, we sought a ligand that would yield Cu^I complexes that would be unlikely to be reactive with O_2 in the absence of the α-ketoacid, so that any oxidative chemistry seen could be traced to α-ketoacid decarboxylation.

Taking all these properties into account, we focused on the bidentate pyridine-imine ligands as depicted in Scheme 3-4. These ligands contain various aryl substituents on the

[96] DFT calculations were performed by Dr. Stefan Huber and Prof. Christopher Cramer at the University of Minnesota as well as Prof. Laura Gagliardi at the University of Geneva.

pyridine ring that may serve to trap a highly reactive Cu^{I}-peracid and/or Cu-oxyl species that would be formed upon oxygenation of the Cu^{I}-α-ketoacid complexes. Like $[Fe^{II}(Tp^{Ph2})(BF)]$, the ortho positions of aryl groups in the present systems are likely to be the most probable sites of hydroxylation. With this expectation, changing the X substituents (from H to OMe) was envisioned to influence the trapping efficiency of such reactive species. Likewise, blocking these potential hydroxylating sites with two methyl groups as seen with L^{Me} might provide an opportunity to investigate exogenous substrate reactivity studies without competing reactions between the ligand hydroxylation and substrate oxidations. The 2,6-diisopropylphenyl substituents on the imine nitrogen donor serve to provide steric bulk necessary for inhibiting dimerization reactions.

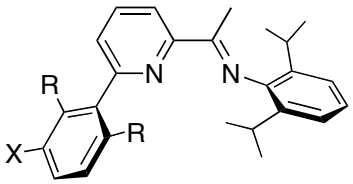

L^{H} (R = X = H)
L^{Me} (R = Me, X = H)
$L^{m\text{-}OMe}$ (R = H, X = OMe)

Scheme 3-4. Schematic representation of ligands.

The syntheses of the ligands used in this study are depicted in Scheme 3-5. Using modifications of known methods,[97,98] we synthesized the aryl appended pyridyl ketone

[97] Scott, N. M.; Schareina, T.; Tok, O.; Kempe, R. "Lithium and potassium amides of sterically demanding aminopyridines." *Eur. J. Inorg. Chem*. **2004**, *16*, 3297-3304.

[98] Bianchini, C.; Mantovani, G.; Meli, A; Migliacci, F.; Laschi, F. "Selective Oligomerization of Ethylene to Linear α-Olefins by Tetrahedral Cobalt(II) Complexes with 6-(Organyl)-2-(imino)pyridyl Ligands: Influence of the Heteroatom in the Organyl Group on the Catalytic Activity." *Organometallics*. **2003**, *22*,

precursors. Without further purification, these precursors were then condensed with excess 2,6-diisopropylaniline in the presence of a catalytic amount of formic acid in refluxing methanol. The analytically pure products were isolated by recrystallization from methanol in yields of 35 ~ 75% and were characterized by ^{1}H and $^{13}C\{^{1}H\}$ NMR spectroscopy and CHN elemental analysis (see the Experimental section for details). Key features in the ^{1}H NMR spectrum denoting the successful incorporation of 2,6-diisopropylaniline to the ketone functionality include the appearance of a septet at ~2.8 ppm for the methine hydrogens and a doublet at ~1.7 ppm for the methyl hydrogens from the isopropyl groups. In addition, all three ligands exhibit a singlet at 2.16 ~ 2.34 ppm for the ketimine hydrogens.

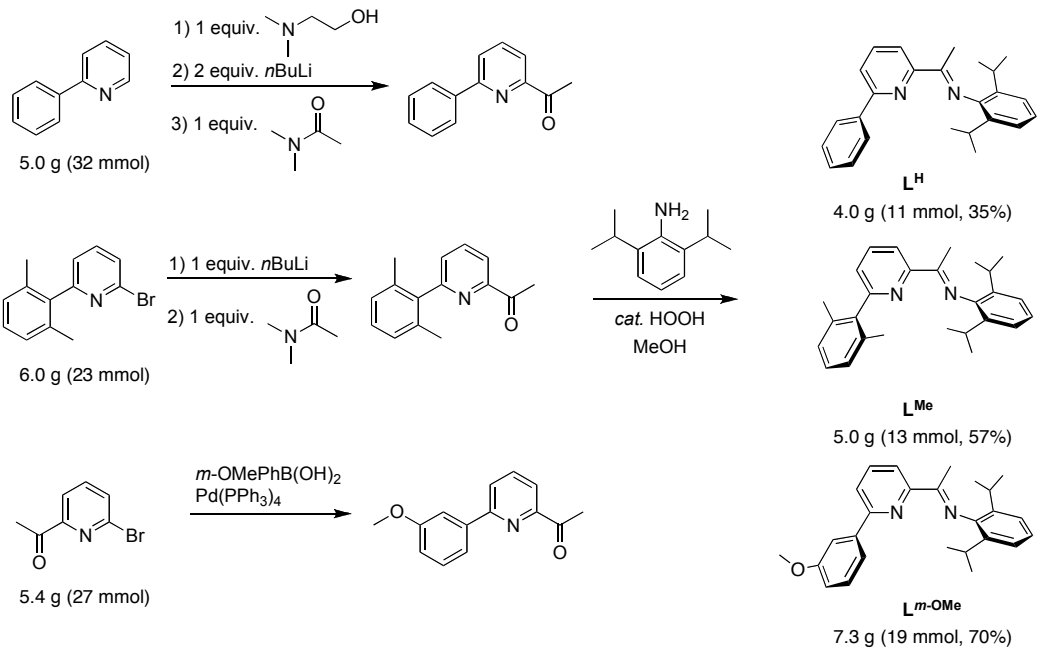

Scheme 3-5. Synthesis of pyridyl-imine ligands.

2545-2547.

3.3. Synthesis and Characterization of Copper(I)-α-Ketocarboxylate Complexes

3.3.1. Synthesis of Copper(I)-α-Ketocarboxylate Complexes

The first approach we took to synthesize a Cu^{I}-α-ketocarboxylate complexes of the ligand L^{Me} involved metathesis reactions of the corresponding copper(I) halide or triflate precursors with the alkali metal salts of the various α-ketoacids. For example, [L^{Me}CuCl] was prepared by mixing an equimolar amount of the CuCl and L^{Me} in THF and was isolated by recrystallisation through a slow diffusion of pentane into a concentrated THF solution of the copper(I) chloride compound (yield 80%). This compound was characterized by ^{1}H and $^{13}C\{^{1}H\}$ NMR spectroscopy (see below in section 3.3.3 for characterization). Then, [L^{Me}CuCl] was reacted with an equimolar amount of the NaBF (BF = benzoylformate) in THF. Unfortunately, this reaction resulted in disproportionation, as indicated by a brown precipitate of copper and greenish-blue solutions comprising copper(II) species.

In an alternative approach, we decided to use the copper(I) complex of more weakly coordinating triflate anion. The complex [L^{Me}CuOTf] was prepared by treatment of the copper(I) chloride compound with AgOTf in THF. After removing the AgCl precipitate by filtration through a plug of celite, the pure copper(I) triflate compound was isolated via a similar manner to that used for the copper(I) chloride precursor (yield 75%), and was characterized by ^{1}H and $^{13}C\{^{1}H\}$ NMR spectroscopy, CHN analysis, and X-ray crystallography (see below in section 3.3.2 and 3.3.3 for the crystal structure and

characterization). Reaction of the copper(I) triflate complex with the NaBF led to the formation of red-brown mixtures, from which we were able to isolated red-brown crystalline compounds (yield 40%). This compound was characterized by X-ray crystallography. It was found to be a dicopper(I) species bridged by a benzoylformate (see in section 3.3.2 for the detailed description of the crystal structure). While the overall structure of this compound is unique, it was not explored further because of our desire to study mononuclear Cu^{I}-α-ketoacid complexes analogous to the α-ketoacid-dependent non-heme iron enzyme active sites. Varying the stoichiometry of the benzoylformate (ranging from 0.5 to 2 equivalents) relative to the copper(I) triflate precursor did not influence the nature of the product, as revealed by ESI-MS measurements for the isolated compounds: the main species in solution has a peak at *m/z* = 1043.4 corresponding to the $[(L^{Me})_2Cu_2(BF)]^+$ ion.

By using $[Cu(Mes)]_4$ (Mes = mesityl) as a copper source and base for deprotonating the α-ketoacids, we were able to synthesize the Cu^{I}-α-ketoacid complexes in high yield (75 ~ 85%). This route involved treatment of $[Cu(Mes)]_4$ (Mes = mesityl) with α-ketoacids such as benzoyl or mesitoyl formic acid in THF followed by addition of the ligands (Scheme 3-6). After recrystallization, all four Cu^{I}-α-ketoacid complexes were isolated as red-brown crystalline solids. The crystal structures of all of the copper(I) complexes are described in section 3.3.2 and the characterization data in section 3.3.3.

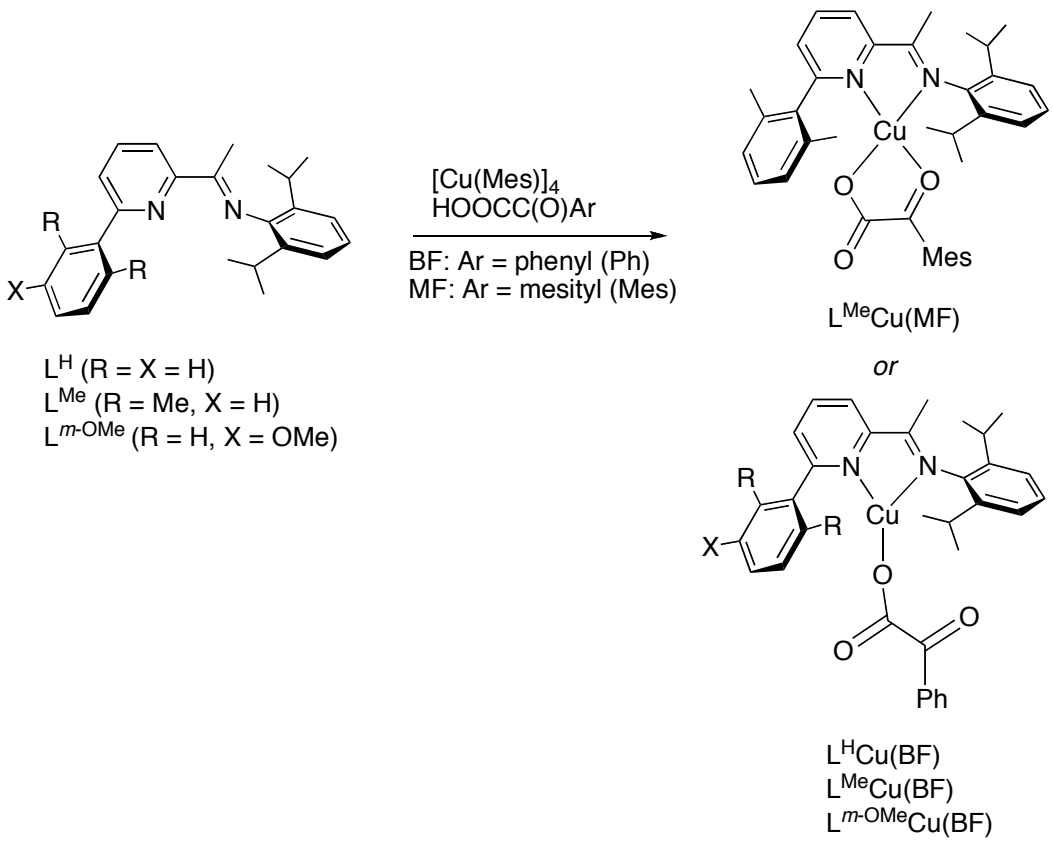

Scheme 3-6. Synthesis of Cu(I)-α-ketocarboxylate complexes.

3.3.2. X-ray Crystal Structures of Copper(I) Complexes

As desribed above, reaction of $[L^{Me}Cu(OTf)]$ with the NaBF led to the formation of red-brown crystalline complex formulated as $[(L^{Me})_2Cu_2(BF)](OTf)\bullet 2THF$. The crystal structure of the compound is depicted in Figure 3-2. This compound is a dicopper(I) species bridged by a benzoylformate in a κ^3-(*O,O,O*) fashion. This binding mode is similar to those seen in dinuclear Fe^{II} complexes of a tetradendate N4 ligand with phenylpyruvate or a derivative.[99] Each copper(I) ion shows a different coordination

[99] Paine, T. K.; Zheng, H.; Que, L., Jr. "Iron Coordination Chemistry of Phenylpyruvate: An Unexpected

environment. The Cu1 site has a distorted tetrahedral geometry consisting of the ligand's N donors and a bidendate BF coordinated via O2 and O3. On the other hand, the Cu2 ion is three-coordinate with the ligand N donors and the carboxylate oxygen (O1) from the benzoylformate forming the coordination sphere. The phenyl group is almost coplanar with the α-ketocarboxylate moiety, with a O2-C1-C2-O3 torsion angle of 10.2(4)°. The C-O bond lengths of the α-ketoacid moiety clearly indicate an electron-localized carboxylate anion (O1-C1 = 1.291(4) Å and O2-C1 = 1.222(4) Å) singly bonded (C1-C2 = 1.531(4) Å) to the α-carbonyl group (O3-C2 = 1.221(4) Å).

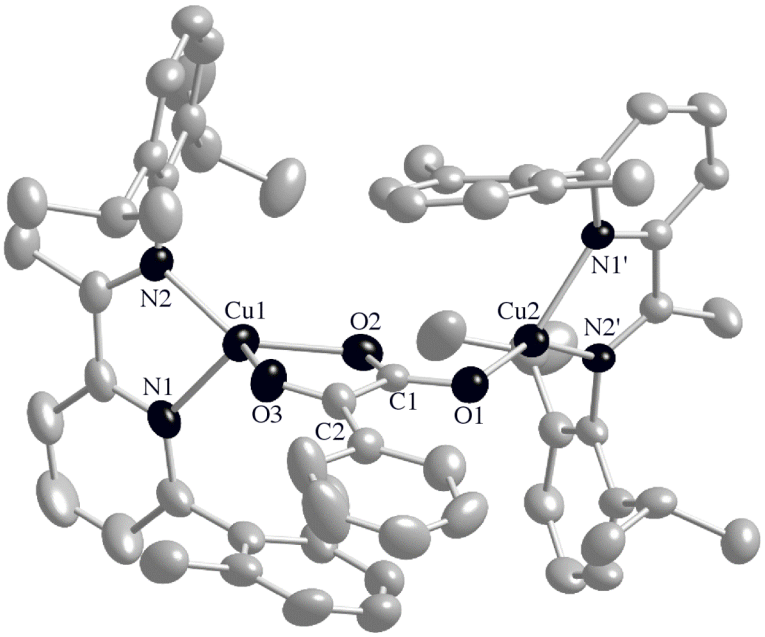

Figure 3-2. X-ray crystal structure of $[(L^{Me})_2Cu_2(BF)](OTf)\bullet 2THF$. All non-hydrogen atoms are shown as 50 % thermal ellipsoids. The counter anion, two THF solvated molecules and hydrogen atoms are omitted for clarity.

κ^3-Bridging Mode That Leads to Oxidative Cleavage of the C2-C3 Bond." Inorg. Chem. 2005, 44, 474-476.

Table 3-1. Selected bond lengths and angles for $[(L^{Me})_2Cu_2(BF)](OTf)^a$

a. Bond Lengths (Å)			
Cu1-O2	2.016(2)	Cu1-O3	2.180(2)
Cu1-N1	2.042(3)	Cu1-N2	1.992(2)
Cu2-O1	1.906(2)	Cu2-N1’	2.071(2)
Cu2-N2’	1.983(2)	O1-C1	1.291(4)
O2-C1	1.222(4)	O3-C2	1.221(4)
C1-C2	1.531(4)		
b. Bond Angles and Torsion Angles (deg)			
O2-Cu1-O3	77.39(9)	O2-Cu1-N1	124.31(10)
O2-Cu1-N2	138.38(10)	O3-Cu1-N1	113.26(10)
O3-Cu1-N2	126.05(10)	N1-Cu1-N2	81.20(11)
O1-Cu2-N1’	126.78(10)	O1-Cu2-N2’	148.75(10)
N1’-Cu2-N2’	80.74(9)	O2-C1-C2-C3	10.2(4)
O1-C1-C2-O3	-168.6(3)	O2-C1-C2-O3	-168.8(3)

[a] Estimated standard deviations are given in parantheses.Single crystals suitable for

Single crystals of Cu^I-α-ketocarboxylate complexes and $[L^{Me}Cu(OTf)]$ suitable for X-ray crystallography were grown by a slow diffusion of pentane into concentrated solutions of the corresponding copper(I) compounds either in THF or CH_2Cl_2. All complexes show similar Cu-N bond distances of 1.97-2.14 Å typical for Cu^I complexes, but they display diverse Cu-O bond distances depending on basicity of the oxy anions (α-

ketocarboxylates vs triflate) and the binding mode of the α-ketocarboxylates to the metal ion. In the crystal structure of [L^{Me}Cu(OTf)], the triflate anion was disordered over two positions, one with a Cu-O1 distance of 1.991(4) Å (52% occupancy) and the other with a Cu-O1' distance of 1.994(4) Å (48% occupancy). In both cases, the triflate anion binds to the copper(I) ion in a monodentate fashion. This Cu-O distance is ca. 0.08 Å longer compared to the corresponding values in LCu(BF) (L = L^{H}, L^{Me}, and $L^{m\text{-}OMe}$), and correlates with the stronger binding of the N2 donor to the copper(I) center (ca. 0.1 Å shorter Cu-N distances than those observed in LCu(BF)). The elongation of the Cu-O bond in [L^{Me}Cu(OTf)] can be ascribed to a weaker basicity of trifluorosulfonate ($pK_a \sim -15$)[100] compared to benzoylformate ($pK_a = 1.21$)[101].

The binding mode of the α-ketoacid to the copper(I) center in these model complexes is also flexible (monodentate vs. bidentate) as seen in the analogous iron(II) compounds. In L^{Me}Cu(MF) (MF = mesitoylformate), the coordination environment of the copper(I) ion is similar to that of the Cu1 center in [$(L^{Me})_2Cu_2$(BF)](OTf). The α-ketocarboxylate binds to a four coordinate Cu^{I} ion in a bidentate fashion via one oxygen from the carboxylate moiety and one oxygen from the α-keto functionality. The geometry is distorted from tetrahedral, as reflected by a τ_4 value of 0.63 (values of 0 and 1 being associated with ideal square planar or tetrahedral geometries, respectively).[81] Also, the α-ketocarboxylate moiety displays an electron-localized carboxylate anion, as evidenced from the C-O bond distances (C1-O1 = 1.261(3) Å, C1-O3 = 1.230(3) Å, C2-O2 =

[100] Scherrer, R. A.; Donovan, S. F. "Automated Potentiometric Titrations in KCl/Water-Saturated Octanol: Method for Quantifying Factors Influencing Ion-Pair Partitioning." *Anal. Chem*. **2009**, *81*, 2768-2778.
[101] Scherrer, R. A.; Donovan, S. F. "Automated Potentiometric Titrations in KCl/Water-Saturated Octanol: Method for Quantifying Factors Influencing Ion-Pair Partitioning." *Anal. Chem*. **2009**, *81*, 2768-2778.

1.223(3) Å, and C1-C2 = 1.545(3) Å). A main structural difference between $L^{Me}Cu(MF)$ and $[(L^{Me})_2Cu_2(BF)](OTf)$ involves the orientation of the aromatic ring with respect to the the α-ketocarboxylate moiety. While the latter shows a coplanar arrangement of the phenyl group, in the former the mesityl group is almost oriented perpendicular to the α-ketocarboxylate plane (~84°). This orientation may be due to steric pressure from the three methyl groups of mesitoylformate (MF), which results in two ortho methyl groups from MF effectively encapsulating the α-ketocarbon. This feature may have important implications for O_2 reactivity (see below). Similar structural features are also seen in the recently reported Fe^{II} complexes of sterically congested α-ketocarboxylates.[102]

In contrast, other copper(I) complexes of the benzoylformate (BF) exhibit three-coordinate Cu^I ions close to a planar T-shaped geometry, where the α-ketocarboxylates bind solely through a carboxylate O atom with the α-keto group oriented approximately orthogonal to the carboxylate group, as indicated by O1-C1-C2-O3 torsion angles of 102.9(3)° - 124.0(2)°.

[102] Friese, S. J.; Kucera, B. E.; Young, V. G.; Que, L., Jr; Tolman, W. B. "Iron(II) Complexes of Sterically Bulky α-Ketocarboxylates. Structural Models for α-Ketoacid-Dependent Nonheme Iron Halogenases." *Inorg. Chem*. **2008**, *47*, 1324-1331.

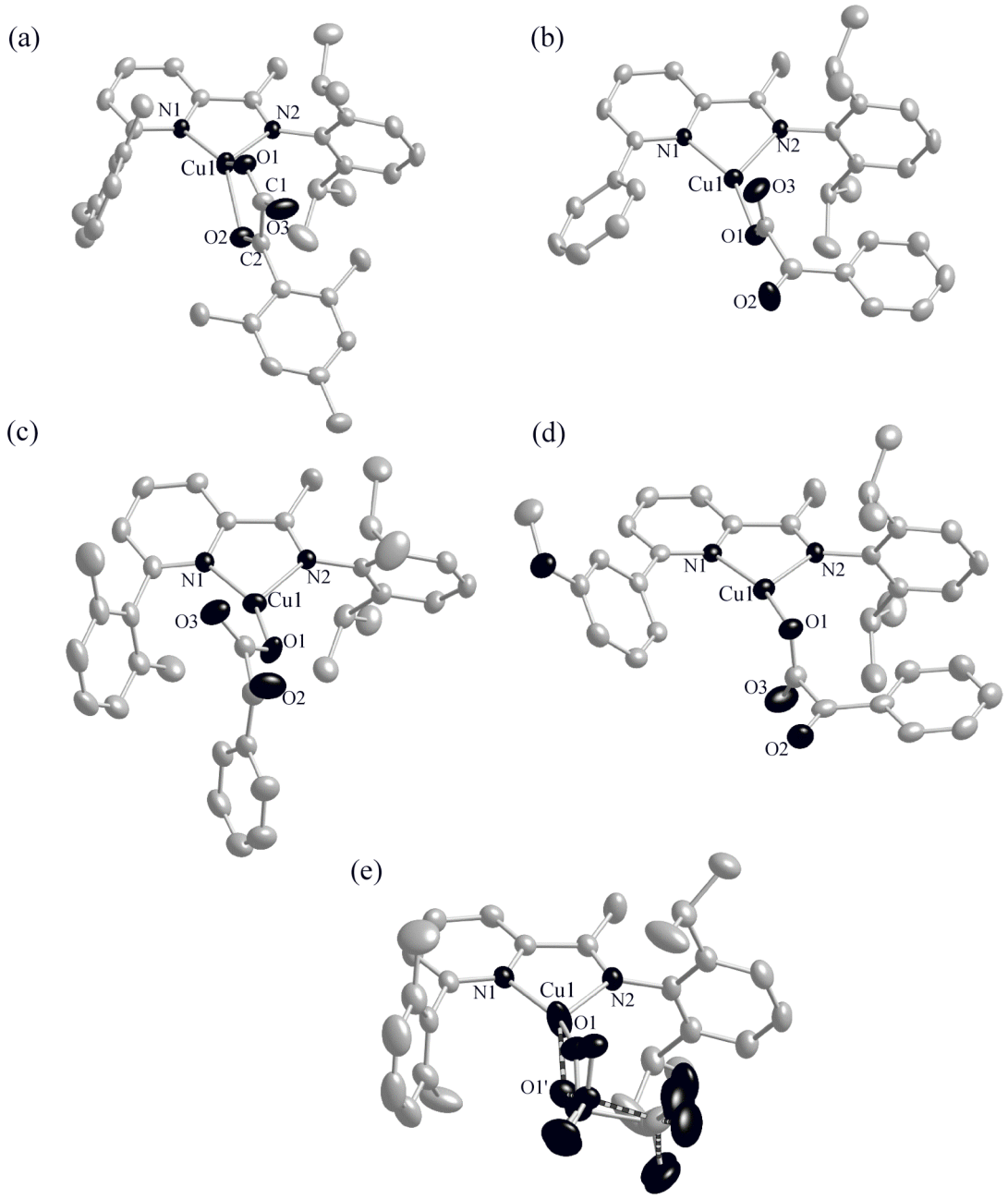

Figure 3-3. Representation of the X-ray crystal structures of $L^{Me}Cu(MF)$ through $L^{Me}Cu(OTf)$. All non-hydrogen atoms are shown as 50 % thermal ellipsoids. Hydrogen atoms are omitted for clarity.

Table 3-2. Selected bond lengths (Å) and angles (deg)[a]

	$L^{Me}Cu(MF)$	$L^{H}Cu(BF)$	$L^{Me}Cu(BF)$	$L^{m\text{-}OMe}Cu(BF)$	$L^{Me}Cu(OTf)$
Cu1-N1	1.9676(19)	1.9831(19)	1.9804(18)	1.969(2)	1.975(2)
Cu1-N2	2.107(2)	2.1113(19)	2.0932(17)	2.140(2)	2.008(2)
Cu-O1	1.9904(19)	1.9042(16)	1.8757(17)	1.9010(19)	1.991(4)
Cu1-O2	2.1815(19)				
N1-Cu1-N2	79.99(8)	80.74(7)	80.55(7)	80.62(9)	80.69(9)
N1-Cu1-O1	137.52(8)	154.80(8)	152.48(6)	158.31(9)	142.95(14)
N2-Cu1-O1	115.31(8)	123.60(8)	126.66(7)	120.90(9)	128.84(14)
O2-Cu1-N1	134.09(8)				
O2-Cu1-N2	112.07(8)				
O1-Cu1-O2	79.78(7)				
C1-O1	1.261(3)	1.279(3)	1.275(2)	1.268(4)	
C1-O3	1.230(3)	1.216(3)	1.217(2)	1.222(4)	
C1-C2	1.545(3)	1.529(3)	1.535(3)	1.532(4)	
C2-O2	1.223(3)	1.216(3)	1.216(3)	1.212(4)	
O1-C1-C2-O2	0.3(3)	103.5(3)	124.0(2)	102.9(3)	

[a] Estimated standard deviations are given in parentheses.

3.3.3. Properties of Copper(I) Complexes in solution

UV-vis spectra of the complexes $L^{Me}Cu(MF)$, $L^{H}Cu(BF)$, and $L^{Me}Cu(OTf)$ in acetone at –80 °C are shown in Figure 3-4; those of $L^{Me}Cu(BF)$ and $L^{m\text{-}OMe}Cu(BF)$ are are almost identical to that of $L^{H}Cu(BF)$ and thus are not shown.

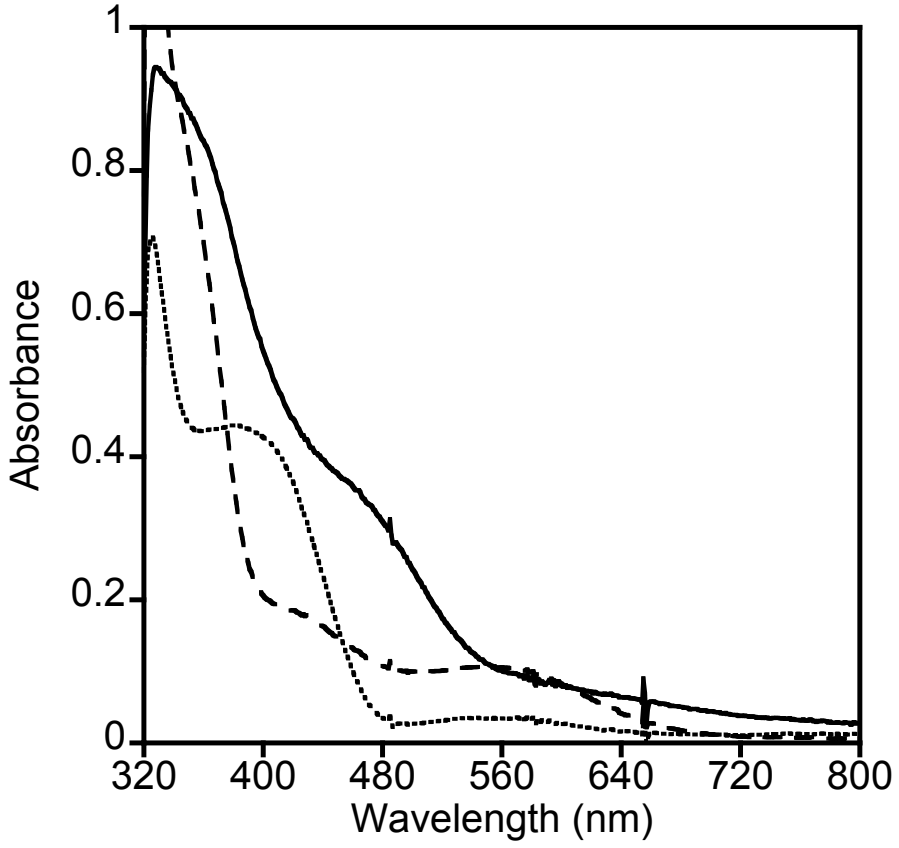

Figure 3-4. UV-vis spectra of 0.25 mM solutions in acetone at –80 °C of $L^{Me}Cu(MF)$ (solid line), $L^{H}Cu(BF)$ (dashed line), and $L^{Me}Cu(OTf)$ (dotted line).

For LCu(BF) complexes having a monodentate α-ketocarboxylate in their solid state structures, only weak visible absorption bands at 410 and 560 nm are observed. The latter band is also seen in $L^{Me}Cu(OTf)$ featuring the monodentate triflate anion, but its intensity is weaker relative to those in LCu(BF). In contrast, the UV-vis spectrum of $L^{Me}Cu(MF)$

displays more intense and broader features ranging from 410 to 550 nm. Though the origin of these features is known with certainty, we postulate that these bands are $Cu^{I} \rightarrow$ α-ketocarboxylate MLCT transitions on the basis of the crystal structure of the complex (bidentate α-ketocarboxylate) and by analogy to the analogous Fe^{II} complexes. In general, the Fe^{II} complexes of a bidentate α-ketocarboxylate exhibit unique visible absorption features originating from $Fe^{II} \rightarrow$ α-ketocarboxylate charge transfer (MLCT) transitions, which are sensitive to the nature of α-ketocarboxylate and the metal's Lewis acidity and coordination number.[5b,62a-b,90-91] In sum, the UV-vis data for the copper complexes appear to indicate that the Cu^{I}-α-ketocarboxylate complexes maintain their structural integrity in solution.

Other relevant evidence to support this assumption comes from ^{1}H and ^{13}C NMR data. For all of the Cu^{I}-α-ketocarboxylate complexes, similar ^{1}H and ^{13}C NMR spectra are observed in CD_2Cl_2 at ambient temperature that exhibit a single set of sharp peaks. To illustrate, ^{1}H NMR spectra for the ligand L^{Me}, $L^{Me}Cu(BF)$ and $L^{Me}Cu(MF)$ are depicted in Figure 3-5. Binding of the copper ion to the N-donor ligand affects the chemical shifts of the ligand protons. The most notable changes are observed in pyridyl (*β*, *β'* and *γ*) and ketimine proton (NC*Me*) signals. The py *β'* and *γ* protons are downfield shifted, but the py *β* is upfield shifted relative to those of the free ligand upon complexation. The ketimine protons are also downfield shifted when the copper ion binds to the ligand. Moreover, the peaks from the α-ketocarboxylate are sharp and well resolved. For example, the ^{1}H NMR spectrum of $L^{Me}Cu(BF)$ displayed peaks between 7.3 and 7.7 ppm with chemical shifts and splitting patterns consistent with assignment as the BF protons. Taken together, the ^{1}H NMR data suggest that in solution the Cu^{I}-α-ketocarboxylate

complexes either retain the structures observed by X-ray diffraction or undergo fluxional processes that are sufficiently rapid to result in an averaged spectrum (cf. bidentate/monodentate α-ketocarboxylate isomerization).

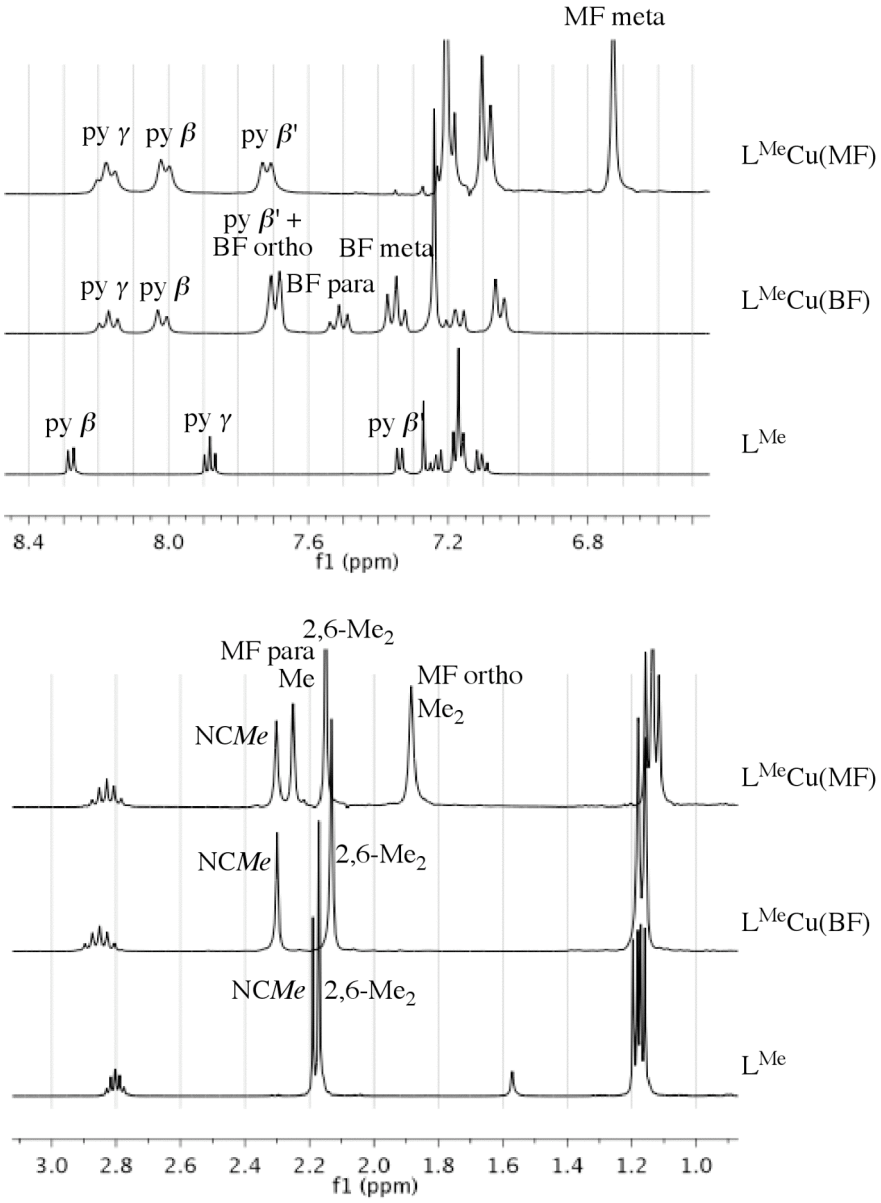

Figure 3-5. ^{1}H NMR spectra of L^{Me}, $L^{Me}Cu(BF)$ and $L^{Me}Cu(MF)$ in CD_2Cl_2. Expanded aromatic regions (above) and aliphatic regions (below). Greek letters designate positions on the pyridine ring, and ortho, meta, and para designate positions on the benzoyl- or mesitoylformate.

To evaluate these hypotheses, Profs. Laura Gagliardi, Christopher Cramer and Dr. Stefan Huber performed density functional calculations at the M06L level[103] on model systems with unsubstituted aryl rings. The calculation indicated that the binding mode of the ketocarboxylate to copper is flexible. Specifically, the monodentate and bidentate structures are energetically similar, with the latter preferred by about 7 kcal/mol. This result is consistent with the observed fluxional behabior in solution.

3.4. Dioxygen Reactivitiy of Copper(I) Complexes

3.4.1. Oxygen reactivity of Copper(I) Complexes

A main goal in this study is to understand how the α-ketocarboxylates influence the oxygenation of the copper(I) complexes and to elucidate whether the oxygenation of the Cu^{I}-α-ketocarboxylate complexes follows a similar reaction pathway as that drawn for α-ketoacid dependent iron enzymes and models. We initially envisioned that the copper(I) complex of the pyridine-imine based bidendate ligand would not afford the oxygenation chemistry in the absense of the α-ketocarboxylate. Consistent with our expectation, the complex $L^{Me}Cu(OTf)$ was unreactive toward O_2 in acetone or THF at –80 °C as indicated by no significant change of the UV-vis spectrum during oxygenation. However, prolonged O_2 bubbling in THF solution at ambient temperature gradually resulted in a

[103] a) M06L: Zhao, Y.; Truhlar, D. G. "A new local density functional for main-group thermochemistry, transition metal bonding, thermochemical kinetics, and noncovalent interactions." *J. Chem. Phys*. **2006**, *125*, 194101. b) CASPT2: Andersson, K.; Malmqvist, P. A.; Roos, B. O. "Second-order perturbation theory with a complete active space self-consistent field reference function." J. Chem. Phys. **1992**, *96*. 1218-1226.

color change from red-brown to greenish-blue. Analysis of the crude oxidized mixtures of $L^{Me}Cu(OTf)$ by ESI-MS indicated formation of a complex mixture of products. Major Cu-containing species were identified as $[L_nCu]^+$ (n = 1 or 2). This result suggests that the oxygenation of $L^{Me}Cu(OTf)$ results in extensive ligand redistribution and the redox processes such as autooxidation of the copper(I) center, instead of any O_2-containing intermediates.

Incorporation of the α-ketocarboxylate anion to the copper(I) ion markedly changes the O_2 reactivity. Depending on the structure of the α-ketocarboxylate and the ligand framework, each Cu^I-α-ketocarboxylate complex showed significantly different O_2 reactivity. Both $L^{Me}Cu^I(MF)$ and $L^{Me}Cu^I(BF)$ were unreactive toward O_2 in acetone or THF at –80 °C. Similar to the case of $L^{Me}Cu(OTf)$ complex, prolonged O_2 bubbling at ambient temperature resulted in extensive ligand redistribution and redox processes. For example, ESI-MS data for the crude oxidized mixtures of $L^{Me}Cu^I(MF)$ indicated formation of a complex mixture of products including both Cu^I and Cu^{II} species with no evidence for decarboxylation to yield 2,4,6-trimethylbenzoic acid. Major Cu^I-containing species were identified as $[L_nCu]^+$ (n = 1 or 2), and we were able to isolate and characterize one such Cu^{II} species from the reaction mixtures. The structural analysis by X-ray crystallography (Figure 3-6) showed that two Cu^{II} ions are bridged by four mesitoylformates via two oxygen atoms from the carboxylates in a paddle wheel geometry (determined only via a partial X-ray diffraction data collection).[104] Each Cu center has an additional THF solvent at an axial position. In this structure, four MF

[104] It ($C_{52}H_{66}Cu_2O_{14}$; M_w = 1042.15) crystallized in the monoclinic space group P1, with a = 9.8398 Å, b = 10.5219 Å, c = 13.3041 Å, α = 96.2210º, β = 107.8550º, γ = 104.490º, V = 1243.48 Å^3, and Z = 1.

ligands show different arrangements. While two MF ligands lying in the plane defined by Cu-Cu axis have O-C-C-O torsion angles of 14 to 15° close to that seen in the parent $L^{Me}Cu(MGA)$ complex, the other two MF ligands display an arrangement much closer to that seen in other LCu(BF) complexes as reflected by O-C-C-O torsion angles of 114 to 117°. These observations reinforce the notion that binding of an α-ketocarboxylate to the copper center is flexible.

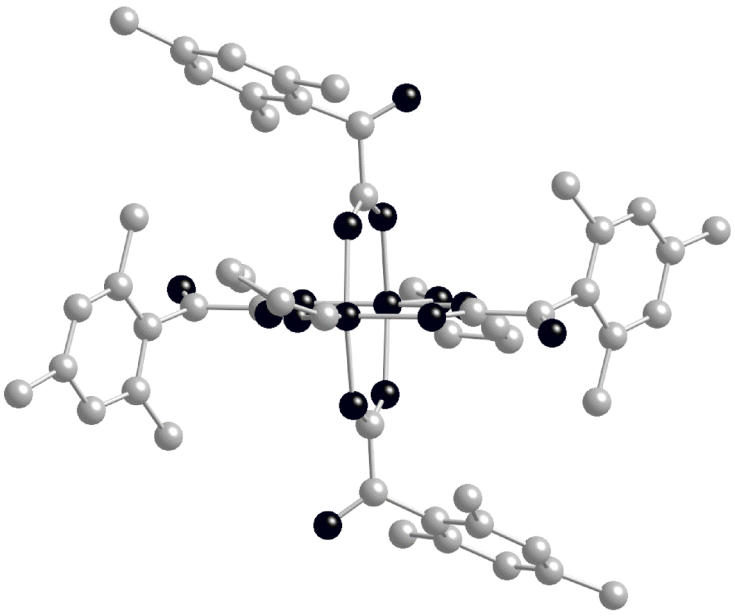

Figure 3-6. Representation of the X-ray crystal structure of $[Cu_2(MF)_4(THF)_2]$. All non-hydrogen atoms are shown isotropically. Hydrogen atoms are omitted for clarity.

Further evidence indicating that decarboxylation did not occur upon oxygenation of $L^{Me}Cu(MF)$ and $L^{Me}Cu(BF)$ came from ^1H NMR analyses on the recovered organic products, showing mainly intact ligand and α-ketocarboxylic acid. The fact that oxidative decarboxylation was not observed for $L^{Me}Cu(MF)$ could be rationalized by its structural features, in particular the perpendicular orientation of the central mesityl ring with

respect to the α-ketocarboxylate moiety. In this arrangement two methyl groups at the 2 and 6 positions of MF effectively shield the ketonic carbon atom from attack by a bound O_2 (assuming that the initial reaction between copper(I) center and O_2 takes place). As a result, oxygenation of $L^{Me}Cu$(MF) yields the autooxidation of the Cu^I center and ligand redistribution instead of inducing the oxidative decarboxylation of the α-ketocarboxylate. These observations parallel those for the oxygenation of the Fe^{II} complexes of the same or related α-ketocarboxylates.[26] The reasons for the lack of decarboxylation of $L^{Me}Cu$(BF) is more difficult to discern. One rationale centers on the weak electron-donating nature of the pyridylimine ligand. Thus, we hypothesize that the initial O_2 binding to the Cu center is not thermodynamically feasible because of their unfavorable redox properties. This hypothesis is in good agreement with calculations showing that the oxygenation is endergonic in the case of model system with unsubstituted aryl rings (see below). Also, calculations on model system indicated that the rate-determining step is a subsequent decarboxylation by the 1:1 Cu/O_2 adduct with a significant kinetic barrier. Given that the ligands L^{Me} and L^H are expected to have similar electron-donating power, but the Cu(BF) complex of the latter does decarboxylate (see below), the lack of reactivity of $L^{Me}Cu$(BF) with O_2 could be traced to the steric bulk of the methyl substituents of the 2,6-dimethylphenyl flanking group blocking the decarboxylation by the 1:1 Cu/O_2 adduct.

In contrast, exposure of solutions of LCu(BF) (L = L^H or $L^{m\text{-}OMe}$) to O_2 in acetone at –80 °C resulted in gradual (~2–4 h) formation of brown solutions, as revealed by a new band at 405 nm (Figure 3-7). However, this band was not perturbed upon warming, suggesting that it is not due to a thermally sensitive Cu/O_2 intermediate that would be

expected to exhibit the characteristic absorption features that decay as the reaction temperature is increased.[5e,11d,38a-b] Instead, the position and intensity of this band is reminiscent of the copper(II)-phenolate complexes that exhibit phenolate to copper(II) charge transfer transitions in a wide range of the visible region.[105] Thus, we hypothesize that this band also has the same origin. In order to prove this hypothesis, we decided to analyze the organic products that were recovered from the oxygenation of $L^{H}Cu(BF)$ and $L^{m\text{-}OMe}Cu(BF)$ by ^{1}H NMR spectroscopy and/or ESI-MS.

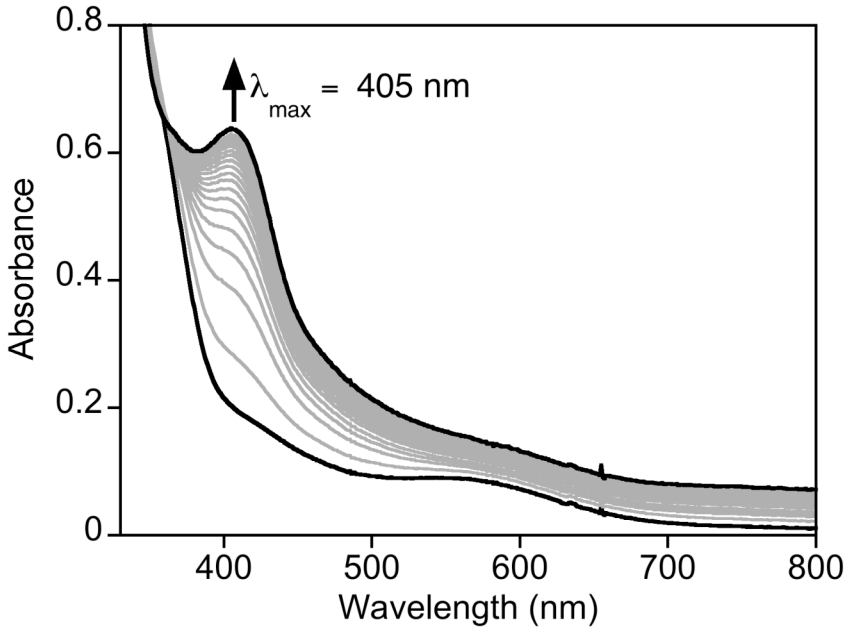

Figure 3-7. UV-vis spectral changes during the reaction of $L^{m\text{-}OMe}Cu(BF)$ with O_2 in acetone at –80 °C (0 → 60 min).

[105] Ainscough, E. W.; Bingham, A. G.; Brodie, A. M.; Husbands, J. M.; Plowman, J. E. "Small molecule analogs for the specific metal-binding site of lactoferrin. Part 2. Phenolato complexes of copper(II) and the nature of the charge-transfer transition in the visible region." *J. Chem. Soc., Dalton Trans*. **1981**, *8*, 1701-1707.

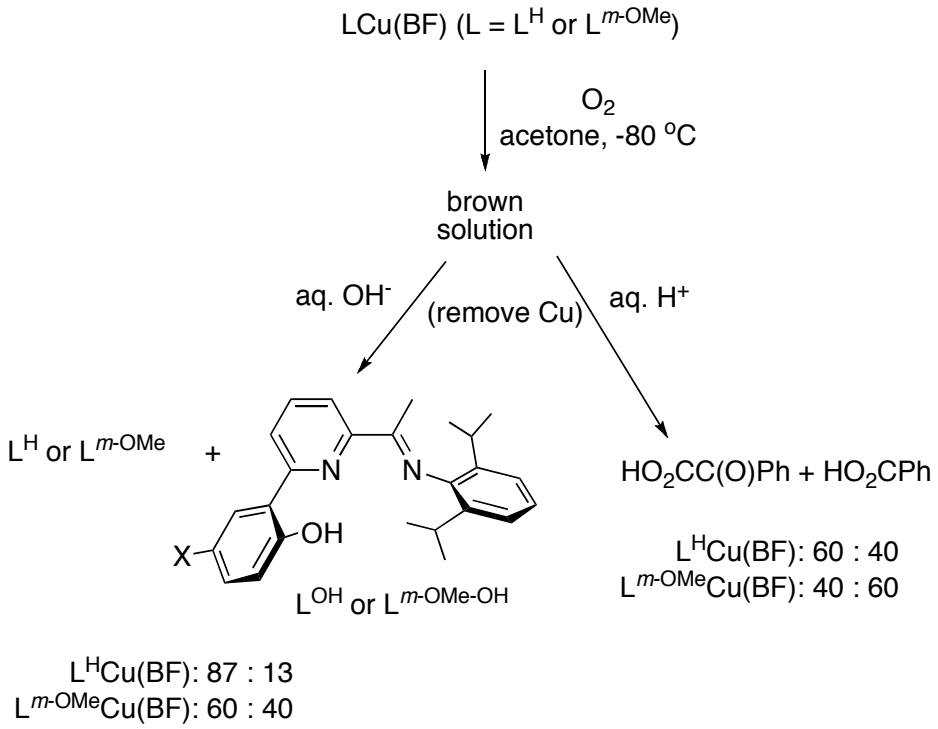

Scheme 3-7. Reactivity of $L^{H}Cu(BF)$ and $L^{m\text{-}OMe}Cu(BF)$ with O_2.

After warming and removal of the solvent, the dried brown residues were redissolved in Et_2O, followed by addition of aq. NH_4OH to detach the copper ion from the ligands. The ligands were then extracted with Et_2O, washed with water, and dried with $MgSO_4$. Removal of the solvent in vacuo led to isolation of a mixture of intact ligands (L^{H} or $L^{m\text{-}OMe}$) and hydroxylated versions (L^{OH} or $L^{m\text{-}OMe\text{-}OH}$), as revealed by the representative ^1H NMR spectrum of the recovered ligand residues for $L^{m\text{-}OMe}Cu(BF)$ (Figure 3-8). It clearly indicates that there are two sets of distinctive peaks. While one set of peaks is identical to those of the intact ligand ($L^{m\text{-}OMe}$), the other is assigned as those of the hydroxylated ligand ($L^{m\text{-}OMe\text{-}OH}$). Evidence for such assignment comes from a singlet peak at ~14 ppm for the proton of the hydroxyl group, similar to that of the related 2-

hydroxyphenylpyridine.[106] Also, positive ion ESI-MS data on the recovered ligand residue exhibits intense peaks at *m/z* values of 403 and 425, with isotope distribution patterns consistent with [$L^{m\text{-OMe-OH}}$ + X^+] (X = H or Na). The combined ^{1}H NMR and ESI-MS data support assignment of the hydroxylated species as the molecular structure shown in Scheme 3-7. This result also supports the assignment of the band at 405 nm of the oxygenated species as the phenolate to copper(II) charge transfer transition.

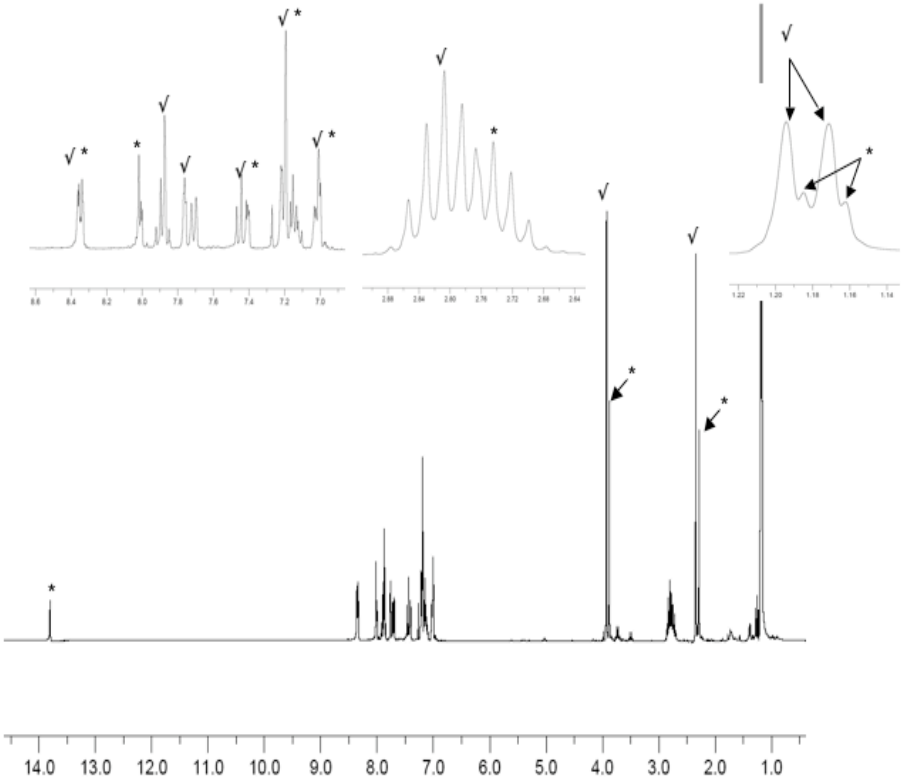

Figure 3-8. ^{1}H NMR spectrum of the recovered ligands containing $L^{m\text{-OMe}}$ (✓) and $L^{m\text{-OMe-OH}}$ (*).

[106] Chen, X.; Hao, X.-S.; Goodhue, C. E.; Yu, J.-Q. "Cu(II)-Catalyzed Functionalizations of Aryl C-H Bonds Using O_2 as an Oxidant." *J. Am. Chem. Soc.* **2006**, *128*, 6790-6791.

An obvious question that arises from the observed ligand hydroxylation concerns whether this reaction takes place by the Cu-based mechanism shown in Scheme 3-3. If so, the reaction should result in formation of the benzoic acid from the benzoylformate. To test this, we also analyzed the acidic products that were recovered from the combined aqueous layers by treatment with conc. HCl(aq) and subsequent extraction with CH_2Cl_2. Consistent with our expectation, ^{1}H NMR data of the recovered acidic residues for $L^{m\text{-}OMe}Cu(BF)$ clearly show a mixture of benzoylformic acid and benzoic acid on the basis of the comparison to those of authentic samples.

Overall recoveries for ligand and acidic products for the oxygenations of both $L^{H}Cu(BF)$ and $L^{m\text{-}OMe}Cu(BF)$ were found to be greater than 95%, but the relative ratio of the product distributions was different. For $L^{H}Cu(BF)$, 13% of hydroxylated ligand and 40% of benzoic acid was observed, whereas these values increased to 40% and 60%, respectively, for $L^{m\text{-}OMe}Cu(BF)$. These different extents of formation of the hydroxylated ligand and benzoic acid for $L^{H}Cu(BF)$ versus $L^{m\text{-}OMe}Cu(BF)$ indicate differing extents of decarboxylation and more efficient arene hydroxylation for $L^{m\text{-}OMe}Cu(BF)$, which contains a more electron-rich arene group that would be expected to more rapidly trap an electrophilic copper-oxygen species.

In order to track the fate of O_2, we prepared two samples by using either $^{16}O_2$ or $^{18}O_2$ for the oxygenation of $L^{m\text{-}OMe}Cu(BF)$. ESI-MS data were obtained for the crude brown oxygenated product solutions (Figures 3-9 and 3-10). With $^{16}O_2$, intense peaks with correct *m/z* and isotope patterns for $[L^{m\text{-}OMe\text{-}O}Cu]^+$ (*m/z* = 464) and $[(L^{m\text{-}OMe\text{-}O})_2Cu_2(benzoate)]^+$ (*m/z* = 1049) were observed. When $^{18}O_2$ was used, these peaks increased by 2 and 6 mass units, respectively. The results clearly indicate that one O atom

from O_2 is incorporated into the ligand and the second into the benzoate.

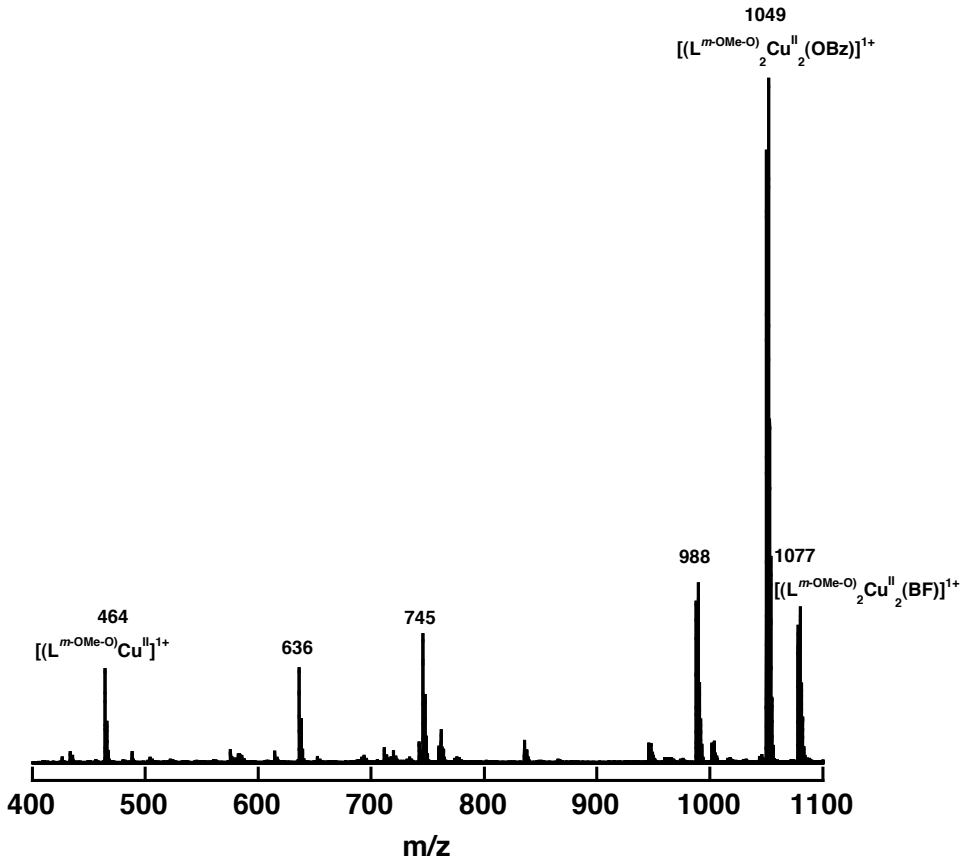

Figure 3-9. ESI-MS data of the brown solution resulting from reaction of $L^{m\text{-}OMe}Cu(BF)$ with $^{16}O_2$ (OBz = benzoate, BF = benzoylformate, $L^{m\text{-}OMe\text{-}O}$ = anion of the hydroxylated ligand, see Scheme 3-7). The isotope envelops at m/z values of 464 and 1049 are shown in detail in Figures **3-10**.

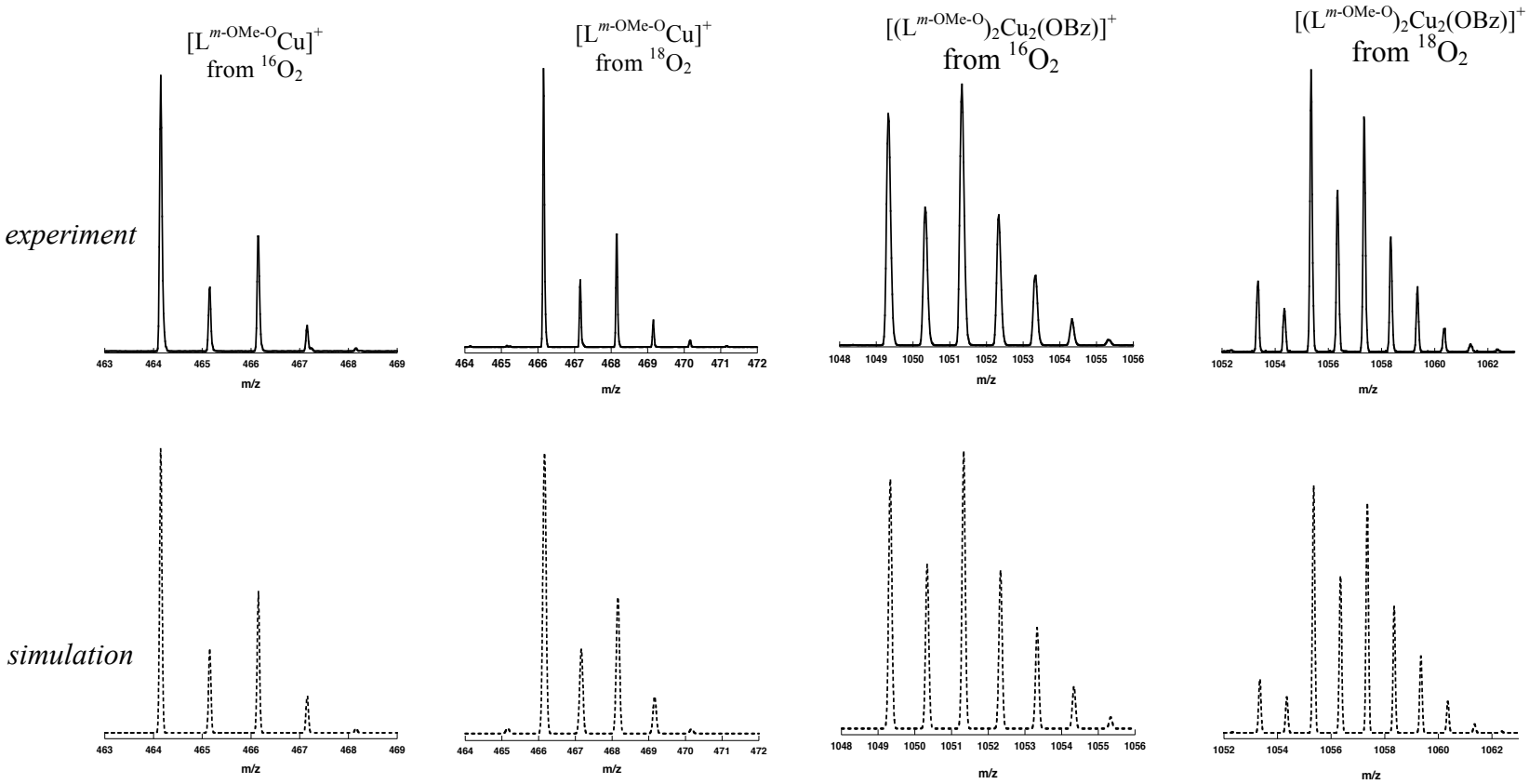

Figure 3-10. Expanded regions of the ESI-MS data of the solution resulting from reaction of $L^{m\text{-OMe}}Cu(BF)$ with $^{16}O_2$ or $^{18}O_2$, with experimental data (top) and simulations (bottom). For the simulation of $[(L^{m\text{-OMe-O}})Cu]^+$ derived from the reaction with $^{18}O_2$, the simulation is for incorporation of one ^{18}O atom. For the simulation of $[(L^{m\text{-OMe-O}})_2Cu_2(OBz)]^+$ derived from the reaction with $^{18}O_2$, the simulation is for a mixture of the compounds with either three or two ^{18}O atoms (4:1 ratio).

Overall, the experimental results described above parallel those seen in the oxygenation of the iron(II) model complex [$Fe^{II}(Tp^{Ph2})$(BF)] (decarboxylation and ligand hydroxylation). Thus, these results are in good agreement with our expectation that reaction of O_2 with the Cu^{I}-α-ketocarboxylate complexes, $L^{H}Cu$(BF) and $L^{m\text{-}OMe}Cu$(BF), follows a reaction pathway akin to that drawn for Cu in Scheme 3-3. That is, the bound α-ketocarboxylate undergoes an O_2-induced decarboxylation (formation of carboxylic acid via a loss of CO_2) to yield a reactive species that could be trapped by the arene ring hydroxylation of the supporting ligand.

3.4.2. Theoretical Evaluation for Oxygenation Mechanism of Copper(I)-α-Ketocarboxylate Complexes

The fact that no oxidative decarboxylation was observed in cases of $L^{Me}Cu$(MF) and $L^{Me}Cu$(BF), and that $L^{Me}Cu$(OTf) was also unreactive with O_2, suggests that involvement of a peroxo– or bis(oxo)dicopper species derived from reaction of the LCu(I) fragment of $L^{H}Cu$(BF) or $L^{m\text{-}OMe}Cu$(BF) with O_2 is unlikely to take place in the process(es) that yield(s) hydroxylated ligand. Rather, the observed results with $L^{H}Cu$(BF) or $L^{m\text{-}OMe}Cu$(BF) are more consistent with a reaction pathway akin to that drawn for Cu in Scheme 3-3. Nevertheless, we were not able to detect any observable intermediates during such processes. Thus, key questions concern what reactive species are responsible for the ligand hydroxylation observed in this study and what chemical steps are involved in the formation of such species. To address these questions, Profs. Laura Gagliardi,

Christopher Cramer and Dr. Stefan Huber computed mechanisms for the reaction of model system (a truncated model lacking aryl substituents) with dioxygen at the M06L density functional level, as shown in Scheme 3-8.

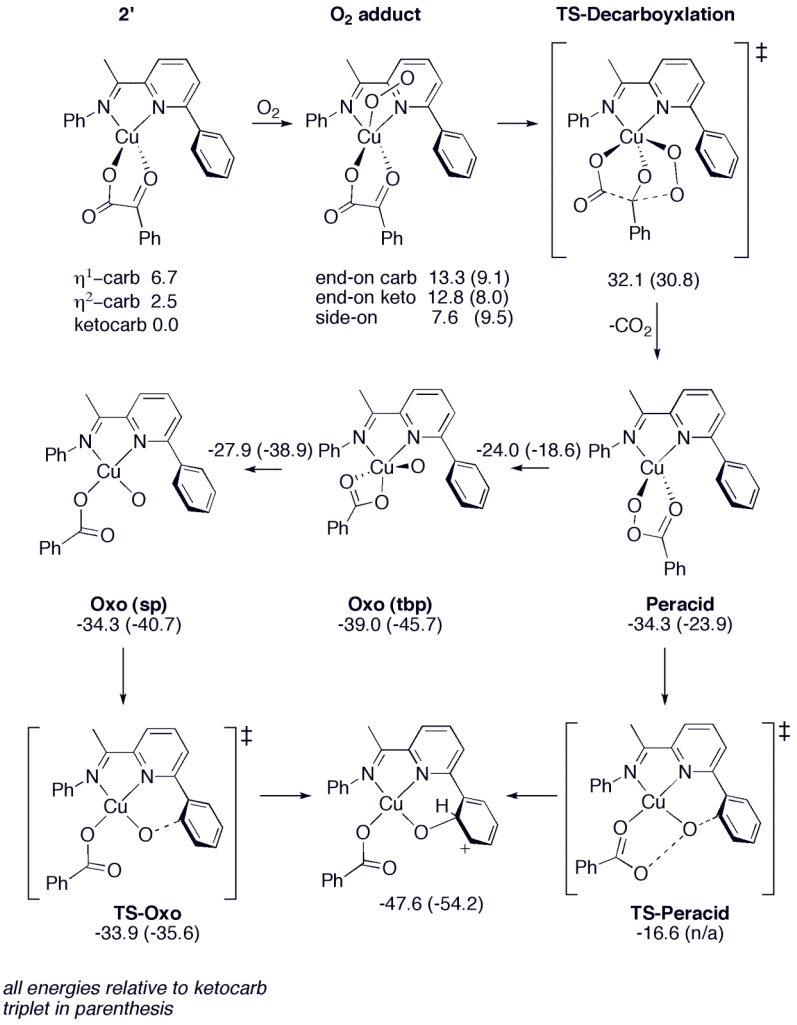

Scheme 3-8. Calculated Mechanisms for O_2-Induced Decarboxylation and Arene Substituent Hydroxylation of Model system. Nomenclature; ketocarb for a bidentate α-ketocarboxylate, η^2-carb for a bidentate carboxylate, η^1-carb for a monodentate carboxylate, side-on for a side-on bound O_2 addut with a modentate caboxylate, end-on keto for an end-on bound O_2 adduct with a bidentate α-ketocarboxylate, and end-on carb for an end-on bound O_2 adduct with a monodentate carboxylate. Free energies (kcal/mol) relative to lowest-energy ketocarboxylate for singlet and triplet (in parentheses) intermediates and TS structures in oxidation reaction mechanisms.

The calculations show that the model system has a bidentate α-ketocarboxylate (ketocarb) in its resting state that is lower in energy compared with those of either a bidentate (η^2-carb) or a monodentate (η^1-carb) carboxylate. Subsequent addition of O_2 leads to formation of an "O_2 adduct" that adopts either of two energetically similar structures: a singlet structure (7.6 kcal/mol) with a side-on bound O_2 fragment, analogous in character to Cu^{III}-peroxo species supported by β-diketiminate ligands,[38c] or a triplet state (8.0 kcal/mol) featuring end-on O_2 coordination (shown). After migration of one O atom of the O_2 fragment to the ketocarbon of the ketocarboxylate, loss of CO_2 generates a singlet Cu^{I}-peracid complex ("Peracid") with a gas-phase free energy of activation of 15.4 kcal/mol. Decarboxylation is predicted overall to be exergonic by about 34 kcal/mol.

Two pathways leading to oxygenation of the 2-pyridyl benzene ring from this peracid complex were characterized. In the first, a singlet transition-state structure involving oxidation of the ligand by the peracid itself was located ("TS-Peracid") as shown in Figure 3-11. This structure features O–O and C–O bond distances of 2.47 and 2.38 Å, respectively, and a Cu–O bond distance of 1.72 Å. Thus, this transition state is "early" with respect to attack at the arene, but "late" with respect to O–O bond breaking, so it appears very "oxo-like" in character. After this transition state, spin crossing is required to reach the triplet ground state of the hydroxylated product. Overall, the direct arene hydroxylation by the "Peracid" intermediate was predicted to be thermodynamically favorable ($\Delta G \sim 20$ kcal/mol).

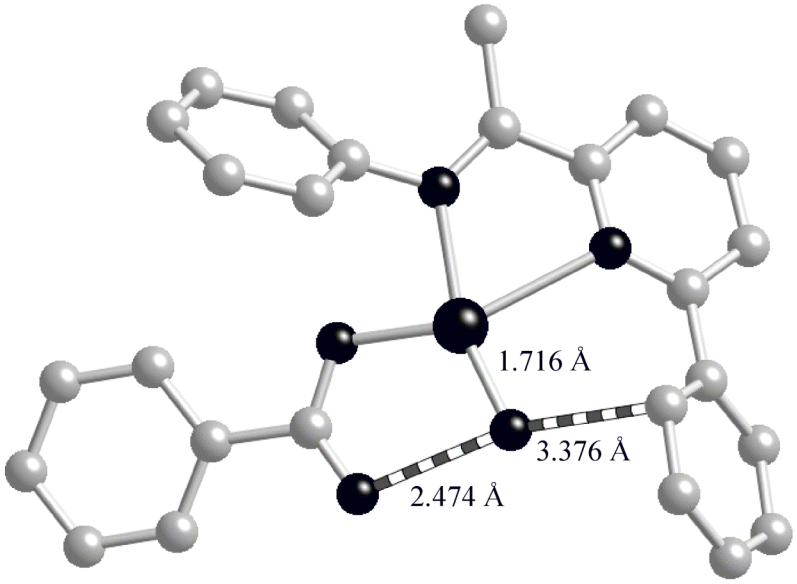

Figure 3-11. Transition state structure of the arene hydroxylation by "Peracid".

In the second pathway, initial cleavage of the peracid O–O bond leads to a stable trigonal bipyramidal copper-oxo intermediate, which isomerizes to a square planar isomer. Both species are best described as triplet Cu^{II}-oxyl species,[2,54b] implying the involvement of the spin crossing event upon conversion of "Peracid" to "Oxo" intermediate. The square planar intermediate effects the arene hydroxylation reaction via a triplet transition-state structure ("TS-Oxo") having Cu–O and O–C bond lengths of 1.84 and 1.93 Å, respectively, as depicted in Figure 3-12. While both paths leading to the same triplet oxygenated cyclohexadienyl cation product were predicted to be endorgonic, the latter pathways were more accessible than the former (highest activation free energies of 10.4 and 17.8 kcal/mol relative to the peracid intermediate, respectively).

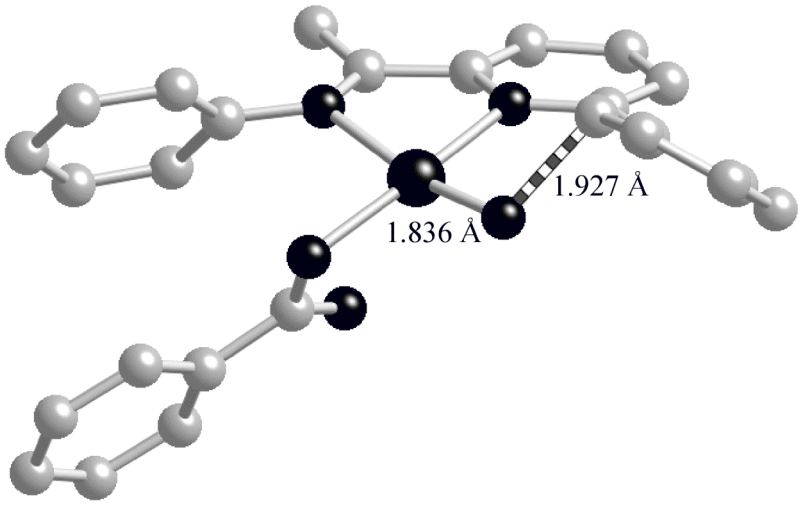

Figure 3-12. Transition state structure of the arene hydroxylation by "Oxo (sp)".

As described above, spin crossings between the singlet and triplet surfaces were expected to take place in both paths. Thus, such processes may permit either or both pathways to contribute to the observed reactivity, as noted in prior studies of Cu^{II}-oxyl reactivity[39] and α-ketoglutarate-dependent non-heme iron reactivity,[107] and their general relevance to iron-based oxidations.[89] Indeed, our preliminary computational prediction that the relevant spin-orbit coupling matrix elements between the singlet and triplet states for the two TS structures originating from the singlet peracid intermediate have values of about 350 cm^{-1} in each case implies that spin crossing should be reasonably efficient along either of the two paths.

In sum, the results from theoretical calculations also support that the Cu^{I}-α-ketoacid

[107] a) Borowski, T.; Bassan, A.; Siegbahn, P. E. M. "A Hybrid Density Functional Study of O-O Bond Cleavage and Phenyl Ring Hydroxylation for a Biomimetic Non-Heme Iron Complex." *Inorg. Chem*. **2004**, *43*, 3277-3291. b) Bassan, A.; Borowski, T.; Siegbahn, P. E. M. "Quantum chemical studies of dioxygen activation by mononuclear non-heme iron enzymes with the 2-His-1-carboxylate facial triad." *Dalton Trans*. **2004**, *20*, 3153-3162.

complexes react with O_2 to yield a transient "Peracid" intermediate via a loss of CO_2. Then, the "Peracid" intermediate either results in the direct ligand hydroxylation or first undergoes the O-O bond cleavage to generate an "Oxo" species that is responsible for the ligand hydroxylation. Nevertheless, we still need to find better systems for stabilizing such species in order to isolate and characterize them. Recent DFT calculations carried out by Dr. Stefan Huber et.al.[108] may provide an interesting insight into stabilizing such species. In this study, the authors investigated the effects of electronic modifications to the truncated model system on the oxygenation mechanisms by introducing substituents on the aromatic rings of the N-donor ligands (from electron-donating to –withdrawing groups). The authors found that stability of more Cu^{II}/Cu^{III}-like intermediates ("O_2 adduct" and "Oxo" species) relative to the more Cu^{I}-like peracid analog increases and reactivity of "Oxo" species in C-H abstraction reactions decreases with more electron-donating N-donor ligands. Testing these computational expectations experimentally remains as a key goal for future research.

3.5. Conclusions and Perspectives

In this chapter, we have described the synthesis and characterization of a series of copper(I)-α-ketocarboxylate complexes, and discussed results from their oxygenation reactions. By virtue of tactically designed supporting ligands, we have been able to intercept intermediate(s) derived from the O_2-induced decarboxylation of the bound α-

[108] Huber, S. M.; Ertem, M. Z.; Aquilante, F.; Gagliardi, L.; Tolman, W. B.; Cramer, C. J. "Generating Cu^{II}-Oxyl/Cu^{III}-Oxo Species from Cu^{I}-α-Ketocarboxylate Complexes and O_2: In Silico Studies on Ligand Effects and C-H-Activation Reactivity." *Chem. Eur. J.* **2009**, *15*, 4886-4895.

ketocarboxylate upon reaction of these complexes with O_2. Such reactions showed dependence on the nature of the supporting ligand and the α-ketocarboxylate used. While $L^{Me}Cu(MF)$ and $L^{Me}Cu(BF)$ are inert toward O_2 at low temperature, reaction of LCu(BF) (L = L^H or $L^{m\text{-}OMe}$) with O_2 resulted in decarboxylation and ligand hydroxylation. The results demonstrate that the oxidative decarboxylation for substrate oxidations by iron(II)−α-ketocarboxylate species in enzymes and model complexes[5b,62a-b,92-94,107] can be extended to copper analogues.

Theoretical calculations by Dr. Stefan Huber, Prof. Christopher Cramer and Laura Gagliardi have provided intriguing mechanistic understanding of the oxygenation process. Notably, two reaction pathways leading to the ligand hydroxylation were identified, involving either copper(I)-peracid or derived copper-oxyl species. These findings can serve to illustrate a new pathway for the generation of novel copper-oxygen intermediates relevant to oxidation catalysis.

Through the ongoing research in this area, the experimental results implicating a possible contribution of [LCu-OOR] (R = H or C(O)R'] or [$LCu^{II}–O^{-\bullet} \leftrightarrow LCu^{III}=O^{2-}$] in some copper-dependent oxidation reactions[55a-b,57-58,] have began to grow. Identification and characterization of such species experimentally and their relevance to the catalytic cycles of enzymes such as DβM and PHM, however, still needs to be explored.

3.6. Experimental Section

General Considerations. All reagents were obtained from commercial sources and used without further purification, unless otherwise noted. The solvents THF, toluene, pentane, and Et_2O were dried over Na/benzophenone and distilled under nitrogen or passed through solvent purification columns (Glass Contour, Laguna, CA). $[Cu_4Mes_4]$ (Mes = mesityl),[80] $[Cu(CH_3CN)_4]O_3SCF_3$,[109] 1-(6'-bromo-pyridin-2'-yl)-ethanone,[39] and 2-bromo-6-(2',6'-dimethylphenyl)pyridine[53] were synthesized following literature procedures. All metal complexes were prepared and stored in a Vacuum Atmospheres inert atmosphere glovebox under a dry nitrogen atmosphere or were manipulated using standard inert atmosphere vacuum and Schlenk techniques. Labeled dioxygen ($^{18}O_2$, 99%) was purchased from Icon Isotopes, Inc and used without further purification.

Physical Methods. NMR spectra were recorded on either Varian VI-300 or VI-500 spectrometers at room temperature. Chemical shifts (δ) for ^1H and ^{13}C NMR spectra are reported versus tetramethylsilane and were referenced to residual protium in the deuterated solvent. UV-vis spectra were recorded on an HP8453 (190-1100 nm) diode array spectrophotometer. Beers Law plots have yet to be obtained, so rather than list UV-vis data as $\lambda_{max}(\varepsilon)$ in the text below, the spectra are shown as absorbance vs. wavelength plots in Figure S5. Low temperature spectra were acquired through the use of a Unisoko low temperature UV-vis cell holder. When necessary, UV-vis spectra were corrected for drifting baselines due to minimal frosting of the UV cells caused by the low-temperature

[109] Kubas, G. J. "Tetrakis(acetonitrile)copper(I) hexafluorophosphate." *Inorg. Synth*. **1979**, *19*, 90-92.

device. This was achieved by subtracting the average of a region with no absorbance (i.e., baseline, typically 950-1000 nm) from the entire spectrum. Elemental analyses were performed by Robertson Microlit Lab. ESI-MS (electrospray ionization mass spectra) were recorded on a Bruker BioTOF II instrument.

3.6.1. Ligand Synthesis

L^H. A solution of 2-dimethylaminoethanol (8.0 mL, 80 mmol) in pentane (100 mL) was treated dropwise with 1.6M *n*BuLi (100 mL, 160 mmol) at 0 °C. After 30 min at 0 °C, a solution of 2-phenylpyridine (5.0 g, 32.0 mmol) in pentane (50 mL) was added dropwise to yield a red-brown species, which was then cooled to -78 °C after 1h at 0 °C. A solution of *N,N*-dimethylacetamide (3.0 mL, 32.0 mmol) in pentane (50 mL) was added carefully at -78 °C. After 1 h at -78 °C, the solution was warmed to room temperature and the reaction mixture was carefully hydrolyzed with H_2O at 0 °C. The aqueous layer was extracted with diethyl ether (2 × 50 mL), dried over Na_2SO_4, and evaporated under vacuum. The crude product, 1-(6'-phenylpyridin-2'-yl)ethanone was directly used to the next step without any further purification. A mixture of the crude 1-(6'-phenylpyridin-2'-yl)ethanone, 2,6-diisopropylaniline (tech 90%, 10.0 g, 51.0 mmol) and formic acid (2 drops) in 100 mL anhydrous MeOH was refluxed for 3 days. The volume of the solvent was reduced to 20 mL under vacuum to yield a yellow microcrytalline material (2.8 g, 7.7 mmol; 25 %) which was isolated by filtration and washing with cold MeOH (2 × 10 mL). Slow evaporation of the mother liquor under

ambient temperature overnight gave the second crop of the product (1.2 g, 3.3 mmol; 10 %), for an overall yield of 35 % based on the starting 2-phenylpyridine. ^{1}H NMR (300 MHz, CD_2Cl_2): δ 8.29-8.32 (m, 1H), 8.12-8.16 (m, 2H), 7.87-7.94 (m, 2H), 7.42-7.54 (m, 3H) 7.06-7.19 (m, 3H), 2.78 (sept, J = 11.5 Hz, 2H), 2.30 (s, 3H), 1.16 (d, J = 11.5 Hz, 6H), 1.14 (d, J = 11.5 Hz, 6H). ^{13}C{^{1}H} NMR (75.0 MHz, CD_2Cl_2): δ 167.94, 156.66, 156.33, 147.17, 139.59, 137.79, 136.34, 129.64, 129.27, 127.34, 124.04, 123.50, 121.65, 120.04, 28.79, 23.55, 23.14, 17.58 ppm. Anal. Calcd for $C_{25}H_{28}N_2$: C, 84.23; H, 7.92; N, 7.86. Found: C, 83.98; H, 8.07; N, 7.83.

L^{Me}. A pale yellow solution containing 2-bromo-6-(2',6'-dimethylphenyl)pyridine (6.0 g, 23.0 mmol) in 100 mL THF was cooled to -80 °C using the dry ice/acetone bath. Under nitrogen, a 1.6 M solution of *n*BuLi in hexane (14.5 mL, 23.0 mmol) was added dropwise with syringe to give a dark red solution. After 30 min, dry *N,N*-dimethylacetamide (2.5 mL, 27.0 mmol) was added and the reaction mixture was then warmed to room temperature and carefully quenched with 50 mL of water. The organic phase was separated and the aqueous phase was washed with dichloromethane (3 × 50 mL). The combined organic layers were dried over Na_2SO_4, filtered, and the solvent was removed under reduced pressure to yield a dark red oil. This crude product containing 1-{6'-(2'',6''-dimethylphenyl)pyridin-2'-yl}ethanone was directly used in the next step without any further purification. The final product, L^{Me} was synthesized following the same procedure as that described in the synthesis of L^{H}, but with the crude 1-{6'-(2'', 6''-dimethylphenyl)pyridin-2'-yl}ethanone. The overall yield was 57 % based on the starting 2-bromo-6-(2', 6'-dimethylphenyl)pyridine. ^{1}H NMR (300 MHz, CD_2Cl_2):

δ 8.29 (d, J = 7.2 Hz, 1H), 7.88 (t, J = 7.8 Hz, 1H), 7.35 (d, J = 7.2 Hz, 1H), 7.25-7.05 (m, 6H), 2.79 (sept, J = 6.9 Hz, 2H), 2.16 (s, 3H), 2.12 (s, 6H), 1.15 (d, J = 6.9 Hz, 12H). ^{13}C{1H} NMR (75.0 MHz, CD_2Cl_2): δ 168.08, 158.98, 156.90, 147.13, 140.98, 137.18, 136.57, 136.39, 128.43, 128.16, 126.29, 124.04, 123.49, 119.60, 28.76, 23.61, 23.13, 20.71, 17.73 ppm. Anal. Calcd for $C_{27}H_{32}N_2$: C, 84.33; H, 8.39; N, 7.28. Found: C, 84.08; H, 8.15; N, 7.19.

$L^{m\text{-}OMe}$. To a mixture of 1-(6'-bromo-pyridin-2'-yl)-ethanone (5.4 g, 27.0 mmol) and $Pd(PPh_3)_4$ in 120 mL toluene was added aqueous Na_2CO_3 (18.0 mL, 2.0 M) and 3-methoxyphenylboronic acid (4.56 g, 30.0 mmol) in 40 mL MeOH under a nitrogen atmosphere and the mixture was refluxed for 8 h. After cooling, dichloromethane (150 mL), aqueous Na_2CO_3 (45.0 mL, 2.0 M) and concentrated ammonium hydroxide (6.0 mL) was added. The organic layer was extracted with dichloromethane (3 × 100 mL), the combined organic layer was dried over magnesium sulfate and the volatile material was removed in vacuo to give crude 1-{6'-(3''-methoxyphenyl)-pyridin-2'-yl}ethanone, which was used directly in the next step without further purification. The final product, $L^{m\text{-}OMe}$ was synthesized following the same procedure as that described in synthesis of L^H, but with the crude 1-{6'-(3''-methoxyphenyl)-pyridin-2'-yl}ethanone. The overall yield was 70 % based on the starting 1-(6'-bromo-pyridin-2'-yl)-ethanone. ^{1}H NMR (300 MHz, $CDCl_3$): δ 8.35 (dd, J = 6.9 and 1.8 Hz, 1H), 7.93-7.85 (m, 2H), 7.77-7.70 (m, 2H), 7.44 (t, J = 8.1 Hz, 1H), 7.22-7.06 (m, 3H), 7.02 (dd, J = 8.1 and 2.4 Hz, 1H), 3.93 (s, 3H), 2.81 (sept, J = 6.9 Hz, 2H), 2.34 (s, 3H), 1.18 (d, J = 6.9 Hz, 12H). ^{13}C{1H} NMR (75.0 MHz, $CDCl_3$): δ 167.54, 160.25, 156.19, 155.84, 146.70, 140.75, 137.43, 136.03,

130.01, 123.71, 123.17, 121.51, 119.90, 119.47, 114.66, 112.81, 55.56, 28.44, 23.42, 23.14, 17.49 ppm. Anal. Calcd for $C_{26}H_{30}N_2O$: C, 80.79; H, 7.82; N, 7.25. Found: C, 80.58; H, 7.89; N, 7.12.

3.6.2. Synthesis of Cu(I)-α-Ketocarboxylate Complexes

General Method for preparation of Cu(I)-α-ketocarboxylate complexes. In an inert atmosphere an equimolar mixture of $[Cu(Mes)]_4$ (0.065 mmol) and α-ketocarboxylic acid (benzoyl- or mesitoylformic acid, 0.26 mmol) in 3 mL THF was stirred for 30 min and the insoluble material was removed by filtration through a plug of celite. The orange colored filtrate was added to a solution of ligand (0.26 mmol) in 2 mL THF. After 30 min, the solvent was removed under vacuum to give a dark reddish-brown powder (yield 75–85%).

[(L^{Me})Cu(O_2CC(O)Mes)]. This complex was recrystallized by a slow diffusion of pentane into a concentrated THF solution of the product at -20 °C. ^{1}H NMR (300 MHz, CD_2Cl_2): δ 8.17 (t, J = 7.5-7.8 Hz, 1H), 8.00 (d, J = 7.5 Hz, 1H), 7.71 (d, J = 7.5 Hz, 1H), 7.07-7.22 (m, 6H), 6.72 (s, 2H), 2.82 (sept, J = 6.6-6.9 Hz, 2H), 2.29 (s, 3H), 2.24 (s, 3H), 2.14 (s, 6H), 1.87 (s, 6H), 1.12 (t, J = 5.7-6.6 Hz, 12H). ^{13}C{1H} NMR (75.0 MHz, CD_2Cl_2): δ 201.65, 168.44, 167.20, 160.75, 151.99, 143.83, 139.48, 138.92, 137.86, 137.41, 136.11, 135.35, 130.00, 129.46, 128.50, 128.25, 126.09, 124.04, 123.25, 28.93, 23.84, 23.55, 21.33, 20.67, 19.63, 17.66 ppm. Anal. Calcd for $C_{38}H_{43}N_2O_3Cu$: C, 71.39; H, 6.78; N, 4.38. Found: C, 71.14; H, 6.59; N, 4.32.

[L^{H}Cu(O_2CC(O)Ph)]. This complex was recrystallized by a slow diffusion of pentane into a concentrated CH_2Cl_2 solution of the product at -20 °C. ^{1}H NMR (300 MHz, d_8-THF): δ 8.17-8.23 (m, 3H), 8.05-8.13 (m, 2H), 7.68 (bd, J = 7.2 Hz, 2H), 7.41-7.53 (m, 4H), 7.33 (t, J = 7.5 Hz, 2H), 7.13-7.23 (m, 3H), 2.96 (sept, J = 6.9 Hz, 2H), 2.34 (s, 3H), 1.17 (d, J = 6.6 Hz, 6H), 1.14 (d, J = 6.9 Hz, 6H). ^{13}C{1H} NMR (75.0 MHz, d_8-THF): δ 192.89, 171.59, 169.96, 158.99, 154.23, 145.65, 140.30, 139.72, 138.19, 133.77, 130.56, 130.42, 129.71, 129.17, 128.91, 127.75, 126.24, 125.98, 124.31, 123.19, 29.34, 24.30, 23.67, 17.74 ppm. Anal. Calcd for $C_{33}H_{33}N_2O_3Cu$: C, 69.64; H, 5.84; N, 4.92. Found: C, 69.91; H, 5.78; N, 4.76.

[(L^{Me})Cu(O_2CC(O)Ph)]. This complex was recrystallized by a slow diffusion of pentane into a concentrated THF solution of the product at -20 °C. ^{1}H NMR (300 MHz, CD_2Cl_2): δ 8.17 (t, J = 7.8 Hz, 1H), 8.02 (d, J = 7.8 Hz, 1H), 7.69 (bd, J = 7.2 Hz, 3H), 7.51 (t, J = 7.5-7.8 Hz, 1H), 7.35 (t, J = 7.5, 2H), 7.04-7.24 (m, 6H), 2.85 (sept, J = 6.9 Hz, 2H), 2.30 (s, 3H), 2.13 (s, 6H), 1.17 (d, J = 6.9 Hz, 12H). ^{13}C{1H} NMR (75.0 MHz, CD_2Cl_2): δ 194.16, 169.14, 168.66, 160.82, 152.04, 143.91, 139.72, 139.33, 137.88, 136.14, 134.70, 133.38, 130.47, 129.95, 129.33, 128.54, 128.23, 126.20, 124.14, 123.25, 29.02, 23.92, 23.39, 20.70, 17.57 ppm. Anal. Calcd for $C_{35}H_{37}N_2O_3Cu$: C, 70.39; H, 6.24; N, 4.69. Found: C, 70.32; H, 6.29; N, 4.71.

[($L^{m\text{-}OMe}$)Cu(O_2CC(O)Ph)]. This complex was recrystallized by a slow diffusion of pentane into a concentrated THF solution of the product at -20 °C. ^{1}H NMR (300 MHz, CD_2Cl_2): δ 8.13 (t, J = 7.8 Hz, 1H), 8.01 (t, J = 7.5 Hz, 2H), 7.78-7.62 (m, 3H), 7.54-7.48 (m, 2H), 7.42-7.27 (m, 6H), 6.98 (dd, J = 8.1 and 1.8 Hz, 1H), 3.81 (s, 3H)

2.90 (sept, J = 6.9 Hz, 2H), 2.31 (s, 3H), 1.21 (d, J = 6.9 Hz, 6H), 1.16 (d, J = 6.9 Hz, 6H). $^{13}C\{1H\}$ NMR (75.0 MHz, CD_2Cl_2): δ 194.07, 170.01, 160.27, 159.35, 143.77, 140.60, 139.74, 138.17, 134.48, 133.53, 130.40, 130.21, 128.70, 127.88, 126.45, 124.27, 123.53, 121.09, 116.50, 113.87, 55.78, 29.02, 24.01, 23.45, 17.84 ppm. Anal. Calcd for $C_{34}H_{35}N_2O_4Cu$: C, 68.15; H, 5.89; N, 4.68. Found: C, 67.92; H, 6.06; N, 4.51.

[$L^{Me}Cu(O_3SCF_3)$]. Upon addition of a yellow solution of a L^{Me} (200 mg, 0.52 mmol) in 3 mL THF to a slurry of a CuCl (26.0 mg, 0.52 mmol) in 2 mL THF, the color of the reaction mixture was immediately changed into dark reddish-brown. After 12 hr, the insoluble material was removed by a filtration through a plug of celite and the solvent was removed under vacuum to give a purple powder. Pure [L^{Me}CuCl] was isolated by recrystallisation through a slow diffusion of pentane into a concentrated THF solution of the product at -20 °C (yield 80%). ^1H NMR (300 MHz, d_8-THF): δ 8.19-8.28 (m, 2H), 7.77 (dd, J = 7.2, 1.2 Hz, 1H), 7.09-7.22 (m, 6H), 2.88 (sept, J = 6.9 Hz, 2H), 2.33 (s, 3H), 2.11 (s, 6H), 1.20 (d, J = 6.9 Hz, 6H), 1.13 (d, J = 6.9 Hz, 6H). $^{13}C\{1H\}$ NMR (75.0 MHz, d_8-THF): δ 169.95, 161.40, 152.34, 144.58, 140.49, 140.11, 138.64, 136.55, 130.42, 129.86, 129.00, 126.58, 124.49, 124.24, 29.43, 24.83, 23.77, 21.16, 17.63 ppm. To a dark reddish-brown solution of [L^{Me}CuCl] (150 mg, 0.31 mmol) in 2 mL THF was added a coloress solution of AgO_3SCF_3 (80.0 mg, 0.31 mmol). After 1 h, the precipitated AgCl was removed by filtration through a plug of celite and the filtrate was dried under vacuum to give a purple powder. X-ray quality single crystals were grown by a slow diffusion of pentane into a concentrated THF solution of the product at -20 °C (yield 75%). ^1H NMR (300 MHz, d_8-THF): δ 8.26-8.34 (m, 2H), 7.81 (dd, J = 6.6, 2.1 Hz, 1H),

7.10-7.24 (m, 6H), 2.89 (sept, J = 6.6-6.9 Hz, 2H), 2.37 (s, 3H), 2.12 (s, 6H), 1.17 (d, J = 6.6 Hz, 6H), 1.13 (d, J = 6.9 Hz, 6H). $^{13}C\{1H\}$ NMR (75.0 MHz, d_8-THF): δ 169.95, 160.58, 152.30, 144.61, 140.63, 140.40 138.76, 136.74, 130.72, 129.52, 128.88, 126.72, 124.96, 124.50, 29.24, 24.09, 23.89, 20.72, 17.91 ppm. Anal. Calcd for $C_{28}H_{32}N_2F_3O_3SCu$: C, 56.32; H, 5.40; N, 4.69. Found: C, 56.32; H, 5.20; N, 4.55.

3.6.2. Oxygenation and Products Analyses of Cu(I)-α-Ketocarboxylate Complexes

Reactions of all copper(I) complexes with O_2 were performed similarly, as described in the following representative example. A 20 mL Schlenk flask containing $L^{m\text{-}OMe}Cu(BF)$ (60.0 mg, 0.1 mmol) in 10 mL acetone was cooled to -80 °C with an acetone / dry ice bath. The mixture was reacted with O_2 by bubbling the gas through the solution at this temperature for 4 h and then it was gradually warmed to room temperature. An aliquot from the brown solution was removed for analysis by ESI-MS (see Figures 3-8 and 3-9). To extract the organic products, the volatile materials were removed from the solution under vacuum. The residue was dissolved in concentrated NH_4OH (2 mL), and the blue mixture was extracted with diethyl ether (3 × 20 mL), dried over anhydrous Na_2SO_4, and dried under vacuum. The residue was analyzed by ESI-MS and ^1H NMR spectroscopy with an internal standard (1,3,5-trimethoxybenzene). The latter indicated that the yield of recovered ligand (starting plus hydroxylated) was > 95 %, with a ratio of $L^{m\text{-}OMe}$ to $L^{m\text{-}OMe\text{-}OH}$ of 60:40 from analysis of the methyl protons on the methoxy

substituent (Figure 3-8). For the case of the reaction with $L^{H}Cu(BF)$, the ratio of L^{H} to L^{OH} was 87:13. ^{1}H NMR of $L^{m\text{-}OMe\text{-}OH}$ ($CDCl_3$): δ = 13.81 (s, $L^{m\text{-}OMe}$-O*H*, 1H), 3.88 (s, 3H), 2.77 (sept, *J* = 6.9 Hz, 2H), 2.29 (s, 3H), 1.17 (d, *J* = 6.9 Hz, 12H) (other resonances were hidden below those of $L^{m\text{-}OMe}$). The aqueous phase was then acidified to pH = 1 with concentrated HCl. The organic product was extracted with CH_2Cl_2 (3 × 20 mL), dried over anhydrous Na_2SO_4, and dried under vacuum. The brown residue was analyzed by ^{1}H NMR spectroscopy with an internal standard (1,3,5-trimethoxybenzene), which revealed an overall yield (benzoylformic and benzoic acids) of > 98 %, and a ratio of benzoylformic acid (BFH) to benzoic acid (HOBz) of 40:60 based on integrated ratios of the *ortho* protons of benzoylformic acid and benzoic acid. For the case of the reaction with $L^{H}Cu(BF)$, the ratio was 60:40. ^{1}H NMR ($CDCl_3$): δ = 8.29 (d, *J* = 7.2 Hz, *ortho* of BFH), 8.14 (d, *J* = 7.2 Hz, *ortho* of HOBz), 7.71 (t, *J* = 7.2 Hz, *meta* of BFH), 7.64 (t, *J* = 7.2 Hz, *meta* of HOBz), 7.58 – 7.45 (m, *para* of BFH and HOBz). The same procedure was used for the reaction of $L^{m\text{-}OMe}Cu(BF)$ with $^{18}O_2$, but instead of bubbling the gas ~20 mL of $^{18}O_2$ was transferred to the reaction vessel by vacuum transfer. ESI-MS data of the crude product solution are shown in Figures 3-9. The reaction of $L^{Me}Cu(OTf)$ with O_2 was performed similarly, but there was no color change at -80 °C, and no attempt was made to analyze the products after warming to room temperature.

Table 3-3. Summary of X-ray Crystallographic Data

	$[(L^{Me})Cu(O_2CC(O)Mes)]$	$[L^{H}Cu(O_2CC(O)Ph)]$
empirical formula	C38 H43 Cu N2 O3	C33 H33 Cu N2 O3 • CH_2Cl_2
formula weight (g/mol)	639.28	654.08
crystal habit, color	red, block	brown, Plate
crystal system	Triclinic	Triclinic
space group	$P\bar{1}$	$P\bar{1}$
a (Å)	8.958(3)	10.2026(12)
b (Å)	11.008(4) Å	12.1789(14)
c (Å)	19.141(11) Å	15.2420(18)
α (deg)	78.74(4)	67.379(2)
β (deg)	78.76(4)	85.964(2)
γ (deg)	66.24(4)	65.239(2)
V ($Å^3$)	1679.9(13)	1578.2(3)
Z	2	2
D_{calc} (g/cm^3)	1.264	1.376
temperature (K)	173(2)	173(2)
Absorption (cm^{-1})	6.88	8.98
θ range (deg)	1.09 to 25.11	1.46 to 25.06
hkl ranges	-10 to 10, -13 to 13, -22 to 22	-12 to 12, -14 to 14, -18 to 17
no. of reflections collected	13556	13378
no. of unique reflections	5878 (R_{int} = 0.0280)	5581 (R_{int} = 0.0305)
Observed reflections ($I > 2\sigma(I)$)[a]	4702	4599
Completeness to θ = 25.11°	98.3 %	99.4 %
Data / restraints / parameters	5878 / 5 / 397	5581 / 0 / 379
R1/wR2 ($I > 2\sigma(I)$)	0.0356 / 0.0893	0.0378 / 0.0799
R1/wR2 (all data)	0.0513 / 0.1013	0.0518 / 0.0853
Goodness-of-fit on F^2	1.059	1.043
Max/min peak ($e.Å^{-3}$)	0.386 / -0.347	0.695 / -0.517

Continued.

	$[(L^{Me})Cu(O_2CC(O)Ph)]$	$[(L^{m\text{-}OMe})Cu(O_2CC(O)Ph)]$
empirical formula	C35 H37 Cu N2 O3	C34 H35 Cu N2 O4
formula weight (g/mol)	597.21	599.18
crystal habit, color	red-brown, Plate	red-brown, block
crystal system	Monoclinic	Triclinic
space group	$P_{2/1}/n$	$P\bar{1}$
a (Å)	13.812(10)	10.1018(11)
b (Å)	14.651(9)	11.7821(13)
c (Å)	15.986(9)	12.8840(14)
α (deg)	90°	86.043(2)
β (deg)	109.14(3)	73.753(2)
γ (deg)	90°	88.886(2)
V ($Å^3$)	3056(3)	1468.7(3)
Z	4	2
D_{calc} (g/cm^3)	1.298	1.355
temperature (K)	173(2)	173(2)
Absorption (cm^{-1})	7.52	7.85
θ range (deg)	1.94 to 25.06	1.65 to 25.06
hkl ranges	-16 to 16, -17 to 17, -19 to 19	-12 to 12, -14 to 14, -15 to 15
no. of reflections collected	28455	14194
no. of unique reflections	5404 (R_{int} = 0.0358)	5179 (R_{int} = 0.0376)
Observed reflections ($I > 2\sigma(I)$)[a]	4529	4047
Completeness to θ = 25.11°	99.7 %	99.5 %
Data / restraints / parameters	5404 / 4 / 377	5179 / 0 / 375
R1/wR2 ($I > 2\sigma(I)$)	0.0303 / 0.0779	0.0451 / 0.1067
R1/wR2 (all data)	0.0415 / 0.0866	0.0644 / 0.1143
Goodness-of-fit on F^2	1.062	1.061
Max/min peak ($e.Å^{-3}$)	0.303 / -0.293	1.017 / -0.627

Continued.

	$[L^{Me}Cu(O_3SCF_3)]$	$[(L^{Me})_2Cu_2(BF)](OTf)\bullet 2THF$
empirical formula	C28 H32 Cu F3 N2 O3 S	C71 H85 Cu2 F3 N4 O8 S
formula weight (g/mol)	597.16	1338.57
crystal habit, color	red, block	red-brown, plate
crystal system	Monoclinic	Triclinic
space group	$P_{2/1}/c$	$P\bar{1}$
a (Å)	13.4571(11)	13.5529(15)
b (Å)	13.8773(10)	14.3127(16)
c (Å)	15.4330(12)	17.867(2)
α (deg)	90°	97.710(2)
β (deg)	99.702(2)	98.017(2)
γ (deg)	90°	90.820(2)
V ($Å^3$)	2840.9(4)	3399.5(7)
Z	4	2
D_{calc} (g/cm^3)	1.396	
temperature (K)	173(2)	173(2)
Absorption (cm^{-1})	8.93	8.28
θ range (deg)	1.99 to 25.03	1.44 to 25.06
hkl ranges	-14 to 16, -16 to 15, -18 to 18	-16 to 16, -17 to 17, -21 to 21
no. of reflections collected	18007	33250
no. of unique reflections	5015 (R_{int} = 0.0228)	12001(R_{int} = 0.0272)
Observed reflections ($I > 2\sigma(I)$)[a]	4477	9764
Completeness to θ = 25.11° or 25.06°	100.0 %	99.5 %
Data / restraints / parameters	5015 / 20 / 368	12001/59/849
R1/wR2 ($I > 2\sigma(I)$)	0.0509 / 0.1118	0.0530/0.1343
R1/wR2 (all data)	0.0567 / 0.1157	0.0669/0.1423
Goodness-of-fit on F^2	1.053	1.042
Max/min peak ($e.Å^{-3}$)	0.744 / -1.724	1.033/ -0.603

$R1 = \Sigma||F_0|-|F_c||/\Sigma|F_0||$. $wR_2 = [\Sigma[w(F_0^2-F_c^2)^2]/\Sigma w(F_0^2)^2]]^{1/2}$ where
$w = q / [\sigma^2 (F_0^2) + (aP)^2 + bP + d + e \times sin(\theta)$.
$GooF = S = [\Sigma[w(F_0^2-F_c^2)^2] / (n-p)]^{1/2}$

CHAPTER 4. SYNTHESIS, CHARACTERIZATION, AND OXO-TRANSFER REAGENT REACTIVITY OF VARIOUS COPPER(I) COMPLEXES

4.1. Introduction

In previous chapter, we demonstrated that reaction of Cu^{I}–α-ketocarboxylate complexes with O_2 led to an oxidative decarboxylation and the derived, highly reactive copper-oxygen intermediate(s) has(have) been intercepted by the supporting N-donor ligand to result in hydroxylation of an arene substituent.[1] Theoretical calculations have provided intriguing mechanistic notions that hydroxylation pathways involve novel [Cu^{I}–OOC(O)R] and [Cu^{II}–$O^{\bullet}$] species. The results show that the oxidative decarboxylation pathway for substrate oxidation by α–ketoglutrate-dependent non-heme iron enzymes[5b,62a-b] can be expanded to copper analogues. The route we pursued in this chemistry could serve as an alternative pathway for the generation of novel mononuclear copper–oxyl species, which have been invoked as an active species in catalysis by PHM and DβM.[23-24,36] However, we could not detect or observe such intermediates during the oxygenation of various Cu^{I}–α-ketocarboxylate complexes by spectroscopic means. Thus, identification and characterization of such species and their relevance to the catalytic cycles of enzymes such as DβM and PHM represent the ongoing research goal in this area.

As discussed in Chapter 3, theoretical calculations by Stefan Huber et al.[108] predict that use of more electron-donating N-donor ligands could increase the stability of the

Cu^{II}-oxyl species relative to the Cu^{I}-peracid analog within series of Cu^{I}–α-ketocarboxylate complexes. In addition, some recent experimental results show that reactions of Cu^{I} complexes with iodosylbenzene lead to the intramolecular ligand hydroxylation or *N*-dealkylation presumably via an intermediacy of the Cu^{II}-oxyl species.[57-58,63] This route has also been utilized to generate the analogous $[Fe^{IV}=O]^{2+}$ species as models for active species in catalysis by various non-heme iron enzymes.[62,64] Similarly, reactions of copper complexes with trimethylamine *N*-oxide (Me_3NO) also induced the intramolecular arene hydroxylations (Scheme 4-1).[110] In these studies, the copper(II) complexes of *N*-benzoylaminoacid ligands reacted with excess Me_3NO to yield the hydroxylation of the appended phenyl ring of the ligands. Interestingly, introduction of the alkylgroups (methyl or phenyl) at the amide nitrogen did not effect the observed reactions. Also, addition of extra spacer groups between either the amide and carboxylate or the amide and benzene ring did not promote such reactions. These results imply ligands' structural importance both in generating the active species and in their reactivity toward intramolecular arene hydroxylation. Recent DFT calculations[56,111] led to provocative mechanistic proposal for the arene hydroxylation pathway that involves the

---

[110] a) Kametani, T.; Ihara, M. "Alkaloid formation through N-oxide intermediates; regioselective synthesis of (±)-corytuberine by redox reaction." *J. Chem. Soc., Perkin Trans. 1* **1980**, *2*, 629-632. b) Capdevielle, P.; Sparfel, D.; Baranne-Lafont, J.; Cuong, N. K.; Maumy, M. "Copper(I) and copper(II) mediated two-electron oxidations of benzylic alcohols and diaryl acetic acids by trimethylamine N-oxide." *J. Chem. Soc., Chem. Commun*. **1990**, *7*, 565-566. c) Reinaud, O.; Capdevielle, P.; Maumy, M. "Copper(II) mediated aromatic hydroxylation by trimethylamine N-oxide." *J. Chem. Soc., Chem. Commun*. **1990**, *7*, 565-568. d) Reinaud, O.; Capdevielle, P.; Maumy, M. "2-(N-Amido)-4-nitrophenol: a new ligand for the copper-mediated hydroxylation of aromatics by trimethylamine N-oxide." *J. Mol. Catal*. **1991**, *68*, L13-L15. e) Rousselet, G.; Capdevielle, P.; Maumy, M. "Copper-induced synthesis of iminiums: trimethylamine oxidation or amine N-oxide conversion." *Tetrahedron Lett*. **1995**, *36*, 4999-5002.

[111] Buijs, W.; Comba, P.; Corneli, D.; Pritzkow, H. "Structural and mechanistic studies of the copper(II)-assisted ortho-hydroxylation of benzoates by trimethylamine N-oxide." *J. Organomet. Chem*. **2002**, *641*, 71-80

$[CuO]^+$ species generated by O–N bond homolysis from an isolated Cu^{II}-$ONMe_3$. The calculations also showed that the derived $[CuO]^+$ intermediate can be best described as a Cu^{II}-$O^{-\bullet}$ having a triplet electronic ground state. In addition, the authors concluded that coordination of both strongly electron-donating amide nitrogen and carboxylate oxygen to copper(II) ion plays a significant role in inducing the O-N bond homolysis of Me_3NO, consistent with lack of reactivity upon the substitution of the hydrogen with the alkyl groups at the amide nitrogen.

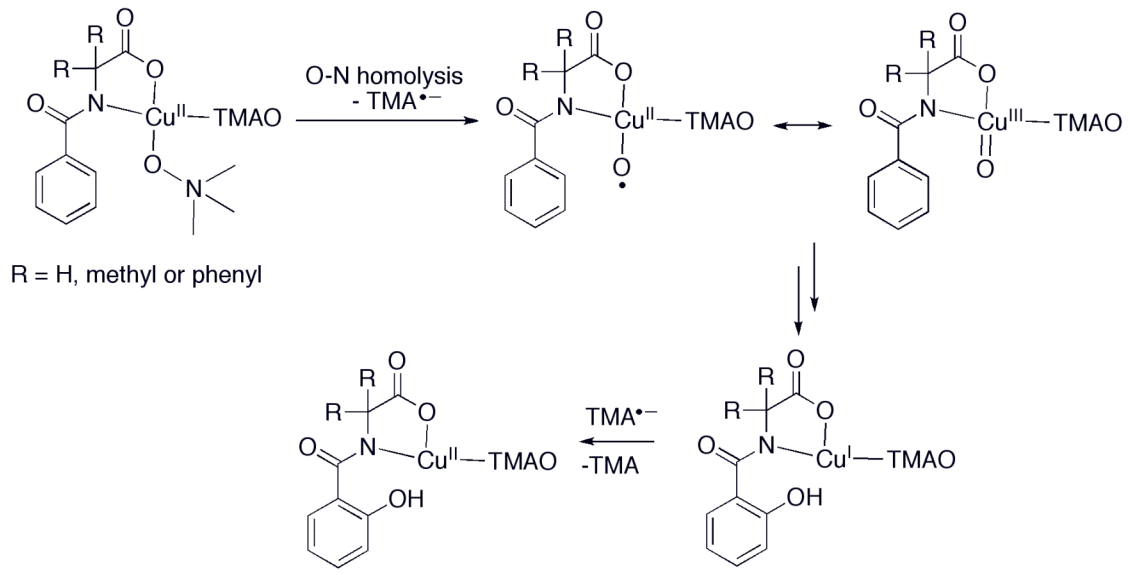

Scheme 4-1. Proposed reaction mechanism for Cu^{II}-assisted arene hydroxylation. TMAO refers to trimethylamine N-oxide and TMA to trimethylamine.

Taking all of aforementioned perspectives in account, we sought to further explore reactions of a wide range of copper(I) complexes with various potential oxo-transfer reagents including iodosylbenzene (PhIO) and *N*-oxides. Of particular interest in this study is to understand how systematic changes of the steric and electronic properties of the supporting ligands affect the interaction between the copper centers and the oxo-

transfer reagents. Moreover, given that other metal centers (e.g., Fe[64d-e,112] and Ru[64f]) reacted with *N*-oxides to form high-valent metal-oxo species ($[M=O]^{2+}$) through the heterolytic N-O bond cleavage, such copper(I) N-oxide adducts might provide a $[CuO]^{+}$ or related species following similar reaction pathways.

In this context, we investigated the reactions of pyridine- and trialkylamine-*N*-oxides with copper(I) complexes of a range of supporting ligands with variable steric and electronic profiles. This chapter will describe the results obtained in this study, some of which have previously been published somewhere.[3]

4.2. Synthesis of Copper(I) Complexes

In general, the electronic and steric properties of the supporting ligands play significant roles in binding and/or activation of small molecules.[5e,11d,38a-b] As noted in Cu/Me_3NO systems, coordination of the deprotonated amide nitrogen and the carboxylate oxygen to the Cu^{II} ion was critical to induce the arene hydroxylation of the supporting ligands by a Cu/O intermediate ($[CuO]^{+}$ species) that presumably formed via a homolytic cleavage of the O-N bond of Me_3NO.

[112] See selected examples: a) Shin, K.; Goff, H. M. "Generation of oxoiron(IV) porphyrin complexes by amine N-oxide oxo-transfer reactions." *J. Am. Chem. Soc.* **1987**, *109*, 3140-3142. b) Nee, Michael W.; Bruice, Thomas C. "Use of the N-oxide of p-cyano-N,N-dimethylaniline as an "oxygen" donor in a cytochrome P-450 model system." *J. Am. Chem. Soc.* **1982**, *104*, 6123-6125.

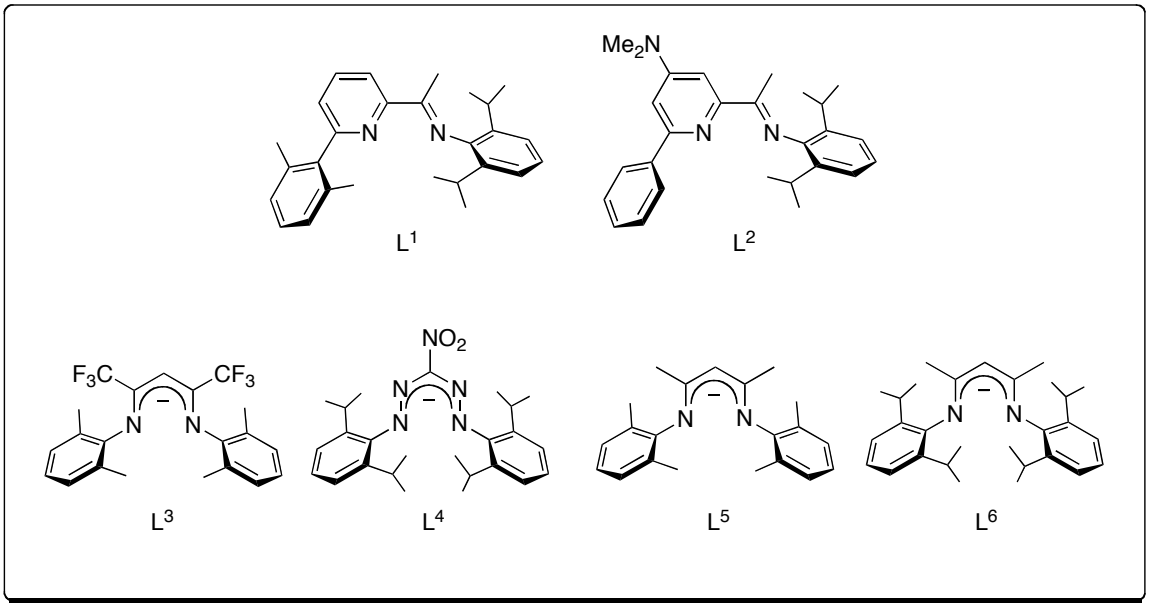

Scheme 4-2. Drawing for ligands.

Previously, we also reported the synthesis and O_2 reactivity of a variety of copper(I) complexes, and showed differing results depending on the steric and electronic profiles of the supporting ligands. While the copper(I) complex of weakly electron-donating ligand (L^1) did not react with O_2,[1] more electron-donating ligands supported the O_2 chemistry to generate either bis(μ-oxo)dicopper species (L = L^3 through L^5)[50] or mononuclear side-on Cu^{III}-peroxo species (L = L^6)[42] (Scheme 4-2). With this knowledge obtained from the dioxygen reactivity studies of these copper(I) complexes, we tried to understand how the N-O bond of N-oxides would be affected by steric and electronic profiles of the various copper(I) complexes.

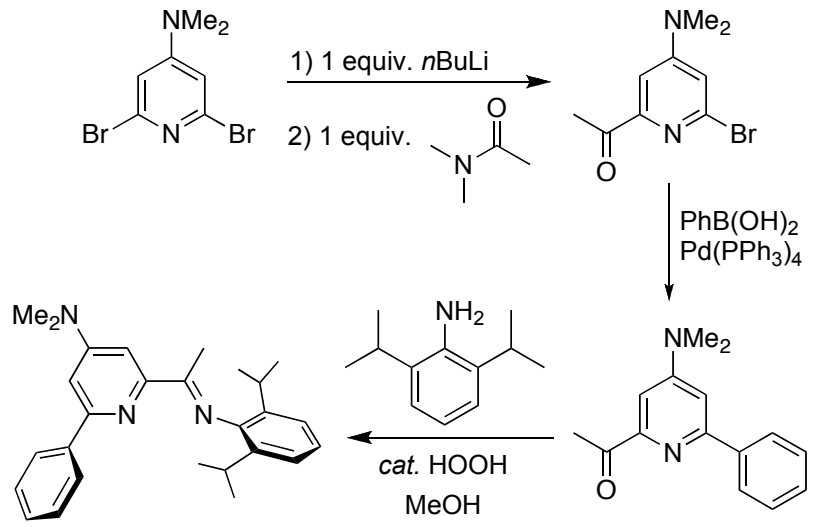

Scheme 4-3. Synthesis of ligand L^2.

All ligands used in this study were prepared following the literature procedures,[1,42,50] except for L^2. For L^2, using known method,[112] we prepared the 2,6-dibromo-4-dimethylaminopyridine, which was then converted to the 1-{6'-bromo-4'-(dimethylamino)pyridin-2'-yl}ethanone. After introducing the phenyl ring to this pyridyl acetone precursor via a Suzuki-Miura coupling reaction, the phenyl appended pyridyl acetone underwent the condensation reactions with excess 2,6-diisopropylaniline in the presence of a catalytic amount of formic acid at the refluxing condition to give the ligand L^2 (scheme 4-3). With these ligands in hand, the corresponding Cu^I complexes were synthesized according to the previous methods (Scheme 4-4). The copper(I) complexes of the pyridyl imine ligands were prepared either by treating the ligand ($L = L^1$) with CuCl and then AgO_3SCF_3 or by reacting the ligand ($L = L^2$) with $[Cu(CH_3CN)_4](O_3SCF_3)$. For

[112] Wayman, K. A.; Sammakia, T. "O-Nucleophilic Amino Alcohol Acyl-Transfer Catalysts: the Effect of Acidity of the Hydroxyl Group on the Activity of the Catalyst." *Org. Letters*. **2003**, *5*, 4105-4108.

the β-diketiminates or formazan lgiands, the copper(I) complexes were synthesized by either adding the protonated ligands to [CuMes] (mes = mesityl) (L = L^3 or L^4) or to the base (*n*-BuLi) and then $[Cu(CH_3CN)_4)]O_3SCF_3$. All copper(I) complexes were characterized by ^1H and $^{13}C\{^1H\}$ NMR spectroscopy, and CHN analyses.

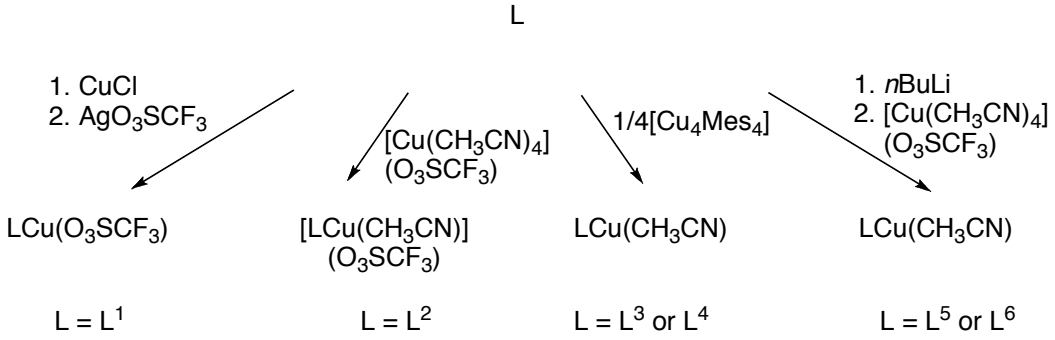

Scheme 4-4. Syntheses of copper(I) complexes.

4.3. Reactions of Copper(I) Complexes with Various N-oxides or Iodosylbenzene

4.3.1. Formation of Stable Copper(I)-N-oxide Complexes

Reactions of $[L^1Cu(O_3SCF_3)]^2$ with substituted pyridine-*N*-oxides (1 equiv) or [LCu(CH3CN)] (L = L^3 or L^4)[1,72-73] with Me_3NO (1 equiv) in THF at room temperature yielded the corresponding Cu^I-*N*-oxide adducts, respectively (Scheme 4-5). After recrystallisation, the products were isolated as red-brown crystalline solids in good yields (65–95%) and they were characterized by ^1H and $^{13}C\{^1H\}$ NMR spectroscopy, CHN

analysis, and X-ray crystallography.

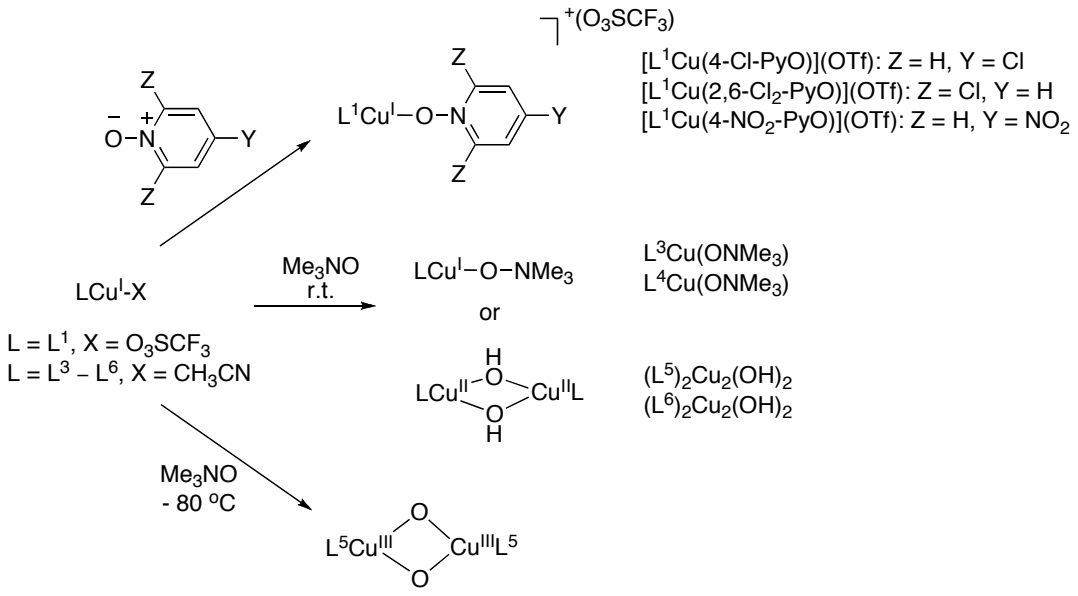

Scheme 4-5. Reactions of Cu^{I} complexes with pyridine- and trimethylamine-*N*-oxides.

4.3.2. X-ray Crystal Structures of Copper(I)-N-oxide Complexes

Single crystals suitable for X-ray crystallography were grown by a slow vapor diffusion of pentane into a concentrate solutions of the corresponding copper(I)-*N*-oxide compounds in THF at –20 °C. As depicted in Figure 4-1, all of the structures feature three-coordinate Cu^{I} ions with a planar geometry (sum of donor-Cu-donor angles of 351–360°) and bent coordination of the *N*-oxide ligands (Cu1-O1-N3 angles of 120–122°). For Cu^{I}-pyridine *N*-oxide complexes of L^{1}, the overall structural features including geometry, bond distances and angles are almost identical to those of Cu^{I}-triflate analog. Minor changes involve the Cu-O and averaged Cu-N distances. The pyridne *N*-oxides

bind to the copper center more strongly compared to the triflate anion, as evident from Cu-O bond distances of 1.88-1.90 Å that is ca. 0.1 Å shorter than the Cu-triflate bond distance (1.991 (4) Å). As a result, the average Cu-N bond distance of 2.03 Å in these Cu^{I}-pyridine *N*-oxide complexes is slightly longer than the corresponding value of 1.99 Å for $L^{I}Cu(OTf)$. Interestingly, for $[L^{1}Cu(2,6\text{-}Cl_2\text{-}PyO)](OTf)$, one of the two chloro substituents weakly interacts with the copper center, with Cu-Cl bond distance of ~2.95 Å. The N–O bond distances of 1.33–1.34 Å for these Cu^{I}-pyridine *N*-oxide complexes are similar to those seen in Cu^{II}-pyridine-*N*-oxide complexes,[113] implying the little activation of *N*-oxide. The pyridine *N*-oxide ring planes are parallel to the dimethylphenyl substituent in L^{1}, consistent with π-stacking interactions. The various substituents of the pyridine *N*-oxides did not greatly influence their bondings with respect to the N-O and Cu-O bond lengths.

Similarly, the overall structures of Cu^{I}-ONM_3 adducts of L^{3} and L^{4} parallel those of the corresponding Cu^{I}-NCMe complexes. However, some structural differences are noticed between $L^{4}Cu(NCMe)$ and $L^{4}Cu(ONM_3)$. While the former shows symmetrical Cu-N bond distances (1.94 and 1.95 Å) in a coordination geometry close to Y-shaped, in the latter case the Cu^{I} ion adopts a geometry close to T-shaped with more divergent Cu-N distances of 1.9093(19) and 2.000(15) Å. This asymmetry of Cu-N bonds in $L^{4}Cu(ONM_3)$ seems to be due to a crystal packing effect because careful examination of the 3-dimensional packing structure of $L^{4}Cu(ONM_3)$ revealed close contacts between the

[113] a) Shi, J.-M.; Chen, J.-N.; Wu, C.-Ju; Liu, L.-D. "Tetrakis(4-nitropyridine-N-oxide-κO)bis(perchlorato)copper(II)." *Acta Crystallogr. E*. **2005**, *61*, m2621-m2622. b) van Albada, G. A.; Mutikainen, I.; Turpeinen, U.; Reedijk, J. "A rare 2D structure of a novel Cu(II) dinuclear-based compound with dicyanamide and 4-nitropyridine-N-oxide as ligands." *Inorg. Chem. Commun*. **2006**, *9*, 441-443.

methyl hydrogens from $ONMe_3$ and the nitro group of the formazanato ligand from the next molecule. These contacts push away the N-oxide from the central position to result in the Y-shaped geometry. The structural distortion from T- to Y-shaped geometry appears to be translated into the asymmetry of Cu-N bonds. Both Cu^I-$ONMe_3$ adducts have N-O bond distances of 1.40–1.41 Å that are similar to that of free Me_3NO (1.404(5) Å),[114] implicating little activation of *N*-oxide. This result could be ascribed to the weak and modest electron-donating character of the ligands used, which are in line with the findings from O_2 reactions of [LCuX] (X = O_3SCF_3 or CH_3CN, L = L^1 or L^3 and L^4) (vide supra). While a number of copper(II)-*N*-oxide complexes are known,[113,115] to our knowledge these complexes represent the first examples of copper(I)-*N*-oxide variants.

[114] Caron, A.; Palenik, G. J.; Goldish, E.; Donohue, J. "The molecular and crystal structure of trimethylamine oxide, $(CH_3)_3NO$." *Acta Crystallogr*. **1964**, *17*, 102-108.

[115] Selected examples: a) Hatfield, W. E.; Muto, Y.; Jonassen, H. B.; Paschal, J. S. "Substituted pyridine N-oxide complexes of copper(II) halides." *Inorg. Chem*. **1965**, *4*, 97-99. b) Richardson, H. W.; Wasson, J. R.; Hatfield, W. E.; Brown, E. V.; Plasz, A. C. "Spectral and magnetic properties of copper(II)-1,5-naphthyridine-1,5-dioxide complexes." *Inorg. Chem*. **1976**, *15*, 2916-2920. c) Carlin, R. L.; De Jongh, L. J. "Structural and magnetic properties of transition metal complexes of pyridine N-oxide." *Chem. Rev*. **1986**, *86*, 659-680.

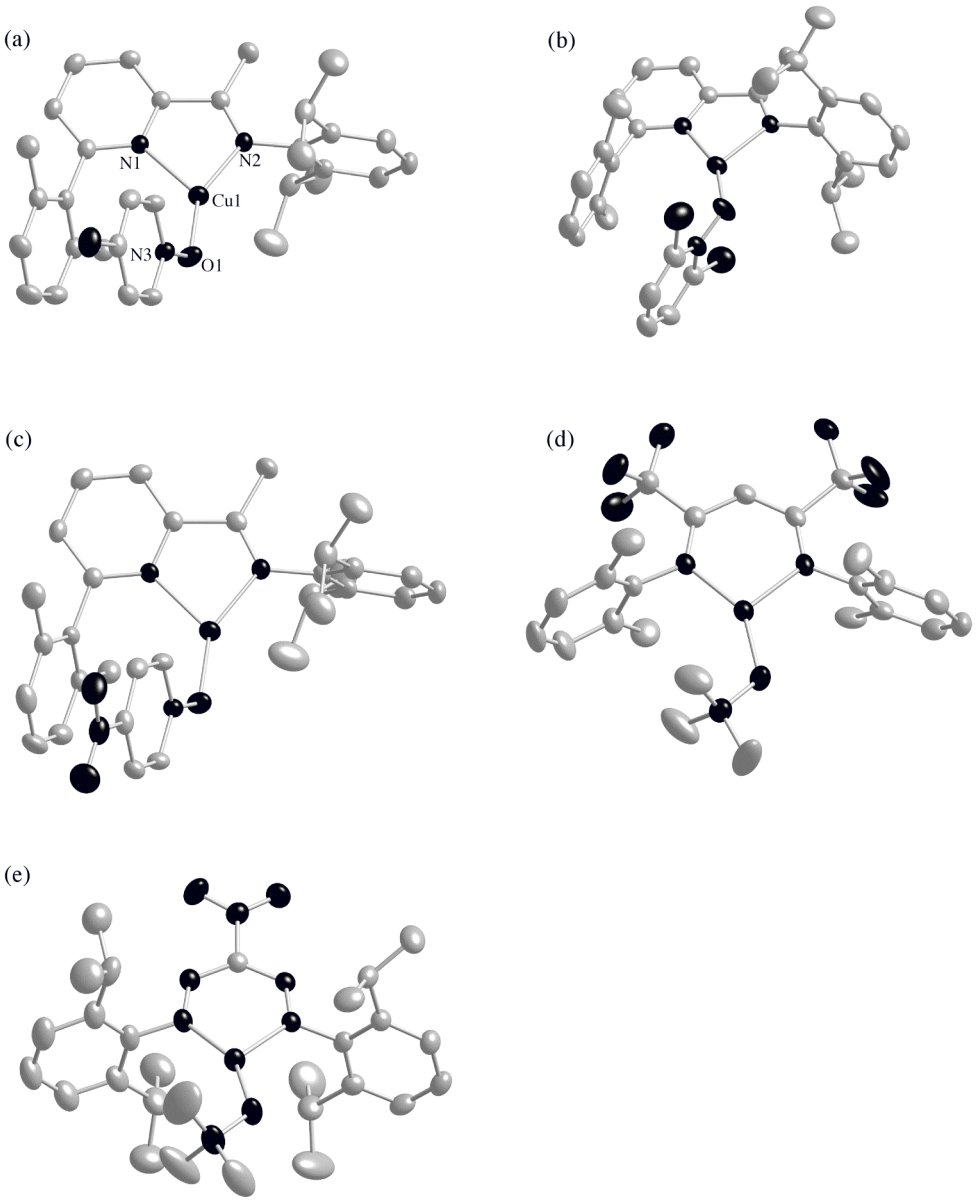

Figure 4-1. Representation of the X-ray crystal structures of Cu^{I}-*N*-oxide adducts. All non-hydrogen atoms are shown as 50 % thermal ellipsoids. For Cu^{I}-pyridine *N*-oxide complexes of L^{1}, only cationic portions are shown. For $L^{4}Cu(ONMe_3)$, disordered THF molecule is omitted for clarity.

Table 4-1. Selected bond lengths (Å) and angles (deg)[a]

	$[L^1Cu(4\text{-}Cl\text{-}PyO)]^+$	$[L^1Cu(2,6\text{-}Cl_2\text{-}PyO)]^+$	$[L^1Cu(4\text{-}NO_2\text{-}PyO)]^+$	$L^3Cu(ONMe_3)$	$L^4Cu(ONMe_3)$
Cu1-N1	2.0876(16)	1.9621(16)	2.066(2)	1.941(2)	1.9093(19)
Cu1-N2	1.9792(16)	2.0857(15)	1.993(2)	2.001(2)	2.0005(19)
Cu-O1	1.9017(14)	1.8763(15)	1.9048(18)	1.9076(18)	1.8853(17)
O1-N3	1.339(2)	1.328(2)	1.330(3)	1.407(3)	1.399(3)
N1-Cu1-N2	80.35(6)	80.58(7)	80.66(9)	90.58(8)	91.79(8)
N1-Cu1-O1	128.09(6)	156.02(7)	128.78(9)	143.82(8)	149.25(8)
N2-Cu1-O1	151.29(7)	122.86(7)	150.72(9)	117.59(8)	118.96(7)
Cu1-O1-N3	119.47(11)	120.24(12)	121.96(16)	121.94(14)	119.94(14)

[a] Estimated standard deviations are given in parantheses.

4.3.3. Properties of Copper(I)-N-oxide Complexes in solution

The ^{1}H NMR spectra of Cu^I-*N*-oxide complexes except for $[L^1Cu(4\text{-Cl or }4\text{-}NO_2\text{-PyO}](OTf)$ complexes in CD_2Cl_2 or C_6D_6 display a single set of sharp peaks at room temperature, indicating that the Cu^I-*N*-oxide complexes maintain their structural integrities in solution. For example, in $LCu(ONMe_3)$ complexes (L = L^3 and L^4) a singlet peak for the methyl protons from the *N*-oxide is observed at 2.59 ppm (for L^3) and 2.87 ppm (for L^4) and the peaks for the supporting ligand have almost identical chemical shifts and splitting pattern to those for the $LCu^I(NCMe)$ analogs. Similarly, except for the peaks

for the ligand protons that are in the range of those for the copper(I)-triflate complex, ^{1}H NMR spectrum of [L^{1}Cu(2,6-Cl$_2$-PyO)](OTf) displayed additional peaks between 7.55 and 7.48 ppm for the *N*-oxide protons.

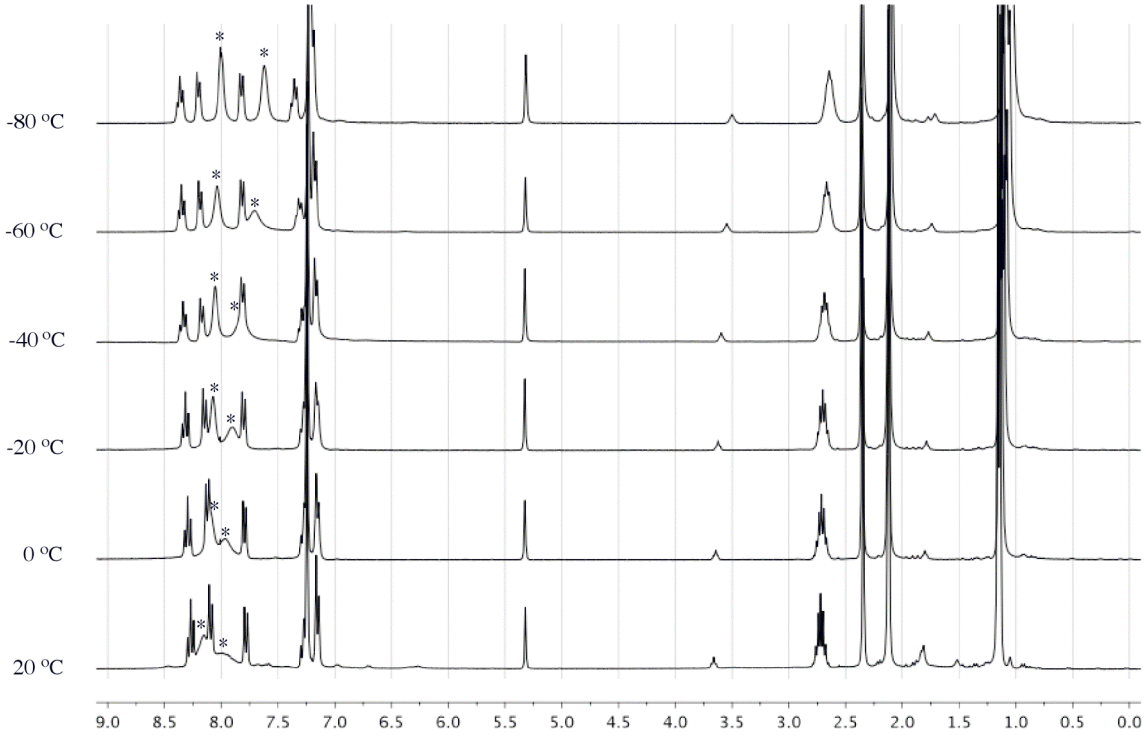

Figure 4-2. Variable temperature ^{1}H NMR spectra of [L^{1}Cu(4-NO$_2$-PyO)](O$_3$SCF$_3$) in CD$_2$Cl$_2$ (300 MHz). Peaks from 4-nitropyridine-*N*-oxide are marked with asterisks.

However, in [L^{1}Cu(4-Cl or 4-NO$_2$-PyO](OTf) complexes the pyridine *N*-oxides appear to undergo rapid fluxional processes. For instance, the ^{1}H NMR spectra of [L^{1}Cu(4-NO$_2$-PyO](OTf) in CD$_2$Cl$_2$ at room temperature exhibit the broad peaks from the pyridine *N*-oxide, but they are split and sharpened upon cooling to –80 °C (Figure 4-2). Thus, we envisioned that the pyridine ring in the pyridine *N*-oxide would undergo a rapid rotational motion through a Cu-O axis at room temperature, but this motion would

be slow down at low temperature due to the π-interaction with the dimethylphenyl substituent in L^1 as seen in their crystal structures. Yet, this rotational motion seems to be much slower or inhibited in the case of [L^1Cu(2,6-Cl_2-PyO)](OTf) at room temperature largely due to the additional weak interaction between one of the two chloro substituents and the copper center as seen in its crystal structure.

Interestingly, thermal stabilities among the copper(I)-*N*-oxide complexes supported by the ligands (L^1 or L^3 and L^4) are different. The copper(I) pyridine *N*-oxide complexes of L^1 are quiet stable in solution. There are no signs of decay by NMR spectroscopy in a d_8-THF solution after 1 day at 80 °C (sealed tube). In contrast, under the same conditions, LCu($ONMe_3$) complexes (L = L^3 and L^4) decompose to paramagnetic species that have yet to be identified. As a representative example, the ^{1}H NMR spectra change of L^4Cu($ONMe_3$) after heating for 4 hours at 80 °C is depicted in Figure 4-3. As evident from the relative ratio of peaks from the ligand to the residual THF solvent, the singlet peak from Me_3NO and most peaks from L^4 disappear, and new peaks from unidentified species appear. Given the comparable N-O bond dissociation energies of ~ 260 kcal/mol among the pyridine *N*-oxides and Me_3NO,[116] the difference in their thermal stabilities would be ascribed to the relative degree of electron donation from the ligands; while L^1 is poor electron-donating, L^3 or L^4 are more electron-donating, but not enough to activate the N-O bond of the *N*-oxides at ambient temperature.

[116] Acree, W. E., Jr.; Pilcher, G.; Ribeiro da Silva, Maria D. M. C. "The dissociation enthalpies of terminal (N-O) bonds in organic compounds." *J. Phys. Chem. Ref. Data*. **2005**, *34*, 553-572.

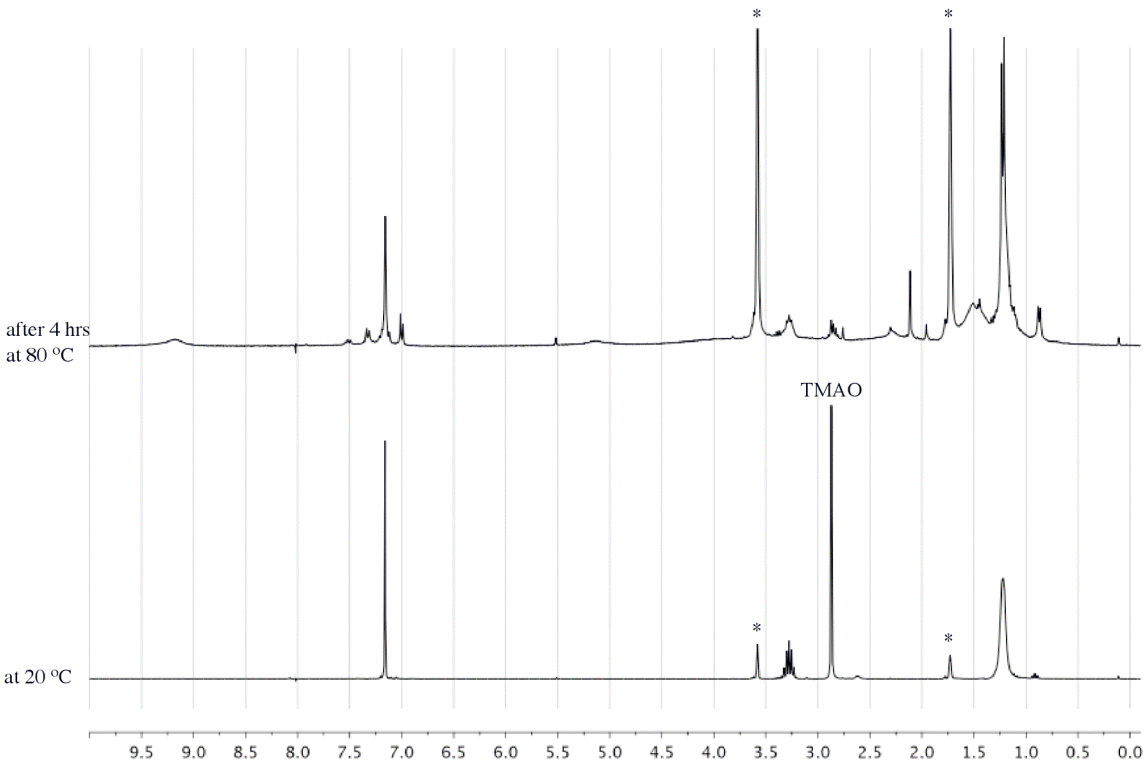

Figure 4-3. ^{1}H NMR spectra change of [L^4Cu(Me_3NO)] in d_8-THF (300 MHz) after heating to 80 °C. Peaks from THF are marked with asterisks. TMAO refers to trimethylamine N-oxide.

4.3.4. Reaction of Copper(I) Complex of L^2 with Iodosylbenzene

Working under hypothesis that stability of Cu^I-pyridine *N*-oxide complexes of L^1 is due to the relatively low degree of electron donation from the ligand L^1, we turned our attention to an analogue of L^1 containing an electron donating *p*-Me_2N group on the pyridyl ring (L^2). First attempt to make the copper(I)-triflate precursor of L^2 following the same procedure to that of $L^1Cu(OTf)^1$ resulted in the copper(I) species having two ligands {[$(L^2)_2$Cu](O_3SCF_3)} as a main product, as evident from a strong ESI-MS peak at *m/z* value of 861 with the isotope distribution pattern consistent to $[(L^2)_2Cu]^+$. The

reduced steric profile of L^2 relative* to that of L^1 (phenyl vs. 2,6-dimethylphenyl, respectively) is thought to be a possible reason for forming the bis-ligand copper(I) complex. Yet, use of the strongly coordinating solvent such as CH_3CN and $[Cu(CH_3CN)_4](O_3SCF_3)$ as a copper source obviates the formation of such bis-ligand copper(I) complex, and results in the $[L^2Cu(CH_3CN)](O_3SCF_3)$ complex by virtue of the coordination of one CH_3CN solvent molecule to the copper center. This compound was characterized by ^1H and $^{13}C\{^1H\}$ NMR spectroscopy and CHN analysis. The key features in the ^1H NMR spectrum denoting the successful incorporation of copper ion to the ligand include that both the methyl hydrogens of the dimethylamino group and the ketimine protons are downfield shifted relative to the free ligand. In addition, the coordination of an acetonitrile to the copper center is evident from a singlet at 2.05 ppm for the methyl hydrogens. Unfortunately, the reaction of $[L^2Cu(CH_3CN)](O_3SCF_3)$ with Me_3NO at room temperature either in THF or CH_3CN solvents led to extensive ligand redistribution and redox processes. From the crude reaction mixtures, we could isolate the known complex $[Cu(Me_3NO)_4]^{2+}$ (determined only via a partial X-ray diffraction data collection)[117] and $[(L^2)_2Cu](O_3SCF_3)$ complex (identified by X-ray crystallography) (Figure 4-4). The crystal structure of $[(L^2)_2Cu](O_3SCF_3)$ complex indicates that it consists of one copper(I) ion, two L^2 ligands, a O_3SCF_3 anion and two THF molecules. The average Cu-N bond distance of 2.074 Å is similar to that (2.03 Å) for Cu^I-pyridne N-oxide complexes of L^1. The coordination geometry of the copper center is distorted from tetrahedral, as reflected by a τ_4 value of 0.59 (values of 0 and 1 being associated with

[117] Drago, R. S.; Donoghue, J. T.; Herlocker, D. W. "Transition metal ion complexes of trimethylamine N-oxide." *Inorg. Chem*. **1965**, *4*, 836-839.

ideal square planar or tetrahedral geometries, respectively).[81] Again, the formation of bis-ligand Cu^{I} species would be ascribed to the reduced steric profile of the ligand L^2.

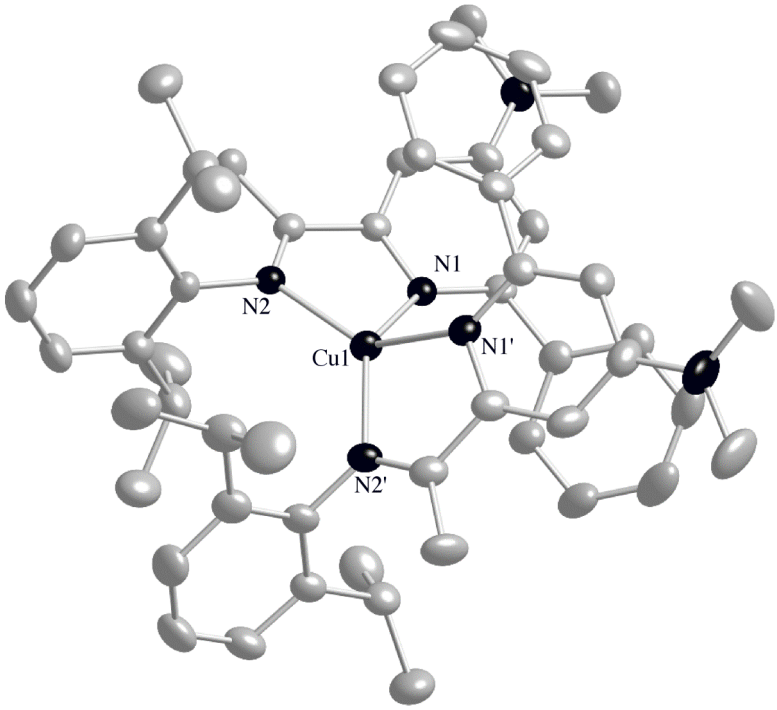

Figure 4-4. Representation of the X-ray crystal structure of $[(L^2)_2Cu](O_3SCF_3)_2$•2THF. All non-hydrogen atoms are shown as 50 % thermal ellipsoids. Only cationic portion is shown and two THF molecules are omitted for clarity.

Table 4-2. Selected bond lengths and angles for $[(L^2)_2Cu](OTf)\bullet 2THF$ [a]

a. Bond Lengths (Å)			
Cu1-N1	2.124(2)	Cu1-N2	2.028(3)
Cu1-N1'	2.103(3)	Cu1-N2'	2.041(2)
b. Bond Angles and Torsion Angles (deg)			
N1-Cu1-N2	80.61(9)	N1-Cu1-N1'	96.99(9)
N1-Cu1-N2'	137.49(9)	N2-Cu1-N1'	138.02(9)
N2-Cu1-N2'	138.36(9)	N1'-Cu1-N2'	80.62(9)

[a] Estimated standard deviations are given in parantheses.

Thus, we sought to react $[L^2Cu(CH_3CN)](O_3SCF_3)$ with stronger oxidant such as PhIO in order to trap a possible $[CuO]^+$ or related species via an intramolecular hydroxylation of the phenyl substituent of the ligand L^2. In accordance with our expectation, such reaction in CH_3CN at room temperature yielded a dicationic tricopper(II) cluster featuring hydroxylated forms of L^2 coordinated to Cu^{II} ions (57% isolated yield). In addition, three copper(II) ions in this cluster are bridged by a central IO_3^- ion to complete four coordinate Cu^{II} ions (Figure 4-5). This cluster was also characterized by CHN analysis and ESI-MS spectrometry. While the overall structure of this cluster is unique, the observation of ligand aryl group hydroxylation by PhIO has parallel in the literature[57-58,63] and similarly may be attributed to a $[CuO]^+$ intermediate or some type of CuOIPh species.

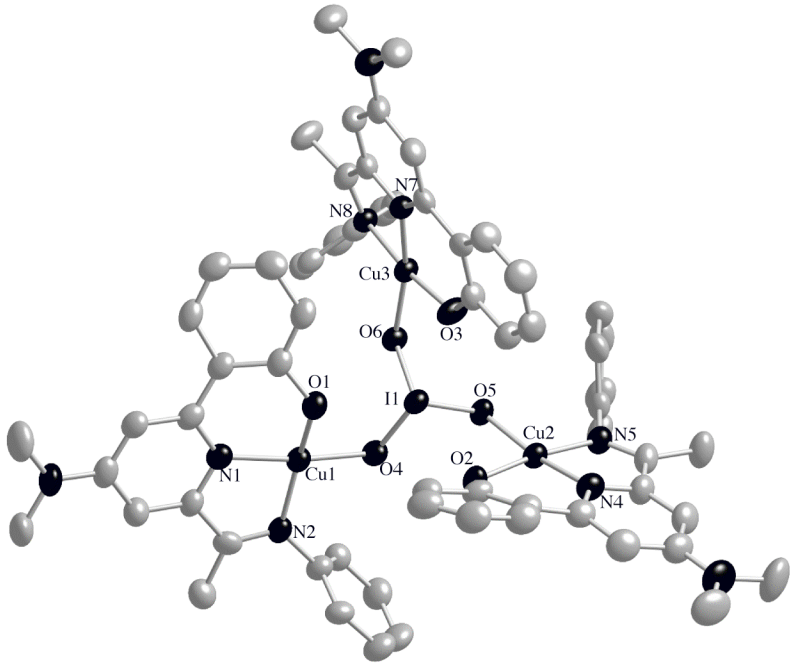

Figure 4-5. Representation of the X-ray structure of the dicationic portion of the tricopper cluster $[(L^o)_3Cu_3(IO_3)](O_3SCF_3)_2 \bullet 2CH_3CN$. The anions and two CH_3CN solvent molecules as well as ligand iPr groups are omitted for clarity. All non-hydrogen atoms are shown as 50 % thermal ellipsoids. L^o refers to the hydroxylated form of L^2.

4.4. Reactions of Copper(I) Complexes of L^5 and L^6 with Me_3NO

By using relatively weak or modest electron-donating ligands, we demonstrate the formation of stable Cu^I-*N*-oxide adducts (L = L^1 or L^3 and L^4) or the observation of oxo-transfer reaction to yield the ligand aryl group hydroxylation by PhIO (L = L^2). For the former cases, the thermal stabilities of such Cu^I-*N*-oxide adducts showed dependence on the electron-donating properties of the ligands; while Cu^I-pyridine *N*-oxide adducts of weakly electron-donating ligand L^1 are very stable in solution, use of modestly electron-donating ligands (L = L^3 and L^4) appeared to thermally induce the N-O bond activation of

the corresponding Cu^{I}-*N*-oxide adducts. These observations suggest that more strongly electron-donating ligands would result in the N-O bond heterolysis of the N-oxides. Thus, we turned our attention to the copper(I) complexes of more electron-donating ligand L^5 and L^6. Addition of Me_3NO to $L^5Cu(CH_3CN)$ in THF at room temperature led to the rapid color change from the pale-yellow to the dark-brown. From this brown solutions we were able to isolate a few crystals of the known[82] complex $[(L^5)_2Cu_2(\mu\text{-}OH)_2]$. Despite the longer reaction time (over 1d) being required, the reaction of $L^6Cu(CH_3CN)$ with Me_3NO under the same condition also led to the formation of the bis(μ-hydroxo)dicopper(II) complex, which was characterized by the X-ray crystallography (Figure 4-6). Gross structural features of $[(L^6)_2Cu_2(\mu\text{-}OH)_2]$ complex are similar to those of the $[(L^3)_2Cu_2(\mu\text{-}OH)_2]$ species.[1] But, the increased steric bulk from the diisopropyl flanking groups of L^6 seems to prevent both hydroxides and β-diketiminate ligands from tightly binding to the copper centers. For instance, average bond distances of Cu-O and Cu-N are 1.941 and 1.96 Å, respectively. These distances are slightly longer than the corresponding values of 1.911 and 1.941 Å for the $[(L^3)_2Cu_2(\mu\text{-}OH)_2]$ complex. Moreover, the Cu-Cu distance also increases by ~ 0.1 Å compared to that (~ 3.02 Å) of the $[(L^3)_2Cu_2(\mu\text{-}OH)_2]$ complex. Both weak bindings of the β-diketiminate ligands and bridging hydroxides and wider Cu-Cu separation seemingly help to minimize unfavorable steric repulsions between two aryl groups at the expense of the reduced dihedral angle between the N atoms of 38.69°.

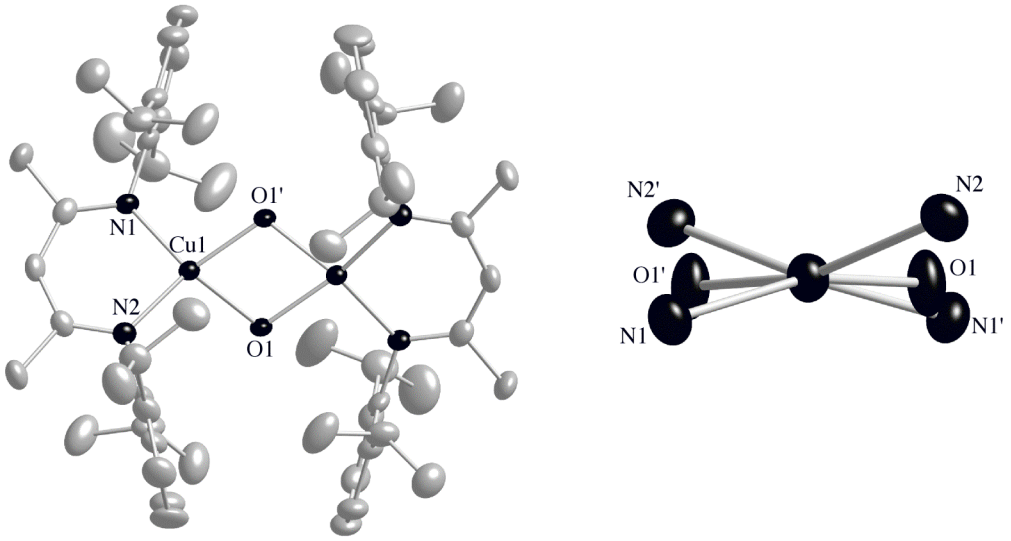

Figure 4-6. Representation of the X-ray structure of $[(L^6)_2Cu_2(\mu\text{-}OH)_2]$ with all non-hydrogen atoms shown as 50% thermal ellipsoids. (left) view along Cu-Cu vector.

Table 4-3. Selected bond lengths and angles for $[(L^6)_2Cu_2(\mu\text{-}OH)_2]$ [a]

a. Bond Lengths (Å)			
Cu1-O1	1.938(3)	Cu1-O1'	1.944(3)
Cu1-N1	1.959(3)	Cu1-N2	1.962(3)
b. Bond Angles and Torsion Angles (deg)			
O1-Cu1-O1'	73.37(15)	O1-Cu1-N1	98.04(12)
O1-Cu1-N2	165.63(13)	O1'-Cu1-N2	98.27(13)
O1'-Cu1-N1	165.34(13)	N1'-Cu1-N2'	80.62(9)

[a] Estimated standard deviations are given in parantheses.

Although we were not able to quantify the yield of the bis(μ-hydroxo)dicopper(II) species derived from the reaction of the copper(I) complexes of L^5 or L^6 with Me_3NO at

room temperature, these results are consistent with our expectation. That is, the more electron-rich copper centers could effect the N-O bond scission of Me_3NO to generate a $[CuO]^+$ or related species that then undergo the hydrogen abstraction from the surrounding medium to produce the final bis(μ-hydroxo)dicopper complexes. However, the source of the hydroxide H-atoms is not clear at this point.

To prove the hypothesis that the bis(μ-hydroxo)dicopper complexes is formed via the N-O bond scission of Me_3NO by the electron-rich copper(I) complexes of L^5 or L^6, we further explored such reactions at low temperature (T < −78 °C). When the copper(I) complex of L^5 reacted with excess Me_3NO in THF at −80 °C, smooth conversion to an intermediate occurred over ~1h (Figure 4-7). The resultant intermediate exhibits the intense absorption band at 423 nm (ε ~ 16 000 M^{-1} cm^{-1} per copper). The position and intensity of this band is in the range of the bis(μ-oxo)dicopper(III) species formed by the oxygenation of $L^5Cu(CH_3CN)$ (λ_{max} = 422 nm, ε = 22 000 M^{-1} cm^{-1}) in THF at −80 °C.[67] This result led us to tentatively assign the species formed from the reaction of $L^5Cu(CH_3CN)$ with Me_3NO as a bis(μ-oxo)dicopper(III) species.

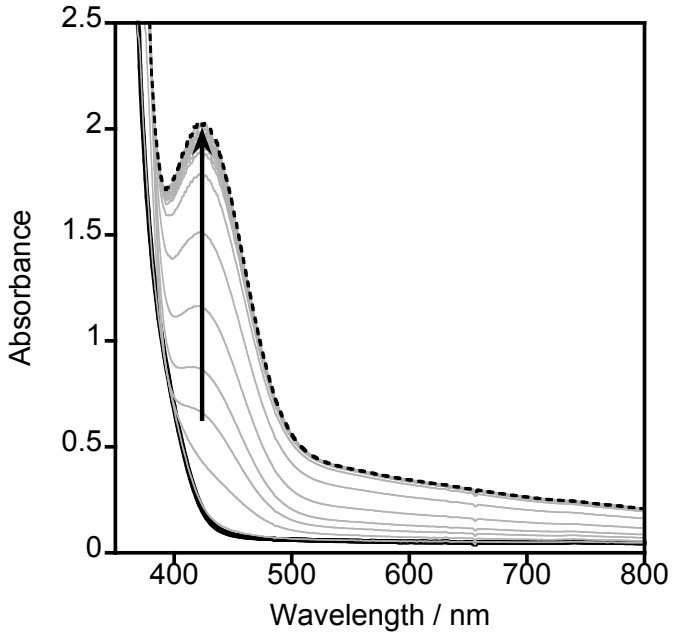

Figure 4-7. UV-vis spectra obtained during the reaction of $L^5Cu(CH_3CN)$ (0.25 mM) with Me_3NO (10 equiv) in THF at −80 °C over 1h (starting spectrum in black solid line, final spectrum in black dotted line).

To confirm this assignment, we performed the resonance Raman experiments on the intermediate and compared the data to those of a sample prepared independently from O_2. As depicted in Figure 4-8, both samples prepared either from Me_3NO or from O_2 display a resonance enhanced peak at 608 cm^{-1} that is identical to the previously reported literature value.[24] On the basis of the UV-vis and resonance Raman spectroscopic properties, we assigned the intermediate as the bis(μ-oxo)dicopper(III) species.

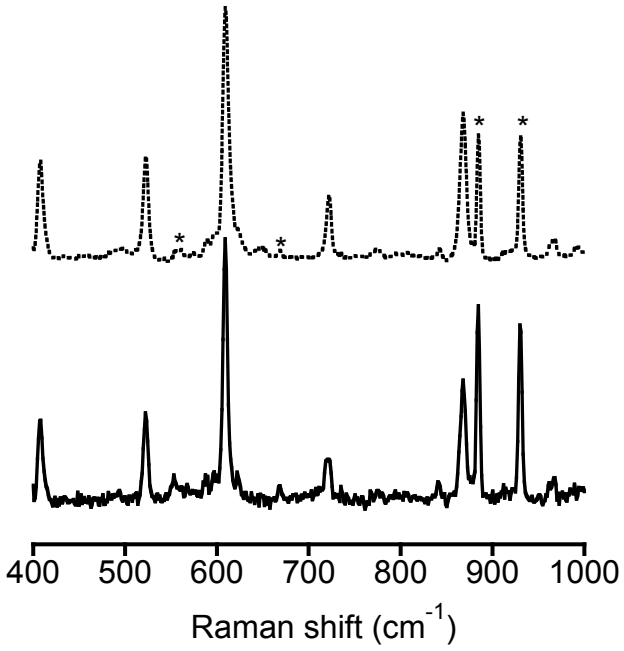

Figure 4-8. Resonance Raman spectra obtained on samples obtained from the reaction of $L^5Cu(CH_3CN)$ in THF at −80 °C with Me_3NO (solid line) or O_2 (dotted line). The spectra were obtained using λ_{ex} = 457.9 nm at −196 °C; solvent peaks are marked with asterisks and the peak assigned as the Cu_2O_2 core vibration is indicated at 608 cm^{-1}.

This result clearly indicates that the copper(I) complex of L^5 effectively induces the heterolytic N-O bond scission of Me_3NO by virtue of the strong electron-donating property of L^5. Although reactions of PhIO with copper(I) complexes that yield other types of products have been reported,[8c,118] to our knowledge this is the first example of a bis(μ-oxo)dicopper complex derived from an oxo transfer reagent.

In contrast, the reaction of $L^6Cu(CH_3CN)$ with excess Me_3NO between −80 and

[118] See, for example: a) Obias, H. V.; Lin, Y.; Murthy, N. N.; Pidcock, E.; Solomon, E. I.; Ralle, M.; Blackburn, N. J.; Neuhold, Y; Zuberbuehler, A. D.; Karlin, K. D. "Peroxo-, Oxo-, and Hydroxo-Bridged Dicopper Complexes: Observation of Exogenous Hydrocarbon Substrate Oxidation" *J. Am. Chem. Soc*. **1998**, *120*, 12960-12961. b) Franklin, C. C.; Vanatta, R. B.; Tai, A.; Valentine, J. S. "Copper ion mediated epoxidation of olefins by iodosylbenzene." *J. Am. Chem. Soc*. **1984**, *106*, 814-816.

25 °C only resulted in minor change in the UV-vis spectrum, with a new weak shoulder feature at 420 nm ($\varepsilon < 1000$ M^{-1} cm^{-1}). This feature remained unchanged at temperature below −10 °C, but the prolonged stirring at room temperature eventually changed the color to the brown. Considering the almost identical electron-donating properties of L^5 and L^6 based on ν(CO) values of 2071[1] and 2070[71] cm^{-1} for the corresponding copper(I) carbonyl complexes, respectively, the steric properties (2,6-dimethylphenyl vs. 2,6-diisopropylphenyl for L^5 and L^6) also appear to play a role in promoting the N-O bond cleavage of Me_3NO.

Combining all data, we proposed possible reaction pathways to the bis(μ-oxo)dicopper complex via a heterolytic N-O bond cleavage of Me_3NO at the copper(I) center (Scheme 4-6). The first route involves an adduct akin to $LCu^I(ONMe_3)$ (L = L^3 and L^4) that subsequently undergoes the N-O bond cleavage to yield a Me_3N and a $[CuO]^+$ species. The produced $[CuO]^+$ species rapidly dimerizes to form the $[Cu_2(\mu\text{-}O)_2]^{2+}$ core. In the other pathway, the Cu^I-$ONMe_3$ adduct first dimerizes in solution to form a $[Cu_2(\mu\text{-}ONMe_3)_2]^{2+}$ species that then undergoes the N-O bond cleavage to produce the $[Cu_2(\mu\text{-}O)_2]^{2+}$ core. Although the more sluggish reaction rate for the copper(I) complex of L^6 that features identical electron-donating but more sterically demanding compared to that of L^5 lies more toward the second pathway, that is, dimerization of the Cu^I-$ONMe_3$ adduct is expected to be more energetically uphill for L^6 due to its increased steric, we recognize that both pathways are equally viable on the basis of all available data so far.

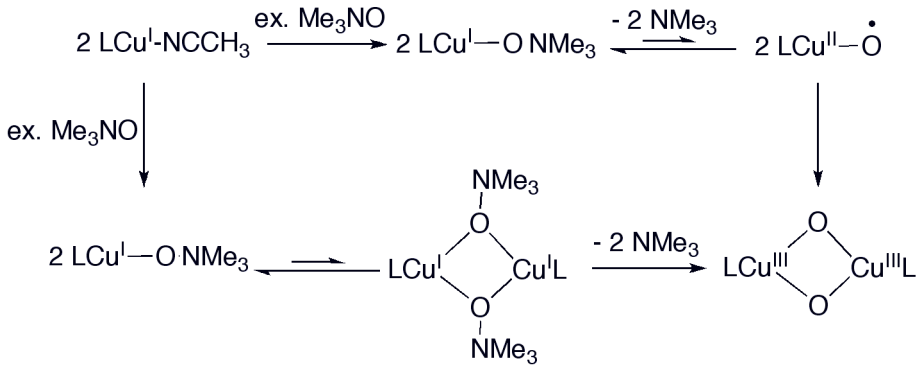

Scheme 4-6. Proposed reaction pathways to a $[Cu_2(\mu\text{-}O)_2]^{2+}$ core.

4.5. Conclusions and Perspectives

In this chapter, we described the results from explorations of the reactivity of copper(I) complexes of L^1 and L^3-L^6 with pyridine- and trimethylamine-*N*-oxides. Such reactions have been found to depend on degree of the electron donation from the ligands. With the relatively weak electron-donating ligands of L^1, L^3, and L^4, we observed the formation of novel, stable Cu^I-*N*-oxide adducts. On contrary, use of the more strongly electron-donating ligands of L^5 or L^6 led to the formation of a bis(μ-OH)$_2$dicopper species at room temperature or a bis(μ-oxo)dicopper core at low temperature for L^5 via an oxo-transfer to the copper(I) centers. For the latter, the rate of the oxo-transfer reaction is also shown to be affected by the steric demand of the ligands. Reaction of the copper(I) complex of L^2 with PhIO yields a unique tricopper cluster derived from aryl substituent hydroxylation.

4.6. Experimental Section

General: All reagents were obtained from commercial sources and used without further purification, unless otherwise noted. The solvents THF, pentane, and Et_2O were dried over Na/benzophenone and distilled under nitrogen or passed through solvent purification columns (Glass Contour, Laguna, CA). The solvent CH_3CN was dried over CaH_2 and distilled under nitrogen prior to use. The compounds $[Cu_4Mes_4]$ (Mes = mesityl),[80] $[Cu(CH_3CN)_4](O_3SCF_3)$,[109] L^1,[1,1] $[(L^1)Cu(O_3SCF_3)]$,[1] $LCu(CH_3CN)$ ($L = L^3$, L^4 and L^5),[3] and 2,6-dibromo-4-(dimethylamino)pyridine[112] were synthesized following literature procedures (see Scheme 2 in main text for ligand identities). All metal complexes were prepared and stored in a Vacuum Atmospheres inert atmosphere glovebox under a dry nitrogen atmosphere or were manipulated using standard inert atmosphere vacuum and Schlenk techniques.

Physical Methods: NMR spectra were recorded on either Varian VI-300 or VI-500 spectrometers at room temperature. Variable low-temperature NMR spectra were recorded on the Varian VI-300 instrument. Chemical shifts (δ) for ^1H and ^{13}C NMR spectra are reported versus tetramethylsilane and were referenced to residual protium in the deuterated solvent. UV-Vis spectra were recorded on an HP8453 (190-1100 nm) diode array spectrophotometer. Low temperature spectra were acquired through the use of a Unisoko low temperature UV-Vis cell holder. When necessary, UV-Vis spectra were corrected for drifting baselines due to minimal frosting of the UV cells caused by the low-temperature device. This was achieved by subtracting the average of a region with no absorbance (i.e., baseline, typically 950-1000 nm) from the entire spectrum. Resonance

Raman spectra were recorded on an Acton 506 spectrometer using a Princeton Instruments LN/CCD-11100-PB/UVAR detector and ST-1385 controller interfaced with Winspec software. The spectra were obtained at −196 °C using a backscattering geometry. A Spectra-Physics 2030-15 argon ion laser with a power of 200 mW at the sample was employed to give the excitation at 457.9 nm. Raman shifts were externally referenced to liquid indene. Elemental analyses were performed by Robertson Microlit Lab. ESI-MS (electrospray ionization mass spectra) were recorded on a Bruker BioTOF II instrument.

2,6-Dibromo-4-(dimethylamino)pyridine. This compound was prepared by the method described in the literature.[15] Yield (22 %). ^{1}H NMR (300 MHz, $CDCl_3$): δ 6.58 (s, *J* 2H), 2.99 (s, 6H). ^{13}C{1H} NMR (75.0 MHz, $CDCl_3$): δ 156.81, 140.94, 109.09, 39.67 ppm.

L^2. *n*-Butyllithium (1.6 M in hexanes, 23.0 mL, 37 mmol) was added via syringe to a solution of 2,6-dibromo-4-(dimethylamino)-pyridine (10.0 g, 36 mmol) in THF (200 mL) at –78 °C and the mixture was allowed to stir for 45 min. Anhydrous *N,N*-dimethylacetamide (810 μL, 10.5 mmol) was added via syringe to the mixture, which was then warmed to room temperature. Saturated sodium carbonate (50 mL) was added and the mixture was extracted with EtOAc (3 x 50 mL). The combined organic layers were dried over $MgSO_4$ and solvent was removed under reduced pressure. Flash chromatography (2:1 hexanes/EtOAc) using silica gel provided 6.19 g (71 %) of 1-{6'-bromo-4'-(dimethylamino)pyridin-2'-yl}ethanone. ^{1}H NMR (300 MHz, $CDCl_3$): δ 7.22 (d, *J* = 2.4 Hz, 1H), 6.75 (d, *J* = 2.4 Hz, 1H), 3.04 (s, 6H), 2.65 (s, 3H). ^{13}C{^{1}H} NMR

(75.0 MHz, $CDCl_3$): δ 200.07, 156.26, 153.94, 142.53, 112.09, 104.49, 39.66, 26.16 ppm. Anal. Calcd for $C_9H_{11}N_2OBr$: C, 44.47; H, 4.56; N, 11.52. Found: C, 44.88; H, 4.78; N, 11.37.

To a mixture of 1-{6'-bromo-4'-(dimethylamino)pyridin-2'-yl}ethanone (3.0 g, 12.3 mmol) and $Pd(PPh_3)_4$ (0.43 g, 0.37 mmol) in toluene (60 mL) was added aqueous Na_2CO_3 (12.0 mL, 2.0 M) and a solution of phenylboronic acid (1.8 g, 15.0 mmol) in MeOH (20 mL) under a nitrogen atmosphere and the mixture was refluxed for 8 h. After cooling, CH_2Cl_2 (80 mL), aqueous Na_2CO_3 (12.0 mL, 2.0 M) and concentrated ammonium hydroxide (3.0 mL) were added. The aqueous layer was extracted with CH_2Cl_2 (3 × 50 mL), the combined organic fractions were dried over $MgSO_4$, and the volatile materials were removed under vacuum to give crude 1-{6'-phenyl-4'-(dimethylamino)pyridin-2'-yl}ethanone, which was used directly in the next step without further purification. A mixture of the crude 1-{6'-phenyl-4'-(dimethylamino)pyridin-2'-yl}ethanone, 2,6-diisopropylaniline (tech 90%, 10.0 g, 51.0 mmol) and formic acid (2 drops) in 100 mL anhydrous MeOH was refluxed for 3 d. The volume of the solvent was reduced to 20 mL under vacuum to yield a gray microcrytalline material (3.1 g, 7.76 mmol; 63 % based on the starting 1-{6'-phenyl-4'-(dimethylamino)pyridin-2'-yl}ethanone), which was isolated by filtration and washing with cold MeOH (2 × 10 mL) (3.1 g, 7.76 mmol; 63% based on the starting 1-{6'-phenyl-4'-(dimethylamino)pyridin-2'-yl}ethanone). ^{1}H NMR (300 MHz, CD_2Cl_2): δ 8.11-8.08 (m, 2H), 7.62 (d, J = 2.4 Hz, 1H), 7.51-7.38 (m, 3H), 7.18-7.04 (m, 4H) 3.14 (s, 6H), 2.80 (sept, J = 6.9 Hz, 2H), 2.26 (s, 3H), 1.16 (d, J = 6.9 Hz, 6H), 1.15 (d, J = 6.9 Hz, 6H). ^{13}C{^{1}H} NMR (75.0 MHz,

CD_2Cl_2): δ 168.69, 159.30, 156.28, 147.39, 140.91, 136.42, 129.13, 128.99, 127.46, 123.81, 123.47, 104.86, 102.85, 39.90, 28.75, 23.51, 23.20, 17.96 ppm. Anal. Calcd for $C_{27}H_{33}N_3$: C, 81.16; H, 8.32; N, 10.52. Found: C, 81.56; H, 8.37; N, 10.47.

[(L^2)Cu(CH_3CN)](O_3SCF_3). A yellow solution of L^2 (100 mg, 0.25 mmol) in CH_3CN (3 mL) was added to a colorless solution of [Cu(CH_3CN)$_4$](O_3SCF_3) (94.3 mg, 0.25 mmol) in CH_3CN (2 mL), resulting in an immediate color change to dark red. After 30 min, the red mixture was filtered through a plug of Celite and the solvent was removed under vacuum to give the product as orange microcrystals. Analytically pure material was obtained by slow diffusion of Et_2O into a concentrated CH_3CN solution of the product at −20 °C (128 mg, 79%). ^{1}H NMR (300 MHz, CD_2Cl_2): δ 7.79-7.76 (m, 2H), 7.57-7.52 (m, 3H), 7.26 (s, 3H), 7.21 (d, J = 2.4, 1H), 6.97 (d, J = 2.4, 1H), 3.24 (s, 6H), 2.72 (sept, J = 6.9 Hz, 2H), 2.31 (s, 3H), 2.05 (s, 3H), 1.18 (d, J = 6.9 Hz, 12H). ^{13}C{^{1}H} NMR (75.0 MHz, CD_2Cl_2): δ 173.24, 159.74, 156.94, 151.37, 143.33, 140.99, 130.32, 128.96, 128.86, 126.86, 124.44, 117.87, 108.13, 107.88, 40.35, 29.07, 24.16, 23.14, 17.60, 3.10 ppm. Anal. Calcd for $C_{30}H_{36}N_4O_3F_3SCu$: C, 55.16; H, 5.55; N, 8.58. Found: C, 55.06; H, 5.57; N, 8.56.

General Method for the Preparation of Copper(I)-N-Oxide Complexes. In an inert atmosphere, to a solution of the [(L^1)Cu(O_3SCF_3)] (100 mg, 0.167 mmol) or [(L^3 or L^4)Cu(CH_3CN)] (0.167 mmol) in THF (5 mL) was added an equimolar amount of the substituted pyridine N-oxide (PyO) or Me_3NO in THF (3 mL). The mixture was stirred for 30 min and then the solvent was removed under vacuum to give a reddish-brown

residue. The products were obtained in analytically pure form by recrystallisation via slow vapor diffusion of pentane into a concentrated THF solution at –20 °C.

[(L^1)Cu(4-Cl-PyO)](O_3SCF_3). This complex was isolated as a dark-red crystalline solid (110 mg, 90 %). ^{1}H NMR (300 MHz, CD_2Cl_2): δ 8.37 (t, J = 7.8 Hz, 1H), 8.23 (d, J = 7.8 Hz, 1H), 7.81 (d, J = 7.8 Hz, 1H), 7.35 (bs, 4H), 7.31-7.14 (m, 6H), 2.72 (sept, J = 6.9 Hz, 2H), 2.39 (s, 3H), 2.13 (s, 6H), 1.18 (d, J = 6.9 Hz, 6H), 1.13 (d, J = 6.9 Hz, 12H). ^{13}C{1H} NMR (75.0 MHz, CD_2Cl_2): δ 170.26, 160.67, 151.73, 143.25, 141.55, 139.87, 137.70, 136.51, 130.59, 130.04, 128.66, 126.77, 124.73, 124.41, 29.16, 23.94, 23.08, 20.78, 17.79 ppm. Anal. Calcd for $C_{33}H_{36}N_3O_4F_3ClSCu$: C, 54.54; H, 4.99; N, 5.78. Found: C, 54.49; H, 4.94; N, 5.70.

[(L^1)Cu(2,6-Cl_2-PyO)](O_3SCF_3). This complex was isolated as a dark-red crystalline solid (108 mg, 85%). ^{1}H NMR (300 MHz, CD_2Cl_2): δ 8.31 (t, J = 7.8 Hz, 1H), 8.16 (d, J = 7.8 Hz, 1H), 7.76 (d, J = 7.8 Hz, 1H), 7.55-7.48 (m, 3H), 7.26 (s, 3H), 6.94-6.90 (m, 3H), 2.76 (sept, J = 6.9 Hz, 2H), 2.38 (s, 3H), 2.07 (s, 6H), 1.21 (d, J = 6.9 Hz, 6H), 1.19 (d, J = 6.9 Hz, 6H). ^{13}C{1H} NMR (75.0 MHz, CD_2Cl_2): δ 170.29, 160.53, 151.27, 143.85, 143.19, 141.25, 137.76, 135.87, 130.45, 129.54, 128.07, 126.81, 124.36, 124.24, 29.21, 23.94, 23.22, 20.67, 17.60 ppm. Anal. Calcd for $C_{33}H_{35}N_3O_4F_3Cl_2SCu$: C, 52.07; H, 4.63; N, 5.52. Found: C, 51.92; H, 4.40; N, 5.35.

[(L^1)Cu(4-NO_2-PyO)](O_3SCF_3). This complex was isolated as a dark-red crystalline solid (107 mg, 87%). ^{1}H NMR (300 MHz, CD_2Cl_2): δ 8.27 (t, J = 7.8 Hz, 1H), 8.16 (bs, 2H), 8.10 (d, J = 7.8 Hz, 1H), 7.99 (bs, 2H), 7.78 (d, J = 7.8, 1H), 7.30-7.14 (m, 6H), 2.72 (sept, J = 6.9 Hz, 2H), 2.34 (s, 3H), 2.12 (s, 6H), 1.15 (d, J = 6.9 Hz, 12H).

$^{13}C\{1H\}$ NMR (75.0 MHz, CD_2Cl_2): δ 194.16, 169.14, 168.66, 160.82, 152.04, 143.91, 139.72, 139.33, 137.88, 136.14, 134.70, 133.38, 130.47, 129.95, 129.33, 128.54, 128.23, 126.20, 124.14, 123.25, 29.02, 23.92, 23.39, 20.70, 17.57 ppm. Anal. Calcd for $C_{33}H_{36}N_4O_6F_3SCu$: C, 53.76; H, 4.92; N, 7.60. Found: C, 53.87; H, 4.96; N, 7.44.

[(L^3)Cu(Me_3NO)]. This complex was isolated as a brown crystalline solid (57 mg, 67%). ^1H NMR (300 MHz, THF-d_8): δ 6.91 (d, J = 7.5 Hz, 4H), 6.74 (t, J = 7.5 Hz, 2H), 5.44 (s, 1H), 2.59 (s, 9H), 2.17 (s, 12H), $^{13}C\{1H\}$ NMR (75.0 MHz, THF-d_8): δ 150.15, 130.03, 128.10, 123.20, 119.88, 82.30, 59.90, 19.23 ppm. Anal. Calcd for $C_{24}H_{28}CuF_6N_3O$: C, 52.22; H, 5.11; N, 7.61. Found: C, 52.06; H, 4.96; N, 7.36.

[(L^4)Cu(Me_3NO)]. This complex was isolated as a brown crystalline solid (78 mg, 88%). ^1H NMR (300 MHz, THF-d_8): δ 7.16 (s, 6H), 3.28 (sept, J = 6.9 Hz, 4H), 2.87 (s, 9H), 1.22 (bs, 24H), $^{13}C\{1H\}$ NMR (75.0 MHz, THF-d_8): δ 151.88, 141.39, 127.27, 123.96, 60.46, 29.09, 29.02, 23.44 ppm. Anal. Calcd for $C_{28}H_{43}CuN_6O_3$: C, 58.46; H, 7.53; N, 14.61. Found: C, 58.27; H, 7.42; N, 14.46.

Reaction of [(L^2)Cu(CH_3CN)](O_3SCF_3) with Me_3NO. To an orange solution of [(L^2)Cu(CH_3CN)](O_3SCF_3) in CH_3CN (3 mL) (100 mg, 0.153 mmol) was added an equimolar amount of Me_3NO as a solid (11.5 mg, 0.153 mmol) and the mixture was stirred for 1 d at ambient temperature, during which time the color changed to red. The reaction mixture was filtered through a plug of Celite to remove any insoluble residue and solvent was removed from the red filtrate in vacuo. Crystallization via slow vapor diffusion of pentane into a concentrated THF solution at –20 °C resulted in the formation of a complex mixture of products that included green and red single crystals which were

identified by manual removal and subsequent X-ray crystallography. The green crystals were found to be $[Cu(Me_3NO)_4](O_3SCF_3)_2$ (determined only via a partial X-ray diffraction data collection),[21] and the red crystals were found to be $[(L^2)_2Cu](O_3SCF_3) \cdot 2THF$ (determined by a complete X-ray crystal structure solution, see Figure 4-4).

Reaction of $L^2Cu(CH_3CN)$ with PhIO, to yield $[(L^2\text{-}O)_3Cu_3(IO_3)](O_3SCF_3)_2$. To an orange solution of $[L^2Cu(CH_3CN)](O_3SCF_3)$ (100 mg, 0.153 mmol) in CH_3CN (3 mL) was added an excess PhIO as a solid (67 mg, 0.306 mmol) and the mixture was stirred for 1 d at ambient temperature, during which time the color changed to brown. The reaction mixture was filtered through a plug of Celite to remove any insoluble residue and the volume of the brown filtrate was reduced to ~ 1 ml under vaccum. The solution was carefully layered with Et_2O (~ 5 ml) and allowed to stand at –20 °C to give the product as reddish-brown crystals (63 mg, 57 %). Anal. Calcd for $C_{91}H_{104}N_{10}F_6O_{12}S_2I_2Cu_3$ ($[(L^2\text{-}O)_3Cu_3(IO_3)](O_3SCF_3)_2$-PhI-$CH_3CN$) C, 50.78; H, 4.87; N, 6.51. Found: C, 50.76; H, 4.96; N, 6.63. The presence of PhI and CH_3CN in the compound was corroborated by NMR spectroscopy.

Room Temperature Reaction of $LCu(CH_3CN)$ (L = L^5 or L^6) with Me_3NO. To a light yellow solution of $LCu(CH_3CN)$ (0.122 mmol) in THF (3 mL) was added an equimolar amount of Me_3NO (0.122 mmol) at ambient temperature accompanied by a rapid color change to a dark brown. The resulting mixture was stirred for 1d to ensure the completion of reaction. The mixture was filtered through a plug of Celite to remove any insoluble residue and the dark brown filtrate was evacuated in vacuo to give a brown powder. Slow diffusion of pentane into a concentrated THF solution at – 20 °C yielded a

few crystals of $(L)_2Cu_2(OH)_2$, which were identified by the X-ray crystal structure determinations.

Low Temperature Reactions of $L^5Cu(CH_3CN)$ with Me_3NO and O_2. (a) UV-vis Spectroscopy. A solution of $L^5Cu(CH_3CN)$ (0.33 mM) in THF (3 mL) in a septum-sealed quartz cuvette was cooled to –80 °C, and a solution of Me_3NO in THF (1 mL, 10 mM,10 equiv.) was added with a gas tight syringe while purging with Ar. For the O_2 reaction, a quartz cuvette containing $L^5Cu(CH_3CN)$ in THF (10 mM, 2 mL) was cooled to –78 °C by submersion in an acetone/dry ice bath. Dry O_2 was then bubbled through the solution for 5 min.

(b) Resonance Raman Spectroscopy. For the O_2 reaction, a sample for analysis by resonance Raman spectroscopic analysis was prepared by transferring the green solution prepared in a quartz cuvette (above) to a precooled NMR tube (–78 °C), which was then immersed in liquid N_2.

To generate the sample derived from Me_3NO, a closed system consisting of a reaction vessel and an addition funnel was used. The reaction vessel was charged with a solution of Me_3NO in THF (1 ml, 100 mM) and a stir bar in the glove box. The addition funnel was charged with a solution of $L^5Cu(CH_3CN)$ in THF (1 ml, 20 mM), attached to the reaction vessel, and the system sealed with a glass stopper. The solution of Me_3NO in the reaction vessel was then frozen by immersion in liquid N_2, after which the solution of the Cu(I) complex was added. The reaction vessel was then transferred to a dry ice/acetone bath and the reaction solution was allowed to warm to –78 °C. The mixture was stirred for 4 h yielding a light green solution that was stored overnight in a –80 °C

freezer to ensure that the reaction was complete. The solution was then transferred to a precooled NMR tube (–78 °C) and immediately frozen in liquid N_2 for subsequent analysis by resonance Raman spectroscopy.

Table 4-4. Summary of X-ray Crystallographic Data

	$[(L^1)Cu(4\text{-}Cl\text{-}PyO)](O_3SCF_3)$	$[L^1Cu(2,6\text{-}Cl_2\text{-}PyO)](O_3SCF_3)$
empirical formula	C33 H36 Cu N3 Cl F3 O4 S	C33 H35 Cu N3 Cl2 F3 O4 S
formula weight (g/mol)	726.70	761.14
crystal habit, color	red, Block	red, Plate
crystal system	Triclinic	Triclinic
space group	$P\bar{1}$	$P\bar{1}$
a (Å)	8.5510(7)	12.019(3)
b (Å)	10.5070(9)	13.674(4)
c (Å)	19.3019(16)	14.148(4)
α (deg)	103.5400(10)	100.573(4)
β (deg)	96.5490(10)	106.928(4)
γ (deg)	97.3330(10)	108.802(4)
V ($Å^3$)	1653.5(2)	2004.6(9)
Z	2	2
D_{calc} (g/cm^3)	1.460	1.261
temperature (K)	173(2)	173(2)
Absorption (cm^{-1})	8.63	7.79
θ range (deg)	2.02 to 25.07	1.58 to 25.10
hkl ranges	-10/10, -12/12, -22/22	-14/14, -16/14, -16/16
no. of reflections collected	16418	17049
no. of unique reflections	5853(R_{int} = 0.0236)	7049(R_{int} = 0.0204)
Observed reflections ($I > 2\sigma(I)$)[a]	5067	6060
Completeness to θ = 25.11°	99.7	98.9
Data / restraints / parameters	5853 / 0 / 422	7049 / 0 / 424
R1/wR2 ($I > 2\sigma(I)$)	0.0310 / 0.0741	0.0335 / 0.0873
R1/wR2 (all data)	0.0387 / 0.0771	0.0392 / 0.0901
Goodness-of-fit on F^2	1.035	1.070
Max/min peak ($e.Å^{-3}$)	0.351 / -0.318	0.586 / -0.381

	[(L^1)Cu(4-NO_2-PyO)](O_3SCF_3)	[L^3Cu(Me_3NO)]
empirical formula	C33 H36 Cu N4 F3 O6 S	C24 H28 Cu N3 F6 O
formula weight (g/mol)	737.26	552.03
crystal habit, color	red, Rod	red, Plate
crystal system	Triclinic	Monoclinic
space group	$P\bar{1}$	$P_{2/1}/c$
a (Å)	8.5410(6)	12.2913(16)
b (Å)	10.5361(7)	13.9744(18)
c (Å)	19.1094(13)	15.579(2)
α (deg)	101.4610(10)	90
β (deg)	95.1540(10)	107.408(2)
γ (deg)	95.4040(10)	90
V ($Å^3$)	1667.4(2)	2004.6(9)
Z	2	4
D_{calc} (g/cm^3)	1.468	1.436
temperature (K)	173(2)	173(2)
Absorption (cm^{-1})	7.85	9.20
θ range (deg)	2.02 to 25.07	1.74 to 25.03
hkl ranges	-10/10, -12/12, -22/22	-14/14, -16/16, -18/18
no. of reflections collected	11999	22947
no. of unique reflections	5846(R_{int} = 0.0423)	4505(R_{int} = 0.0417)
Observed reflections ($I > 2\sigma(I)$)[a]	4209	3692
Completeness to θ = 25.11°	99.2	99.9
Data / restraints / parameters	5846 / 0 / 440	4505 / 0 / 323
R1/wR2 ($I > 2\sigma(I)$)	0.0365 / 0.0826	0.0371 / 0.0851
R1/wR2 (all data)	0.0589 / 0.0999	0.0499 / 0.0900
Goodness-of-fit on F^2	0.942	1.029
Max/min peak ($e.Å^{-3}$)	0.343 / -0.356	0.422 / -0.288

	$[L^4Cu(Me_3NO)]$	$[(L^2)_2Cu](O_3SCF_3)$
empirical formula	2(C28 H43 Cu N6 O3)• C4 H8 O	C55 H66 Cu N6 F3 O3 S • 2(C4 H8 O)
formula weight (g/mol)	1222.55	1155.95
crystal habit, color	brown, Block	red, Plate
crystal system	Monoclinic	Monoclinic
space group	$P_{2/1}$/c	$P_{2/1}$/c
a (Å)	16.7649(14)	13.1455(11)
b (Å)	10.8596(9)	40.113(4)
c (Å)	19.0628(16)	11.4694(10)
α (deg)	90	90
β (deg)	110.371(2)	100.664(2)
γ (deg)	90	90
V ($Å^3$)	3253.5(5)	5943.5(9)
Z	2	4
D_{calc} (g/cm^3)	1.248	1.292
temperature (K)	173(2)	173(2)
Absorption (cm^{-1})	7.11	4.66
θ range (deg)	2.19 to 25.04	1.66 to 25.05
hkl ranges	-19/19, -12/12, -22/22	-15/14, -47/47, -13/16
no. of reflections collected	26227	36278
no. of unique reflections	5748(R_{int} = 0.0470)	10513(R_{int} = 0.0432)
Observed reflections ($I > 2\sigma(I)$)[a]	4593	7660
Completeness to θ = 25.11°	99.9	99.9
Data / restraints / parameters	5748 / 34 / 390	10513 / 0 / 726
R1/wR2 ($I > 2\sigma(I)$)	0.0390 / 0.1058	0.0499 / 0.1186
R1/wR2 (all data)	0.0523 / 0.1131	0.0777 / 0.1332
Goodness-of-fit on F^2	1.058	1.043
Max/min peak ($e.Å^{-3}$)	0.667 / -0.421	0.561 / -0.388

	$[(L^2\text{-}O)_3Cu_3(IO_3)]\ (O_3SCF_3)_2$	$[(L^6)_2Cu(OH)_2]$
empirical formula	C81 H96 Cu3 N9 O6 I • 2(C F3 O3 S) • 2(C2 H3 N)	C58 H82 Cu2 N4 O2
formula weight (g/mol)	1989.44	994.36
crystal habit, color	red, Block	brown, Plate
crystal system	Triclinic	Monoclinic
space group	$P\,\bar{1}$	$P_{2/n}$
a (Å)	13.468(2)	23.0719(16)
b (Å)	18.175(3)	10.7138(7)
c (Å)	21.349(4)	23.4203(17)
α (deg)	65.920(2)	90
β (deg)	78.452(2)	107.3850(10)
γ (deg)	88.273(2)	90
V ($Å^3$)	4666.9(13)	5524.8(7)
Z	2	4
D_{calc} (g/cm^3)	1.416	1.195
temperature (K)	173(2)	173(2)
Absorption (cm^{-1})	11.28	8.12
θ range (deg)	1.55 to 25.07	1.09 to 25.05
hkl ranges	-16/16, -21/21, -25/25	-27/17, -9/12, -27/27
no. of reflections collected	45011	26301
no. of unique reflections	16475(R_{int} = 0.0637)	9698(R_{int} = 0.0500)
Observed reflections ($I > 2\sigma(I)$)[a]	9753	5980
Completeness to θ = 25.11°	99.3	98.9
Data / restraints / parameters	16475 / 0 / 1099	9698 / 6 / 641
R1/wR2 ($I > 2\sigma(I)$)	0.0588 / 0.1552	0.0461 / 0.1015
R1/wR2 (all data)	0.1269 / 0.1905	0.0951 / 0.1251
Goodness-of-fit on F^2	1.074	1.036
Max/min peak ($e.Å^{-3}$)	1.950 / -0.813	0.439 / -0.517

$R1 = \Sigma||F_0|-|F_c||/\Sigma|F_0||$. $wR_2 = [\Sigma[w(F_0^2-F_c^2)^2]/\ \Sigma w(F_0^2)^2]]^{1/2}$ where $w = q / [\sigma^2 (F_0^2) + (aP)^2 + bP + d + e \times sin(\theta)$. $GooF = S = [\Sigma[w(F_0^2-F_c^2)^2] / (n-p)]^{1/2}$

Bibliography

[1] Hong, S.; Hill, L. M. R.; Gupta, A. K.; Naab, B. D.; Gilroy, J. B.; Hicks, R. G.; Cramer, C. J.; Tolman, W. B. "Effects of Electron-Deficient β-Diketiminate and Formazan Supporting Ligands on Copper(I)-Mediated Dioxygen Activation." *Inorg. Chem*. **2009**, *48*, 4514-4523.

[2] Hong, S.; Huber, S. M.; Gagliardi, L.; Cramer, C. C.; Tolman, W. B. "Copper(I)-α-Ketocarboxylate Complexes: Characterization and O_2 Reactions That Yield Copper-Oxygen Intermediates Capable of Hydroxylating Arenes." *J. Am. Chem. Soc*. **2007**, *129*, 14190-14192.

[3] Hong, S.; Gupta, A. K.; Tolman, W. B. "Intermediates in Reactions of Copper(I) Complexes with N-Oxides: From the Formation of Stable Adducts to Oxo Transfer." *Inorg. Chem*. **2009**, *48*, 6323-6325.

[4] Bielski, Benon H. J.; Cabelli, Diane E.; Arudi, Ravindra L.; Ross, Alberta B. "Reactivity of perhydroxyl/superoxide radicals in aqueous solution." *J. Phys. Chem. Ref. Data*. **1985**, *14*, 1041-1100.

[5] a) Holm, R. H.; Kennepohl,P.; Solomon. E. I. "Structural and Functional Aspects of Metal Sites in Biology" *Chem. Rev*. **1996**, *96*, 2239-2314. b) Costas, M.; Mehn. M. P.; Jensen. M. P.; Que Jr., L. "Dioxygen Activation at Mononuclear Nonheme Iron Active Sites: Enzymes, Models, and Intermediates" *Chem. Rev*. **2004**, *104*, 939-986. c) Siegbahn, P. E. M.; Borowski, T. "Modeling Enzymatic Reactions Involving Transition Metals" *Acc. Chem. Res*. **2006**, *39*, 729-738. d) Nam, W. "Dioxygen Activation by Metalloenzymes and Models" *Acc. Chem. Res*. **2007**, *40*, 465. e) Mirica, L. M.; Ottenwaelder, X.; Stack, T. D. P. "Structure and Spectroscopy of Copper−Dioxygen Complexes" *Chem. Rev*. **2004**, *104*, 1013-1045.

[6] a) Heirwegh, K.; Borginon, H.; Lontie, R. "Separation and absorption spectra of α- and β-hemocyanin of Helix pomatia." *Biochim. Biophys. Acta*. **1961**, *48*, 517-526. b) Van Holde, K. E. "Physical studies of hemocyanins. III. Circular dichroism and absorption spectra." *Biochemistry*. **1967**, *6*, 93-99.

[7] a) Freedman, T. B.; Loehr, J. S.; Loehr, T. M. "A resonance Raman study of the copper protein, hemocyanin. New evidence for the structure of the oxygen-binding site." *J. Am. Chem. Soc*. **1976**, *98*, 2809-2815. a) Ling, J-S; Nestor, L. P.; Czernuszewicz, R. S.; Spiro, T. G.; Fraczkiewicz, R.; Sharma, K. D.; Loehr, T. M.; Sanders-Loehr, J. "Common Oxygen Binding Site in Hemocyanins from Arthropods and Mollusks. Evidence from Raman Spectroscopy and Normal Coordinate Analysis." *J. Am. Chem. Soc*. **1994**, 116, 7682-7691.

[8] a) Kitajima, N. Fujisawa, K.; Morooka, Y.; Toriumi, K. "μ-η^2:η^2-Peroxo binuclear copper complex, $[Cu(HB(3,5\text{-}(Me_2CH)_2pz)_3)]_2(O_2)$." *J. Am. Chem. Soc*. **1989**. *111*, 8975-8976. b) Kitajima, N.; Koda, T.; Hashimoto, S.; Kitagawa, T.; Morooka, Y. "An accurate synthetic model of oxyhemocyanin." *J. Chem. Soc. Chem. Commun*. **1988**, *2*, 151-152. c) Kitajima, N.; Koda, T.; Hashimoto, S.; Kitagawa, T.; Morooka, Y. "Synthesis and characterization of the dinuclear copper(II) complexes $[Cu(HB(3,5\text{-}Me_2pz)_3)]_2X$ ($X = O^{2-}$, $(OH)_2^{2-}$, CO_3^{2-}, O_2^{2-})." *J. Am. Chem. Soc*. **1991**, *113*, 5664-5671. d) Kitajima, N.; Fujisawa, K.; Fujimoto, C.; Morooka, Y.; Hashimoto, S.; Kitagawa, T.; Toriumi, K.;

Tatsumi, K.; Nakamura, A. "A new model for dioxygen binding in hemocyanin. Synthesis, characterization, and molecular structure of the μ-η^2:η^2 peroxo dinuclear copper(II) complexes, $[Cu(HB(3,5\text{-}R_2pz)_3)]_2(O_2)$ (R = isopropyl and Ph)." *J. Am. Chem. Soc*. **1992**, *114*, 1277-1291.
[9] Magnus, K. A.; Ton-That, H.; Carpenter, J. E. "Recent Structural Work on the Oxygen Transport Protein Hemocyanin." *Chem. Rev*. **1994**, *94*, 727-735.
[10] Cuff, M. E.; Miller, K.I.; Van Holde, K. E.; Hendrickson, W. A. "Crystal structure of a functional unit from Octopus hemocyanin." *J. Mol. Biol*. **1998**, *278*, 855-870.
[11] a) Lippard, S. J.; Berg, J. M. "*Principles of Bioinorganic Chemistry"* b) Blackman, A. G.; Tolman, W. B. "Copper-Dioxygen and Copper-Oxo Species Relevant to Copper Oxygenases and Oxidases" Structure & Bonding, Vol. 97; Springer-Verlag: Berlin, 2000; Vol. 97, pp 179-211. c) Solomon, E. I.; Chen, P.; Metz, M.; Lee, S. K.; Palmer, A. E. "Oxygen Binding, Activation, and Reduction to Water by Copper Proteins." *Angew. Chem. Int. Ed.* **2001**, *40*, 4570-4590. d) Lewis, E. A.; Tolman, W. B. "Reactivity of Dioxygen-Copper Systems" *Chem. Rev.* **2004**, *104*, 1047-1076.
[12] Solomon, E. I.; Sundaram, U. M.; Machonkin, T. E. "Multicopper Oxidases and Oxygenases." *Chem. Rev*. **1996**, *96*, 2563-2605.
[13] a) Stewart, L.C.; Klinman, J.P. "Dopamine Beta-Hydroxylase of Adrenal Chromaffin Granules: Structure and Function" *Ann. Rev. Biochem*. **1998**, *57*, 551-590. b) Eipper, B. A.; Stoffers, P. A.; Mains, R. E. "The Biosynthesis of Neuropeptides: Peptide alpha-Amidation" *Annu. Rev. Neurosci.* **1992**, *15*, 57–85. c) Klinman, J.P. "The copper-enzyme family of dopamine β-monooxygenase and peptidylglycine α-hydroxylating monooxygenase: resolving the chemical pathway for substrate hydroxylation. *J. Biol. Chem*. **2006**, 281, 3013-3016.
[14] a) Lamoroux, A.; Vigny, A.; Faucon Biguet, V.; Darmon, M. C.; Frank, R.; Henry, J. P.; Mallet, J. "The primary structure of human dopamine-β-hydroxylase: insights into the relationship between the soluble and the membrane-bound forms of the enzyme" *EMBO J.* **1987**, *6*, 3931–3937. b) Southan, C.; Kruse, L. I. "Sequence similarity between dopamine β-hydroxylase and peptide α-amidating enzyme: Evidence for a conserved catalytic domain" *FEBS Lett.* **1989**, *255*, 116-120. c) Eipper, B. A.; Quon, A. S. W.; Mains, R. E.; Boswell, J. S.; Blackburn, N. J. "The Catalytic Core of Peptidylglycine α-Hydroxylating Monooxygenase: Investigation by Site-Directed Mutagenesis, Cu X-ray Absorption Spectroscopy, and Electron Paramagnetic Resonance" *Biochemistry.* **1995**, *34*, 2857–2865.
[15] a) Klinman, J. P.; Krueger, M.; Brenner, M.; Edmondson, D. E. "Evidence for two copper atoms/subunit in dopamine β-monooxygenase catalysis." *J. Biol. Chem*. **1984**, *259*, 3399-3402. b) Blackburn, N. J.; Concannon, M.; Shahiyan, S. K.; Mabbs, F. E.; Collison, D. "Active Site of Dopamine β-Hydroxylase. Comparison of Enzyme Derivatives Containing Four and Eight Copper Atoms per Tetramer Using Potentiometry and EPR Spectroscopy" *Biochemistry*. **1988**, *27*, 6001-6008. c) Blackburn, N. J.; Pettingill, T. M.; Seagraves, K. S.; Shigeta, R. T. "Characterization of a carbon monoxide complex of reduced dopamine beta-hydroxylase. Evidence for inequivalence of the Cu(I) centers" *J. Biol. Chem*. **1990**, *265*, 15383-15386. d) Stewart, L. C.; Klinman, J. P. "Characterization of Alternate Reductant Binding and Electron Transfer in the Dopamine

β-Monooxygenase Reaction" *Biochemistry*. **1987**, *26*, 5302-5309. e) Reedy, B. J.; Blackburn, N. J. "Preparation and Characterization of Half-Apo Dopamine β–hydroxylase by Selective Removal of Cu_A. Identification of a Sulfur Ligand at the Dioxygen Binding Site by EXAFS and FTIR Spectroscop" *J.Am.Chem.Soc*. **1994**, *116*, 1924-1931.

[16] a) Eipper, B. A.; Quon, A. S. W.; Mains, R. E.; Boswell, J. S.; Blackburn, N. J. "The Catalytic Core of Peptidylglycine α-Hydroxylating Monooxygenase: Investigation by Site-Directed Mutagenesis, Cu X-ray Absorption Spectroscopy, and Electron Paramagnetic Resonance." *Biochemistry*. **1995**, *34*, 2857-65. b) Boswell, J. S.; Reedy, B. J.; Kulathila, R.; Merkler, D.; Blackburn, N. J. "Structural investigations on the coordination environment of the active-site copper centers of recombinant bifunctional peptidylglycine α-amidating enzyme." *Biochemistry*. **1996**, *35*, 12241-50. c) Blackburn, N. J.; Rhames, F. C.; Ralle, M.; Jaron, S. "Major changes in copper coordination accompany reduction of peptidylglycine monooxygenase: implications for electron transfer and the catalytic mechanism." *J. Biol. Inorg. Chem*. **2000**, *5*, 341-353.

[17] a) Prigge, S. T.; Kolhekar, A. S.; Eipper, B. A.; Mains, R. E.; Amzel, L. M. "Amidation of bioactive peptides: the structure of peptidylglycine alpha- hydroxylating monooxygenase." *Science*. **1997**, *278*, 1300-1305. b) Prigge, S.T.; Kolhekar, A.S.; Eipper, B.A.; Mains, R.E.; Amzel, L.M. "Substrate-mediated electron transfer in peptidylglycine α-hydroxylating monooxygenase." *Nat Struct Biol*. **1999**, *6*, 976-983. c) Prigge, Sean. T.; Eipper, Betty. A.; Mains, Richard. E.; Amzel, L. Mario. "Dioxygen binds end-on to mononuclear copper in a precatalytic enzyme complex." *Science*. **2004**, *304*, 864-867.

[18] Gubelmann, M. H.; Williams, A. F. "The structures and reactivity of dioxygen complexes of the transition metals." *Struct. Bonding (Berlin)*. **1983**, *55*, 1-65.

[19] Jaron, S.; Blackburn, N. J. "Does superoxide channel between the copper centers in peptidylglycine monooxygenase? A new mechanism based on carbon monoxide reactivity." *Biochemistry*. **1999**, *38*, 15086-15096.

[20] Bell, J.; El Meskini, R.; D'Amato, D.; Mains, R. E.; Eipper, B. A. "Mechanistic Investigation of Peptidylglycine α-Hydroxylating Monooxygenase via Intrinsic Tryptophan Fluorescence and Mutagenesis." *Biochemistry*. **2003**, *42*, 7133-7142.

[21] Francisco, W. A.; Wille, G.; Smith, A. J.; Merkler, D. J.; Klinman, J. P. "Investigation of the Pathway for Inter-Copper Electron Transfer in Peptidylglycine α-Amidating Monooxygenase." *J. Am. Chem. Soc*. **2004**, *126*, 13168-13169.

[22] a) Fitzpatrick, Paul F.; Flory, Donald R., Jr.; Villafranca, Joseph J. "3-Phenylpropenes as mechanism-based inhibitors of dopamine β-hydroxylase: evidence for a radical mechanism." *Biochemistry*. **1985**, *24*, 2108-2114. b) Fitzpatrick, Paul F.; Villafranca, Joseph J. "Mechanism-based inhibitors of dopamine β-hydroxylase containing acetylenic or cyclopropyl groups." *J. Am. Chem. Soc*. **1985**, *107*, 5022-5023. c) Fitzpatrick, P. F.; Villafranca, J. J. "Mechanism-based inhibitors of dopamine β-hydroxylase. *Arch. Biochem. Biophys*. **1987**, *257*, 231-250. d) Zabriskie, T. M.; Cheng, H.; Vederas, J. C. "Mechanism-based inactivation of peptidylglycine α-hydroxylating monooxygenase (PHM) by a substrate analog, D-phenylalanyl-L-phenylalanyl-D-vinylglycine: inhibition of formation of peptide C-terminal amides." *J. Am. Chem. Soc*. **1992**, *114*, 2270-2272. e)

Kulathila, R.; Merkler, K. A.; Merkler, D, J.; Kulathila, R. "Enzymic formation of C-terminal amides." *Nat. Pro. Rep*. **1999**, *16*, 145-154.
[23] Evans, John. P.; Ahn, Kyunghye.; Klinman, Judith. P. "Evidence that dioxygen and substrate activation are tightly coupled in dopamine β-monooxygenase. Implications for the reactive oxygen species." *J. Biol. Chem*. **2003**, *278*, 49691-49698.
[24] Chen. P.; Solomon. E. I. "Oxygen activation by the noncoupled binuclear copper site in peptidylglycine α-hydroxylating monooxygenase. Reaction mechanism and role of the noncoupled nature of the active site." *J. Am. Chem. Soc*. **2004**, *126*, 4991-5000.
[25] Tian, G.; Berry, J. A.; Klinman, J. P. "Oxygen-18 kinetic isotope effects in the dopamine β-monooxygenase reaction: Evidence for a new chemical mechanism in non-heme, metallomonooxygenase." *Biochemistry*. **1994**. *33*. 226-234.
[26] Francisco, W. A.; Blackburn, N. J.; Klinman, J. P. "Oxygen and Hydrogen Isotope Effects in an Active Site Tyrosine to Phenylalanine Mutant of Peptidylglycine α-Hydroxylating Monooxygenase: Mechanistic Implications." *Biochemistry*. **2003**, *42*, 1813-1819.
[27] Miller, S. M.; Klinman, J. P. "Magnitude of intrinsic isotope effects in the dopamine β-monooxygenase reaction." *Biochemistry*. **1983**, *22*, 3091-3096.
[28] Miller, S. M.; Klinman, J. P. "Secondary isotope effects and structure-reactivity correlations in the dopamine β-monooxygenase reaction: evidence for a chemical mechanism." *Biochemistry*. **1985**, *24*, 2114-2127.
[29] Francisco, W. A.; Merkler, D. J.; Blackburn, N. J.; Klinman, J. P. "Kinetic Mechanism and Intrinsic Isotope Effects for the Peptidylglycine α-Amidating Enzyme Reaction." *Biochemistry*. **1998**, *37*, 8244-8252.
[30] Francisco, W. A.; Knapp, M. J.; Blackburn, N. J.; Klinman, J. P. "Hydrogen Tunneling in Peptidylglycine α-Hydroxylating Monooxygenase." *J. Am. Chem. Soc*. **2002**, *124*, 8194-8195.
[31] Weast, R. C., Ed. (1971) *CRC Handbook of Chemistry and Physics*, 51st ed., The Chemical Rubber Co., Cleveland, OH.
[32] Armstrong, D. A.; Yu, D.; Rauk, A. "Oxidative damage to the glycyl α-carbon site in proteins: an ab initio study of the C-H bond dissociation energy and the reduction potential of the C-centered radical." *Can. J. Chem*. **1996**, *74*, 1192-1199.
[33] Ahn, N.; Klinman, J. P. "Mechanism of modulation of dopamine β-monooxygenase by pH and fumarate as deduced from initial rate and primary deuterium isotope effect studies." *Biochemistry*. **1983**, *22*, 3096-3106.
[34] Ponce, A.; Gray, H. B.; Winkler, J. R. "Electron Tunneling through Water: Oxidative Quenching of Electronically Excited $Ru(tpy)_2^{2+}$ (tpy = 2,2':6,2"-terpyridine) by Ferric Ions in Aqueous Glasses at 77 K. *J. Am. Chem. Soc*. **2000**, *122*, 8187-8191.
[35] Kunishita, A.; Kubo, M.; Sugimoto, H.; Ogura, T.; Sato, K.; Takui, T.; Itoh, S. "Mononuclear Copper(II)- Superoxo Complexes that Mimic the Structure and Reactivity of the Active Centers of PHM and DβM." *J. Am. Chem. Soc*. **2009**, *131*, 2788-2789.
[36] a) Kamachi, T.; Kihara, N.; Shiota, Y.; Yoshizawa, K. "Computational Exploration of the Catalytic Mechanism of Dopamine β-Monooxygenase: Modeling of Its Mononuclear Copper Active Sites." *Inorg. Chem*. **2005**, *44*, 4226-4236. b) Yoshizawa, K.; Kihara, N.; Kamachi, T.; Shiota, Y. "Catalytic Mechanism of Dopamine β-Monooxygenase

Mediated by Cu(III)-Oxo." *Inorg. Chem*. **2006**, *45*, 3034-3041. c) Crespo, A.; Marti, M. A.; Roitberg, A. E.; Amzel, L. M.; Estrin, D. A. "The catalytic mechanism of peptidylglycine α-hydroxylating monooxygenase investigated by computer simulation." *J. Am. Chem. Soc*. **2006**, *128*, 12817-12828.

[37] Sono, M.; Roach, M. P.; Coulter, E. D.; Dawson, J. H. "Heme-Containing Oxygenases." *Chem. Rev*. **1996**, *96*, 2841-2887.

[38] a) Hatcher, L. Q.; Karlin, K. D. "Oxidant types in copper-dioxygen chemistry: the ligand coordination defines the Cu_n-O_2 structure and subsequent reactivity." *J. Biol. Inorg. Chem*. **2004**, *9*, 669-683. b) Itoh, S. "Mononuclear copper active-oxygen complexes." *Curr. Opin. Chem. Biol*. **2006**, *10*, 115-122. c) Cramer, C. J.; Tolman, W. B. "Mononuclear Cu-O_2 Complexes: Geometries, Spectroscopic Properties, Electronic Structures, and Reactivity." *Acc. Chem. Res*. **2007**, *40*, 601-608. d) Suzuki, M. "Ligand Effects on Dioxygen Activation by Copper and Nickel Complexes: Reactivity and Intermediates." *Acc. Chem. Res*. **2007**, *40*, 609-617. e) Itoh, S.; Fukuzumi, S. "Dioxygen activation by copper complexes. Mechanistic insights into copper monooxygenases and copper oxidases." *Bull. Chem. Soc. Jpn.* **2002**, *75*, 2081–2095. f) Schindler, S. "Reactivity of Copper(I) Complexes Towards Dioxygen." *Eur. J. Inorg. Chem.* **2000**, 2311–2326.

[39] Schroeder, D.; Holthausen, M. C.; Schwarz, H. "Radical-Like Activation of Alkanes by the Ligated Copper Oxide Cation (Phenanthroline)CuO^+." *J. Phys. Chem. B* **2004**, *108*, 14407-14416.

[40] a) Weitzer, M.; Schindler, S.; Brehm, G.; Schneider, S.; Hoermann, E.; Jung, B.; Kaderli, S.; Zuberbuehler, A. D. "Reversible Binding of Dioxygen by the Copper(I) Complex with Tris(2-dimethylaminoethyl)amine (Me6tren) Ligand." *Inorg. Chem*. **2003**, *42*, 1800-1806. b) Zhang, C. X.; Kaderli, S.; Costas, M.; Kim, E.; Neuhold, Y.; Karlin, K. D.; Zuberbuehler, A. D. "Copper(I)-Dioxygen Reactivity of [(L)CuI]+ (L = Tris(2-pyridylmethyl)amine): Kinetic/Thermodynamic and Spectroscopic Studies Concerning the Formation of Cu-O2 and Cu2-O2 Adducts as a Function of Solvent Medium and 4-Pyridyl Ligand Substituent Variations." *Inorg. Chem*. **2003**, *42*, 1807-1824. c) Börzel, H.; Comba, P.; Hagen, K. S.; Kerscher, M.; Pritzkow, H.; Schatz, M.; Schindler, S.; Walter, O. "Copper-Bispidine Coordination Chemistry: Syntheses, Structures, Solution Properties, and Oxygenation Reactivity." *Inorg. Chem*. **2002**, *41*, 5440-5452. d) Karlin, K. D.; Kaderli, S.; Zueberbuehler, A. D. "Kinetics and Thermodynamics of Copper(I)/Dioxygen Interaction." *Acc. Chem. Res*. **1997**, *30*, 139-147. e) Karlin, K. D.; Tolman, W. B.; Kaderli, S.; Zuberbuehler, A. D. "Kinetic and thermodynamic parameters of copper-dioxygen interaction with different oxygen binding modes." *J. Mol. Catal. A: Chem*. **1997**, *117*, 215-222.

[41] Fujisawa, K.; Tanaka, M.; Moro-oka, Y.; Kitajima, N. "A Monomeric Side-On Superoxocopper(II) Complex: Cu(O_2)(HB(3-tBu-5-iPrpz)3)." *J. Am. Chem. Soc.* **1994**, *116*, 12079–12080.

[42] Aboelella, N. W.; Lewis, E. A.; Reynolds, A. M.; Brennessel, W. W.; Cramer, C. J.; Tolman, W. B. "Snapshots of Dioxygen Activation by Copper: The Structure of a 1:1 Cu/O_2 Adduct and Its Use in Syntheses of Asymmetric Bis(μ-oxo) Complexes." *J. Am. Chem. Soc.* **2002**, *124*, 10660–10661.

[43] Reynolds, A. M.; Gherman, B. F.; Cramer, C. J.; Tolman, W. B. "Characterization of a 1:1 Cu/O2 Adduct Supported by an Anilido-Imine Ligand." *Inorg. Chem.* **2005**, *44*, 6989–6997.
[44] Würtele, C.; Gaoutchenova, E.; Harms, K.; Holthausen, M. C.; Sundermeyer, J.; Schindler, S. "Crystallographic Characterization of a Synthetic 1:1 End-On Copper Dioxygen Adduct Complex." *Angew. Chem., Int. Ed.* **2006**, *45*, 3867–3869.
[45] Chen, P.; Root, D. E; Campochiaro, C.; Fujisawa, K.; Solomon, E. I. "Spectroscopic and electronic structure studies of the diamagnetic side-on Cu^{II}-superoxo complex Cu(O2)[HB(3-R-5-^{i}Prpz)3]: Antiferromagnetic coupling versus Covalent delocalization." *J. Am. Chem. Soc*. **2003**, *125*, 466-474.
[46] Cramer, C. J.; Tolman, W. B.; Theopold, K. H.; Rheingold, A. L. "Variable Character of O-O and M-O Bonding in Side-on (η2) 1:1 Metal Complexes of O_2." *Proc. Natl. Acad. Sci. U.S.A.* **2003**, *100*, 3635–3640.
[47] Egan, J. W., Jr.; Haggerty, B. S.; Rheingold, A. L.; Sendlinger, S. C.; Theopold, K. H. "Crystal structure of a side-on superoxo complex of cobalt and hydrogen abstraction by a reactive terminal oxo ligand." *J. Am. Chem. Soc*. **1990**. *112*. 2445-2446.
[48] Schatz, M.; Raab, V.; Foxon, S. P.; Brehm, G.; Schneider, S.; Reiher, M.; Holthausen, M. C.; Sundermeyer, J.; Schindler, S. "Dioxygen complexes: Combined spectroscopic and theoretical evidence for a persistent end-on copper superoxo complex." *Angew. Chem. Int. Ed*. **2004**. *43*. 4360-4363.
[49] a) Hill, H. A. O.; Tew, D. G. "Dioxygen, Superoxide and Peroxide. In *Comprehensive Coordination Chemistry*; Wilkinson, G., Gillard, R. D., McCleverty, J. A., Eds.; Pergamon: Oxford, 1987; Vol. 2, pp 315–333. b) Nakamoto, K. *Infrared and Raman Spectra of Inorganic and Coordination Compounds, Part B*, 5th ed.;Wiley-Interscience: New York, 1997; pp 154–168.
[50] Spencer, D. J. E.; Aboelella, N. W.; Reynolds, A. M.; Holland, P. L.; Tolman, W. B. β-Diketiminate Ligand Backbone Structural Effects on Cu(I)/O_2 Reactivity: Unique Copper-Superoxo and Bis(μ-oxo) Complexes. *J. Am. Chem. Soc.* **2002**, *124*, 2108–2809.
[51] Aboelella, N. W.; Kryatov, S. V.; Gherman, B. F.; Brennessel, W. W.; Young, V. G., Jr.; Sarangi, R.; Rybak-Akimova, E. V.; Hodgson, K. O.; Hedman, B.; Solomon, E. I.; Cramer, C. J.; Tolman, W. B. "Dioxygen Activation at a Single Copper Site: Structure, Bonding, and Mechanism of Formation of 1:1 Cu/O_2 Adducts." *J. Am. Chem. Soc.* **2004**, *126*, 16896–16911.
[52] Reynolds, A. M.; Lewis, E. L.; Aboelella, N. W.; Tolman, W. B. "Reactivity of a 1:1 copper–oxygen complex: Isolation of a Cu(II)-*o*-iminosemiquinonato species." *Chem. Commun.* **2005**, 2014–2016.
[53] Gherman, B. F.; Tolman, W. B.; Cramer, C. J. "Characterization of the structure and reactivity of monocopper-oxygen complexes supported by β-diketiminate and anilido-imine ligands." *J. Comput. Chem*. **2006**, *27*, 1950-1961.
[54] a) Nakao, Y.; Hirao, K.; Taketsugu, T. "Theoretical study of first-row transition metal oxide cations." *J. Chem. Phys*. **2001**, *114*, 7935-7940. b) Decker, A.; Solomon, E. I. "Dioxygen activation by copper, heme and non-heme iron enzymes: comparison of electronic structures and reactivities." *Curr. Opin. Chem. Biol*. **2005**, *9*, 152-163.
[55] a) Kunishita, A.; Teraoka, J.; Scanlon, J. D.; Matsumoto, T.; Suzuki, M.; Cramer, C. J.;

Itoh, S. "Aromatic Hydroxylation Reactivity of a Mononuclear Cu(II)-Alkylperoxo Complex." *J. Am. Chem. Soc*. **2007**, *129*, 7248-7249. b) Kunishita, A.; Ishimaru, H.; Nakashima, S.; Ogura, T.; Itoh, S. "Reactivity of Mononuclear Alkylperoxo Copper(II) Complex. O-O Bond Cleavage and C-H Bond Activation." *J. Am. Chem. Soc*. **2008**, *130*, 4244-4245.

[56] Comba, P.; Knoppe, S.; Martin, B.; Rajaraman, G.; Rolli, C.; Shapiro, B.; Stork, T. "Copper(II)-mediated aromatic ortho-hydroxylation: a hybrid DFT and ab initio exploration." *Chem. Eur. J*. **2008**, *14*, 344-357.

[57] Maiti, D.; Lee, D-H.; Gaoutchenova, K.; Wuertele, C.; Holthausen, M. C.; Narducci, S., Amy, A.; Sundermeyer, J.; Schindler, S.; Karlin, K. D. "Reactions of a copper(II) superoxo complex lead to C-H and O-H substrate oxygenation: modeling copper-monooxygenase C-H hydroxylation." *Angew. Chem. Int. Ed*. **2008**, *47*, 82-85.

[58] Maiti, D.; Narducci. S. Amy, A.; Karlin, K. D. "Copper-Hydroperoxo-Mediated N-Debenzylation Chemistry Mimicking Aspects of Copper Monooxygenases." *Inorg. Chem*. **2008**, *47*, 8736-8747.

[59] Maiti, D.; Fry, H. C.; Woertink, J. S.; Vance, M. A.; Solomon, E. I.; Karlin, K. D. "A 1:1 Copper-Dioxygen Adduct is an End-on Bound Superoxo Copper(II) Complex which Undergoes Oxygenation Reactions with Phenols." *J. Am. Chem. Soc*. **2007**. *129*. 264-265.

[60] Maiti, D; Narducci Sarjeant, A. A.; Karlin, K. D. "Copper(II)-Hydroperoxo Complex Induced Oxidative N-Dealkylation Chemistry." *J. Am. Chem. Soc*. **2007**, *129*, 6720-6721.

[61] a) Shearer, J.; Zhang, C. X.; Zakharov, L. N.; Rheingold, A. L.; Karlin, K. D. "Substrate oxidation by copper-dioxygen adducts: mechanistic considerations." *J. Am. Chem. Soc*. **2005**, *127*, 5469-5483. b) Itoh, K.; Hayashi, H.; Furutachi, H.; Matsumoto, T.; Nagatomo, S.; Tosha, T.; Terada, S.; Fujinami, S.; Suzuki, M.; Kitagawa, T. "Synthesis and Reactivity of a (μ-1,1-Hydroperoxo)(μ-hydroxo)dicopper(II) Complex: Ligand Hydroxylation by a Bridging Hydroperoxo Ligand." *J. Am. Chem. Soc*. **2005**, *127*, 5212-5223.

[62] a) Abu-Omar, M. M.; Loaiza, A.; Hontzeas, N. "Reaction mechanisms of mononuclear non-heme iron oxygenases." *Chem. Rev*. **2005**. *105*. 2227-2252. b) Hausinger, R. P. "Fe(II)/α-ketoglutarate-dependent hydroxylases and related enzymes." *Crit. Rev. Biochem. Mol. Biol.* **2004**. *39*. 21–68. c) Krebs, C.; Fujimori, D. G.; Walsh, C. T.; Bollinger, J. M., Jr. "Non-Heme Fe(IV)-Oxo Intermediates." *Acc. Chem. Res*. **2007**. *40*. 484-492.

[63] Reglier, M.; Amadei, E.; Tadayoni, R.; Waegell, B. "Pyridine nucleus hydroxylation with copper oxygenase models." *J. Chem. Soc., Chem. Commun*. **1989**. *8*. 447-450.

[64] Selected examples: a) Que, L., Jr. "The road to non-heme oxoferryls and beyond." *Acc. Chem. Res*. **2007**. *40*. 493-500. b) Rohde, J.-U.; In, J.-H.; Lim, M. H.; Brennessel, W. W.; Bukowski, M. R.; Stubna, A.; Münck, E.; Nam, W.; Que, L., Jr. "Crystallographic and Spectroscopic Evidence for a Nonheme Fe^{IV}=O Complex." *Science* **2003**. *299*. 1037–1039. c) Song, W.; Seo, M. S.; DeBeer George, S.; Ohta, T.; Song, R.; Kang, M.; Tosha, T.; Kitagawa, T.; Solomon, E. I.; Nam, W. "Synthesis, Characterization, and Reactivities of Manganese(V)-Oxo Porphyrin Complexes." *J. Am. Chem. Soc.* **2007**. *129*. 1268-1277. d) Rowe, G. T.; Rybak-Akimova, E, V.; Caradonna, J. P. "Unraveling the Reactive Species of a Functional Non-Heme Iron Monooxygenase Model Using Stopped-Flow

UV-Vis Spectroscopy." *Inorg. Chem*. **2007**. *46*. 10594-10606. e) Qin, K.; Incarvito, C. D.; Rheingold, A. L.; Theopold, K. H. "Hydrogen Atom Abstraction by a Chromium(IV) Oxo Complex Derived from O_2." *J. Am. Chem. Soc.* **2002**. *124*. 14008-14009. f) Gross, Z.; Ini, S. "Dual Role of Pyridine N-Oxides in Ruthenium Porphyrin-Catalyzed Asymmetric Epoxidation of Olefins." *Inorg. Chem*. **1999**. *38*. 1446-1449.

[65] Bollinger, J. M., Jr.; Krebs, C. "Enzymatic C-H activation by metal-superoxo intermediates." *Curr. Opin. Chem. Biol.* **2007**, *11*, 151-158.

[66] Selected recent reviews: see references 5e,11d,38a,38b.

[67] Spencer, D. J. E.; Reynolds, A. M.; Holland, P. L.; Jazdzewski, B. A.; Duboc-Toia, C.; Le Pape, L.; Yokota, S.; Tachi, Y.; Itoh, S.; Tolman, W. B. "Copper Chemistry of β-Diketiminate Ligands: Monomer/Dimer Equilibria and a New Class of Bis(μ-oxo)dicopper Compounds." *Inorg. Chem*. **2002**, *41*, 6307-6321.

[68] Sarangi, R.; Aboelella, N.; Fujisawa, K.; Tolman, W. B.; Hedman, B.; Hodgson, K. O.; Solomon, E. I. "X-ray Absorption Edge Spectroscopy and Computational Studies on $LCuO_2$ Species: Superoxide-Cu^{II} versus Peroxide-Cu^{III} Bonding." *J. Am. Chem. Soc.* **2006**, *128*, 8286-8296.

[69] a) Vaska, L. "Dioxygen-Metal Complexes: Toward a Unified View." *Acc. Chem. Res.* **1976**, *9*, 175–183. b) Valentine, J. S. "The dioxygen ligand in mononuclear group VIII transition metal complexes." *Chem. Rev.* **1973**, *73*, 235–245. c) Gubelmann, M. H.; Williams, A. F. "The structure and reactivity of dioxygen complexes of the transition metals." *Struct. Bonding (Berlin, Ger.)* **1983**, *55*, 1–65.

[70] DuBois, J. L.; Mukherjee, P.; Stack, T. D. P.; Hedman, B.; Solomon, E. I.; Hodgson, K. O. "A Systematic K-edge x-ray Absorption Spectroscopic Study of Cu(III) Sites." *J. Am. Chem. Soc*. **2000**, *122*, 5775-5787.

[71] Hill, L. M. R.; Gherman, B. F.; Aboelella, N. W.; Cramer, C. J.; Tolman, W. B. "Electronic tuning of β- diketiminate ligands with fluorinated substituents: effects on the O2-reactivity of mononuclear Cu(I) complexes." *Dalton Trans*. **2006**, *41*, 4944-4953.

[72] Gilroy, J. B.; Otieno, P. O.; Ferguson, M. J.; McDonald, R.; Hicks, R. G. "Synthesis and Characterization of 3-Cyano- and 3-Nitroformazans, Nitrogen-Rich Analogues of β-Diketimine Ligands." *Inorg. Chem*. **2008**, *47*, 1279-1286.

[73] Gilroy, J. B.; Patrick, B. O.; McDonald, R.; Hicks, R. G. "Transition Metal Complexes of 3-Cyano- and 3-Nitroformazans." *Inorg. Chem*. **2008**, *47*, 1287-1294.

[74] Gilroy, J. B.; Ferguson, M. J.; McDonald, R.; Hicks, R. G. "Synthesis and characterization of palladium complexes of 3-nitroformazans." *Inorg. Chim. Acta*. **2008**, *361*, 3388-3393.

[75] Koivisto, B. D.; Hicks, R. G. "The magnetochemistry of verdazyl radical-based materials." *Coord. Chem. Rev*. **2005**, *249*, 2612-2630.

[76] Gilroy, J. B.; Ferguson, M. J.; McDonald, R.; Patrick, B. O.; Hicks, R. G. "Formazans as β-diketiminate analogues. Structural characterization of boratatetrazines and their reduction to borataverdazyl radical anions." *Chem. Commun*. **2007**, *2*, 126-128.

[77] Resonance raman experiments were preformed by Aalo K. Gupta, and preliminary EPR data and analysis were performed by our collaborator at the Medical College of Wisconsin, Prof. William Antholine.

[78] Theoretical calculations were performed by our collaborator at the University of Minnesota, Prof. Christopher Cramer.

[79] Carey, D. T.; Cope-Eatough, E. K.; Vilaplana-Mafe, E.; Mair, F. S.; Pritchard, R. G.; Warren, J. E.; Woods, R. J. "Structures and reactions of monomeric and dimeric lithium diazapentadienyl complexes with electrophiles: synthesis of α-C,C'-dialkyl-β-diimines, and dissolution-reversible synthesis of an α-alkoxylithium-b-diimine." *Dalton Trans*. **2003**, *6*, 1083-1093.

[80] Tsuda, T.; Yazawa, T.; Watanabe, K.; Fujii, T.; Saegusa, T. "Preparation of thermally stable and soluble mesitylcopper(I) and its application in organic synthesis." *J. Org. Chem*. **1981**, *46*, 192-194.

[81] Yang, L.; Powell, D. R.; Houser, R. P. "Structural variation in copper(I) complexes with pyridylmethylamide ligands: structural analysis with a new four-coordinate geometry index, τ_4." *Dalton Trans*. **2007**, *9*, 955-964.

[82] Dai, X.; Warren, T. H. "Dioxygen activation by a neutral β-diketiminato copper(I) ethylene complex." *Chem. Commun*. **2001**, *19*, 1998-1999.

[83] Henson, M. J.; Mukherjee, P.; Root, D. E.; Stack, T. D. P.; Solomon, E. I. "Spectroscopic and Electronic Structural Studies of the $Cu(III)_2$ Bis-μ-oxo Core and Its Relation to the Side-On Peroxo-Bridged Dimer." *J. Am. Chem. Soc*. **1999**. *121*. 10332-10345.

[84] Holland, P. L.; Cramer, C. J.; Wilkinson, E. C.; Mahapatra, S.; Rodgers, K. R.; Itoh, S.; Taki, M.; Fukuzumi, S.; Que, L., Jr.; Tolman, W. B. "Resonance Raman spectroscopy as a probe of the bis(μ-oxo)dicopper core." *J. Am. Chem. Soc*. **2000**. *122*. 792-802.

[85] Cramer, C. J. "*Essentials of Computational Chemistry: Theories and Models*, 2nd ed.; John Wiley & Sons: Chichester, U.K., 2004; pp 501-504.

[86] Estiú, G. L.; Zerner, M. C. "Calculations on the Electronic Structure and UV-Visible Spectrum of Oxyhemocyanin." *J. Am. Chem. Soc*. **1999**. *121*. 1893-1901.

[87] Attempts to identify product of oxidation of the solvent via gas chromatography/mass spectrometry analysis after allowing the intermediate to decompose were unsuccessful, however.

[88] Gilroy, J. B.; McKinnon, S. D. J.; Kennepohl, P.; Zsombor, M. S.; Ferguson, M. J.; Thompson, L. K.; Hicks, R. G. "Probing Electronic Communication in Stable Benzene-Bridged Verdazyl Diradicals." *J. Org. Chem*. **2007**. *72*. 8062-8069.

[89] For examples, see: a) Nam, W. "High-Valent Iron(IV)-Oxo Complexes of Heme and Non-Heme Ligands in Oxygenation Reactions." *Acc. Chem. Res*. **2007**, *40*, 522-531. b) Shaik, S.; Hirao, H.; Kumar, D. "Reactivity of High-Valent Iron-Oxo Species in Enzymes and Synthetic Reagents: A Tale of Many States." *Acc. Chem. Res*. **2007**, *40*, 532-542. c) Shaik, S.; Kumar, D.; de Visser, S. P.; Altun, A.; Thiel, W. "Theoretical perspective on the structure and mechanism of cytochrome P 450 enzymes." *Chem. Rev*. **2005**, *105*, 2279-2328. d) Harvey, J. N.; Poli, R.; Smith, K. M. "Understanding the reactivity of transition metal complexes involving multiple spin states." *Coord. Chem. Rev*. **2003**, *238-239*, 347-361. e) Bautz, J.; Comba, P.; Lopez de Laorden, C.; Menzel, M.; Rajaraman, G. "Biomimetic high-valent non-heme iron oxidants for the cis-dihydroxylation and epoxidation of olefins." *Angew. Chem. Int. Ed*. **2007**, *46*, 8067-8070. f) Kryatov, S. V.; Rybak-Akimova, E. V.; Schindler, S. "Kinetics and Mechanisms of Formation and

Reactivity of Non-heme Iron Oxygen Intermediates." *Chem. Rev*. **2005**, *105*, 2175-2226.
[90] Hegg, E. L.; Que, L, Jr. "The 2-His-1-carboxylate facial triad. An emerging structural motif in mononuclear non-heme iron(II) enzymes." *Eur. J. Biochem*. **1997**, *250*, 625-629.
[91] Zhang, Z.; Ren, J. S.; Harlos, K.; McKinnon, C. H.; Clifton, I. J.; Schofield, C. J. "Crystal structure of a clavaminate synthase-Fe(II)-2-oxoglutarate-substrate-NO complex: evidence for metal centered rearrangements." *FEBS. Lett*. **2002**, *517*, 7-12.
[92] a) Chiou, Y.-M.; Que, L., Jr. "Models for α-Keto Acid-Dependent Non-heme Iron Enzymes: Structures and Reactivity of $[Fe^{II}(L)(O_2CCOPh)](ClO_4)$ Complexes." *J. Am. Chem. Soc*. **1995**, *117*, 3999-4013. b) Chiou, Y.-M.; Que, L., Jr. "Model Studies of α-Keto Acid-Dependent Nonheme Iron Enzymes: Nitric Oxide Adducts of $[Fe^{II}(L)(O_2CCOPh)](ClO_4)$ Complexes." *Inorg. Chem*. **1995**, *34*, 3270-3278. c) Hegg, E. L.; Ho, R. Y. N.; Que, L., Jr. "Oxygen Activation and Arene Hydroxylation by Functional Mimics of α-Keto Acid-Dependent Iron(II) Dioxygenases." *J. Am. Chem. Soc*. **1999**, *121*, 1972-1973. d) Mehn, M. P.; Fujisawa, K.; Hegg, E. L.; Que, L., Jr. "Oxygen activation by nonheme iron(II) complexes: α-Keto carboxylate versus carboxylate." *J. Am. Chem. Soc*. **2003**, *125*, 7828-7842. f) Mukherjee, A.; Martinho, M.; Bominaar, E. L.; Muenck, E.; Que, L., Jr. "Shape-selective interception by hydrocarbons of the O2-derived oxidant of a biomimetic nonheme iron complex." *Angew. Chem., Int. Ed*. **2009**, *48*, 1780-1783.
[93] Ha, E. H.; Ho, R. Y. N.; Kisiel, J. F.; Valentine, J. S. "Modeling the Reactivity of α-Ketoglutarate-Dependent Non-Heme Iron(II)-Containing Enzymes." *Inorg. Chem*. **1995**, *34*. 2265-2266.
[94] Hikichi, S.; Ogihara, T.; Fujisawa, K.; Kitajima, N.; Akita, M.; Moro-oka, Y. "Synthesis and Characterization of the Benzoylformato Ferrous Complexes with Hindered Tris(pyrazolyl)borate Ligand as a Structural Model for Mononuclear Non-Heme Iron Enzymes." *Inorg. Chem*. **1997**, *36*, 4539-4547.
[95] a) Pavel, E. G.; Zhou, J.; Busby, R. W.; Gunsior, M.; Townsend, C. A.; Solomon, E. I. "Circular Dichroism and Magnetic Circular Dichroism Spectroscopic Studies of the Non-Heme Ferrous Active Site in Clavaminate Synthase and Its Interaction with α-Ketoglutarate Cosubstrate." *J. Am. Chem. Soc*. **1998**, *120*, 743-753. b) Ryle, M. J.; Padmakumar, R.; Hausinger, R. P. "Stopped-Flow Kinetic Analysis of Escherichia coli Taurine/α-Ketoglutarate Dioxygenase: Interactions with α-Ketoglutarate, Taurine, and Oxygen." *Biochemistry*. **1999**, *38*, 15278-15286.
[96] DFT calculations were performed by Dr. Stefan Huber and Prof. Christopher Cramer at the University of Minnesota as well as Prof. Laura Gagliardi at the University of Geneva.
[97] Scott, N. M.; Schareina, T.; Tok, O.; Kempe, R. "Lithium and potassium amides of sterically demanding aminopyridines." *Eur. J. Inorg. Chem*. **2004**, *16*, 3297-3304.
[98] Bianchini, C.; Mantovani, G.; Meli, A; Migliacci, F.; Laschi, F. "Selective Oligomerization of Ethylene to Linear α-Olefins by Tetrahedral Cobalt(II) Complexes with 6-(Organyl)-2-(imino)pyridyl Ligands: Influence of the Heteroatom in the Organyl Group on the Catalytic Activity." *Organometallics*. **2003**, *22*, 2545-2547.
[99] Paine, T. K.; Zheng, H.; Que, L., Jr. "Iron Coordination Chemistry of Phenylpyruvate: An Unexpected κ^3-Bridging Mode That Leads to Oxidative Cleavage of the C2-C3 Bond." Inorg. Chem. 2005, 44, 474-476.

[100] Scherrer, R. A.; Donovan, S. F. "Automated Potentiometric Titrations in KCl/Water-Saturated Octanol: Method for Quantifying Factors Influencing Ion-Pair Partitioning." *Anal. Chem*. **2009**, *81*, 2768-2778.
[101] Scherrer, R. A.; Donovan, S. F. "Automated Potentiometric Titrations in KCl/Water-Saturated Octanol: Method for Quantifying Factors Influencing Ion-Pair Partitioning." *Anal. Chem*. **2009**, *81*, 2768-2778.
[102] Friese, S. J.; Kucera, B. E.; Young, V. G.; Que, L., Jr; Tolman, W. B. "Iron(II) Complexes of Sterically Bulky α-Ketocarboxylates. Structural Models for α-Ketoacid-Dependent Nonheme Iron Halogenases." *Inorg. Chem*. **2008**, *47*, 1324-1331.
[103] a) M06L: Zhao, Y.; Truhlar, D. G. "A new local density functional for main-group thermochemistry, transition metal bonding, thermochemical kinetics, and noncovalent interactions." *J. Chem. Phys*. **2006**, *125*, 194101. b) CASPT2: Andersson, K.; Malmqvist, P. A.; Roos, B. O. "Second-order perturbation theory with a complete active space self-consistent field reference function." J. Chem. Phys. **1992**, *96*. 1218-1226.
[104] It ($C_{52}H_{66}Cu_2O_{14}$; M_w = 1042.15) crystallized in the monoclinic space group P1, with a = 9.8398 Å, b = 10.5219 Å, c = 13.3041 Å, α = 96.2210º, β = 107.8550º, γ = 104.490º, V = 1243.48 Å^3, and Z = 1.
[105] Ainscough, E. W.; Bingham, A. G.; Brodie, A. M.; Husbands, J. M.; Plowman, J. E. "Small molecule analogs for the specific metal-binding site of lactoferrin. Part 2. Phenolato complexes of copper(II) and the nature of the charge-transfer transition in the visible region." *J. Chem. Soc., Dalton Trans*. **1981**, *8*, 1701-1707.
[106] Chen, X.; Hao, X.-S.; Goodhue, C. E.; Yu, J.-Q. "Cu(II)-Catalyzed Functionalizations of Aryl C-H Bonds Using O_2 as an Oxidant." *J. Am. Chem. Soc*. **2006**, *128*, 6790-6791.
[107] a) Borowski, T.; Bassan, A.; Siegbahn, P. E. M. "A Hybrid Density Functional Study of O-O Bond Cleavage and Phenyl Ring Hydroxylation for a Biomimetic Non-Heme Iron Complex." *Inorg. Chem*. **2004**, *43*, 3277-3291. b) Bassan, A.; Borowski, T.; Siegbahn, P. E. M. "Quantum chemical studies of dioxygen activation by mononuclear non-heme iron enzymes with the 2-His-1-carboxylate facial triad." *Dalton Trans*. **2004**, *20*, 3153-3162.
[108] Huber, S. M.; Ertem, M. Z.; Aquilante, F.; Gagliardi, L.; Tolman, W. B.; Cramer, C. J. "Generating Cu^{II}-Oxyl/Cu^{III}-Oxo Species from Cu^{I}-α-Ketocarboxylate Complexes and O_2: In Silico Studies on Ligand Effects and C-H-Activation Reactivity." *Chem. Eur. J*. **2009**, *15*, 4886-4895.
[109] Kubas, G. J. "Tetrakis(acetonitrile)copper(I) hexafluorophosphate." *Inorg. Synth*. **1979**, *19*, 90-92.
[110] a) Kametani, T.; Ihara, M. "Alkaloid formation through N-oxide intermediates; regioselective synthesis of (±)-corytuberine by redox reaction." *J. Chem. Soc., Perkin Trans. I* **1980**, *2*, 629-632. b) Capdevielle, P.; Sparfel, D.; Baranne-Lafont, J.; Cuong, N. K.; Maumy, M. "Copper(I) and copper(II) mediated two-electron oxidations of benzylic alcohols and diaryl acetic acids by trimethylamine N-oxide." *J. Chem. Soc., Chem. Commun*. **1990**, *7*, 565-566. c) Reinaud, O.; Capdevielle, P.; Maumy, M. "Copper(II) mediated aromatic hydroxylation by trimethylamine N-oxide." *J. Chem. Soc., Chem. Commun*. **1990**, *7*, 565-568. d) Reinaud, O.; Capdevielle, P.; Maumy, M. "2-(N-Amido)-4-nitrophenol: a new ligand for the copper-mediated hydroxylation of aromatics by trimethylamine N-oxide." *J. Mol. Catal*. **1991**, *68*, L13-L15. e) Rousselet, G.;

Capdevielle, P.; Maumy, M. "Copper-induced synthesis of iminiums: trimethylamine oxidation or amine N-oxide conversion." *Tetrahedron Lett*. **1995**, *36*, 4999-5002.

[111] Buijs, W.; Comba, P.; Corneli, D.; Pritzkow, H. "Structural and mechanistic studies of the copper(II)-assisted ortho-hydroxylation of benzoates by trimethylamine N-oxide." *J. Organomet. Chem*. **2002**, *641*, 71-80

[112] See selected examples: a) Shin, K.; Goff, H. M. "Generation of oxoiron(IV) porphyrin complexes by amine N-oxide oxo-transfer reactions." *J. Am. Chem. Soc*. **1987**, *109*, 3140-3142. b) Nee, Michael W.; Bruice, Thomas C. "Use of the N-oxide of p-cyano-N,N-dimethylaniline as an "oxygen" donor in a cytochrome P-450 model system." *J. Am. Chem. Soc*. **1982**, *104*, 6123-6125.

[112] Wayman, K. A.; Sammakia, T. "O-Nucleophilic Amino Alcohol Acyl-Transfer Catalysts: the Effect of Acidity of the Hydroxyl Group on the Activity of the Catalyst." *Org. Letters*. **2003**, *5*, 4105-4108.

[113] a) Shi, J.-M.; Chen, J.-N.; Wu, C.-Ju; Liu, L.-D. "Tetrakis(4-nitropyridine-N-oxide-κO)bis(perchlorato)copper(II)." *Acta Crystallogr. E*. **2005**, *61*, m2621-m2622. b) van Albada, G. A.; Mutikainen, I.; Turpeinen, U.; Reedijk, J. "A rare 2D structure of a novel Cu(II) dinuclear-based compound with dicyanamide and 4-nitropyridine-N-oxide as ligands." *Inorg. Chem. Commun*. **2006**, *9*, 441-443.

[114] Caron, A.; Palenik, G. J.; Goldish, E.; Donohue, J. "The molecular and crystal structure of trimethylamine oxide, $(CH_3)_3NO$." *Acta Crystallogr*. **1964**, *17*, 102-108.

[115] Selected examples: a) Hatfield, W. E.; Muto, Y.; Jonassen, H. B.; Paschal, J. S. "Substituted pyridine N-oxide complexes of copper(II) halides." *Inorg. Chem*. **1965**, *4*, 97-99. b) Richardson, H. W.; Wasson, J. R.; Hatfield, W. E.; Brown, E. V.; Plasz, A. C. "Spectral and magnetic properties of copper(II)-1,5-naphthyridine-1,5-dioxide complexes." *Inorg. Chem*. **1976**, *15*, 2916-2920. c) Carlin, R. L.; De Jongh, L. J. "Structural and magnetic properties of transition metal complexes of pyridine N-oxide." *Chem. Rev*. **1986**, *86*, 659-680.

[116] Acree, W. E., Jr.; Pilcher, G.; Ribeiro da Silva, Maria D. M. C. "The dissociation enthalpies of terminal (N-O) bonds in organic compounds." *J. Phys. Chem. Ref. Data*. **2005**, *34*, 553-572.

[117] Drago, R. S.; Donoghue, J. T.; Herlocker, D. W. "Transition metal ion complexes of trimethylamine N-oxide." *Inorg. Chem*. **1965**, *4*, 836-839.

[118] See, for example: a) Obias, H. V.; Lin, Y.; Murthy, N. N.; Pidcock, E.; Solomon, E. I.; Ralle, M.; Blackburn, N. J.; Neuhold, Y; Zuberbuehler, A. D.; Karlin, K. D. "Peroxo-, Oxo-, and Hydroxo-Bridged Dicopper Complexes: Observation of Exogenous Hydrocarbon Substrate Oxidation" *J. Am. Chem. Soc*. **1998**, *120*, 12960-12961. b) Franklin, C. C.; Vanatta, R. B.; Tai, A.; Valentine, J. S. "Copper ion mediated epoxidation of olefins by iodosylbenzene." *J. Am. Chem. Soc*. **1984**, *106*, 814-816.